

Научном већу Института за физику Београд

Београд, 11. Децембра 2019. године

Предмет:

Молба за покретање поступка за избор у звање научни сарадник

С обзиром да испуњавам критеријуме прописане од стране Министарства просвете, науке и технолошког развоја за стицање звања научни сарадник, молим Научно веће Института за физику Београд да покрене поступак за мој избор у наведено звање.

У прилогу достављам:

1. Мишљење руководиоца пројекта са предлогом чланова комисије за избор у звање
2. Стручну биографију
3. Преглед научне активности
4. Елементе за квалитативну и квантитативну оцену научног доприноса са доказима
5. Списак објављених научних радова и њихове копије
6. Податке о цитираности
7. Уверење о одбрањеној докторској дисертацији

Са поштовањем, др Давид Кнежевић

Научном већу Института за физику Београд

Предмет:

Молба за покретање поступка за избор у звање научни сарадник

Др Давид Кнежевић запослен је у Институту за физику у Београду од маја 2017. године. Ангажован је на пројекту основних истраживања Министарства просвете, науке и технолошког развоја Републике Србије ОИ171002, под називом *Нуклеарне методе истраживања ретких догађаја и космичког зрачења*. У оквиру пројекта бави се истраживањима у гама спектроскопији, физици неутрона и физици атомског језгра. С обзиром да испуњава све предвиђене услове за избор у звање научног сарадника, у складу са Правилником о поступку, начину вредновања и квантитативном исказивању научноистраживачких резултата истраживача Министарства просвете, науке и технолошког развоја Републике Србије, сагласан сам са покретањем поступка за избор др Давида Кнежевића у звање научни сарадник.

За састав комисије за избор др Давида Кнежевића у звање научни сарадник предлагам:

1. др Владимир Удовичић, виши научни сарадник, Институт за физику у Београду
2. др Александар Драгић, виши научни сарадник, Институт за физику у Београду
3. проф. др Миодраг Крмар, редовни професор, Природно-математички факултет у Новом Саду

Руководилац пројекта

проф. др Иштван Бикит

Стручна биографија др Давида Кнежевића

Давид Кнежевић рођен је 03.06.1988. године у Книну, република Хрватска. Основне студије физике завршио је 2011. године на природно-математичком факултету у Новом Саду. Мастер студије физике завршио је 2012. године на природно-математичком факултету у Новом Саду одбраном мастер рада *Компаративна анализа симулиране и експерименталне ефикасности германијумског детектора*. Исте године уписао је докторске студије на истој установи и завршио их 30.09.2019. године одбраном докторске дисертације *Експериментално одређивање параметара нуклеарне структуре активационим техникама*, урађену под менторством доцента др Николе Јованчевића са природно-математичког факултета у Новом Саду.

Давид Кнежевић је рођен 03.06.1988. у Книну, република Хрватска. Основне академске студије физике је похађао на Природно-математичком факултету у Новом Саду (2007-2011) и завршио са просечном оценом 10. Мастер студије је завршио на истом факултету (2011-2012) са просеком 9,93 одбранивши мастер рад „Компаративна анализа симулиране и експерименталне ефикасности германијумског детектора“. 2012. уписује докторске академске студије физике на истом факултету и завршава их 30.09.2019. године одбраном докторске дисертације *Експериментално одређивање параметара нуклеарне структуре активационим техникама*, урађену под менторством доцента др Николе Јованчевића са природно-математичког факултета у Новом Саду. Од маја 2017. године Давид Кнежевић је запослен у Институту за физику у Београду као истраживач сарадник у Нискофонској лабораторији за нуклеарну физику Института за физику у Београду, у оквиру пројекта основних истраживања „Нуклеарне методе истраживања ретких догађаја и космичког зрачења“ (ОИ171002) Министарства просвете, науке и технолошког развоја Републике Србије, којим руководи проф. Емеритус др Иштван Бикит. У току школске 2016/17, 2017/18 и 2018/19 и 2019/20 године учествује у извођењу наставе на Природно-математичком факултету Универзитета у Новом Саду, као сарадник у настави на предметима Савремена експериментална физика 3, увод у нуклеарну физику и виши курс нуклеарне физике. У току је завршетак рада на практикуму из области нуклеарне физике за студенте Природно-математичког факултета чији је коаутор.

До сада, Давид Кнежевић има три рада објављена у часопису категорије М21, два рада објављена у часопису категорије М22, четири рада у часопису категорије М23, четири саопштења са међународних скупова штампана у целини (М33), један рад у часопису категорије М53 и два рада у зборнику радова са националног научног скупа објављена у целини (категорија М63).

Од учешћа на конференцијама, летњим школама и радионицама, издваја се:

1. Joint ICTP-IAEA School on Nuclear Data Measurements for Science and Applications 19-30 October 2015, Trieste, Italy
2. 2015 Student Practice in JINR Fields of Research (3rd stage), 07-25 September 2015, Dubna, Russia.
3. 9th International Physics Conference of the Balkan Physical Union – BPU9 , 24-27 August 2015 , Istanbul University , Istanbul , Turkey.
4. Scientific Workshop on Nuclear Fission dynamics and the Emission of Prompt Neutrons and Gamma Rays, 20-22 Jun 2017, Varna, Bulgaria.

5. 27th Seminar on Activation Analysis and Gamma Spectrometry (SAAGAS 27), 24-27 February, 2019, Garching, Germany
6. Scientific Workshop on Nuclear Fission Dynamics and the Emission of Prompt Neutrons and Gamma Rays, 24-26 September 2019 Barga, Italy

Од учешћа на експериментима, издваја се:

1. Measuring the Level Density and the Radiative Strength Function of ^{108}Ag and ^{110}Ag by the Two-Step Gamma Cascades Method, at FRM II, Munich, Germany, 2016.
2. Measuring the Level Density and the Radiative Strength Function of ^{94}Nb by the Two-Step Gamma Cascades Method, at MTA EK, BNC, Budapest, CHANDA project, 2016.
3. Measuring the Level Density and the the Radiative Strength Function of ^{104}Rh by the Two-Step Gamma Cascades Method, at FRM II, Munich, Germany, 2017.
4. Measuring the Level Density and the Radiative Strength Function of ^{56}Mn by the Two-Step Gamma Cascade Method, at FRM II, Munich, Germany, 2017.
5. Measuring the Level Density and the Radiative Strength Function of ^{94}Nb by the Two-Step Gamma Cascades, at MTA EK, BNC, Budapest, 2017. (additional beam time).
6. Spectroscopy above the shape isomer in ^{238}U , at CNRS - ALTO installation, Orsay, France, 2018.

Преглед научне активности др Давида Кнежевића

Давид Кнежевић се бави истраживањима у области неутронске физике, захвата термалних неутрона, физике атомског језгра и гама спектрометрије. Током досадашњег рада кандидат је учествовао у великом броју експеримената и овладао радом са HPGe детекторима, обрадом података у гама спектрометрији, као и основним моделима језгра. На 4 експеримента који се тичу захвата термалних неутрона, и који су извршени на истраживачким реакторима у Будимпешти и Гархингу, кандидат је учествовао у свим корацима, од постављања експерименталне поставке до коначне обраде података.

Главни токови истраживања у којима кандидат тренутно учествује су:

1. Добијање спектроскопских података о језгрима (гама прелази и енергетски нивоу) коришћењем термалног захвата неутрона и $(n_{th}, 2\gamma)$ реакције
2. Добијање информација о функцији густине нивоа и функцији јачине прелаза за атомска језгра коришћењем термалног захвата неутрона и $(n_{th}, 2\gamma)$ реакције, у спрези са практичним моделом каскадног гама распада неутронских резонанци, развијеним у Дубни
3. Истраживања везана за интеракцију неутрона са HPGe детекторима

Преглед основних резултата научних истраживања кандидата биће презентован у виду резимеа најрелевантнијих радова које је објавио у међународним часописима.

- **D. Knežević**, N. Jovančević, M. Krmar, J. Petrović, Modeling of neutron spectrum in the gamma spectroscopy measurements with Ge-detectors, Nuclear Instruments and Methods in Physics Research Section A, Volume 833, 23-26, 2016. (M21)

У овом раду испитиван је нови метод за процену неутронског спектра пристуног у гама спектрометријским мерењима са Ge детекторима на основу интеракције неутрона са атомима детектора, а без присуства било каквог детектора за неутроне. Метод се заснива на рачунању неутронског спектра коришћењем метода деконволуције, где се на основу активности германијумских изотопа након интеракције са неутронима, доступних података о ефикасним пресецима и почетном проценом спектра рачуна највероватнија расподела неутрона по енергијама на месту детектора. Резултати показују да овај метод може да пружи корисне информације о неутронском спектру.

- Anđelić B., **Knežević D.**, Jovančević N., Krmar M., Petrović J., Toth A., Medić Ž., Hansman J., Presence of neutrons in the low-level background environment estimated by the analysis of the 595.8 keV gamma peak, Nuclear Instruments and Methods in Physics Research Section A, Volume 852, 80-84, 2017. (M21)

У овом раду анализирана је могућност одређивања присуства неутрона у нискофонским Ge детекторским системима коришћењем детектованих интензитета гама пика од 595.8 keV. Како овај гама пик може потицати и од интеракција брзих и спорих неутрона (путем $^{73}\text{Ge}(n, g)^{74}\text{Ge}$ и $^{74}\text{Ge}(n, n')^{74}\text{Ge}$ реакција) постоји могућност да се флуks и спорих и брзих неутрона одреди само на основу детектованог интензитета овог једног пика. Да би се испитала та могућност извршена су мерења са

^{252}Cf неутронским извором у близини Ge детектора. Спектар неутрона ^{252}Cf је модификован коришћењем различитих слојева PVC пластике различите дебљине између извора и детектора. Добијени резултати показују да се гама пик енергије од 595.8 keV може користити за одређивање флукса брзих неутрона. Такође, резултати показују да је ова гама линија осетљивија на присуство термалних неутрона од гама пика енергије од 139.9 keV ($^{74}\text{Ge}(n,\gamma)^{75}\text{mGe}$) која се стандардно користи за одређивање присуства спорих неутрона. Резултати представљени у овом раду могу довести од унапређења техника одређивања присуства неутрона у нискофосним гама спектрометријским системима.

- **David Knezevic**, Nikola Jovancevic, Anatoly M Sukhovoij, Aleksandar Dragic, Liudmila V Mitsyna, László Szentmiklósi, Tamás Belgya, Stephan Oberstedt, Miodrag Krmar, Ilija Arsenic, Vu D Cong, Study of gamma transitions and level scheme of ^{94}Nb using the $^{93}\text{Nb}(n,\gamma)^{94}\text{Nb}$ reaction, Nuclear Physics A, volume 993, 121645, January 2020, <https://doi.org/10.1016/j.nuclphysa.2019.121645> (M22)

У овом раду извршена је анализа података прикупљена методом двоструких гама каскада за језгро ^{94}Nb . Експеримент је извршен на истраживачком реактору у Будимпешти, Мађарска. Експериментална поставка се састојала од два HPGe детектора, мете, снопа термалних неутрона, и аквизиционог система који може да снима амплитуду догађаја и време када је догађај детектован. Двосутруке гама каскаде представљају два узастопна прелаза се енергије захвата неутрона на основно или неко од нископобуђених стања. Анализом добијених података одређен је интензитет, енергија примарног и секундарног гама кванта, као и интермедијални ниво у прелазу за 216 каскада. Упоредивањем са базом података утврђено је да се 27 примарних транзиција, 29 интермедијалних нивоа, као и 183 секундарне транзиције могу препоручити као нови спектроскопски подаци.

- **David Knezevic**, Nikola Jovancevic, Anatoly M Sukhovoij, Aleksandar Dragic, Liudmila V Mitsyna, Zsolt Revay, Christian Stieghorst, Stephan Oberstedt, Miodrag Krmar, Ilija Arsenic, Dimitrije Maletic, Dejan Jokovic, Study of gamma ray transitions and level scheme of Mn^{2556} using the $\text{Mn}^{2555}(n,\gamma)$ reaction, Nuclear Physics A, volume 992, 121628, December 2019, <https://doi.org/10.1016/j.nuclphysa.2019.121628> (M22)

У овом раду извршена је анализа података прикупљена методом двоструких гама каскада за језгро ^{56}Mn . Експеримент је извршен на истраживачком реактору у Гархингу, Немачка. Експериментална поставка се састојала од два HPGe детектора, мете, снопа термалних неутрона, и аквизиционог система који може да снима амплитуду догађаја и време када је догађај детектован. Двосутруке гама каскаде представљају два узастопна прелаза се енергије захвата неутрона на основно или неко од нископобуђених стања. Анализом добијених података одређен је интензитет, енергија примарног и секундарног гама кванта, као и интермедијални ниво у прелазу за 71 каскаду. Упоредивањем са базом података утврђено је да се 23 примарне транзиције, 24 интермедијална нивоа, као и 32 секундарне транзиције могу препоручити као нови спектроскопски подаци.

- N. Jovančević, LV Mitsyna, AM Sukhovoij, **D. Knežević**, M. Krmar, J. Petrović, S Oberstedt, A Dragić, F-J Hamsch, VD Cong, Study of Nuclear Structure Parameters by Using the (n,γ) Reaction, Journal of the Korean Physical Society, volume 75(2), July 2019, pages 100-116, DOI: 10.3938/jkps.75.100 (M23)

У овом раду извршен је преглед могућности практичног модела каскадног гама распада неутронских резонанци развијеног у Дубни, Русија. Овај модел може да, на основу одређивања интензитета двоструких гама каскада између енергије захвата неутрона за одређено језгро и основног или неког од нископобуђених нивоа, омогући симултано одређивање функције густине стања и функције густине прелаза. У раду су презентовани резултати добијени применом овог модела за више од 40 језгара.

- D. C. Vu, A. M. Sukhovoј, S. Zeinalov, N. Jovančević, **D. Knežević**, M. Krmar, A. Dragić, Representation of radiative strength functions within a practical model of cascade gamma decay, Physics of Atomic Nuclei, Vol. 80(2), 237-250, 2017.

У овом раду извршен је преглед могућности практичног модела каскадног гама распада неутронских резонанци развијеног у Дубни, Русија. За разлику од претходног рада на листи, у овом раду је извршена анализа утицаја динамике интеракције између фермионских и бозонских нуклеарних стања на облик атомског језгра и приказани су резултати добијени за до сада (преко 40) испитана језгра.

Елементи за квалитативну оцену научног доприноса

1 Квалитет научних резултата

1.1 Значај научних резултата

Најзначајнији научни допринос кандидата представља рад на развоју новог практичног модела каскадног гама распада неутронских резонанци који омогућава симултано одређивање функције густине стања и функције јачине прелаза у експериментима у којима се детектују гама кванти након захвата термалних неутрона на мети. Такође, рад на прикупљању нови спектроскопских података за језгра коришћењем методе двоструких гама каскада.

Метода двоструких гама каскада се детекцији два коинциденциона гама кванта који се каскадно емитују након захвата термалних неутрона на језгрима мете. Ове каскаде представљају прелазак са енергије захвата неутрона до основног или неког од нископобуђених стања емисијом два гама кванта. Ова метода омогућава добијање нових спектроскопских података о језгрима, попут енергија нивоа, као и енергија гама прелаза и примењива је на велики број средње тешких и тешких језгара. Такође, ова метода омогућава ограничавање потенцијалних вредности спинова за нове нивое, као и за нивое које постоје у бази података а за које нису познате вредности спина

Практични модел каскадног гама распада неутронских резонанци је развијен на Обједињеном институту за нуклеарна истраживања у Дубни, Русија. Модел омогућава симултано одређивање функције густине стања и функције густине прелаза и заснива се на суперпроводном моделу језгра. Модел се константно развија и кандидат учествује у развоју овог модела и прикупљању нових експерименталних података од 2016.

1.2 Параметри квалитета часописа

Кандидат др Давид Кнежевић објавио је укупно 9 радова у међународним часописима и то:

- 2 рада у врхунском међународном часопису *Nuclear Instruments and Methods in Physics Research Section A* (IF=1.362, IF=1.336, SNIP=1.234)
- 1 рад у врхунском међународном часопису *Radiation Measurements* (IF=1.213, SNIP=1.099)
- 2 рада у истакнутом међународном часопису *Nuclear Physics A* (IF=1.463, SNIP=0.902)
- 1 рад у међународном часопису *Journal of the Korean Physical Society* (IF=0.630, SNIP=0.380)
- 1 рад у међународном часопису *Physics of Atomic Nuclei* (IF=0.524, SNIP=0.536)
- 1 рад у међународном часопису *Acta Physica Polonica B* (IF=0.609, SNIP=0.453)
- 1 рад у међународном часопису *Physics Procedia* (IF=0.660, SNIP=0.856)

Укупан импакт фактор објављених радова је 9.26.

1.3 Подаци о цитираности

Према бази SCOPUS, радови др Давида Кнежевића цитирани су 17 пута, од тога 16 пута изузимајући аутоцитате.

1.4 Додатни библиометријски показатељи

	ИФ	М	СНИП
Укупно	9.26	46	7.596
Усредњено по чланку	1.029	5.111	0.844
Усредњено по аутору	1.195	6.284	1.040

2 Нормирање броја коауторских радова, патената и техничких решења

Сви радови спадају у категорију експерименталних радова у природно-математичким наукама, тако да се радови са 7 и мање коаутора узимају са пуном тежином, а радови са више коаутора нормирају се по формули датој у Правилнику о поступку и начину вредновања и квантитативном исказивању научноистраживачких резултата истраживача, па укупан број М бодова кандидата са нормирањем износи 36.03 бода.

3 Учешће у пројектима, потпројектима и пројектним задацима

Кандидат је од маја 2017. године ангажован на пројекту ОИ171002 "Нуклеарне методе истраживања ретких догађаја и космичког зрачења" Министарства просвете, науке и технолошког развоја Републике Србије, под руководством др Иштвана Бикита.

4 Утицај научних резултата

Утицај научних резултата кандидата описани су у тачкама ?? и ?? овог одељка, као и у прилогу о цитираности.

5 Конкретан допринос кандидата у реализацији радова у научним центрима у земљи и иностранству

Кандидат је највећи део своје истраживачке делатности реализовао у Институту за физику Београд и на Природно-математичком факултету Универзитета у Новом Саду, као и у сарадњи са научним центрима из иностранства, и то на истраживачким реакторима FRMII, Гархинг, Немачка, и BNC, Будимпешта, Мађарска, као и у сарадњи са Обједињеним институтом за нуклеарна истраживања у Дубни, Русија. Допринос кандидата се огледа у постављању експеримената, прикупљању и анализи података, рада на развоју практичног модела каскадног гама распада неутронских резонанци, као и у презентацији и интерперетацији резултата и писању радова.

Елементи за квантитативну оцену научног доприноса

Остварени М-бодови по категоријама публикација

Категорија	М-бодова по публикацији	Број публикација	Укупно М-бодова	Укупно М-бодова нормирано
M21	8	3	24	22.666
M22	5	2	10	5.277
M23	3	4	12	8.086
M33	1	4	4	3.222
M53	1	1	1	1
M63	1	2	2	2
M70	6	1	6	6

Поређење оствареног броја М-поена са минималним условима потребним за избор у звање научног сарадника

	Потребно	Остварено
Укупно	16	48.251
M10+M20+M31+M32+M33+M41+M42	10	39.251
M11+M12+M21+M22+M23	6	36.027

Списак публикација Давида Кнежевића

Радови у врхунским међународним часописима (категорија M21):

1. **D. Knežević**, N. Jovančević, M. Krmar, J. Petrović, Modeling of neutron spectrum in the gamma spectroscopy measurements with Ge-detectors, Nuclear Instruments and Methods in Physics Research Section A, Volume 833, 23-26, 2016.
2. Anđelić B., **Knežević D.**, Jovančević N., Krmar M., Petrović J., Toth A., Medić Ž., Hansman J., Presence of neutrons in the low-level background environment estimated by the analysis of the 595.8 keV gamma peak, Nuclear Instruments and Methods in Physics Research Section A, Volume 852, 80-84, 2017.
3. I. Bikit, D. Mrdja, K. Bikit, S. Grujić, **D. Knežević**, S. Forkapić, U. Kozmidis-Luburić, Radon adsorption by zeolite, Radiation Measurements, Volume 72, January 2015, Pages 70-74, ISSN 1350-4487, <http://dx.doi.org/10.1016/j.radmeas.2014.12.001>

Радови у истакнутим међународним часописима (категорија M22):

1. **David Knezevic**, Nikola Jovancevic, Anatoly M Sukhovej, Aleksandar Dragic, Liudmila V Mitsyna, László Szentmiklósi, Tamás Belgya, Stephan Oberstedt, Miodrag Krmar, Ilija Arsenic, Vu D Cong, Study of gamma transitions and level scheme of ^{94}Nb using the $^{93}\text{Nb} (n_{th}, 2\gamma)$ reaction, Nuclear Physics A, volume 993, 121645, January 2020, <https://doi.org/10.1016/j.nuclphysa.2019.121645>
2. **David Knezevic**, Nikola Jovancevic, Anatoly M Sukhovej, Aleksandar Dragic, Liudmila V Mitsyna, Zsolt Revay, Christian Stieghorst, Stephan Oberstedt, Miodrag Krmar, Ilija Arsenic, Dimitrije Maletic, Dejan Jokovic, Study of gamma ray transitions and level scheme of Mn2556 using the Mn2555 ($n_{th}, 2\gamma$) reaction, Nuclear Physics A, volume 992, 121628, December 2019, <https://doi.org/10.1016/j.nuclphysa.2019.121628>

Радови у међународним часописима (категорија M23):

1. N. Jovančević, LV Mitsyna, AM Sukhovej, **D. Knežević**, M. Krmar, J. Petrović, S Oberstedt, A Dragić, F-J Hambsch, VD Cong, Study of Nuclear Structure Parameters by Using the ($n_{th}, 2\gamma$) Reaction, Journal of the Korean Physical Society, volume 75(2), July 2019, pages 100-116, DOI: 10.3938/jkps.75.100.
2. D. C. Vu, A. M. Sukhovej, S. Zeinalov, N. Jovančević, **D. Knežević**, M. Krmar, A. Dragić, Representation of radiative strength functions within a practical model of cascade gamma decay, Physics of Atomic Nuclei, Vol. 80(2), 237-250, 2017.
3. N.Jovancevic, M.Lebois... **D. Knezevic**,... D.Gestvang, Spectroscopy of Neutron Induced Reactions with the v-ball Spectrometer, Acta Physica Polonica Series B 50(3):297, March 2019, DOI: 10.5506/APhysPolB.50.297.
4. K. Bikit, D. Mrđa, I. Bikit, J. Slivka, M. Veskovic, **D. Knežević**, Studies of the Low-energy Gamma Background, Physics Procedia, Volume 59, 2014, Pages 56-62, ISSN 1875-3892, <http://dx.doi.org/10.1016/j.phpro.2014.10.009>.

Саопштења са међународног скупа штампана у целини (категорија M33):

1. A. M. Sukhovej, L. V. Mitsyna, Sh. Zeinalov, D. C. Vu, N. Jovančević, **D. Knežević**, M. Krmar, A. Dragić, Verification of the Partical Model of Cascade Gamma-Decay, XXIV International Seminar on Interaction of Neutrons with Nuclei, Proceeding of the International Conference, Dubna, ISBN 978-5-9530-0465-7, 122, 2016.
2. D.C. Vu, A.M. Sukhovej, L. V. Mitsyna, Sh. Zeinalov, N. Jovančević, **D. Knežević**, M. Krmar, A. Dragić, Representation of the radiative strength function in the practical model of cascade gamma-decay, XXIV International Seminar on Interaction of Neutrons with Nuclei, Proceeding of the International Conference, Dubna, ISBN 978-5-9530-0465-7, 134, 2016.
3. **D. Knežević**, N. Jovančević, M. Krmar, Estimation of neutron spectrum in the low-level gamma spectroscopy system using unfolding procedure, AIP Conference Proceedings, 1722, 030006, 2016.
4. **Knezevic, D.**, Jovancevic, N., Sukhovej, A. M., Mitsyna, L. V., Krmar, M., Cong, V. D., ... & Dragic, A. (2018). Determination of the nuclear level densities and radiative strength function for 43 nuclei in the mass interval $28 \leq A \leq 200$. In EPJ Web of Conferences (Vol. 169, p. 00007). EDP Sciences.

Радови у научном часопису (категорија M53):

1. **Knezevic, D.**, Jovancevic, N., Sukhovej, A. M., & Mitsyna, L. V. (2018). Testing the modified dependence of the radiative strength function on different excitation energies in the light nucleus ^{28}Al . Journal of Research in Physics, 39(1), 47-63.

Радови у зборнику радова са националног научног скупа објављени у целини (категорија M63):

1. Н. Јованчевић, **Д. Кнежевић**, М. Крмар, Ј. Николов, Н. Тодоровић, С. Илић, Утицај промена мионског флукса на ниво фонске активности у нискофонским гама спектрометријским мерењима, Зборник радова, XXIX Симпозијум ДЗЗСЦГ, Сребрно језеро, ИСБН 978-86-7306-144-3, 551, 2017.
2. Н. Јованчевић, **Д. Кнежевић**, М. Крмар, Ј. Николов, Н. Тодоровић, Ј. Петровић, Одређивање енергетског спектра неутрона присутног у гама спектрометријским мерењима са германијумским детекторима, Зборник радова, XXIX Симпозијум ДЗЗСЦГ, Сребрно језеро, ИСБН 978-86-7306-144-3, 558, 2017.

Одбрањена докторска дисертација (M70)

1. **Д. Кнежевић**, Експериментално одређивање параметара нуклеарне структуре активационим техникама, Универзитет у Новом Саду, Природно-математички факултет, 2019.

Knežević, David

[View potential author matches](#)

 <http://orcid.org/0000-0003-2081-8400>

Affiliation(s): 

University of Belgrade, Belgrade, Serbia [View more](#) 

Subject area: [Physics and Astronomy](#)

Documents by author

11

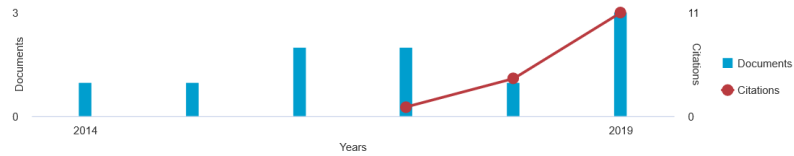
Total citations

17 by 16 documents

h-index: 


3

Document and citation trends:



Profile actions

 [Edit author profile](#)

 [Connect to ORCID](#) 

 [Alerts](#)

[Set citation alert](#)

[Set document alert](#)

 [Learn more about Scopus Profiles](#) 



David Knežević 

11 Documents

[View Mendeley profile](#) 

11 Documents

[Cited by 16 documents](#)

[99 co-authors](#)

[Topics](#)

Estimation of neutron spectrum in the low-level gamma spectroscopy system using unfolding procedure

D. Knežević, N. Jovančević, and M. Krmar

Citation: [AIP Conference Proceedings](#) **1722**, 030006 (2016); doi: 10.1063/1.4944129

View online: <http://dx.doi.org/10.1063/1.4944129>

View Table of Contents: <http://scitation.aip.org/content/aip/proceeding/aipcp/1722?ver=pdfcov>

Published by the [AIP Publishing](#)

Articles you may be interested in

[Study of Neutron Induced Activity in Low-Background Gamma Spectroscopy Systems](#)

[AIP Conf. Proc.](#) **1165**, 439 (2009); 10.1063/1.3232147

[A Comparison of Low-level Gamma-spectrometers within the GERDA Collaboration](#)

[AIP Conf. Proc.](#) **897**, 26 (2007); 10.1063/1.2722064

[Low-level contamination](#)

[Phys. Today](#) **18**, 93 (1965); 10.1063/1.3047369

[Low-Level Low-Frequency Detection System](#)

[Rev. Sci. Instrum.](#) **33**, 1200 (1962); 10.1063/1.1717729

[A Low-Level Radon Counting System](#)

[Rev. Sci. Instrum.](#) **25**, 153 (1954); 10.1063/1.1771009

Estimation of Neutron Spectrum in the Low-level Gamma Spectroscopy System Using Unfolding Procedure

Knežević D.^{1, a)}, Jovančević N.¹ and Krmar M.¹

¹University of Novi Sad, Faculty of Science, Department of Physics, Trg Dositeja Obradovića 3, 21000, Novi Sad, Serbia

^{a)} Corresponding author: david.knezevic@df.uns.ac.rs

Abstract. The radiation resulting from neutron interactions with Ge nuclei in active volume of HPGe detectors is one of the main concerns in low-level gamma spectroscopy measurements [1,2]. It is usually not possible to measure directly spectrum of neutrons which strike detector. This paper explore the possibility of estimation of neutron spectrum using measured activities of certain $\text{Ge}(n,\gamma)$ and $\text{Ge}(n,n')$ reactions (obtained from low-level gamma measurements), available ENDF cross section data and unfolding procedures. In this work HPGe detector with passive shield made from commercial low background lead was used for the measurement. The most important objective of this study was to reconstruct muon induced neutron spectrum created in the shield of the HPGe detector. MAXED [3] and GRAVEL [4] algorithms for neutron spectra unfolding were used. The results of those two algorithms were compared and we analyzed the sensitivity of the unfolding procedure to the various input parameters.

INTRODUCTION

This paper explores the possibility to use unfolding algorithms in order to calculate the neutron spectrum present in the HPGe detector system without measuring directly the neutron spectrum, but only using the neutron induced germanium gamma lines. Neutron induced processes are one of the main sources of background in gamma spectroscopy measurements. Neutrons are always present to some degree in gamma spectroscopy systems. Neutrons that create background in gamma spectroscopy systems originate from natural radioactivity of radionuclides from the detector system surroundings and from cosmic rays. Gamma activity is produced by neutron interaction with detector system materials. As one of the primary background sources, analysis of neutron induced gamma activity is of great importance in low-level gamma spectroscopy measurements. Main source of background inducing neutrons in low-level gamma spectroscopy measurements are cosmic muons.

We can calculate the activity of the reaction k using the equation:

$$A_k = \sum_i \sigma_{ik} \Phi_i \quad (1)$$

In the equation, σ_{ik} is the corresponding cross section and Φ_i is the neutron spectrum content in energy bin i . From eq. (1), the neutron fluence spectrum Φ_i can be determined by the unfolding procedure using cross sections and measured activities. For the unfolding procedure unfolding algorithms MAXED and GRAVEL were used. These techniques start with an initial default spectrum. A-priori information, necessary for the construction of the initial guess spectrum, can be obtained from the available experimental data concerning neutron production by muons in lead [5].

MEASURED ACTIVITIES OF NEUTRON INDUCED GAMMA ACTIVITY

For the measurement of the activities of neutron induced gamma lines the HPGe detector from Canberra, serial number GX10021, was used. Detector is a coaxial n-type detector, with U-shaped cryostat configuration. Relative efficiency of the detector is 100%, and the active volume is 380 cm³. Detector is surrounded by passive lead shield, Canberra model 777B. Total mass of the shield is 1633 kg.

The experimental data was acquired by recording the background spectrum for 5886293 s (~68 days), in order to get the satisfying statistics of the detected gamma rays which are created due to interaction of neutrons with germanium nuclei inside the detector. In Table 1. the activities of the detected gamma peaks that were used in this paper are shown. Four inelastic scattering reactions of neutrons (dominant at high energies), and four radiative neutron capture reactions (dominant at low energies) were used.

TABLE 1. Activities of neutron induced reactions.

Reactions	Measured Activity [10 ⁻²⁴ Bq/atom]
$^{72}\text{Ge}(n,\gamma)^{73\text{m}}\text{Ge}$	0.347(25)
$^{74}\text{Ge}(n,\gamma)^{75\text{m}}\text{Ge}$	0.322(25)
$^{70}\text{Ge}(n,\gamma)^{71\text{m}}\text{Ge}$	0.84(4)
$^{76}\text{Ge}(n,\gamma)^{77\text{m}}\text{Ge}$	2.5(4)
$^{76}\text{Ge}(n,n')^{76}\text{Ge}$	5.7(5)
$^{74}\text{Ge}(n,n')^{74}\text{Ge}$	6.83(20)
$^{72}\text{Ge}(n,n')^{72}\text{Ge}$	1.44(5)
$^{70}\text{Ge}(n,n')^{70}\text{Ge}$	2.49(24)

THE SPECTRUM UNFOLDING PROCEDURE

Maxed and Gravel

MAXED and GRAVEL are unfolding algorithms. Unfolding algorithms use measured gamma activity, response function (cross section) and a priori estimate of the spectrum in order to find the spectrum (in this case the neutron spectrum inside the active volume of HPGe detector).

GRAVEL is an iterative algorithm that uses an a priori estimate of spectrum to determine next iterative steps in order to get the solution spectrum, while MAXED uses the principle of maximum entropy, which chooses the final spectrum to be the one that requires the minimum of additional assumption (in a mathematical way) about the spectrum shape based on an a priori estimate of the spectrum.

Cross Sections Data

Cross section for the measured neutron induces reaction were taken from the ENDF database, from ENDF/B-VII.1 library. When extracting the data for usage in unfolding algorithms some approximations had to be made in order to optimize the number of data points, since large number of data points increases the complexity of the system of equation represented by eq. (1). For inelastic scattering cross sections there are no problems, since the cross section curves are fairly simple and can be described by a relatively small number of points (~100). Capture cross sections required different approach due to resonance region, where the cross section can change up to five orders of magnitude. To solve this, the average values of cross sections for data points inside the resonance region were calculated and used in unfolding algorithms.

A Priori Neutron Spectrum

A priori spectrum in unfolding methods is used as a starting point for unfolding algorithms in determination of the solution spectrum. Since most of the neutrons in our setup comes from muon interaction with lead shielding, for a

priori spectrum we used the empirical equation [5] for the general spectrum shape of neutrons that originate from muon interaction with lead shielding. For neutrons with energies in 1-4 MeV, we used the equation:

$$\frac{dN(E)}{dE} \propto E^{5/11} e^{-E/\theta} \quad (2)$$

Where E is neutron energy, and θ is effective nuclear temperature and its value is 1.22 MeV. For neutron energies above 4 MeV, the equation takes the following form:

$$\frac{dN(E)}{dE} \propto e^{-E/E_d} \quad (3)$$

where E_d is the parameter that in the 4.5-10 MeV interval has the value of 8 ± 1 MeV, and in the 10-50 MeV interval it has the value 8.6 ± 0.5 MeV.

RESULTS

Figure 1. shows the obtained results. The left graph (a) shows the result obtained with GRAVEL and MAXED from the a priori spectrum. Above 1 MeV, both unfolding algorithms are in good agreement with the a priori estimate. Below 1 MeV, the results obtained by unfolding algorithms show disagreement with the a priori spectrum, and some data points differ by factor of 3. This disagreement is most probably due to the fact that the energy region below 1 MeV is not covered by the eq. (2). The lower part of the neutron energy curve was estimated simply by extending the eq. (2) below 1 MeV. Extended work on the energy region below 1 MeV should be done in order to improve the results, and can be used for the investigation of this energy region. The right graph (b) shows the sensitivity of unfolding algorithms (the results shown are for the GRAVEL unfolding algorithm only, since MAXED shown approximately the same behaviour) to the different binnings of the cross sections. The obtained results show that the binning can influence the results greatly, and this fact is clearly seen for the 0.4 MeV step where results are in clear disagreement with the a priori spectrum. Other two binnings show approximately the same results. The stability of the solution for different bins should be tested in more detail.

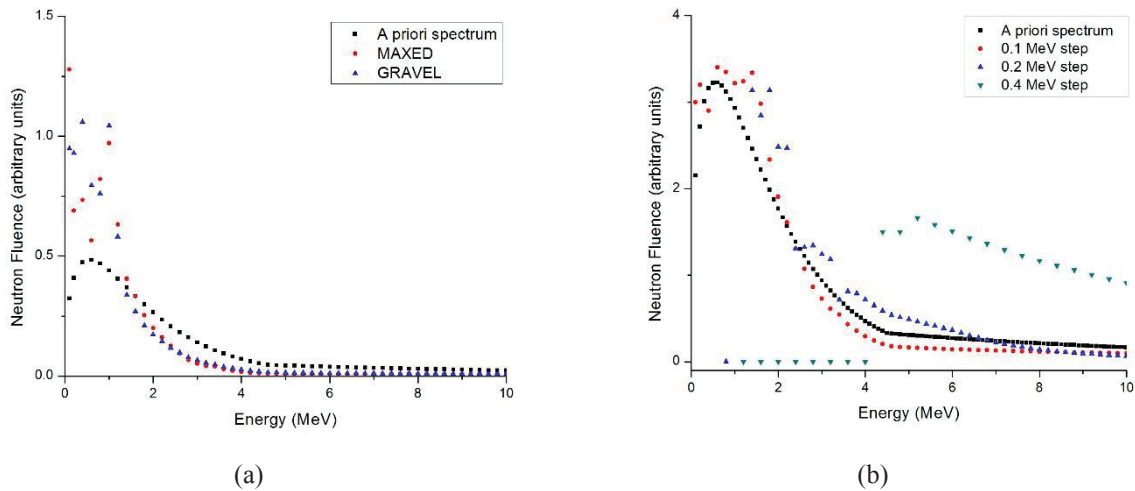


FIGURE 1. The obtained results with MAXED and GRAVEL algorithms (a), and sensitivity of the solution spectrum to different binning of the cross sections for GRAVEL algorithm (the MAXED algorithm shown approximately the same behavior) (b). Since only the general shape of the spectrum is considered in this paper, the values of the data points were scaled differently in (a) and (b) in order to show the results more clearly.

CONCLUSION

In this paper, we explored the possibility of estimating the neutron spectrum inside the HPGe detector with unfolding algorithms using only neutron induced germanium gamma-lines. Obtained results show that this approach could be useful for estimation of the neutron spectrum, and that further work should be done in this field, since it would be highly useful to have the possibility to estimate the neutron spectrum for experiments in which the direct measurement of neutron spectrum is not possible.

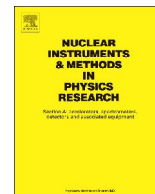
For future work, there is a number of things to consider in order to improve the results. Better statistics of the measurement would reduce the errors of the measured activities, thus giving us greater confidence in obtained activities. Second thing to consider is the lower energy part (around and below the resonance region) of the a priori spectrum. Additional information should be collected about the general shape of this part of neutron spectrum. Also, choice of data points from cross section inside the resonance region has to be optimized to represent the real shape as close as possible using as little data points as possible. Since above 10 MeV (n, 2n) and (n, 3n) reactions also contribute to the production of capture peaks, this should be included in the future work to see if the contribution of these reactions would alter the results. Efficiencies used for the calculation of activities were calculated using Monte Carlo simulation. Precise dimensions of the detector are not well known, so additional uncertainties are introduced to the experiment. Future work will also include the usage of neutron induced lines in Ge from neutrons coming from Cf source. Since the spectrum of Cf is well known, the sensitivity of the unfolding methods to other unfolding parameters will be tested.

ACKNOWLEDGMENTS

The authors would like to thank the Serbian Ministry of Education, Science and Technological Development for the funding.

REFERENCES

1. N. Jovancevic, M. Krmar, D. Mrda, J. Slivka, I. Bikit, [Nucl. Instr. and Meth. A](#), Volume 612, Issue 2, p. 303–308.
2. M. Krmar, J. Hansman, N. Jovančević, N. Lalović, J. Slivka, D. Joković, D. Maletić, [Nucl. Instr. and Meth. A](#), Volume 709, p. 8-11.
3. M. Reginatto, P. Goldhagen, S. Neumann, [Nucl. Instr. and Meth. A](#), Volume 476, p.242-246.
4. YongHao Chen, XiMeng Chen, JiaRong Lei, Li An, XiaoDong Zhang, JianXiong Shao, Pu Zheng, XinHua Wang, [Science China Physics, Mechanics & Astronomy](#), Volume 57, Issue 10, p. 1885-1890.
5. W.U. Schröder, U. Jahnke, K.H. Lindenberger, G. Röschert, R. Engfer, H.K. Walter, “Spectra of Neutron from μ Capture Thallium, Lead and Bismuth”, [Z.Phys.](#) 268 (Springer-Verlag, 1974), p.p. 57-64



Presence of neutrons in the low-level background environment estimated by the analysis of the 595.8 keV gamma peak



Brankica Anđelić, David Knežević, Nikola Jovančević, Miodrag Krmar, Jovana Petrović, Arpad Toth, Žarko Medić, Jan Hansman

Department of Physics, Faculty of Science, University of Novi Sad, Trg Dositeja Obradovica 3, 2100 Novi Sad, Serbia

ARTICLE INFO

Keywords:

Low-background gamma spectroscopy
Neutron capture
Inelastic scattering of neutrons
HPGe detector
Evaporated neutron spectra

ABSTRACT

In order to explore possible improvements of the existing techniques developed to estimate the neutron fluence in low-background Ge-spectroscopy systems, gamma spectra were collected by a HPGe detector in the presence of the ^{252}Cf spontaneous fission neutron source. The spectra were taken with and without a Cd envelope on the detector dipstick, with different thicknesses of plastic used to slow down neutrons. We have analyzed the complex 595.8 keV gamma peak, as well as several more gamma peaks following the neutron interactions in the detector itself and surroundings materials. The investigation shows that some changes of the initial neutron spectra can be monitored by the analysis of the 595.8 keV gamma peak. We have found good agreement in the intensity changes between the long-tail component of the 595.8 keV and the 691 keV gamma peak ($^{72}\text{Ge}(n,n')^{72}\text{Ge}$ reaction), usually used for the estimation of the fast neutron fluence. Results also suggest that the thermal neutrons can have a stronger influence on creation of the Gaussian-like part of 595.8 keV peak, than on the 139 keV one following $^{74}\text{Ge}(n,\gamma)^{75\text{m}}\text{Ge}$ reaction and used in the standard methods (Škoro et al., 1992) [8] for determination of the thermal neutron flux.

1. Introduction

Reduction of different background effects induced by neutrons is very important in different types of low background gamma measurements, such as dark matter search experiments, rare nuclear events research or measurements of the low level environmental activity [1–7]. Consequently, efforts are made in order to improve methods that are used for estimation of the level of neutron presence in the Ge-spectroscopy systems during low-level background gamma measurements. [8–10]. Except for the low-background measurements, it is also important to know the background neutron contribution in different types of prompt neutron activation experiments [11].

Neutrons in the low-background gamma spectroscopy systems usually come from muon interactions, spontaneous fission of heavy elements and (α,n) reactions of α -emitters of the U- and Th-series with light elements in the surrounding rocks [12]. In the ground level laboratory, neutrons are mainly produced by muon capture in a lead shield of the gamma-ray spectroscopy systems [13]. There are a number of studies about the neutron induced activity during gamma spectroscopy measurements [8,13–17]. All of those analyses show that gamma peaks following neutron capture and scattering reactions with the detector itself (and surrounding materials) can give measurable contribution to the background spectra.

Peaks created in the neutron interactions with the detector and surroundings materials can be used for the determination of the

neutron presence during gamma spectroscopy measurements. Methods for determination of the slow neutron flux, using intensity of the 139.9 keV gamma peak (following the $^{74}\text{Ge}(n,\gamma)^{75\text{m}}\text{Ge}$ reaction) and the intensity of the 691.0 keV gamma peak for fast neutrons (the $^{72}\text{Ge}(n,n')^{72}\text{Ge}$ reaction), were proposed in Ref. [8]. However, results of the study [10] suggested that, alongside thermal neutron capture, excitation of the 139.9 keV level in $^{75\text{m}}\text{Ge}$ can also take place via some other mechanisms (for example, fast neutron interactions).

To investigate the possibility of using certain gamma peaks to estimate the presence of the neutrons, we performed measurements with the ^{252}Cf neutron source placed near the HPGe detector. The ^{252}Cf neutron energy spectrum is a standard evaporation spectrum. Its shape is very similar to the energy spectrum of background neutrons in deep underground laboratories, although in a sea level laboratory fast component of background neutron spectrum is not negligible [18–20]. In this work, investigation of the neutron induced gamma peaks in different neutron fluence was done by moderation of the original ^{252}Cf spontaneous fission neutron spectra with PVC plastic sheets. It was the easiest way to obtain different measurement conditions concerning the number of neutrons reaching the active volume of the HPGe detector. Different intensities of the neutron induced gamma peaks obtained in different measurements geometries (thickness of plastic sheets) were thereby analyzed.

Here, we have studied the possibility of using the 595.8 keV gamma peak for estimation of the neutron presence in the HPGe detector

system. The gamma quanta, having the above-mentioned energy, can be emitted through the prompt de-excitation of the ^{74}Ge nuclei following two different processes: the neutron captures on the ^{73}Ge and the inelastic neutron scattering on the ^{74}Ge . The study [10] suggests that in the detected spectra a standard narrow Gaussian shape 595.8 keV gamma peak appears only when there is significant presence of the thermal neutrons. Fast neutrons will interact through inelastic scattering, producing a broad, long tail peak. The presence of this long tail peak is the underlying reason why the 595.8 keV gamma peak in collected gamma spectra has a characteristic structure, being a result of overlapping of a standard Gaussian shape peak, from the capture reaction, and a long tail peak following the neutron inelastic scattering on the Ge nuclei inside the detector. Therefore, in one relatively complex peak one can find the integral contribution of the thermal and also fast neutrons. For the analysis of the complex 595.8 keV gamma peak, the fitting procedure [3,21,22] was employed to differentiate between the contributions of the capture, on one hand, and the inelastic scattering on the other hand, to the overall peak intensity. A number of different gamma peaks were created in the interactions of Ge and surrounding materials with thermal neutrons, as well as in the interactions with fast neutrons. The intensities of those peaks depend on the measurement geometry (i.e. thickness of the plastic covering the neutron source). Obtained intensities of resolved components of the 595.8 keV gamma peak were compared with intensities of other gamma peaks to check whether they follow the same trends.

2. Experimental setup

The experimental setup was located in the low-background laboratory of the Department of Physics in Novi Sad (80 m amsl). The coaxial closed end HPGe detector with horizontal dipstick and a relative efficiency of 22.3 %, was used in the measurements. The HPGe is placed inside a cube chamber made of pre-World War II iron with a useful cube-shaped inner volume of 1 m^3 . Iron walls are 25 cm thick and the total mass of the shield is approximately 20 tons [10,17].

Detector was exposed to the ^{252}Cf spontaneous fission neutrons. The source strength was 4.5×10^3 neutrons per second into 4π sr. The ^{252}Cf source was located in simple paraffin collimator. This was done to prevent some neutrons, which are not initially emitted in the direction of the detector, to reach active volume of the detector after scattering inside low-background iron chamber. The ^{252}Cf source was placed in a Marinelli container (inner diameter 10.6 cm, outer diameter 16.0 cm, height 20.5 cm, bottom thickness 3.0 cm) with wall thickness of 2 mm. The Marinelli container was filled with melted paraffin and located below the HPGe detector (Fig. 1). Some degree of neutron collimation was obtained in this geometry by 17.5 cm long paraffin tube in very

narrow space of the low-background iron chamber. According to very simplified calculation based on measured values of the TVL for different light materials as paraffin or polyethylene [23], it was estimated that in the 3 cm thick walls of the Marinelli container about 50% of neutrons will be absorbed. To attenuate the gamma radiation of the accumulated fission products, the neutron source was placed in a 2 cm thick iron box. The measurements were carried out with different thicknesses of the PVC plates placed between the detector and the neutron source. The purpose of the PVC plates was to absorb and slow down neutrons. Thus, we obtained the simplest setup in which the detector was exposed to different neutron fluences. Six different thicknesses of the PVC plates (7 mm, 14 mm, 26 mm, 45 mm, 68 mm and 93 mm) were used. The measurements were performed for every thickness of the PVC plastic with and without the Cd envelope over the detector dipstick. Cadmium envelope served as an efficient absorber of the thermal neutrons. In this experimental configuration influence of the thermal neutrons was detected. The collection time for all spectra was approximately the same $\sim 150,000$ s.

3. Measurements and results

3.1. Rough insight in neutron fluence

Experimental setup presented in Fig. 1 was the simplest one which exposes the HPGe detector to different numbers of neutrons. It can be expected that the number (and energy spectra) of neutrons reaching detector is a result of a trade-off between thermalization and attenuation of neutrons. Intensities of several gamma lines emitted after neutron interactions in the surrounding materials can be used as a kind of an index showing how adding PVC attenuators can affect the number of neutrons striking active volume of the detector.

In the spectra recorded with the cadmium cap located around the detector dipstick, 651.1 keV and 558.4 keV peaks, following neutron capture on ^{113}Cd are detected. Detected intensity of both gamma lines following $^{113}\text{Cd}(n,\gamma)^{114}\text{Cd}$ reaction can be useful for a rough estimation of the slow neutron number at the very place of the active volume of the detector. Obtained values of the 558 keV and 651.3 keV gamma peaks intensities are presented in Fig. 2.

It can be seen that the count rates of the cadmium peaks do not change significantly with the thicknesses of the PVC plates. Measured intensities vary just up to 20% in the full range of the plastic thicknesses. The cross section for $^{113}\text{Cd}(n,\gamma)^{114}\text{Cd}$ reaction in the thermal region is a couple order of magnitude higher than the cross section in the resonant region. Thus, it can be expected that the results presented in Fig. 2 indicate, that the number of thermal neutrons does not change significantly and the Ge crystal in the detector dipstick is exposed to thermal neutron fluence which is not dependent on thickness of the plastic attenuators. One possible explanation for a nearly constant number of thermal neutrons striking the detector, which should be verified, is that they result from a trade-off between two effects: the thermalization of fast neutrons and the neutron absorption. This can be found in detail for different moderator materials in the study Ref. [24].

In all recorded spectra, prominent 846.8 keV gamma peak was observed. The origin of this peak is the $^{56}\text{Fe}(n,n')\gamma$ gamma reaction. This reaction took place in the walls of the iron shield. Considering that for an inelastic neutron scattering neutron energy should be higher than some threshold energy, the intensity of this peak could be a good indicator for monitoring the presence of fast neutrons. The detected intensity of the 846.8 keV $^{56}\text{Fe}(n,n')\gamma$ peak measured for different thicknesses of the plastic plates is presented in Fig. 3. Count rates of this gamma peak decrease with the increase of the thickness of the PVC because of the slowing down of the neutrons in the PVC. It is evident that plastic PVC attenuators can reduce the number of fast neutrons. The change in the intensity of the 846.8 keV $^{56}\text{Fe}(n,n')\gamma$ peak has the same trend in presence of the Cd layer since the interactions of slow

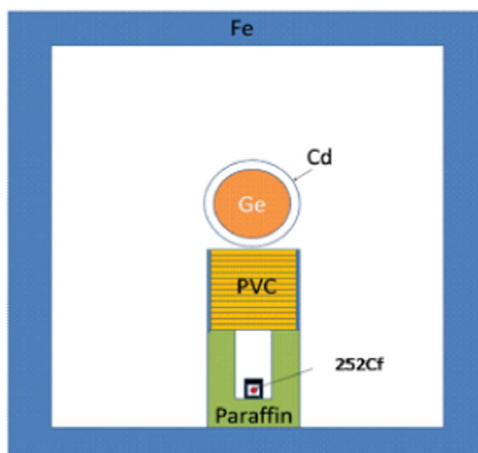


Fig. 1. Scheme of the experimental setup (not in scale).

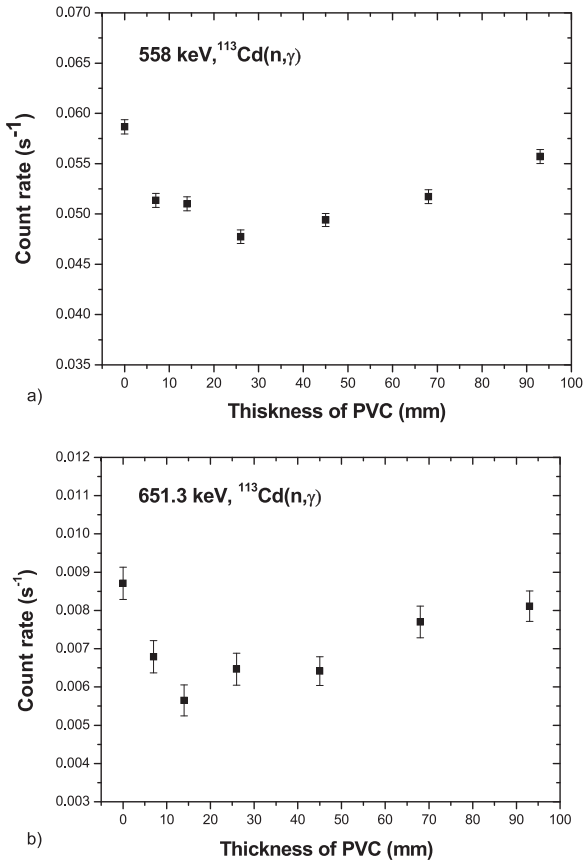


Fig. 2. Detected intensity of a) 558 keV and b) 651.3 keV for the $^{113}\text{Cd}(n,\gamma)^{114}\text{Cd}$ reaction.

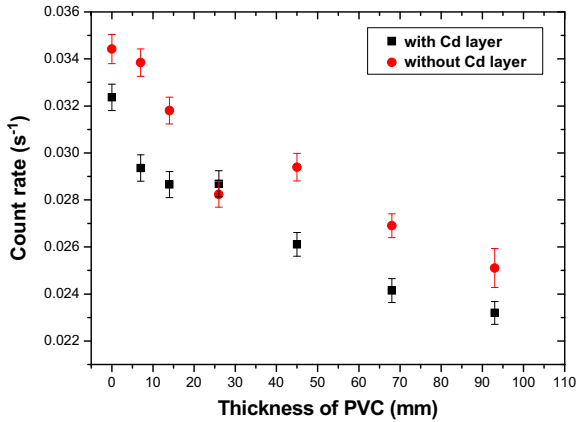


Fig. 3. Detected intensity of the 846.8 keV $^{56}\text{Fe}(n,n')^{56}\text{Fe}$ gamma peak for different thickness of PVC plastic with and without Cd layer around HPGe detector.

neutrons do not have an influence on the detection of this gamma peak.

We have to mention here that in our analysis we considered just the statistical uncertainty of detected gamma peaks. However, the jump in the count rate at 45 mm of PVC Fig. 6 can come from some systematic error. We do not have the possibility to repeat those measurements at the current time, but these results can be basis for future investigation.

3.2. Analysis of 595.8 keV gamma peak

The analysis of the 595.8 keV gamma peak was of particular interest in this work. As already noted, gamma quanta having this energy can be emitted through a prompt de-excitation of the ^{74}Ge nuclei following two different processes: a) the slow neutron captures on the ^{73}Ge , b)

the inelastic neutron scattering on the ^{74}Ge . Thus, this gamma peak, in collected gamma spectra, has a characteristic structure; due to the summation of a standard Gaussian shape peak from the capture reaction and a long tail peak following the neutron inelastic scattering on the Ge nuclei inside the detector. It is necessary to deconvolute this structure by a fitting procedure and to separate the contribution to the overall counts detected in interactions of slow and fast neutrons. Resolved intensities of the narrow Gaussian-shape and the long tail peaks obtained by the deconvolution of the 595.8 keV gamma peak can provide an insight into the presence of fast and slow neutrons in the area of the active volume of the Ge detector.

The most important problem which should be addressed in the deconvolution procedure is the overlapping of the $\text{Ge}(n,\gamma)$ and $\text{Ge}(n,n')$ and interference of the background peaks. This particular issue arises from choosing the function for fitting the asymmetric peaks induced by fast neutrons. This problem was already discussed by other authors [3,22] and in our analysis the neutron induced peaks were fitted by the following function:

$$C(E) = a_0 \text{ERFC} \left[-\frac{(E - E_0)}{\sigma_0} \right] \cdot \text{Exp} \left[-\frac{(E - E_0)}{\Delta} \right] + \sum_{i=1}^n a_i \cdot \text{Exp} \left[-\frac{1}{2\sigma_i^2} (E - E_i)^2 \right] + F \quad (1)$$

where the first term corresponds to the $\text{Ge}(n,n')$ peak; in the second term, the expression inside the summation is a Gaussian function which corresponds to any symmetric gamma peak in the fitting region; the parameter F refers to the background (here to be a linear function). The Gaussian symmetric gamma peaks can be the $\text{Ge}(n,\gamma)$ gamma peaks or any other gamma peak corresponding to the detection of some background gamma line. The parameters of the fit are: a_0 , a_i , E_0 , E_i , σ_0 , σ_i and Δ . E_0 and E_i and they correspond to the energy of the detected gamma peaks; a_0 and a_i are the maximum amplitudes of those peaks. Parameters σ_0 and σ_i should correspond to the energy resolution of the detector and they were determined by the peak full-width at half-maximum (FWHM). The characteristic of the exponential tail of $\text{Ge}(n,n')$ peaks is determined by the Δ parameter.

First step in the fitting procedure is to fix the level of the background continuum. It was shown in Ref. [3] that the quality of the results obtained by the fit of the $\text{Ge}(n,n')$ peaks depends on the energy region chosen for the fit. The next step was the variation of the fitting region for certain energy of the asymmetric peak. The energy region was varied between 30 keV and 40 keV. Different values of the level of the background continuum and energy region were used to get the fit which give the value of χ^2/NDF as close to 1 as possible. Furthermore, the uncertainties of fitting parameters were analyzed to get the optimal set of values. The gamma peaks were fitted by ROOT data analysis toolkit [25]. Fitting procedure was applied on the 691 keV $^{72}\text{Ge}(n,n')$ gamma peak, which has the simplest structure, with one well developed peak (723.3 keV ^{154}Eu , product of ^{252}Cf fission, contained in sealed source). The result of the fit is depicted on Fig. 4.

The same technique was used for deconvolution of the 595.8 keV gamma peak. It can be seen in Fig. 5 that, in the observed energy region, except for the standard narrow $^{73}\text{Ge}(n,\gamma)$ and broad $^{74}\text{Ge}(n,n')$ gamma lines, three additional background gamma peaks appeared (609.3 keV $^{214}\text{Bi}(\text{U})$, 603 keV from fission product ^{154}Eu and 641 keV from fission product ^{145}Ba). The contribution of the background continuum, as well as the background gamma peaks, were subtracted and the intensities of $^{73}\text{Ge}(n,\gamma)$ and $^{74}\text{Ge}(n,n')$ gamma peaks were obtained.

3.3. $\text{Ge}(n,n')$ component of the 595.8 keV gamma peak

The intensities of the $^{74}\text{Ge}(n,n')$ component of the 595.8 keV gamma peaks, obtained after deconvolution are presented in Fig. 6. It can be seen that the intensity of the long tail 595.8 keV gamma peak,

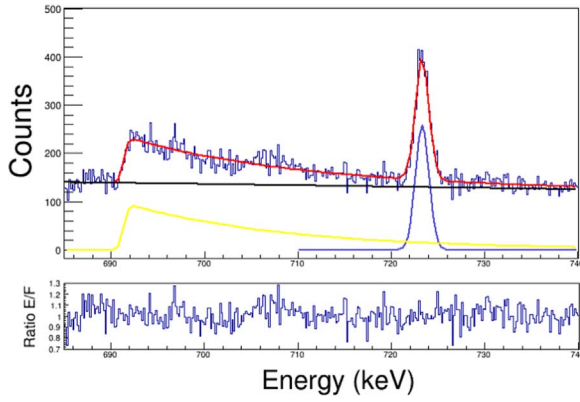


Fig. 4. The part of gamma spectrum in region around the 691 keV $\text{Ge}(n,n')$ gamma peak with the 7 mm of PVC between the Ge-detector and the ^{252}Cf source and the Cd envelope around detector. The lines show the fitting results for the $^{72}\text{Ge}(n,n')$ and background peak (upper graph). Down graph – ratio of experimental spectra to fitting function.

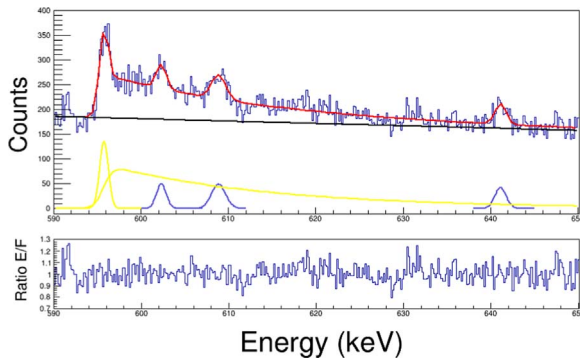


Fig. 5. The part of gamma spectrum in region around the 595.8 keV $\text{Ge}(n,n')$ gamma peak with 7 mm of PVC between the Ge-detector and the ^{252}Cf source. The lines show the fitting results for the $^{74}\text{Ge}(n,n')$, $^{73}\text{Ge}(n,\gamma)$ and background peaks (upper graph). Down graph – ratio of experimental spectra to the fitting function.

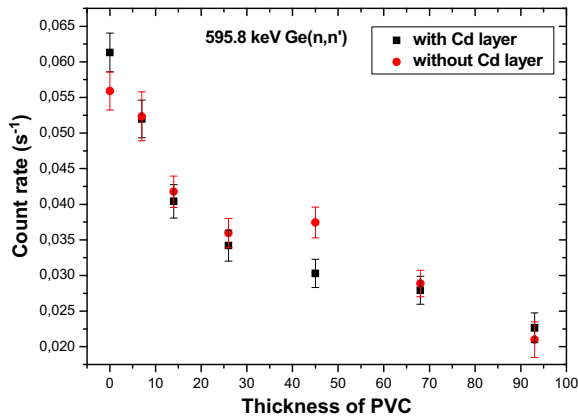


Fig. 6. Detected intensity of the 595.8 keV $^{74}\text{Ge}(n,n')$ gamma peak for different thickness of PVC plastic with and without Cd layer around the HPGe detector.

measured for different thicknesses of the plastic plates located between the neutron source and the HPGe detector, has an apparent decreasing trend. As mentioned above, the same trend was observed in analysis of 846.8 keV $^{56}\text{Fe}(n,n')$ gamma peak (Fig. 3). Considering that only fast neutrons can initiate the (n,n') reaction, presence of the Cd envelope has no influence on the obtained intensities of the separated long tail peak.

To check the obtained results, comparison with the detected intensity of the 691 keV $^{72}\text{Ge}(n,n')$ gamma peaks was performed. The intensity of the 691 keV gamma peak decreases with the increase of plastic thickness, as expected. There are no significant differences

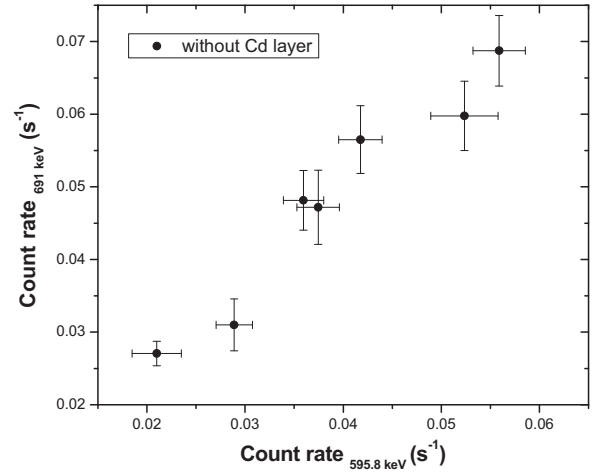


Fig. 7. Correlation between measured intensities of 691 keV and 595.8 keV peaks (without Cd layer around the HPGe detector).

between the measurements done with and without the Cd envelope. Considering that the 691 keV gamma line was frequently used in estimation of the fast neutron fluence [8], let us consider whether it is possible to do the same using the long-tail component of the 595.8 keV gamma peak. Fig. 7 presents a scatter graph showing correlation between the intensities of the two mentioned peaks recorded in this experiment.

The results in Fig. 7 shows strong linear correlation between the 595.8 keV $^{73}\text{Ge}(n,\gamma)$ and 691 keV $^{72}\text{Ge}(n,n')$ gamma peaks with linear slope coefficient 1.24(4). This means that the 595.8 keV can be also used as a standard for the determination of the fast neutron fluence.

3.3.1. $\text{Ge}(n,\gamma)$ component of 595.8 keV gamma peak

The intensity of the 595.8 keV $^{73}\text{Ge}(n,\gamma)$ gamma peak, obtained by deconvolution, has an almost constant value, not dependent on the plastic thickness (Fig. 8). The constant trend of the measured intensities, depicted in Fig. 8 can be expected considering the results obtained by the measurements of the cadmium gamma peaks (Fig. 2). It is evident that the simple experimental setup used in this experiment can provide different values of thermal neutron fluence at the very place of the detector dipstick.

Very similar results were obtained when the 139.9 keV line was used to estimate the thermal neutron fluence. Results are presented on Fig. 9.

Although experimental setup in this experiment did not allow us to provide different values of thermal neutron fluence at the place of the active volume of the HPGe detector to be able to compare neutron

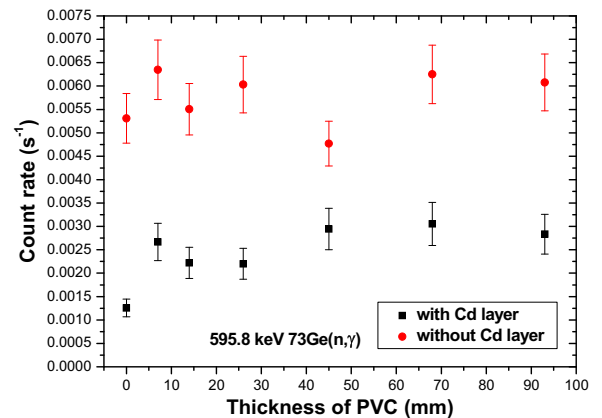


Fig. 8. Detected intensity of the 595.8 keV $^{73}\text{Ge}(n,\gamma)$ gamma peak for different thickness of PVC plastic with and without Cd layer around the HPGe detector.

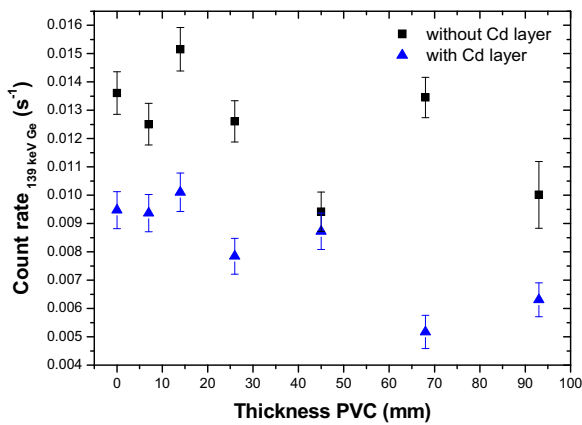


Fig. 9. Detected intensity of the 139.9 keV $^{74}\text{Ge}(\text{n},\gamma)$ gamma peak for different thickness of PVC plastic with and without Cd layer around the HPGe detector.

fluence estimation by the 139.9 keV and the (n,γ) component of the 595.8 keV gamma peak, there is still one possible indicator. We have also calculated the ratio of contribution of thermal neutrons to detected intensity of Ge(n,γ) peaks using the following equation:

$$R(\%) = 100\% \cdot \left(1 - \frac{N_{\text{withCd}}}{N_{\text{withoutCd}}} \right) \quad (2)$$

where N_{withCd} and $N_{\text{withoutCd}}$ are the intensities of gamma peaks measured with and without Cd envelope respectively. The obtained mean ratio R (for different thicknesses of PVC) for the 139.9 keV and 595.8 keV peak were 33(16)% and 57(12)%, respectively. This result can be a kind of an indication that the thermal neutrons have a stronger influence on creation of the 595.8 keV peak, than on the 139 keV one. Unfortunately, uncertainties are relatively large and for more exact confirmation that the 595.8 keV gamma line has some advantage over the 139.9 keV one, more investigations should be done.

4. Conclusions

In this work we have measured the gamma spectra using the low-background Ge-spectroscopy system in an iron shield, in the presence of the ^{252}Cf neutron source. A spontaneous fission neutron spectrum was moderated by PVC plastic plates placed between the HPGe detector and the neutron source. In our experimental setup it was possible to analyze several characteristic gamma peaks originating from the interactions of the neutrons with the isotopes of Ge and couple more surrounding materials. Special care was paid to the 595.8 keV peak because it contains records of simultaneous interaction of the thermal and fast neutrons with the Ge detector.

Preliminary results presented in this paper are quite encouraging: the 595.8 keV peak can be used in the estimation of the neutron fluence at the place of the active volume of the Ge detector. In the high energy region, above the threshold of the $\text{Ge}(\text{n},\text{n}')$ nuclear reactions, very good coincidence between the long-tail component of the 595.8 keV and the 691 keV gamma peaks, usually used for the estimation of fast neutron fluence, was observed. Simple experimental setup unfortunately could not provide us with the variety of thermal neutron fluencies at the place of detector, however it was observed that even in these circumstances

intensity of the sharp gamma peak at the beginning of the long-tail 595.8 keV peak, obtained in neutron capture process, shows a similar trend to the intensity of the 139.9 keV peak. Measured intensities of both mentioned peaks follow the same trends as the gamma peaks obtained in the $^{113}\text{Cd}(\text{n},\gamma)^{114}\text{Cd}$ reaction. It can be expected that the (n,γ) part of the 595.8 keV peak has a potential to be used for estimation of the thermal neutron fluence.

Let us review some noticeable disadvantages and advantages of the method for estimation of neutron fluence based on the measurement of the 595.8 keV peak in gamma spectra. The structure of the 595.8 keV gamma peak is not simple and a sophisticated fit procedure has to be employed. However, the shapes of the sharp Gauss-like gamma lines and the long-tail peak are well known. Moreover, it was noticed that the intensity of the (n,γ) part of the 595.8 keV peak is about two times lower than intensity of the 139.9 keV gamma line, which could introduce some uncertainty, especially if the cases of low thermal neutron fluencies. Significant advantage of the suggested method based on the 595.8 keV gamma peak is the fact that both fast and slow neutron fluence can be determined using just one energy peak. For some rough estimation of thermal to fast neutron fluence ratio, not even the relative energy efficiency of detector needs to be calculated.

Considering that in our experiment no measurements in different fields of thermal neutrons were possible, it is valuable to repeat similar measurements in some other experimental setups. This is especially important in order to confirm the assumption that the intensity of the Gauss-like part of 595.8 keV gamma peak is less dependent on fast neutrons than the usually used 139.9 keV one.

References

- [1] G. Heusser, Nucl. Instrum. Methods A 369 (1996) 539.
- [2] R. Wordel, et al., Nucl. Instrum. Methods A 369 (1996) 557.
- [3] E. Gete, et al., Nucl. Instrum. Methods A 388 (1997) 212.
- [4] N. Jovančević, M. Krmar, Phys. Procedia 31 (2012) 1–190.
- [5] S. Croft, et al., Nucl. Instrum. Methods A 505 (2003) 536–539.
- [6] Da Silva, et al., Nucl. Instrum. Methods Phys. Res. A 354 (1995) 553.
- [7] Y. Feige, et al., J. Geophys. Res. 73 (1968) 3135–3142.
- [8] G.P. Škoro, et al., Nucl. Instrum. Methods A 316 (1992) 333.
- [9] N. Jovančević, M. Krmar, Appl. Radiat. Isot. 69 (2011) 629–635.
- [10] N. Jovančević, et al., Nucl. Instrum. Methods A 612 (2009) 303–308.
- [11] A. Dragić, et al., Phys. Procedia 59 (2014) 125.
- [12] G. Heusser, Background in ionizing radiation detection, in: M. Garcia-Leon, R. Gracia-Tenorio (Eds.), Low-Level Measurements of Radioactivity in the Environment, World Scientific, Singapore, 1994, pp. 69–112.
- [13] G. Heusser, Annu. Rev. Nucl. Part Sci. 45 (1995) 543–590.
- [14] M. Krmar, et al., Nucl. Instrum. Methods A 709 (2013) 8–11.
- [15] M. Krmar, et al., Appl. Radiat. Isot. 70 (1) (2012) 269–273.
- [16] S. Niese, Underground laboratories for low-level radioactivity measurements, in: P.P. Povinec (Ed.), Analysis of Environmental Radionuclides, Elsevier, Amsterdam, 2008, pp. 209–239.
- [17] I. Bikit, et al., Nucl. Instrum. Methods A 606 (2009) 495.
- [18] C.W. Mannhart et al., 1989, IAEA Technical Report INDC(NDS)220/L, p.305, IAEA, Vienna.
- [19] W.V. Schröder, et al., Z. Phys. 239 (1974) 57.
- [20] The ENDF. Evaluated Nuclear Data File, (<https://www-nds.iaea.org/exfor/endf.htm>) (on 4/9/2016).
- [21] G. Fehrenbacher, et al., Nucl. Instrum. Methods A 372 (1996) 239.
- [22] T. Siiskonen, H. Toivonen, Nucl. Instrum. Methods A 540 (2005) 403.
- [23] NCRP Report 79, Neutron contamination from medical electron accelerators (1984).
- [24] Study of the optimal performance of a neutron activation analysis facility based on a DD neutron Generator. In: Proceedings of Neutron Generators for Analytical Purposes, IAEA Radiation Technology Reports Series No. 1, Vienna (2012).
- [25] ROOT cern, (<https://root.cern.ch>) (on 4/9/2016).



Modeling of neutron spectrum in the gamma spectroscopy measurements with Ge-detectors



D. Knežević, N. Jovančević*, M. Krmar, J. Petrović

University of Novi Sad, Faculty of Sciences, Department of Physics, Trg Dositeja Obradovića 3, 21000 Novi Sad, Serbia

ARTICLE INFO

Article history:

Received 20 April 2016

Received in revised form

23 June 2016

Accepted 1 July 2016

Available online 1 July 2016

Keywords:

Gamma spectroscopy

Neutron spectra

Unfolding procedures

Ge - detectors

ABSTRACT

In this study, we present a novel approach for estimation of neutron spectra that are present during gamma spectroscopy measurements performed by a Ge detector. This method is based on the calculation of the neutron spectra by using an unfolding procedure, where the activity of the Ge isotopes, produced by the neutron reactions, and the available cross section data for those reactions are the input parameters. This new approach was tested by background gamma spectroscopy measurements with a HPGe detector. Obtained results show that this method can provide useful information about the neutron spectra at the position of the Ge detectors.

© 2016 Elsevier B.V. All rights reserved.

1. Introduction

Detectible gamma activity can be produced by neutron interactions with the Ge-detector itself and surrounding materials, via captures and scattering reactions [1]. As one of the primary background sources, analysis of neutron presence is of great importance in low-background experiments, as well as in different kinds of prompt neutron activation measurements [2]. Analysis of neutron interactions with the Ge-detector was the subject of numerous studies [1–16]. However, today still we are faced with an old issue - the determination of neutron spectra in the Ge-detector during gamma spectroscopy measurements [17–19]. Thus, we present here a novel approach in order to resolve this issue, that is based on very well known unfolding methods used in neutron activation analysis [20]. This approach is based on the fact that the activity induced by neutrons for the activated radionuclide, k , is proportional to the product of the cross-section for a production of certain radionuclide and the neutron fluence rate:

$$A_k = \sum_i \sigma_{ik} \cdot \Phi_i; \quad i = 1, 2, \dots, c; \quad k = 1, 2, \dots, m \quad (1)$$

where σ_{ik} are the corresponding cross section functions and Φ_i is the neutron fluence rate for a certain energy bin E_i . The index k runs over the number of used radionuclides, and m is the number of radionuclides. The maximum value for the index i , c , denotes the number of bins in the neutron spectra and the cross section function. From Eq. (1), the neutron spectra Φ_i can be determined

by the unfolding procedure. In this approach we denote the activity of the Ge isotopes induced by different neutron reactions as A_k . For the reactions of interest, the available ENDF data cross section data, σ_{ik} , were used [21]. This method gives us the possibility to model neutron spectra at the position of the Ge-detector.

It should be emphasized that this approach is different from others applied in previous studies [17–19], which are based on the analysis of the detector response functions for certain neutron induced gamma peaks by Monte Carlo simulations.

In our present work, this new method was tested by modeling of the background neutron spectra during gamma spectroscopy measurements with the HPGe detector at our laboratory located at sea level [11,22]. Present neutrons are mostly created by muon captures on the Pb nuclei of the lead shield [11]. For the unfolding procedure the GRAVEL unfolding algorithm was used [23,24].

2. Measurements of neutron induced gamma activity

For the measurement of the neutron induced gamma activity, the HPGe detector from Canberra, serial number GX10021, was used. This detector is a coaxial n-type detector, with a U-shaped cryostat configuration. The relative efficiency of this detector is 100%, and the active volume is 380 cm³. The detector is surrounded by a passive lead shield, Canberra model 777B., weighing 1633 kg and being 15 cm thick. The detector is located in the low background laboratory of the Faculty of Sciences in Novi Sad (80 m asl) [22].

The experimental data was acquired by recording the background spectrum during 5886293 s (~68 days), in order to get

* Corresponding author.

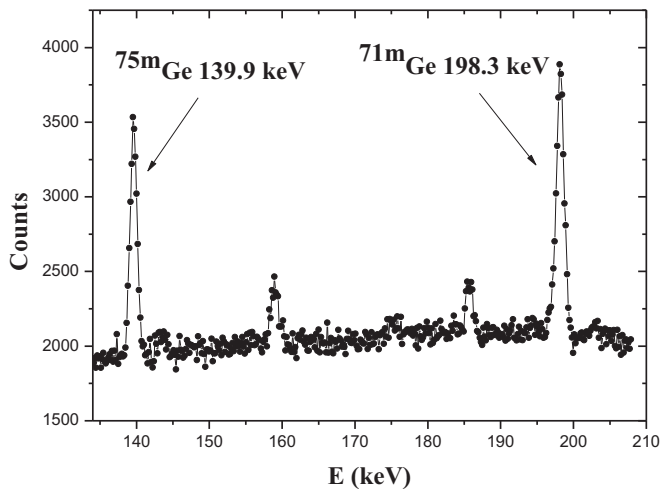


Fig. 1. Low energy part of the spectrum with the neutron induced Ge gamma peaks collected with the HPGe detector in the lead shield.

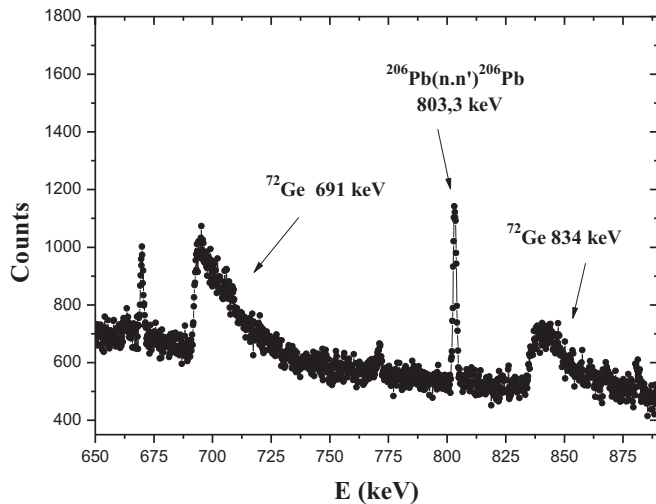


Fig. 2. The part of the spectrum with the neutron induced Ge(n,n') gamma peaks collected with the HPGe detector in the lead shield.

Table 1

General information about detected Ge-gamma peaks and corresponding values of the count rates.

Energy (keV)	Nuclide	Reactions	Count rates (s ⁻¹)
66.7	^{73m} Ge	⁷² Ge(n,γ) ^{73m} Ge ⁷⁴ Ge(n,2n) ^{73m} Ge	2.10(12)
139.9	^{75m} Ge	⁷⁴ Ge(n,γ) ^{75m} Ge ⁷⁶ Ge(n,2n) ^{75m} Ge	1.77(11)
198.3	^{71m} Ge	⁷⁰ Ge(n,γ) ^{71m} Ge ⁷² Ge(n,2n) ^{71m} Ge ⁷³ Ge(n,3n) ^{71m} Ge	2.43(11)
562.8	⁷⁶ Ge	⁷⁶ Ge(n,n') ⁷⁶ Ge	2.51(22)
691.3	⁷² Ge	⁷² Ge(n,n') ⁷² Ge	6.67(21)

satisfying statistics of the detected gamma rays, which are created due to the interactions of neutrons with the germanium nuclei. On Figs. 1 and 2, parts of the collected spectrum with characteristic neutron induced gamma peaks are shown [11,25]. Identified Ge gamma peaks, their origin and intensities are presented in Table 1. The gamma peaks that have suitable detected statistic are chosen for the analysis [11,18].

The intensities of standard narrow Gaussian shape peaks (66.7 keV, 139 keV and 198.3 keV) were determined by the CANBERA softer GENIE2000. To obtain the intensity of the long tail asymmetric Ge(n,n') 562.8 keV and 691.0 keV peaks, their shape was fitted by the following function [4,25]:

$$C(E) = a_0 \text{ERFC} \left[-\frac{(E - E_0)}{\sigma_0} \right] \cdot \text{Exp} \left[-\frac{(E - E_0)}{\Delta} \right] + \sum_{i=1}^n a_i \cdot \text{Exp} \left[-\frac{1}{2\sigma_i^2} (E - E_i)^2 \right] + F \quad (2)$$

In the equation above, the first term corresponds to the Ge(n,n') peak. In the second term, the expression inside the summation is a Gaussian function which corresponds to any symmetric gamma peak in the fitting region. Those peaks can be the Ge(n,γ) gamma peaks or any other gamma peaks corresponding to the background gamma lines. The parameter F refers to the background continuum which is assumed to be a linear function here. The parameters of the fit were: a_0 , a_i , E_0 , E_i , σ_0 , σ_i and Δ . In this case E_0 and E_i correspond to the energies of the detected gamma peaks; a_0 and a_i are the maximum amplitudes of those peaks. Parameters σ_0 and σ_i were determined by the peak full-width at half-maximum (FWHM) and should correspond to the energy resolution of the detector. The Δ parameter determines the characteristic of the exponential tail of Ge(n,n') peaks.

First step in the fitting procedure was to fix the level of background continuum. It was shown in Ref. [4], that the quality of the results obtained by the fit of Ge(n,n') peaks depends on the energy region chosen for the fit. The next step was to vary the fitting region for a chosen energy of the asymmetric peak between 30 keV and 40 keV. Different values of the level of background continuum and energy region were used to get the fit with the value of χ^2/NDF as close to unity as possible. Additionally, the errors of the fitting parameters were analyzed to get the optimal set values. The gamma peaks were fitted by the ROOT data analysis toolkit [31].

Based on detected gamma peak intensities, the activity for production of certain Ge isotopes per atom of natural germanium is calculated by [11,18]:

$$A_k = \frac{C \cdot M}{t \cdot p \cdot (\epsilon + \alpha) \cdot m \cdot N_a} \quad (3)$$

where C is the detected number of counts for certain gamma peak, t is the measurement time, p is the gamma-ray emission probability [26], α is the conversion coefficient [27], ϵ is the full energy peak efficiency (calculated by the Geant4 toolkit [11,28]), M is the Ge molar mass, m is the mass of the Ge crystal and N_a is the Avogadro constant. Obtained values of activities, A_k are shown in Table 2.

3. Cross sections data

Cross sections for the Ge isotope production were obtained by summing the cross sections for different neutron reactions (as

Table 2

The activities, A_k , of Ge isotopes.

Ge isotope	A_k [10 ⁻²⁴ Bq/atom]
^{71m} Ge	0.173(9)
^{73m} Ge	0.095(7)
^{75m} Ge	0.118(9)
⁷² Ge	0.398(13)
⁷⁶ Ge	0.44(4)

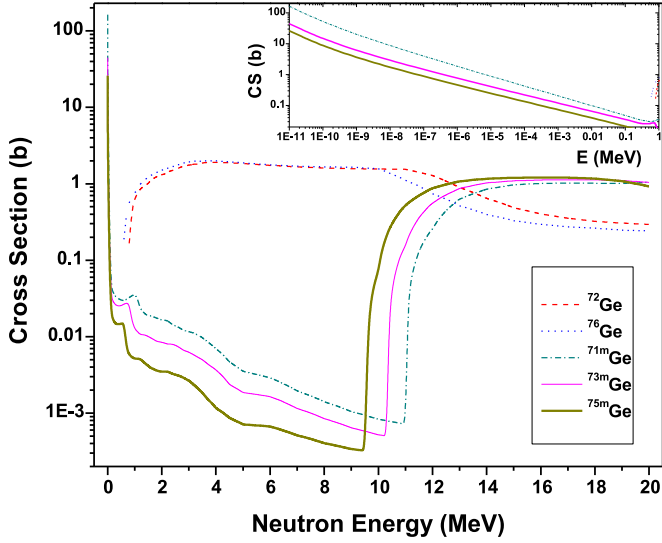


Fig. 3. The cross section functions for Ge isotopes production via neutron reactions (with magnified low energy region) [21].

listed in Table 1). The cross sections for neutron reactions were taken from the ENDF database, specifically from the ENDF/B-VII.1 library [21], as presented on Fig. 3. In order to be used in the unfolding algorithm, the cross section functions were divided into 200 energy bins. Since the cross section functions cover a fairly wide energy range, we have the possibility to determine the neutron spectrum up to 20 MeV.

3.1. A priori neutron spectrum

A priori spectrum in unfolding methods is used as a starting point for the unfolding algorithm in determination of the solution spectrum. The main sources of background neutrons are the spontaneous fission of U and Th, (α, n) nuclear reactions as well as cosmic rays [1]. At ground and shallow depth laboratories, most of the neutrons come from the muon interactions with high-Z shielding materials [11]. Having in mind this was also the case in our measurements, we used the empirical equation (available from the literature [29]) as an a priori spectrum for the general shape of neutrons spectrum. For neutron energies between 1 MeV and 4 MeV, the spectrum is well described by:

$$\frac{dN(E)}{dE} \propto E^{5/11} e^{-E/\theta} \quad (4)$$

where E is the neutron energy, and θ is the effective nuclear temperature and its value is 1.22 MeV. For the neutron energies above 4 MeV, the spectrum takes the following form:

$$\frac{dN(E)}{dE} \propto e^{-E/E_d} \quad (5)$$

where E_d is the parameter that for the energy range 4.5–10 MeV has the value of 8 ± 1 MeV, and for the 10–50 MeV range it takes the value 8.6 ± 0.5 MeV. Our default spectrum is shown in Fig. 4.

4. Unfolding results

In this work, we used the GRAVEL algorithm for the unfolding procedures [24,29]. GRAVEL is an iterative unfolding algorithm that starts with a guess default function. In this technique, from the J -th iteration of the neutron fluence rate (Φ_i^J , for energy bin E_i) the next iteration, Φ_i^{J+1} , will be calculated by:

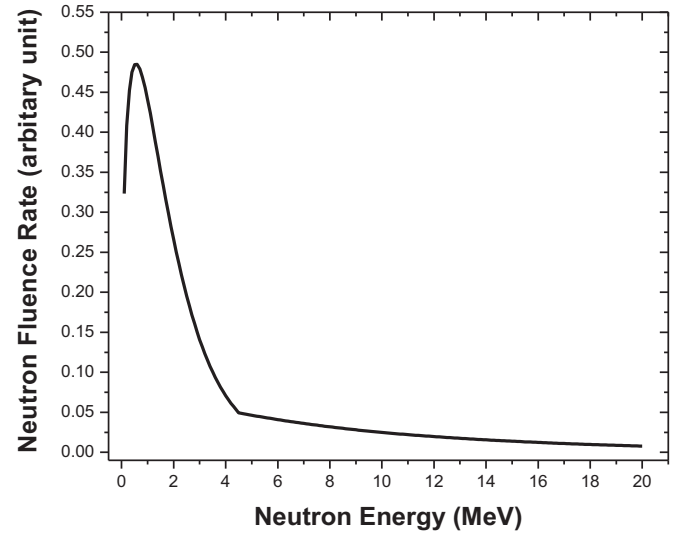


Fig. 4. Default neutron spectrum used in analysis [29].

$$\Phi_i^{J+1} = \Phi_i^J \cdot f(A_k, \varepsilon_k, \sigma_{ki}, \Phi_i^J) \quad (6)$$

The function f is defined as follows:

$$f = \exp \left(\frac{\sum_k W_{ik}^J \log \left(\frac{A_k}{\sum_i \sigma_{ki} \Phi_i^J} \right)}{\sum_k W_{ik}^J} \right), \quad W_{ik}^J = \frac{\sigma_{ki} \cdot \Phi_i^J \cdot A_k^2}{\sum_i \sigma_{ki} \cdot \Phi_i^J \cdot \varepsilon_k^2} \quad (7)$$

where W_{ik}^J is the weight factor, A_k is the measured activity, ε_k is the measurement uncertainty, and σ_{ki} is the cross section for production of k -th Ge isotope and energy bin E_i (Fig. 3). It should be noted that the standard sensitivity analysis and uncertainty propagation cannot be performed by the GRAVEL algorithm. However, the solution spectrum is always non-negative.

The unfolding was performed for 200 energy bins covering the energy range up to 20 MeV. After every integration the parameter χ^2 per degree of freedom n (equal to the number of used radio-nuclides) was calculated:

$$\chi^2/n = \frac{1}{n} \sum_k \frac{(\sum_i \sigma_{ki} \Phi_i - A_k)}{\varepsilon_k} \quad (8)$$

The iteration procedure is stopped when the solution leads to $\chi^2/n \approx 1$. The unfolding neutron spectrum function is given in Fig. 5, together with the default function.

In order to validate the obtained results, the activity (A_c) is calculated for both, default and final neutron spectrum functions, and compared with the measured data (A_m). In Table 3, the sums of squared values, S , are presented and defined by:

$$S = \frac{1}{(p-1)} \sum_{i=1}^p \left(\frac{A_{ci} - A_{mi}}{A_{mi}} \right)^2 \quad (9)$$

where p is the number of the Ge isotopes (in this case $p = 5$).

The results from Table 3. Show that the unfolding procedure converges to a better description of the measured activity data than the initial a priori neutron spectrum. There is an increase of the unfolding spectrum in the low energy range in comparison to the default spectrum. The reason behind this can be the change in energy of the neutron (emitted in muon capture process) through scattering in surrounding materials. In the region above 10 MeV, the determined spectrum function has higher values than the default function (Fig. 5) which can be used as a starting point for further investigations.

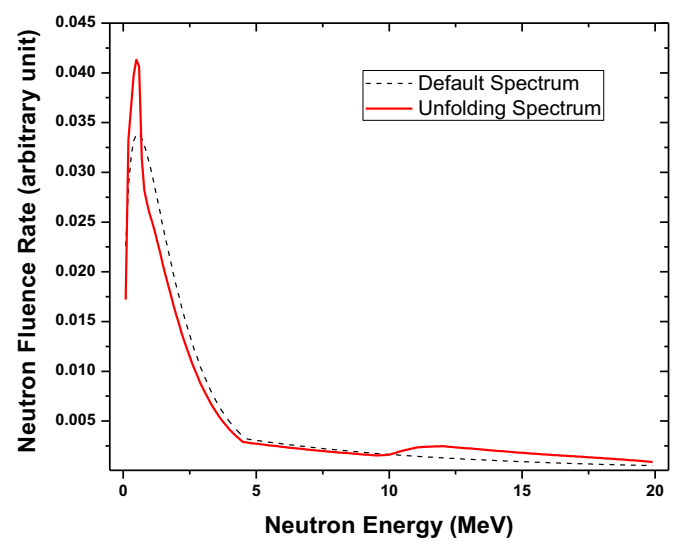


Fig. 5. The obtained unfolded neutron spectrum with GRAVEL algorithm compared with default one. The integral for both spectra is normalized to unity.

Table 3
Relations between calculated A_c and measured A_m activity.

Radionuclide	$\frac{A_c - A_m}{A_m}$ default	$\frac{A_c - A_m}{A_m}$ final
^{73m}Ge	−0.16197	0.07832
^{71m}Ge	0.04694	0.02852
^{75m}Ge	−0.42702	−0.15732
^{72}Ge	0.04293	0.00726
^{76}Ge	0.03737	0.02377
S	0.053506	0.008079

5. Conclusion

In this work, we have analyzed the possibility of estimating the neutron spectrum inside the HPGe detector with an unfolding procedure. This new approach was tested by modeling of the background neutron spectrum. The resulting unfolded spectrum (Fig. 5) describes the neutron presence in the low-background gamma spectroscopy system located in the laboratory at sea level in a satisfactory way.

The obtained results show that this technique could provide useful information about the neutron spectrum in measurements with the Ge – detectors. However, this measurement can also be a starting point for future studies. For future analyses there are a few things to consider in order to improve the results. Better statistics of the measurements would reduce the errors of the measured activities, thus giving us greater confidence in the obtained

activities. We would also consider experiments with different neutron fields, such as the ^{252}Cf spontaneous fission neutron source. Future work will also include the usage of different unfolding algorithms, since other authors reported deviations between them [30]. In this work as a priory neutron spectrum we used compound function based on the available empirical data. As an alternative for default neutron spectrum simplified functions such as Maxwellian function, can be used. The choice of the a priory neutron spectrum function would depend on the characteristics of neutron fields, a feature that can also be studied in the future. After all of the improvements suggested above and after performing tests, this method could become a standard for the determination of the neutron spectra during gamma spectroscopy measurements with the Ge – detectors.

References

- [1] G. Heusser, Nucl. Instrum. Methods Phys. Res. A 369 (1996) 539.
- [2] A. Dragić, et al., Phys. Procedia 59 (2014) 125.
- [3] R. Wordel, et al., Nucl. Instrum. Methods Phys. Res. A 369 (1996) 557.
- [4] E. Gete, et al., Nucl. Instrum. Methods Phys. Res. A 388 (1997) 212.
- [5] N. Jovančević, M. Krmar, Phys. Procedia 31 (2012) 93–98.
- [6] S. Croft, et al., Nucl. Instrum. Methods Phys. Res. A 505 (2003) 536–539.
- [7] Da Silva, et al., Nucl. Instrum. Methods Phys. Res. A 354 (1995) 553.
- [8] Y. Feige, et al., J. Geophys. Res. 73 (1968) 3135–3142.
- [9] G.P. Škoro, et al., Nucl. Instrum. Methods Phys. Res. A 316 (1992) 333.
- [10] N. Jovančević, M. Krmar, Appl. Rad. Isot. 69 (2011) 629–635.
- [11] N. Jovančević, et al., Nucl. Instrum. Methods Phys. Res. A 612 (2009) 303–308.
- [12] G. Heusser, Background in ionizing radiation detection, in: M. Garcia-Leon, R. Gracia-Tenorio (Eds.), Low-Level Measurements of Radioactivity in the Environment, World Scientific, Singapore, 1994, pp. 69–112.
- [13] G. Heusser, Annu. Rev. Nucl. Part. Sci. 45 (1995) 543–590.
- [14] M. Krmar, et al., Nucl. Instrum. Methods Phys. Res. A 70 (2013) 8–11.
- [15] M. Krmar, et al., Appl. Rad. Isot. 70 (1) (2012) 269–273.
- [16] S. Niese, Underground laboratories for low-level radioactivity measurements, in: P.P. Povinec (Ed.), Analysis of Environmental Radionuclides, Elsevier, Amsterdam, 2008, pp. 209–239.
- [17] C. Chund, Y.R. Chen, Nucl. Instrum. Methods Phys. Res. A 301 (1991) 328–336.
- [18] J.E. Naye, Nucl. Instrum. Methods Phys. Res. A 368 (1996) 832–846.
- [19] G. Fehrenbacher, et al., Nucl. Instrum. Methods Phys. Res. A 372 (1996) 239.
- [20] A. Trkov, V. Radulović, J. Radioanal. Nucl. Chem. 304 (2015) 763–778.
- [21] The ENDF, Evaluated Nuclear Data File, (<https://www-nds.iaea.org/exfor/endl.htm>).
- [22] I. Bikit, et al., Nucl. Instrum. Methods Phys. Res. A 606 (2009) 495.
- [23] M. Reginatto, et al., Health Phys. 77 (1999) 579.
- [24] W. Goffe, Studies in Nonlinear Dynamics and Econometrics, Berkeley Electronic Press 1996, pp. 169–176.
- [25] T. Siiskonen, H. Toivonen, Nucl. Instrum. Methods Phys. Res. A 540 (2005) 403.
- [26] National Nuclear Data Center, Brookhaven National Laboratory, (<http://www.nndc.bnl.gov/>).
- [27] LBNL Isotopes Project- LUNDS University, Nuclear Data Dissemination Homepage, (<http://je.lbl.gov/toi.html>).
- [28] S. Agostinelli, et al., Nucl. Instrum. Methods Phys. Res. A 506 (2003) 250.
- [29] W.V. Schröder, et al., Z. Phys. 239 (1974) 57.
- [30] R. Behrens, JINST 4 P03027, 2009.
- [31] ROOT cern, (<https://root.cern.ch>).



Radon adsorption by zeolite



I. Bikit^{a,*}, D. Mrdja^a, K. Bikit^a, S. Grujic^b, D. Knezevic^a, S. Forkapic^a,
U. Kozmidis-Luburic^b

^a University of Novi Sad, Faculty of Sciences, Trg Dositeja Obradovica 4, 21000 Novi Sad, Serbia

^b University of Novi Sad, Faculty of Technical Sciences, Trg Dositeja Obradovica 6, 21000 Novi Sad, Serbia

HIGHLIGHTS

- Measurements of radon adsorption by various zeolite granulation are done.
- Adsorption coefficients for natural zeolite and activated charcoal are determined.
- The adsorption coefficients for activated charcoal and natural zeolite are compared.

ARTICLE INFO

Article history:

Received 4 September 2014

Received in revised form

26 November 2014

Accepted 1 December 2014

Available online 2 December 2014

Keywords:

Radon

Zeolite granulation

Adsorption coefficient

ABSTRACT

Due to well defined three dimensional nano- and micro-porous structure, one of the most important properties of zeolite is its surface adsorption capacity. Nevertheless, a natural zeolite adsorption capability of ^{222}Rn has not been thoroughly investigated. The objective of this paper is to review the research concerning the application of natural zeolite in ^{222}Rn adsorption. To achieve this goal the investigation based on measurements of radon adsorption by various zeolite granulation was done. Ball mill is used to achieve different granulations of zeolite in the range of μm – mm , whereas the particle size distributions are determined by particle size analyzer, Mastersizer 2000. The zeolite samples were exposed to elevated radon concentrations up to 1800 Bq/m^3 inside a closed chamber (volume $\approx 5.4 \times 10^{-3} \text{ m}^3$). The absorbed radon quantity was measured by high resolution gamma spectroscopy. The influence of particle size was measured and discussed. We found that the adsorption coefficients that were obtained in our experiment for natural zeolite samples for different granulations are similar to adsorbing coefficients for silica gel, but they are an order of magnitude lower than radon adsorbing coefficient for synthetic zeolite. The adsorption coefficient for activated charcoal derived in our experiment ($\approx 3 \text{ m}^3/\text{kg}$) is in average 50 times higher comparing to the adsorption coefficients obtained for zeolite samples ($0.038 \text{ m}^3/\text{kg}$ – $0.11 \text{ m}^3/\text{kg}$). All adsorbing coefficients are determined for very low relative humidity of air of about 7%, since our simple experimental setup did not allow possibility to change the relative humidity, or temperature. In addition, we explored the perturbation of radon concentration inside small-volume radon chamber caused by the presence of adsorbing sample and influence of this perturbation on obtained values of adsorbing coefficients.

© 2014 Elsevier Ltd. All rights reserved.

1. Introduction

Due to the gaseous properties of radon, it is easily emanated from ground or building materials and it can reach high levels of activity in poorly ventilated buildings. Hence, the regular measurement of radon is necessary in order to control the radioactivity

levels and take appropriate measures in case of elevated concentrations. Since the late 1980s the main method for short-term measurement of radon concentration indoors is usage of activated charcoal canisters. In the recent years there is an increase in number of studies oriented toward measurement of radon adsorption by alternative types of adsorbing material, and one of those materials is zeolite. It is a naturally occurring mineral group consisting of many different minerals, and it has special porous crystalline structure (Baerlocher et al., 2007). Zeolites can be adapted for a variety of uses, and its ability to adsorb radon should

* Corresponding author. University of Novi Sad, Faculty of Sciences, Department of Physics, Trg Dositeja Obradovica 4, 21000 Novi Sad, Serbia.

E-mail address: bikit@df.uns.ac.rs (I. Bikit).

be investigated in detail. Studies that measured adsorption of radon by zeolite have shown relatively good adsorbing properties of both, natural and synthetic zeolites (Mortazavi et al., 2009; Paschalides et al., 2010). However, their adsorption properties can vary greatly, due to the pore size distribution and composition of natural ores, as well as the degradation of adsorption characteristics over time due to sensitivity towards ionizing radiation in synthetic zeolites (Hedström et al., 2012). Few article reported data on the subject, although the ability of natural zeolites to adsorb radioisotopes is known; for example *Clinoptilolite* was used extensively in dealing with the effects of Chernobyl accident, while *Chabazite* has been used in the Three Mile Island clean-up (Dyer et al., 2000).

It should be also emphasized that removal of radon from indoor air by contacting the air with a silver-exchanged zeolite was patented (Patent US 7381244 B2).

2. Experiment

For radon adsorption measurements, we used highly porous natural zeolite material, produced by FiMö-Aquaristik GmbH, Germany. We used this material from original, hermetically closed fabric boxes, without its exposure to higher temperatures. Different granulations of this material are obtained by different times of milling (10, 20 and 40 min). Milling was performed in a planetary ball mill Fritsch Pulverisette 5. A hardened steel vial (250 cm³ volume) and hardened steel balls (10 mm in diameter) were used. The mass of the milled sample was 50 g, and the angular velocity of the supporting disc and vial were 400 and 800 rpm, respectively. Particle size distribution was determined using a Malvern Mastersizer 2000 particle size analyzer capable of analyzing particles between 0.01 and 2000 μm . This analyzer records the light pattern scattered from a field of particles at different angles. The device then uses an analytical procedure to determine the particle size

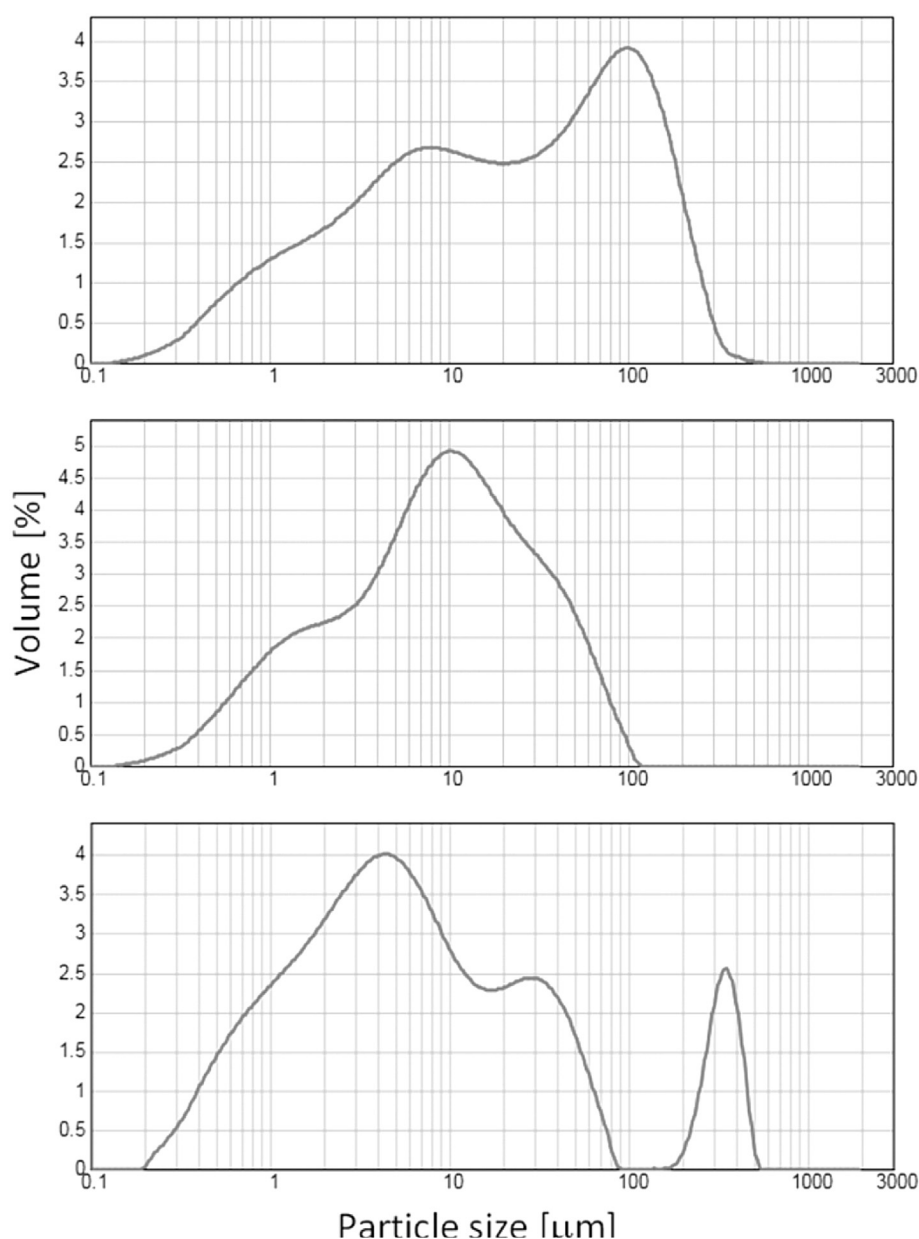


Fig. 1. Particle size distributions for different milling times (from top to bottom: 10 min, 20 min and 40 min).

distribution that created the patterns. The wavelengths of light used during measurement were 632.8 nm and 740 nm. The particle size distributions for different milling times are presented in Fig. 1.

The first measurement of radon adsorption was performed without milling of zeolite (i.e. with zeolite grain size 5–10 mm), and then pulverized samples were used. Only in the first measurement, together with zeolite sample, the activated charcoal canister was present. All the samples were placed in metal canisters that were opened during the exposure to radon within glass chamber and closed immediately after exposure to avoid changes in moisture content of the sample and, potentially more importantly, loss of adsorbed radon from the zeolite.

The experimental setup designed to test the radon adsorption by zeolite is presented in Fig. 2. Zeolite samples were exposed to radon concentrations of about 1400–1800 Bq/m³, during 48 h for each sample, by placing them inside a chamber with thick glass walls, whose volume is $5.4 \cdot 10^{-3}$ m³. The changes of radon concentration inside the chamber over time were continuously measured by alpha-spectrometer RAD7. Circulation of air at a rate of 0.5 l/min is provided thanks to the pump that is an integral component of the alpha-spectrometer, without mixing the air inside the chamber with the outside air. The air inside this closed system contained radon that emanated from the zirconium-oxide ($m = 0.9$ kg), containing Ra-226 radionuclide (4.10 ± 0.20 kBq/kg) which was placed at the chamber bottom. Humidity absorption was performed by passing the air through a column of calcium sulfate (CaSO₄). Each sample was also measured by low-level gamma spectrometry system before exposure to radon elevated concentrations and after exposure.

3. Results and discussion

The concentrations of radon depending on time inside the glass chamber, measured by alpha-spectrometer RAD7, during all exposures of zeolite samples to radon, are presented in Fig. 3. The detected decreases of radon concentrations after inserting the samples (zeolite + activated charcoal, or zeolite only) inside the glass chamber were not caused only due to radon adsorption, but also as a result of radon loss during the sample replacement. Our test by short opening of glass chamber showed that the estimated radon loss can reach up to 40%.

The results of gamma-spectrometry measurements, performed in order to precisely quantify the adsorption characteristics of various zeolite granulations, are presented in Table 1. Relative uncertainties of presented net intensities of 352 keV gamma ray line, associated with lead-214, a short-lived decay product associated with radon-222, expressed at 95% confidence level, are about 10%.

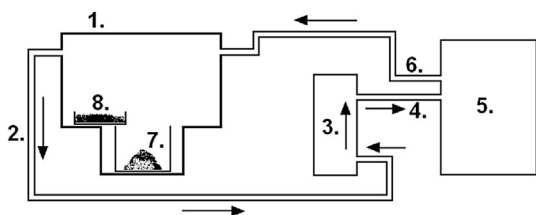


Fig. 2. The experimental setup designed to test the radon adsorption by zeolite 1. Chamber with thick glass walls, 2. Plastic tube, 3. Humidity absorber (CaSO₄), 4. Input plastic tube, 5. Alpha spectrometer (RAD7), 6. Output plastic tube, 7. Zirconium-oxide containing Ra-226, 8. Zeolite. The direction in which the air moves through the closed system is labeled by arrows. The temperature of air and relative humidity were measured by devices that are integral parts of RAD7 device. However, in this experimental setup the temperature of the air and its relative humidity were not adjustable parameters.

From results presented in Fig. 3 and Table 1 it is obvious that radon adsorption by zeolite samples is much less efficient than by activated charcoal. This fact does not necessarily represents a disadvantage, especially in the case of high radon concentrations (500–1500 Bq/m³) where zeolite can be used as an indicator of elevated indoor radon concentrations, which could be measured if zeolite adsorption coefficient is known. The granulation of zeolite samples doesn't significantly influence its radon adsorption characteristics. However, we found better adsorption by zeolite sample milled for 20 min, which can be attributed to the relatively uniform particle size distribution, with average value of 10 μm. In further investigations, the radon adsorption characteristics of zeolite for longer exposure times should be explored (in presented experiment, only one exposure interval of 48 h was used).

Although relatively simple, our experimental setup provided the possibility for estimation of adsorption coefficients of Rn-222 gas on activated charcoal, as well as on zeolite. This coefficient, k (m³/kg), characterizes the capacity that sorbent material has in adsorbing of radon, and can be determined in the following way (López and Canoba, 2002):

$$k = Q/C,$$

where Q is radon activity adsorbed by unit of mass of sorbent material (Bq/kg), and C is concentration of Rn-222 in air during exposure of sorbent material (Bq/m³). In our case the time interval of exposure to radon of activated charcoal and each zeolite sample was 48 h. The temperature of air inside the glass chamber was in interval (25–30) °C, while the relative humidity was about 7%.

Knowing the net intensity of 352 keV post-radon line for activated charcoal after exposure (Table 1), gamma emission probability for this line ($p_\gamma = 0.371$), and detection efficiency at this energy of our HPGe detector for cylindrical geometry of measured sample ($\epsilon = (30 \pm 3) \times 10^{-3}$), we found $Q = 153 \pm 23$ Bq/kg for activated charcoal. As can be seen from Fig. 3 (time interval 2–3), the radon concentration inside glass chamber dropped quickly (within 1 h) in the presence of activated charcoal, reaching the constant level of $C = 50 \pm 6$ Bq/m³ for next 48 h. From these values of Q and C , we found $k_{\text{activated charcoal}} = 3.1 \pm 0.6$ m³/kg. This is in a relatively good agreement with previously reported values for adsorption coefficient of radon on activated charcoal at room temperature ($2\text{--}6$ m³/kg, Cohen and Cohen, 1983; Ren and Lin, 1987; Scarpitta, 1995), although these reported values are related to higher relative humidity, which represent in a better way realistic indoor conditions.

Using similar procedure we found the corresponding value of $Q = 42 \pm 6$ Bq/kg for zeolite (40 min milling). However, the average radon concentration for 48 h exposure interval for this zeolite sample (time interval 6–7 in Fig. 3) was relatively high, $C = 1.10 \pm 0.09$ kBq/m³, giving the corresponding value of $k_{\text{zeolite (40 min milling)}} = 0.038 \pm 0.006$ m³/kg.

Based on values given in Table 1 and Fig. 3, the adsorption coefficients of zeolite samples with 20 min milling and 10 min milling are found to be 0.11 ± 0.021 m³/kg and 0.046 ± 0.009 m³/kg, respectively. The relative uncertainties of derived adsorption coefficients reach up to 20%.

The obtained values for adsorption coefficients of these zeolite samples with different granulations are 25–75 times lower than corresponding value of activated charcoal in our experiment. These values for zeolite samples are very similar to the adsorbing coefficients of radon previously reported for silica gel (0.022–0.065 m³/kg) for relatively broad temperature range 5–35 °C (Ackley, 1975).

The possible disadvantage of our experiment is the use of a radon chamber with a very small volume (only 5.4 L), while the

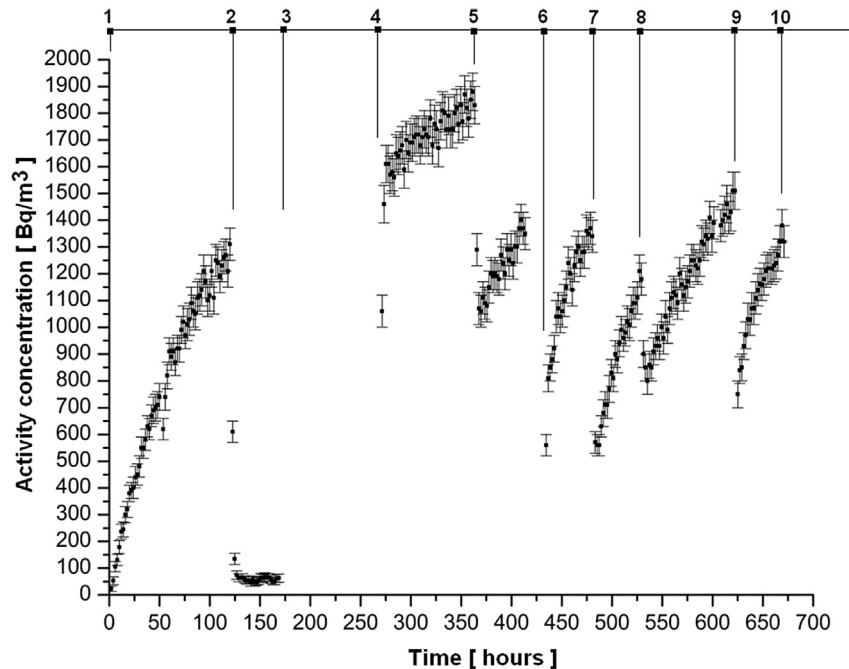


Fig. 3. Time dependence of radon concentration inside the glass chamber. Explanation for corresponding time intervals: 1–2 – only zirconium-oxide closed inside glass chamber; 2–3 – activated charcoal + zeolite, not milled (grain size 5–10 mm); 3–4 – without measurement (only zirconium-oxide closed inside glass chamber); 4–5 – only zirconium-oxide closed inside glass chamber; 5–6 – test of radon loss by short opening (5 s) of glass chamber; 6–7 – exposure of the finest zeolite fraction (40 min milling); 7–8 – exposure of zeolite fraction, 20 min milled; 8–9 – only zirconium-oxide closed inside glass chamber; 9–10 – exposure of zeolite fraction, 10 min milled. Error bars are presented for each single measurement.

Table 1

Gamma-spectrometry measurements of samples.

Sample	Intensity of post-radon 352 keV line before sample exposure to radon [c/(s kg)]	Intensity of post-radon 352 keV line after sample exposure to radon [c/(s kg)]	Net intensity of post-radon 352 keV line due to radon adsorption by sample [c/(s kg)]
Activated charcoal	–	1.87 ± 0.17	1.87 ± 0.17
Zeolite (not milled)	0.23 ± 0.02	0.78 ± 0.06	0.55 ± 0.06
Zeolite (40 min milling)	0.23 ± 0.02	0.70 ± 0.05	0.47 ± 0.05
Zeolite (20 min milling)	0.23 ± 0.02	1.18 ± 0.10	0.95 ± 0.10
Zeolite (10 min milling)	0.23 ± 0.02	0.75 ± 0.06	0.52 ± 0.06

equivalent air-volume of the activated charcoal canister (with a typical 70 g weight) is about 210 L (this directly follows from adsorption coefficient value of $\approx 3 \text{ m}^3/\text{kg}$, i.e. $0.07 \text{ kg} \times 3 \text{ m}^3/\text{kg} = 0.21 \text{ m}^3$). This is strikingly apparent from Fig. 3 at the interval 2–3, where Rn-222 concentration dropped at very low level when active charcoal of 75 g was present. In principle, the sample to be exposed in the radon chamber should not affect the radon concentration of the chamber. However, we did not possess strong enough Ra-226 source to produce high Rn-222 concentration within a big volume. Thus, we repeated measurement by activated charcoal sample, but with mass of only 5 g (15 times lower mass than in previous measurement) in order to obtain value for adsorption coefficient under new conditions and compare it with previous value of $\approx 3 \text{ m}^3/\text{kg}$. Even with this mass, the equivalent air-volume of the activated charcoal (15 L) is still higher than volume of our radon chamber, but we expected a smaller perturbation of radon concentration inside chamber. The use of activated

charcoal sample with mass below 1 g (equivalent air-volume 3 L) would, on the other hand, increase the measurement uncertainty of intensity of 352 keV gamma line, necessary for final determination of adsorption coefficient.

The exposure time for this small activated charcoal sample within radon chamber was 48 h and radon concentration inside chamber registered by RAD7 device is presented in Fig. 4.

As can be seen from Fig. 4, we could not avoid the decrease of radon concentration within radon chamber, although in this measurement we reached average concentration of $C_1 = 370 (15) \text{ Bq/m}^3$, which is about 7 times higher, than in first measurement with 75 g of activated charcoal. After exposure, using gamma spectrometry measurement, we found $Q_1 = 1.6 \pm 0.3 \text{ kBq/kg}$ for activated charcoal sample of 5 g mass. The obtained values C_1 and Q_1 imply the following value for adsorption coefficient of activated charcoal: $k = Q_1/C_1 = 4.3 \pm 0.8 \text{ m}^3/\text{kg}$. This is about 40% higher than our first result for adsorption coefficient of activated charcoal, but it

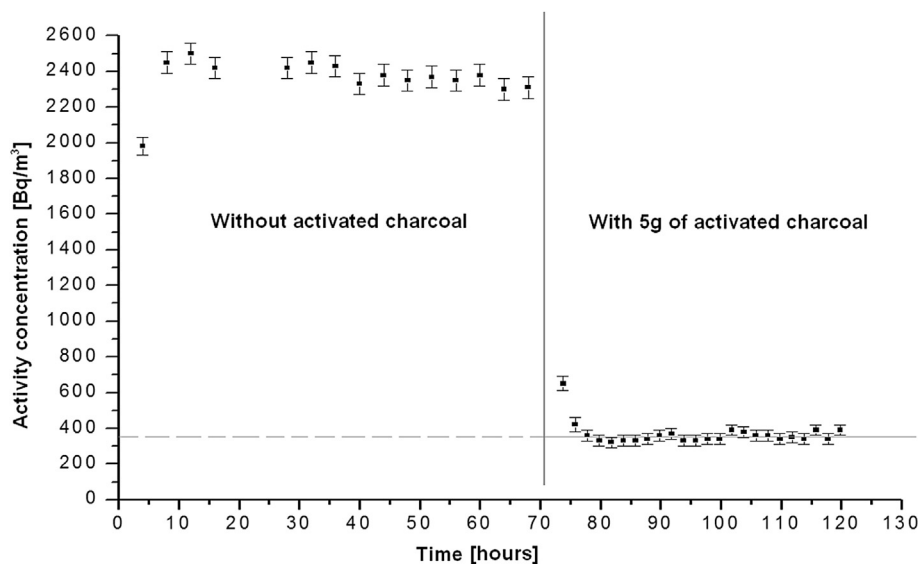


Fig. 4. Time dependence of radon concentration inside the glass chamber without activated charcoal, and with 5 g of activated charcoal sample inside the chamber.

shows relatively good consistency between obtained results for significantly different perturbations of initial radon concentration (both results are in agreement within measurement uncertainties). This further means that adsorption coefficients we obtained for natural zeolite samples are less influenced by radon perturbation effect inside radon chamber, since the magnitude of these perturbations were relatively small in comparison with perturbation caused by activated charcoal.

4. Conclusions

Our results suggest that zeolite, with some constrains, can be used both, to radon measurements (in the case of higher radon concentrations (Sextro, 1987; Ennemoser et al., 1993)) and radon suppression in the air of dwellings, especially having in mind inexpensiveness of the zeolite and its wide availability. However, the measurement of radon concentrations in the range 50–400 Bq/m³ based on radon adsorption on natural zeolite, probably could not be possible (we estimated that the lowest measurable radon concentration is about 500 Bq/m³). In addition, a huge amount of this material is required for reduction of indoor radon concentration, compared to activated charcoal.

For the optimal grain size of the zeolite sample (achieved by 20 min milling), the exposure of the zeolite to the average radon concentration of about 800 Bq/m³, during 48 h, resulted in an activity increase of the 352 keV post-radon line of about $1 \text{ c s}^{-1} \text{ kg}^{-1}$ (35% nominal efficiency HPGe). The adsorption coefficients that were obtained in our experiment for natural zeolite samples (0.038 m³/kg–0.11 m³/kg) are comparable with adsorbing coefficients for silica gel, but they are an order of magnitude lower than radon adsorbing coefficient for 5A synthetic zeolite (Paschalides et al., 2010), and in average about 50 times lower than corresponding value that we found for activated charcoal ($\approx 3 \text{ m}^3/\text{kg}$). The standardization of zeolite for routine Rn-222 measurements (similar as the EPA procedure (EPA 520/5-87-005, 1987) for activated charcoal) needs more detailed studies.

Acknowledgments

The authors acknowledge the financial support of the Provincial Secretariat for Science and Technological Development within the project Development and application low-background alpha, beta spectroscopy for investigating of radionuclides in the nature, and Ministry of Education and Science of Serbia, within the projects Nuclear Methods Investigations of Rare Processes and Cosmic Rays No.171002 and Biosensing Technologies and Global System for Continuous Research and Integrated Management of ecosystems No.43002.

References

- Ackley, R.D., 1975. Removal of Radon-220 from HTGR Fuel Reprocessing and Refabrication Off-Gas Streams by Adsorption (Based on a Literature Survey). Oak Ridge National Laboratory Libraries, p. 15. ORNL-TM-4883.
- Baerlocher, Christian, McCusker, Lynne B., Olson, David H., 2007. Atlas of Zeolite Framework Types, sixth revised ed., ISBN 978-0-444-53064-6
- Cohen, B.L., Cohen, E.S., 1983. Theory and practice of radon monitoring with charcoal adsorption. *Health Phys.* 45, 501–508.
- Dyer, A., Las, T., Zubair, M., 2000. The use of natural zeolites for radioactive waste treatment: studies on leaching from zeolite/cement composites. *J. Radioanal. Nucl. Chem.* 243 (3), 839–841.
- Ennemoser, O., et al., 1993. Unusually high indoor radon concentrations. *Atmos. Environ.* 27A (14), 2169–2172.
- EPA 520/5-87-005, 1987. EERF Standard Operating Procedures for Rn-222 Measurement Using Charcoal Canisters.
- Hedström, H., Foreman, M., Ekberg, C., Ramebäck, H., 2012. Radon capture with silver exchanged zeolites. *Radiochim. Acta* 100 (6), 395–399.
- López, F.O., Canoba, A.C., 2002. ²²²Rn gas diffusion and determination of its adsorption coefficient on activated charcoal. *J. Radioanal. Nucl. Chem.* 252 (3), 515–521.
- Mortazavi, S.M.J., Mehdizadeh, S., Zehtabian, M., Sina, S., 2009. Development of an economical radon-resistant construction technique that is applicable in national radon-reduction programmes. *Int. J. Low Radiat.* 6 (2), 113–118.
- Paschalides, J.S., Marinakis, G.S., Petropoulos, N.P., 2010. Passive, integrated measurement of radon using 5A synthetic zeolite and blue silica gel. *Appl. Radiat. Isot.* 68 (1), 155–163.
- Ren, T., Lin, L., 1987. A passive integrating indoor radon detector with activated carbon. *Radiat. Prot. Dosim.* 19, 121–124.
- Scarpitta, S.C., 1995. A theoretical model for ²²²Rn adsorption on activated charcoal canisters in humid air based on Polanyi's potential theory. *Health Phys.* 68, 332–339.
- Sextro, R.G., 1987. Understanding the origin of radon indoors - building a predictive capability. *Atmos. Environ.* 21 (2), 431–438.

See discussions, stats, and author profiles for this publication at: <https://www.researchgate.net/publication/323577872>

Determination of the nuclear level densities and radiative strength function for 43 nuclei in the mass interval $28 \leq A \leq 200$

Article in The European Physical Journal Conferences · January 2018

DOI: 10.1051/epjconf/201816900007

CITATIONS

0

READS

31

11 authors, including:



David Knežević

University of Novi Sad

9 PUBLICATIONS 4 CITATIONS

[SEE PROFILE](#)



Nikola Jovancevic

University of Novi Sad

38 PUBLICATIONS 85 CITATIONS

[SEE PROFILE](#)



Marija Krmar

Institut Gosa

12 PUBLICATIONS 88 CITATIONS

[SEE PROFILE](#)



Franz-Josef Hamsch

European Commission

448 PUBLICATIONS 2,712 CITATIONS

[SEE PROFILE](#)

Some of the authors of this publication are also working on these related projects:



Younger Dryas Impact Hypothesis [View project](#)



International Standard Neutron Cross Section Evaluation [View project](#)

Determination of the nuclear level densities and radiative strength function for 43 nuclei in the mass interval $28 \leq A \leq 200$

David Knezevic^{1,5}, Nikola Jovancevic^{1,*}, Anatoly M. Sukhovo², Ludmila V. Mitsyna², Miodrag Krmar¹, Vu D. Cong², Franz-Josef Hamsch⁴, Stephan Oberstedt⁴, Zsolt Revay³, Christian Stieghorst³, and Aleksandar Dragic⁵

¹University of Novi Sad, Faculty of Science, Department of Physics, Trg Dositeja Obradovica 3, 21000 Novi Sad, Serbia

²Joint Institute for Nuclear Research, 141980 Moscow region, Dubna, Russia

³Technische Universität München, Forschungsneutronenquelle Heinz Maier-Leibnitz (FRM II), Lichtenbergstr. 1, 85747 Garching, Germany

⁴European Commission, Joint Research Centre, Directorate G – Nuclear Safety and Security, Unit G.2, Retieseweg 111, 2440 Geel, Belgium

⁵Institute of Physics Belgrade, Pregrevica 118, 11080 Zemun, Serbia

Abstract. The determination of nuclear level densities and radiative strength functions is one of the most important tasks in low-energy nuclear physics. Accurate experimental values of these parameters are critical for the study of the fundamental properties of nuclear structure. The step-like structure in the dependence of the level densities ρ on the excitation energy of nuclei E_{ex} is observed in the two-step gamma cascade measurements for nuclei in the $28 \leq A \leq 200$ mass region. This characteristic structure can be explained only if a co-existence of quasi-particles and phonons, as well as their interaction in a nucleus, are taken into account in the process of gamma-decay. Here we present a new improvement to the Dubna practical model for the determination of nuclear level densities and radiative strength functions. The new practical model guarantees a good description of the available intensities of the two step gamma cascades, comparable to the experimental data accuracy.

1 Introduction

The development of theoretical models of nuclear structures requires a set of experimental information of the excited levels density, ρ , (with given quantum numbers) and of the values of the partial width (radiative strength function), Γ , of all possible decay channels. Correct interpretation of the dynamics of the nuclear transitions, in a broad variety from the simple low-lying levels (e.g., quasi-particle or phonon structure) to the very complex compound-states is possible by the theoretical calculations if those experimental data are available. One of the most suitable techniques for determination of required nuclear mater parameters (ρ and Γ) is the two-step gamma cascades methods based on measurement of gamma coincidences following neutron capture [1].

*e-mail: nikola.jovancevic@df.uns.ac.rs

Based on the experimental data collected by two-step gamma cascades experiment a model for description the gamma-decay of neutron resonance was developed at JINR, Dubna [2, 3]. In this model the level density ρ of quasi-particles in any nucleus is defined using the known model of n -quasi-particle levels. Here we presented the improved version of this model taking into account shell inhomogeneities of the single-particle level spectra and their influence on the functions: $\rho = \varphi(E_{ex})$ and $\Gamma = \psi(E_1)$, where E_{ex} is the excitation energy and E_1 is primary transition energy. The experimental results of two step gamma cascades intensity for 43 nuclei in the $28 \leq A \leq 200$ mass region were fitting by this model. This provide us possibility to extract parameters of nuclear structure such as breaking thresholds of the second and the third Cooper pairs, ratio of the collective level density to the total one or level parity.

2 Dubna two-step gamma cascades method

The two-step gamma-cascades method for obtaining information about the nuclear structure parameters following the thermal neutron captures was developed at FLNP, JINR, DUBNA [2, 3]. From amount of gamma-gamma coincidences the method allows to choose registration events of full energy of two-gamma transition cascade with a sufficiently low background. And the experimental intensity distributions of cascades to the final levels of compound-nucleus with excited energy below ~ 500 – 800 keV are obtained from these coincidences. Using the nuclear spectroscopy procedures allows decomposing the initial spectrum on primary and secondary transmission components of cascades with an acceptable uncertainty [2, 3].

The basic idea of this method comes from specific dependence of the two-step gamma- cascade intensity on the partial radiative width Γ and the density of excited levels:

$$I_{\gamma\gamma} = \sum_{\lambda,f} \sum_i \frac{\Gamma_{\lambda i}}{\Gamma_{\lambda}} \frac{\Gamma_{if}}{\Gamma_i} = \sum_{\lambda,f} \frac{\Gamma_{\lambda i}}{\langle \Gamma_{\lambda i} \rangle m_{\lambda i}} n_{\lambda i} \frac{\Gamma_{if}}{\langle \Gamma_{if} \rangle m_{if}} \quad (1)$$

where $\Gamma_{\lambda i}$ and Γ_{if} are the partial radiative widths corresponding to the primary and to the secondary transitions; $n_{\lambda i} = \rho \Delta E_i$ is the number of the excited intermediate levels in a certain interval of the excitation energy ΔE_i ; $\langle \Gamma_{\lambda i} \rangle$ and $\langle \Gamma_{if} \rangle$ are the average values of the corresponding intervals of the nucleus excitation energy widths; $m_{\lambda i}$ and m_{if} are the number of levels in the same intervals. When this method was developed for the first time it was based on an interactive calculation. Using iterative process with “randomly” chosen functions ρ and Γ , it is possible to obtain the most probable values of level density and radiative width (or radiative strength function).

3 Model of the gamma-decay of neutron resonance

Here we present improved version of the model for the gamma-decay of neutron resonance [2] which can explain the experimental data based on combination of phenomenological and theoretical representations.

The level density, described by an expression for density ρ_l of Fermi levels, was taken from the model of density Ω_n of n -quasi-particle states [4]:

$$\rho_l = \frac{(2J+1) \exp\left(-\left(J+1/2\right)^2 / 2\sigma^2\right)}{2 \sqrt{2\pi} \sigma^3} \cdot \Omega_n(E_{ex}), \Omega_n(E_{ex}) = \frac{g^n (E_{ex} - U_l)^{n-1}}{((n/2)!)^2 (n-1)!} \quad (2)$$

Here J is the spin quantum number, $g = 6a/\pi^2$ is the density of the single-particle states near Fermi-surface, σ is the cut-off factor (a and σ values were taken from the back-shifted Fermi-gas model

[5]), and U_l , is the energy of the l -th Cooper pair breaking threshold. The effect of the collective enhancement was also included in this model by the coefficient C_{col} of the collective enhancement of the vibrational level density (or both vibrational and rotational ones for deformed nuclei). For a given excitation energy, E_{ex} , the phenomenological coefficient is determined by a theoretical description that can be found in Ref. [3]:

$$C_{coll} = A_l \exp(\sqrt{(E_{ex} - U_l)/E_v} - (E_{ex} - U_l)/E_\mu) + \beta \quad (3)$$

where A_l are parameters of density for the vibrational levels above the breaking point for each l -th Cooper pair, E_μ and E_v determine the change in the nuclear entropy and the change of the quasi-particles excitation energies, respectively. Coefficients A_l for different pairs are fitted independently, as it was done in Ref. [2]. Coefficient β is used for a description of the rotation level density.

Radiative strength functions for $E1$ - and $M1$ -transitions are determined in this model by Ref. [6]:

$$k(E1, E_\gamma) + k(M1, E_\gamma) = w \frac{1}{3\pi^2 \hbar^2 c^2 A^{2/3}} \frac{\sigma_G \Gamma_G^2 (E_\gamma^2 + \kappa 4\pi^2 T^2)}{(E_\gamma^2 - E_G^2)^2 + E_\gamma^2 \Gamma_G^2} + P\delta^- \exp(\alpha_p(E_\gamma - E_p)) + P\delta^+ \exp(\beta_p(E_p - E_\gamma)) \quad (4)$$

with fitting normalization parameter w and coefficient κ ; thermodynamic temperature T ; the location of the center of the giant dipole resonance E_G , with width Γ_G and cross section σ_G in the maximum for each nucleus. For description of experimental data of Ref. [3] it is necessary to add one or several narrow peaks to the strength function is based on the data of Ref. [3]. The second summand of Eq. (5) corresponds to the left slope of the peak (energies below the maximum), and the third summand is the right slope (energies above the maximum). Position E_p in the energy scale, amplitudes $P\delta^+$ and $P\delta^-$ and slope parameters α_p and β_p are fitted for each peak independently. At $E_1 \approx B_n$ the fitted ratios Γ_{M1}/Γ_{E1} of $E1$ - and $M1$ -strength functions are normalized to known experimental values, and their sum Γ_λ is normalized to the total radiation width of the resonance.

The influence of the shell correction δE on the density of the quasi-particle levels were tested in this work. It was done by using the $a(A)$ value, which depends on the excitation energy, included linearly in the parameter of the single-particle density g (see Eq. (2)). For a nucleus with mass A and excitation energy E_{ex} , $a(A)$ is expressed, as [3]:

$$a(A) = \tilde{a}(1 + ((1 - \exp(\gamma E_{ex}))\delta E/E_{ex})) \quad (5)$$

where asymptotic value is $\tilde{a} = 0.114 \cdot A + 0.162 \cdot A^{2/3}$ and $\gamma = 0.054$. The δE values slightly varied relative to their evaluations [3] in order to keep an average spacing between neutron resonances (see [2]).

In our model the set of common parameters for fitting (see Eqs. (2, 3)) were:

- 1) the break up thresholds energies U_l up to $l=4$,
- 2) the E_μ and E_v parameters, which are common for all Cooper pairs
- 3) the mutually independent parameters A_l of the density of vibrational levels above the break up threshold U_l
- 4) the coefficients w , κ and β
- 5) the ratio r of negative parity and the total level density.

Those parameters were used for the description of the intensity $I_{\gamma\gamma}(E_1)$ for 43 nuclei, in the framework of the proposed model.

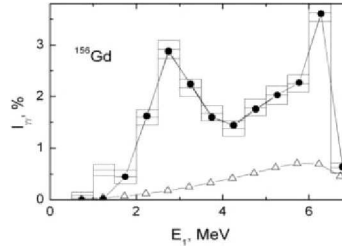


Figure 1. Histogram - experimental cascade intensity and its uncertainties for ^{156}Gd as function of primary cascade quanta E_1 . Points - the best fit of the presented practical model; triangles - a calculation of $I_{\gamma\gamma}$ using models of Ref. [5, 6]. Recorded threshold for cascade gammas is $E_\gamma = 520$ keV.

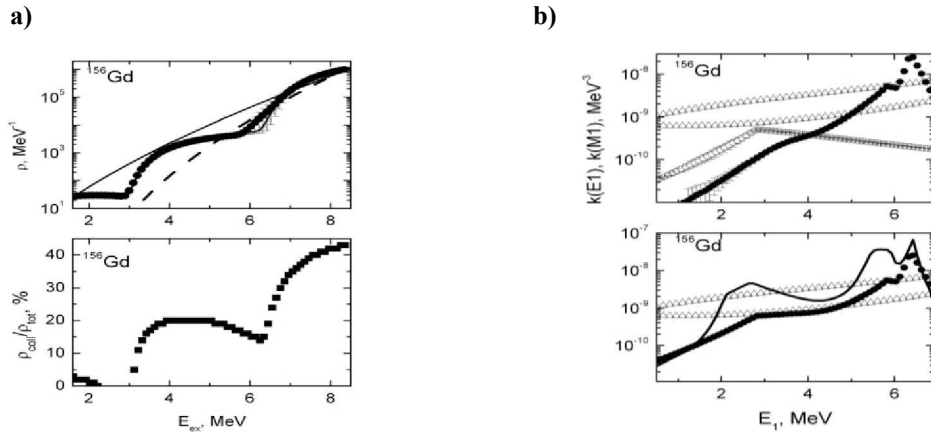


Figure 2. a) Level density of ^{156}Gd . *Top*: points are the best fit of level density (uncertainties – scatter of fits for different sets of initial parameters); dashed and solid lines are the level density calculated using the model of Ref. [5], with taking into account the shell correction δE (6) and without δE , correspondingly. *Bottom*: fitted ratio of density of collective levels to the total level density. **b)** Strength function for ^{156}Gd . *Top*: solid points are the best fit of the strength function of $E1$ -transitions; open points are the best fit of the strength function of $M1$ -transitions. *Bottom*: solid points are a sum of $E1$ - and $M1$ - strength functions; dash line is the sum of strength functions multiplied by $\rho_{\text{mod}}/\rho_{\text{exp}}$ ratio (Ref. [7]). Calculations using the model of Ref. [6] (lower triangles) and using the model of Ref. [8] (upper triangles) were fulfilled with $k(M1) = \text{const}$.

4 Results and discussion

A solution of the system of Eq. (1) is performed by the Monte-Carlo method. The nonlinearity of the strongly correlated equations of the system (1) produces an uncertainty of extracting the ρ and Γ parameters from $I_{\gamma\gamma}$ intensities.

Experimental data on $I_{\gamma\gamma}(E_1)$ are usually obtained with a small total uncertainty and averaged over 500 keV energy intervals. The results for ^{156}Gd are shown, in more detail, in Figs. 1–2. The best fits to $I_{\gamma\gamma}(E_1)$, as well as the fitted level densities and strength functions, are compared to corresponding values calculated using the statistical model. The results and corresponding calculations of level density and radiative strength function for the rest of the investigated nuclei will not be shown in

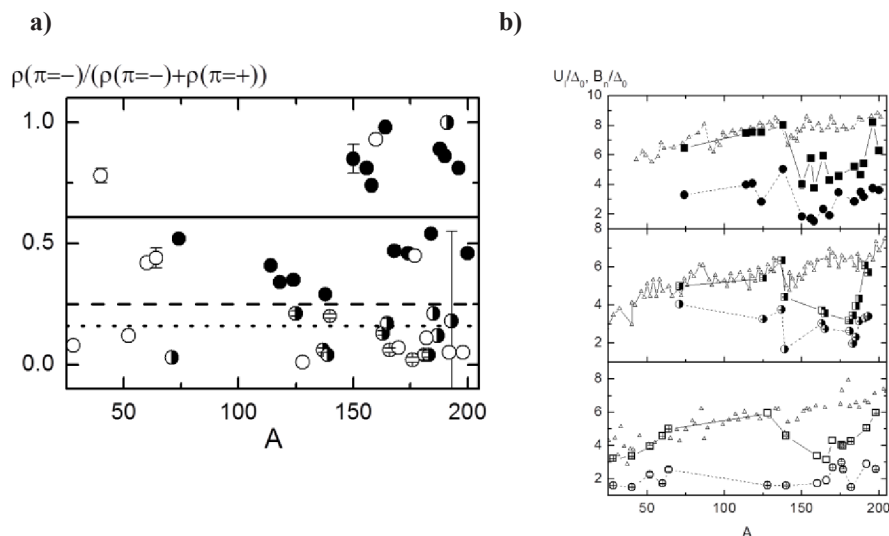


Figure 3. **a)** A-dependence of the ratios U_l/Δ_0 , for the second (points) and the third (squares) Cooper pairs. Full points – even-even, half-open points are even-odd and open points are odd-odd compound nuclei. Triangles – the mass dependence of B_n/Δ_0 ratio. **b)** Mass dependence of the ratio of the level density with negative parity to the total level density at the upper energy border of the E_d and their averages for even-even nuclei (solid lines), even-odd (dashed lines) and odd-odd nuclei (dotted lines). Full points – even-even, half-open points – even-odd and open points – odd-odd compound nuclei.

this publication. However, we are presented here obtained results for some of parameters of nuclear structure.

One important parameter is the breaking thresholds for Cooper pairs. In the present analysis was confirmed the previous results about the connection between the shape of the investigated nucleus and the breaking thresholds. That was established for the first time in our prior analysis [3]. As the breaking thresholds differ for nuclei with various nucleon parities and depend on the average pairing energy (Δ_0) of the last nucleon, the mass dependencies for the ratios of the break up thresholds of the second and the third Cooper pairs to Δ_0 , as well as the mass dependence of the binding energy to Δ_0 , are presented in Fig. 3. As it can be seen in Fig. 3, there is a noticeable difference in U_2/Δ_0 and U_3/Δ_0 ratios for spherical and deformed nuclei in contrast to B_n/Δ_0 .

In this work it was also obtained information about levels parity. For determination of the part $r = \rho(\pi-)/(\rho(\pi-) + \rho(\pi+))$ of levels $\rho(\pi-)$ with negative parity, a linear extrapolation for r value was applied in the $E_d \leq E_{ex} \leq B_n$ energy interval. At that, in the B_n point we use generally accepted assumption, that $\rho(\pi-) = 0.5(\rho(\pi-) + \rho(\pi+))$, and $\rho(\pi-)$ value in this energy point was fixed, and at the E_d energy the $\rho(\pi-)$ value varied.

The calculated ratios of density of the levels with negative parity to the total level density are shown in Fig. 3. The averages of these ratios are 0.61(22), 0.25(28) and 0.16(16) for even-even, even-odd and odd-odd nuclei, respectively (and for odd-even ^{177}Lu it is 0.65(1)). Hence, the behavior of the gamma-decay process is different for nuclei of various nucleon parities.

5 Conclusion

In this work we presented new variant of model for gamma decay of neutron resonance, taking into account shell inhomogeneities of the single-particle level spectra. We used this model for fitting the experimental intensity of two-step gamma cascades and to obtain information about parameters of nuclear structure.

The data on Cooper pair break-up energies, obtained with a high accuracy, are sufficient to conclude that the dynamics of interaction between superfluid and normal phases of a nucleus depends on its' shape. Our model allows for a separate determination of the density of vibrational levels between the breaking thresholds of the Cooper pairs.

Unfortunately, an existence of the sources of uncertainties of the sought ρ and Γ functions is a fundamental problem, and it is inevitable for any nuclear model used for experimental data analysis and for predictions of the spectra and cross sections. There are also fluctuations of the intensities of gamma-transitions in different nuclei, which has a contribution to the systematical error. Nevertheless, the practical model showed one possibility to describe the data of the two-step experiments with the accuracy that exceeds the statistical one.

For future development of reliable model of cascade gamma decay new experimental data are necessary. Because of that, ^{108}Ag , ^{110}Ag , ^{104}Rh and ^{56}Mn nuclei will be investigated by two step gamma cascade method.

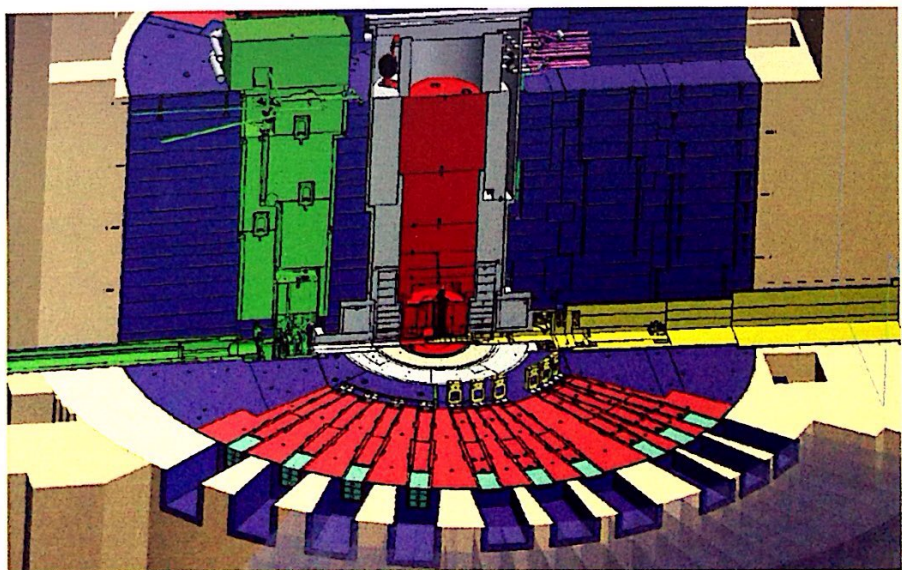
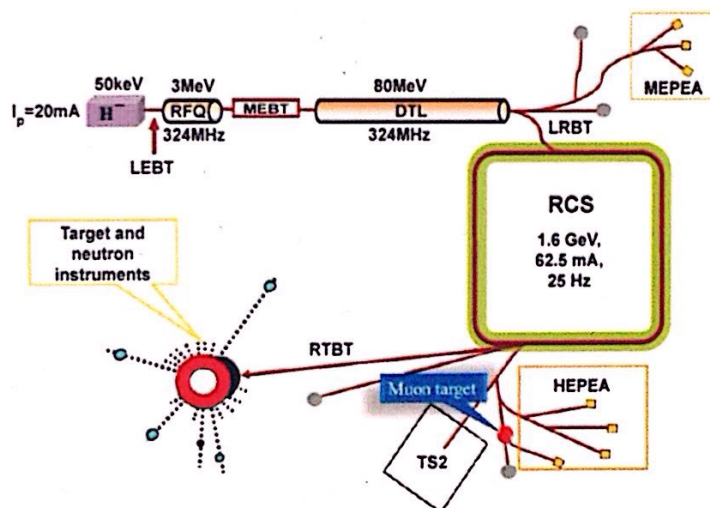
References

- [1] V.G. Soloviev, Nuclear Physics A **586**(2), 265 (1995)
- [2] A.M. Sukhovoj, Phys. Atom. Nucl. **78**, 230 (2015)
- [3] A.M. Sukhovoj, L.V. Mitsyna, N. Jovancevic, Phys. Atom. Nucl. **79**, 313 (2016)
- [4] V.M. Strutinsky, in Proceedings of the International Congress on Nuclear Physics, Paris, France, p. 617 (1958)
- [5] W. Dilg, W. Schantl, H. Vonach, and M. Uhl, Nucl. Phys. A **217**, 269 (1973)
- [6] S.G. Kadenskij, V.P. Markushev and W.I. Furman, Sov. J. Nucl. Phys. **37**, 165 (1983)
- [7] N. Jovancevic, A.M. Sukhovoj, W.I. Furman, and V.A. Khitrov, in Proceedings of XX ISINN, Preprint E3-2013-22, p. 157 (Dubna, 2013); <http://isinn.jinr.ru/past-isinns.html>
- [8] P. Axel, Phys. Rev. **126**, 671 (1962)

ISINN-24

Neutron Spectroscopy,
Nuclear Structure,
Related Topics

Chinese Spallation Neutron Source



Dubna 2017

Joint Institute for Nuclear Research

**FUNDAMENTAL
INTERACTIONS & NEUTRONS,
NUCLEAR STRUCTURE,
ULTRACOLD NEUTRONS,
RELATED TOPICS**

*XXIV International Seminar
on Interaction of Neutrons with Nuclei*

Dubna, Russia, May 24–27, 2016

Proceedings of the Seminar

Dubna • 2017

УДК 539.125.5(042)
ББК 22.383.2я431+22.383.5я431+22.383.25я431
F97

Organizing Committee

W. I. Furman (*co-chairman*), V. N. Shvetsov (*co-chairman*),
E. V. Lychagin (*scientific secretary*), Yu. N. Kopatch,
P. V. Sedyshev, L. V. Mitsyna, M. V. Frontasyeva

Secretariat: T. S. Donskova (*seminar co-ordinator*),
N. A. Malysheva, T. L. Pikelner

The contributions are reproduced directly from the originals presented
by the Organizing Committee.

Fundamental Interactions & Neutrons, Nuclear Structure, Ultracold Neutrons, Related
F97 Topics: Proceedings of the XXIV International Seminar on Interaction of Neutrons with
Nuclei (Dubna, Russia, May 24–27, 2016). — Dubna: JINR, 2017. — 442 p.
ISBN 978-5-9530-0465-7

This collection of papers reflects the present state of neutron-aided investigations of the properties of the nucleus, including fundamental symmetries, properties of the neutron itself, neutron-excited reactions, and the parameters of the nucleus that determine the reaction cross section, as well as the latest theoretical development of all these problems. The works on experimental investigations in the physics of fission by neutrons of various energies are presented in great detail. The current state of experiments on the physics of ultracold neutrons and facilities to obtain them is described at length. The status achieved by now of the latest (from the viewpoint of technique) experiments and environment studies is covered as well.

Фундаментальные взаимодействия и нейтроны, структура ядра, ультрахолодные нейтроны, связанные темы: Труды XXIV Международного семинара по взаимодействию нейтронов с ядрами (Дубна, Россия, 24–27 мая 2016 г.). — Дубна: ОИЯИ, 2017. — 442 с.

ISBN 978-5-9530-0465-7

В сборнике представлено современное состояние исследований свойств ядра с помощью нейтронов: фундаментальных симметрий и свойств самого нейтрона, возбуждаемых им реакций и параметров ядра, определяющих их сечения, а также последние теоретические разработки всех этих вопросов. Очень детально представлены работы по всем аспектам, связанным с экспериментальными исследованиями физики деления ядра нейтронами различных энергий. Достаточно полно описано современное состояние экспериментов по физике ультрахолодных нейтронов и установок для их получения, а также достигнутый к настоящему времени статус методически новейших экспериментов и результаты экологических исследований.

УДК 539.125.5(042)
ББК 22.383.2я431+22.383.5я431+22.383.25я431

ISBN 978-5-9530-0465-7

© Joint Institute for Nuclear
Research, 2017

Nuclear Structure, Nuclear Data

Determination of Group Neutron Cross-Sections and Their Integral Characteristics for Minor Actinides by GRUCON Code Based on Estimated Data of ENDFB, JENDL, JEFF, BNAB

Grigoriev Yu.V., Koptelov E.A., Libanova O.N., Mezentsseva Zh.V.,
Novikov-Borodin A.V., Sinitsa V.V.77

Tuning Effect in Nuclear and Neutron Resonance Data

Sukhoruchkin S.I., Soroko Z.N., Sukhoruchkin D.S.86

New Method of Spacing Analysis of All Nuclei

Sukhoruchkin S.I., Sukhoruchkin D.S.98

New Nuclear Binding Energies and Their Analysis

Sukhoruchkin S.I., Sukhoruchkin D.S.110

Verification of the Practical Model of Cascade Gamma-Decay ✓

Sukhovoj A.M., Mitsyna L.V., Zeinalov Sh., Vu D.C., Jovancevic N., Knezevic D.,
Krmr M., Dragic A.122

Representation of the Radiative Strength Functions in the Practical Model of Cascade Gamma-Decay ✓

Vu D.C., Sukhovoj A.M., Mitsyna L.V., Zeinalov Sh., Jovancevic N., Knezevic D.,
Krmr M., Dragic A.134

Reactions with Fast Neutrons

Prompt-Gamma Neutron Activation Analysis in Mining

Hramco C., Grozdanov D.N., Aliyev F.A., Kopatch Yu.N., Gundorin N.A.,
Bystritsky V.M., Borzakov S.B., Ruskov I.N., Skoy V.R.157

Alpha-Cluster Formation Factor in (n, α) Reaction Cross Sections

Khuukhenkhuu G., Munkhsaikhan J., Odsuren M., Galsandamdin G.,
Gledenov Yu.M., Sansarbayar E., and Sedysheva M.V.166

Measurement of the Energy Distributions of Neutrons from $^7\text{Li}(d,n)^8\text{Be}$ Reaction at Deuteron Energy 2.9 MeV by Activation Method

Mitrofanov K.V., Piksaikin V.M., Zolotarev K.I., Egorov A.S.,
Gremyachkin D.E.175

Verification of the Practical Model of Cascade Gamma-Decay

Sukhovej A.M.¹, Mitsyna L.V.¹, Zeinalov Sh.¹, Vu D.C.^{1,2},
Jovancevic N.³, Knezevic D.³, Krmar M.³, Dragic A.⁴

¹*Joint Institute for Nuclear Research, Dubna, 141980, Russia*

²*Vietnam Academy of Science and Technology Institute of Physics, Hanoi, Vietnam*

³*University of Novi Sad, Faculty of Science, Department of Physics, Novi Sad, Serbia*

⁴*Institute of Physics, Belgrade, Serbia*

Abstract

To determine simultaneously both the level density ρ and the partial widths Γ of nuclear reaction products is possible only by fitting the intensities of the cascades between fixed initial, any intermediate and some final levels. Experimental total gamma-spectra with their calculations by the practical model of the gamma-decay were compared. Verification of ρ and Γ values obtained earlier and evaluation of the achieved accuracy of the practical model were done. Determined using the practical model ρ and Γ systematic uncertainties led to a conclusion that the calculated accuracy of spectra of products from any nuclear reaction will be several percents.

Introduction

An adequate and correct mathematical model of nucleus is need for understanding and subsequent prediction of the nuclear-physical parameters for any nuclei. The basis of this model is experimental determination of both the excited level density ρ and the widths Γ of partial processes of excitation and decay of any given level. In the case if the space D_λ between excited levels is less than detector resolution FWHM only an average of ρ and Γ parameters may be determined.

Excitation energy E_{ex} determines unambiguously and simultaneously both the level density and the strength functions $k = \Gamma / (A^{2/3} \cdot E_\gamma^3 \cdot D_\lambda)$ for any nucleus with A mass number and energy E_γ for emitted gamma-rays below neutron binding energy B_n . It means that level density and partial radiative widths (or corresponding strength functions k) must be determined simultaneously from the system of equations, which connects experimental data with the sought parameters of $\rho = f(q_1, q_2, \dots)$ and $k = \phi(p_1, p_2, \dots)$ functional dependencies.

With regard to ordinary spectra of emission of reaction products and reaction cross sections at any energy E_{ex} they are determined by the ρ and Γ product normalized on a constant. As a strong correlation of ρ and Γ is inevitable in this case, the simultaneous determination of these values is impossible without using any subjective assumptions or untested hypothesis. Correspondingly, calculation of cross sections of nucleon reactions gives an addition to an uncertainty connected with errors of emission widths for nucleon products.

All experimental information about nuclear structure is determined only by shapes of ρ and Γ dependencies on energy. And low count of ρ and Γ absolute values measured in several energy points is not enough to understand all nucleus properties. Measuring the intensities of any two-step cascades between compound-state and some group of the low-lying nuclear levels allows to determine shapes both of level density dependence on the excitation energy

and of average dependence of decay widths of intermediate levels on energy of emitted products at the compound-state decay. Now it was done in Dubna for 43 nuclei in the mass region $28 \leq A \leq 200$ for a measured part of intensities of primary gamma-transitions of two-step cascades [1, 2].

Experimental data on Fermi- and Bose-system interaction

Experimental research of the dynamics of interaction of Fermi- and Bose-states of nuclear matter allows to obtain a new fundamentally information about this nuclear process, so properties of nucleus and of macro systems (as objects for this process investigation) differ in principle. For example, to date in Dubna the unique information is obtained [3, 4] about possible dependency of breaking thresholds of some Cooper pairs of nucleons on the nuclear shape, what is presented in Fig. 1. It is found that the region of deformed nuclei at $A > 150$ the second and the third breaking pairs thresholds are smaller than these thresholds for spherical nuclei. To observe something like that in a superconducting macro system of electron gas is impossible, at least, in the absence of a technique of production of special nanosystem contained combinations of linear nano objects (type of conductor/inculator).

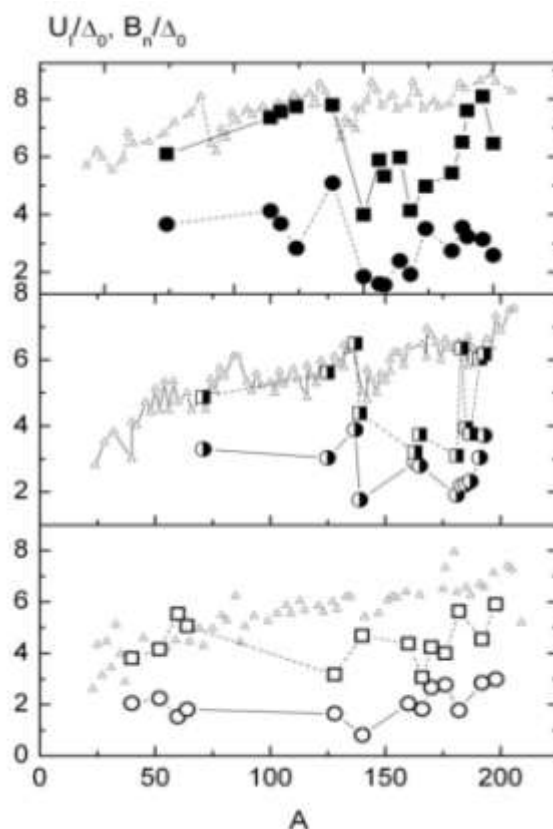


Fig.1. Mass dependencies of ratios of breaking thresholds U_i for the second (points) and the third (squares) Cooper pairs to the approximated average pairing energy Δ_0 for even-even compound nuclei (upper part), for even-odd nuclei (in the middle) and for odd-odd compound nuclei (bottom part). Triangles are known mass dependencies of B_n/Δ_0 .

The intensities $I_{\gamma\gamma}(E_1)$ of two-step cascades between neutron resonance (or another compound-state) λ and some group of low-lying nuclear levels f through any intermediate levels i for a fixed energy E_1 of primary transition are written by a system of equations of type:

$$I_{\gamma\gamma}(E_1) = \sum_{\lambda,f} \sum_i \frac{\Gamma_{\lambda i}}{\Gamma_{\lambda}} \frac{\Gamma_{if}}{\Gamma_i} = \sum_{\lambda,f} \frac{\Gamma_{\lambda i}}{\langle \Gamma_{\lambda i} \rangle m_{\lambda i}} n_{\lambda i} \frac{\Gamma_{if}}{\langle \Gamma_{if} \rangle m_{if}}, \quad (1)$$

where $m_{\lambda i}$ is a number of levels of excited primary gamma-transitions in intervals from the energy of initial level λ to an energy of intermediate level i , m_{if} is a number of levels of excited secondary transitions in intervals from the energy of intermediate level i to energy of the final level f , $n_{\lambda i}$ is a number of intermediate cascade levels in a set of small energy intervals. From the system (1), which connects an unknown level number n (or m) and unknown partial widths, a set of p and q parameters of the model functions $\rho=f(p_1, p_2, \dots)$ and $\Gamma=\phi(q_1, q_2, \dots)$ with some uncertainty is determined.

The experimental spectrum of the two-step cascade intensity is a sum of infinite set of possible pairs of mirror-symmetrical distributions. Ignoring this circumstance [5, 6] distorts entirely a picture of investigated process [7, 8]. Actually, using nuclear-spectroscopy methods the experimental spectra of cascades between initial and finite levels may be factorized on two mirror-symmetrical distributions as functions of energy of primary and secondary quanta of the cascades [9] with an acceptable systematic error. In a case of approximation of pure experimental spectra [5, 6] (without an execution of above-mentioned procedure) a likelihood function values can't give a reliable result for desired ρ and Γ values.

A necessary condition for determination of reliable ρ and Γ functions is an existence of the experimental data on branching coefficients of partial radiative widths of decay of all possible levels i onto limited group of final low-lying levels. In other words, the experiment is needed for recording all possible cascades connected known initial level λ of the nucleus and finite level f through any intermediate levels i . The required result can be obtained only if to take into account Boson part of nuclear excitations and theoretical (or phenomenological) assumptions of ρ and Γ functions for describing the intensity distributions of all primary quanta of cascades and branching coefficients $B_r(E_2)$ for any secondary quanta. There is a nonrecoverable systematic error of nuclear parameters determined such a way. This error causes are experimental systematic errors and mismatch of models for ρ and Γ to their obtained distributions.

We used the model [10] with varied weight and thermodynamic temperature, which gives a possibility for initialization of Γ functions in a wide range of their initial values. For ρ initialization both the function [12] elaborated for a growing number of quasi-particles of a level density and some phenomenological assumptions [13] were used. Besides, inasmuch as experimental spectra of two-step cascades are measured only for some part of intensities of primary gamma-transitions, an uncertainty of the best ρ and Γ fits gives an addition to inevitable systematic uncertainty.

In spite of the fact that an inevitable systematic uncertainty exists, the calculation results are good enough. To evaluate a quality of the ρ and Γ obtained data is possible by comparison of experimental and calculated gamma-spectra (Fig. 2–6).

Features of the total gamma-spectra at thermal neutron capture

Assumed by us normalization of total gamma-spectrum satisfies the condition $\sum I_\gamma E_\gamma = B_n$, where I_γ is an intensity, E_γ is a gamma-quantum energy, and B_n is a neutron binding energy. Consequently, a sum of all possible cascades with any quanta multiplicity doesn't depend on ρ and Γ function types. For determination of shapes of ρ and Γ functions it is need to use only individual cascades ($I_\gamma E_\gamma = \varphi(E_\gamma)$ dependencies). For example, strength function increasing for a part of cascades (Fig.2) is obligatory accompanied by a change both level density and strength functions for the rest cascades.

A distortion of information extracted from the comparison of experimental spectrum with a calculated one is caused by a difference of shapes of these spectra only. And valid information can be obtained if to compare the experiment with two or more calculated spectra. It was done by developed in Dubna practical model of cascade gamma-decay with different representations for the radiative strength functions and for coefficient of vibrational level density enhancement. Two of these representations with various shapes of several (not more than four) local peaks in the functional dependencies on energy of $E1$ - and $M1$ -primarily transitions of two-step cascades are presented below.

In a framework of quasi-particle model of nucleus authors of [14] calculated a shape of fragmentation of strength of one-particle states at their different deviation from Fermi-surface. Calculated fragmentation sufficiently depended on energies of initial quasi-particle state and of photon excitation. A practical result of these calculations is asymmetry of distribution of strength of fragmented state. If to suppose that local peaks in cascade gamma-spectra (Fig. 2) appear in consequence of defined process we could wait that these peaks are asymmetric. We described each of them by a simple analytical function and added several peaks to a smooth energy dependency expected on a base of modified model [10] for both mutlipolarities with varied thermodynamic temperature T and normalization parameter w :

$$k(E1, E_\gamma), k(M1, E_\gamma) = w \frac{1}{3\pi^2 \hbar^2 c^2 A^{2/3}} \frac{\sigma_G \Gamma_G^2 (E_\gamma^2 + \kappa 4\pi^2 T^2)}{(E_\gamma^2 - E_G^2)^2 + E_G^2 \Gamma_G^2} + \text{several local peaks.} \quad (2)$$

Here E_G , Γ_G and σ_G are location of the center, width and cross section in maximum of giant dipole resonance, correspondingly.

In the first variant of calculations each of the local peaks was described as:

$$P\delta^- \exp(\alpha_p(E_\gamma - E_p)) + P\delta^+ \exp(\beta_p(E_p - E_\gamma)), \quad (3)$$

where the first summand is a left slope of peak (energies below maximum) and the second summand is a right slope (energies above maximum). Position E_p , amplitude P and slope parameters α_p , δ^- and β_p , δ^+ for each peak are determined independently.

In the second case each of the local peaks was described by asymmetric Lorentzian curve:

$$k = W_i \frac{(E_\gamma^2 + (\alpha_i(E_i - E_\gamma)/E_\gamma))\Gamma_i^2}{(E_\gamma^2 - E_i^2)^2 + E_\gamma^2 \Gamma_i^2}. \quad (4)$$

Parameters for each i -th peak are similar to ones in model [KMF]: center position E_i , width Γ_i , amplitude W_i and asymmetry parameter $\alpha_i \sim T^2$. Expression $\alpha_i(E_i - E_\gamma)/E_\gamma$ grows with

increasing $B_n - E_i$ value from zero in the center of peak to maximum at B_n energy and decreases at excitation energy fall. Peaks of $E1$ - and $M1$ -strength functions are presented by the same expressions.

In Fig. 2 the experimental intensities of two-step cascades and their best fits for 12 nuclei are compared. A quality of measured intensity fitting (χ^2) for all nuclei in cases of (3) and (4) peak shapes is practically the same what gave a possibility to test surely the obtained ρ and Γ values for the total gamma-spectra calculation. If ρ and Γ functions from the statistical model of nucleus are used in calculations there is a mismatch what is seen also in Fig.2. At upper row of Figs. 3–6 the best fits of densities for intermediate cascade levels are presented.

Fractures of level density curves for spherical nuclei correspond to breaking thresholds of the second Cooper pairs, and fitted breaking thresholds of the third pair for these nuclei are near or above neutron binding energy. For deformed and transition nuclei the breaking thresholds of the fourth pair were found also near B_n .

Calculated total gamma-spectra

The fitted data for two chosen forms (2, 3) of the local peaks of strength functions are shown in Figs. 3–6. Fitted ρ values were compared with calculated ones from back shifted Fermi-gas model [11] and from model with taking into account an influence of shell inhomogeneities on a density of single-particle states near Fermi surface [13]. And sums of the strength functions of $E1$ - and $M1$ -transitions and calculated total gamma-spectra (for 10 nuclei – at capture of thermal neutrons [15]; and for ^{198}Au , ^{128}I [16] – at capture of fast neutrons) are also shown in Figs. 3–6.

For any cascade quantum a fixed threshold 520 keV was chosen because of too complex shape of annihilation line 511 keV and too small cascade primary transition intensities $E_1 < 511$ keV. So an intensity of the total experimental gamma-spectrum was compared with a calculated one in $0.52 < E_\gamma < B_n - E_d$ interval of gamma-quanta energy only.

In all cases the total calculated and experimental gamma-spectra were normalized on a sum of $I_\gamma E_\gamma$ products. For a model variant (2) two calculation results of total gamma-spectra were presented in Figs. 3–6. Calculations were done with and without a compensation of local reduction of level density taken into account [1–4] by corresponding coefficient of increasing of strength functions:

$$M = \rho_{\text{mod}} / \rho_{\text{exp}}, \quad (5)$$

where ρ_{exp} is a level density obtained from experimental data, and ρ_{mod} is level density from Fermi-gas model. The level densities and radiative strength functions obtained from theoretical representations of statistical model of nucleus and ones calculated using presented model are compared in Figs. 3–6.

Results of all fittings shown in Figs. 3–6 indicate unambiguously that level density and radiative strength functions for correct calculations of any nuclear-physical parameters had to take into account effects of nucleon pairing and existence of the levels with sizeable vibrational components of wave-functions near neutron binding energy and, most likely, at higher energies.

In the Table there are ratios $2(I_{\text{exp}} - I_{\text{cal}})^2 / (I_{\text{exp}} + I_{\text{cal}})$ of total gamma-spectra intensities in percents for 12 chosen nuclei. In I and II columns are the calculations with use of peak shapes (3) of strengths functions, and calculations in III and IV columns were done using peak shapes (4). In calculations presented in I and III columns it was supposed that level

densities and strength functions are independent ($M=1$), and in calculations from II and IV columns a compensation (5) was taken into account.

Table 2. $2(S_{\text{exp}}-S_{\text{cal}})^2/(S_{\text{exp}}+S_{\text{cal}})$ ratios of total gamma-spectra

Nucleus	I	II	III	IV
⁶⁰ Co	36	34	22	20
¹¹⁴ Cd	26	28	24	26
¹²⁸ I	15	9	15	9
¹⁵⁰ Sm	20	24	17	9.5
¹⁵⁶ Gd	15	15	19	19
¹⁵⁸ Gd	20	20	20	20
¹⁶⁸ Er	32	34	11	17
¹⁸² Ta	13	16	17	14
¹⁹² Ir	18	13	26	11
¹⁹⁶ Pt	22	16	22	15
¹⁹⁸ Au	20	17	15	8
²⁰⁰ Hg	34	28	30	30

Comparing the data of calculations presented in the Table we can do a following resume.

- 1) The main features of total gamma-spectra (at $E_\gamma = 2-3$ MeV and some below the neutron binding energy) are reproduced by calculations accurately enough.
- 2) Description of the local peaks in radiative strength functions by two exponents (3) gives greater distortion between calculated and experimental total gamma-spectra than Lorentzian description (4).
- 3) In many ways an existence of distortion is caused by insufficient statistical accuracy of data on intensities of measured cascades (changes of level density and radiative strength functions are noticeable if χ^2 of the data from Fig. 2 vary within a few percents). If to use Monte-Carlo method for the system (1) solving the likelihood function always has the same inaccuracy.
- 4) Practically it is not possible to describe sums of radiative strength functions with a maximal accuracy by smooth functional dependencies because there are peaks caused by influence of structure of wave-functions of nuclear fragmented state on matrix elements of all cascade transitions. There is no any reason of an absence of similar dependence in cascades with multiplicity of 3 quanta or more. This proposition means that to describe exactly a total gamma-spectrum only by nuclear parameters obtained from $I_{\gamma\gamma}$ fittings (Fig.2) is unachievable.
- 5) An evaluation of systematic errors of calculated total gamma-spectra allows to wait an accuracy of the practical model of some percents for calculating the spectra of nuclear reaction products. It may be achieved if a statistic accuracy of an experiment on cascade intensity measuring will be, at least, 3–10 times more than now. In order to increase the practical model accuracy it is need also to develop a theoretical model of vibrational level density with taking into account both sequential breaking of Cooper pairs of neutrons and protons (an appearance of mixed neutron-proton pairs may be possible at some excitation energies also) and corresponding change of quasi-particle level density.

Conclusion

A comparison of results obtained in different variants of Dubna model with an available set of experimental $I_{\gamma\gamma}$ data shows that determination of breaking threshold of the second Cooper nucleon pair was done with an excellent accuracy. It isn't possible to determine from the $I_{\gamma\gamma}$ data the breaking threshold of the first Cooper pair because density of low-lying levels is small. But it is need to take its existence into account in $I_{\gamma\gamma}$ analysis so the condition of equality of fitted and experimental level densities had to be kept in the point E_d of transition from discrete individual levels to a range of unresolved ones.

An uncertainty of the breaking threshold determination for each consequent pair grows because number of quasi-particles (and an appropriate derivative dp/dE_{ex} [Str]) quickly increase. In addition, an increase of correlation between the breaking threshold of consequent Cooper pairs and a coefficient of vibrational level density inancement may give the similar effect.

An existence of the sources of uncertainties of the sought ρ and Γ functions is a fundamental problem and it is inevitable for any nuclear model used for experimental data analysis and for prediction of spectra and cross sections.

References

- [1] A.M. Sukhovoij, Phys. Atom. Nucl. **78**, 230 (2015).
- [2] L.V. Mitsyna, A.M. Sukhovoij, in *Proceedings of XXII International Seminar on Interaction of Neutrons with Nuclei, Dubna, May 2014*, Preprint № E3-2015-13 (Dubna, 2015), p. 245; <http://isinn.jinr.ru/past-isinns.html>.
- [3] A.M. Sukhovoij, L.V. Mitsyna, and N. Jovancevich, Phys. Atom. Nucl. **79**, 313 (2016).
- [4] L.V. Mitsyna, A.M. Sukhovoij, in *Proceedings of XXIII International Seminar on Interaction of Neutrons with Nuclei, Dubna, May 2015*, Preprint № E3-2016-12 (Dubna, 2015), p. 299; <http://isinn.jinr.ru/past-isinns.html>.
- [5] M. Krticka et al., Phys. Rev., C. **77**, 054319(2008).
- [6] A. Voinov et al., Phys. Rev., C. **81**, 054607(2010).
- [7] A.M. Sukhovoij, V.A. Khitrov, Phys. At. Nucl., **72**, 1426(2009)
- [8] A.M. Sukhovoij, and V.A. Khitrov, in *Proceedings of XVIII International Seminar on Interaction of Neutrons with Nuclei, Dubna, May 2002*, Preprint № E3-2011-26 (Dubna, 2011), p. 180; <http://isinn.jinr.ru/past-isinns.html>.
- [9] S.T. Boneva, A.M. Sukhovoij, V.A. Khitrov, and A.V. Voinov, Nucl. Phys. **589**, 293 (1995).
- [10] S.G. Kadmsensky, V.P. Markushev and W.I. Furman, Sov. J. Nucl. Phys. **37**, 165 (1983).
- [11] W. Dilg, W. Schantl, H. Vonach, and M. Uhl, Nucl. Phys. A **217**, 269 (1973).
- [12] V.M. Strutinsky, in *Proceedings of the International Congress on Nuclear Physics, Paris, France, 1958*, p. 617.
- [13] V. Ignatyuk, Report INDC-233(L), IAEA (Vienna, 1985).
- [14] L.A. Malov and V.G. Soloviev, Sov. J. Nucl. Phys. **26**, 384 (1977).
- [15] L.V. Groshev et al., Nuc. Data Table, **5** (1-20) 1968.
- [16] J. Voignier., S. Joly, G. Greinier, Nucl. Sci. Eng., **93**(1986) 43.

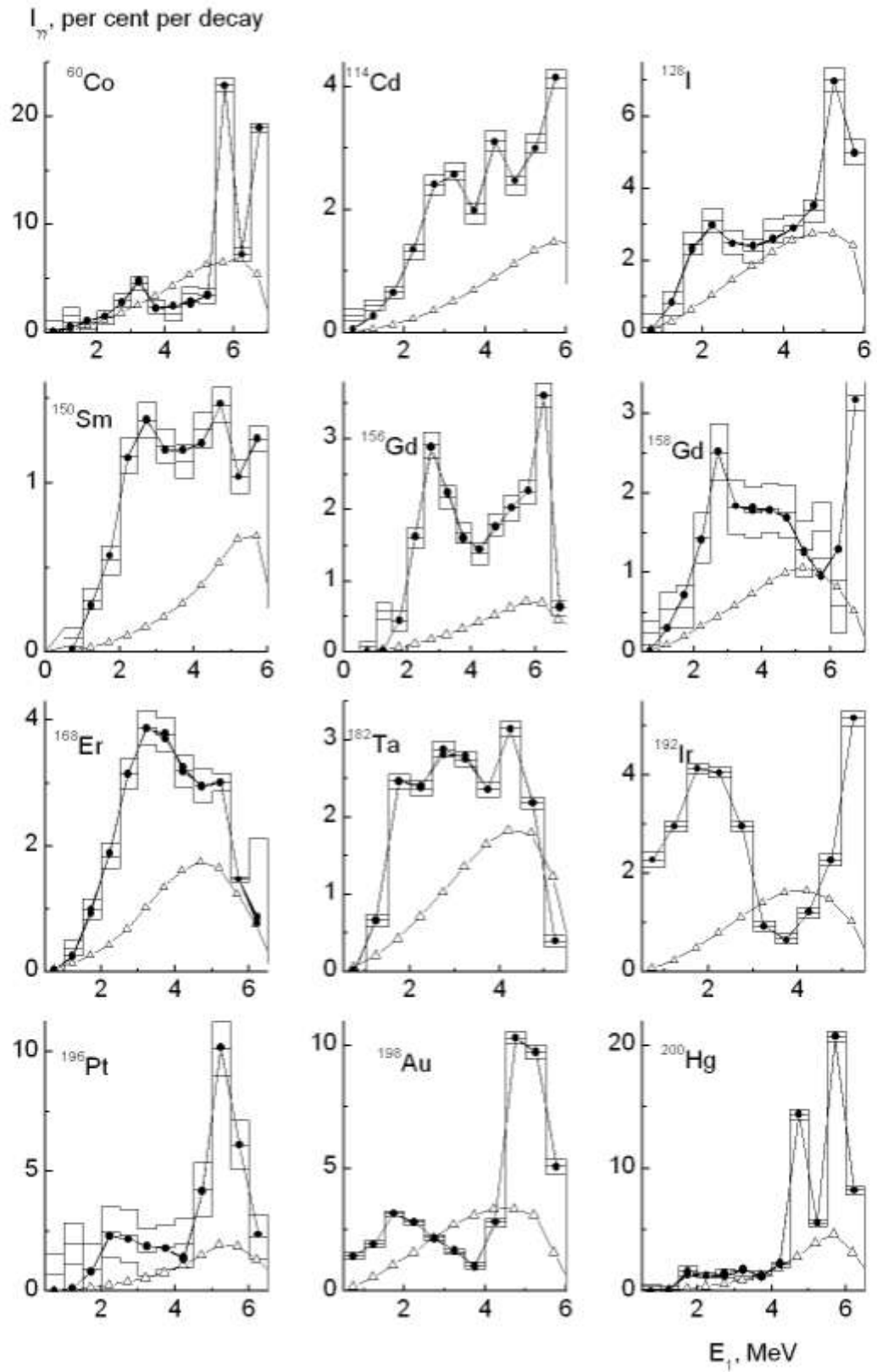


Fig.2. Fitting the experimental intensities I_γ for investigated nuclei. Histogram is experiment with its errors, black points are the best fitted values, triangles are calculations by models [10, 11].

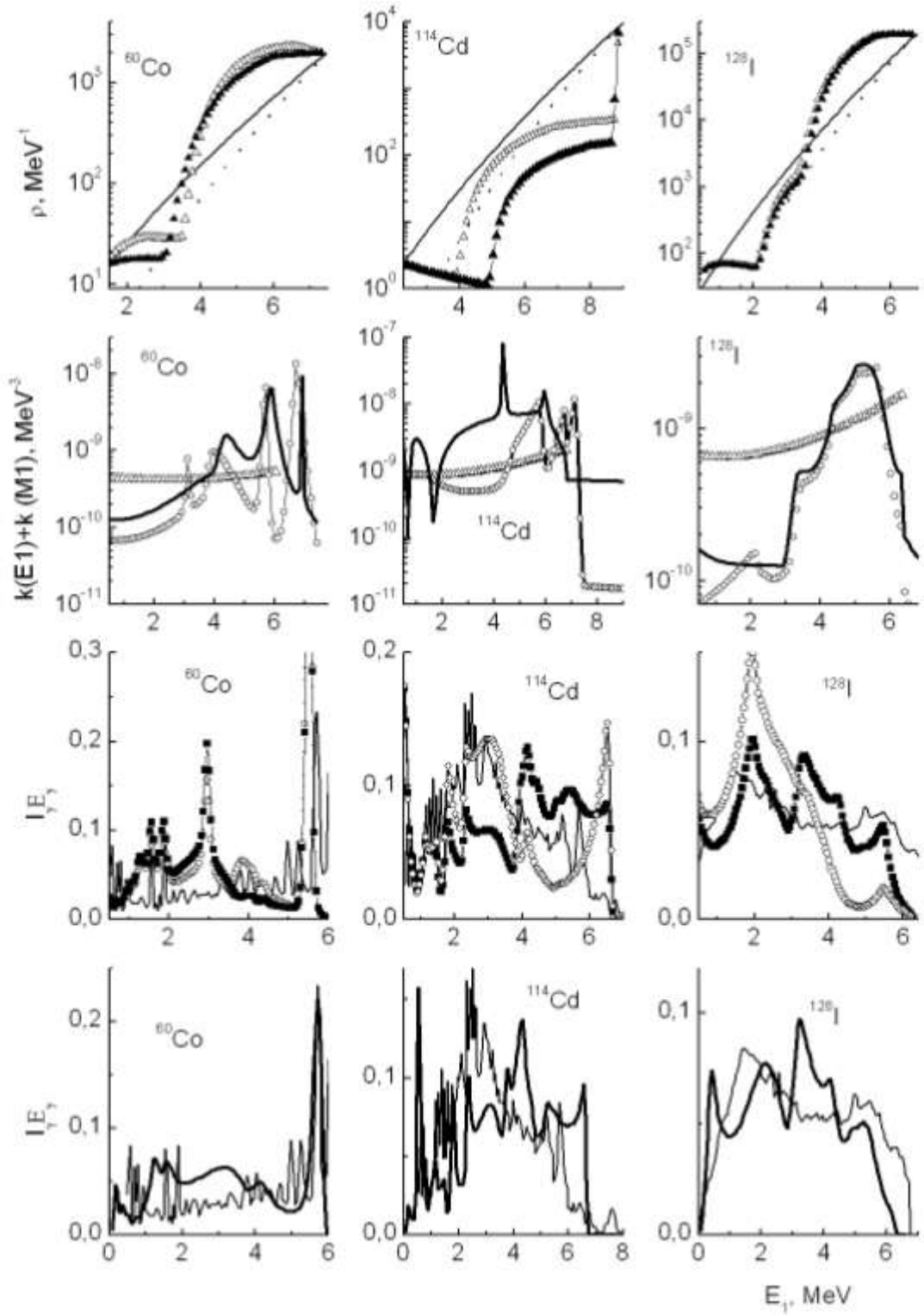


Fig.3. Upper row: level densities calculated with use of function (3) (open triangles), with function (4) (black triangles), and model calculations (solid line – model [11], dashed line – model [13]). Second row: strength functions with local peaks described by exponents (3) (open points), by asymmetric Lorentzian curve (4) (black points), and calculation by model [10] in a sum with $k(M1)=\text{const}$ (triangles). Third row: the best fits of the total gamma spectra if local peaks described as (3) (open points) and as (4) (squares), and experimental one (bottom line). Down row: the total gamma spectra calculated using function (4) and condition (5) (bold solid line) and experimental one (solid line).

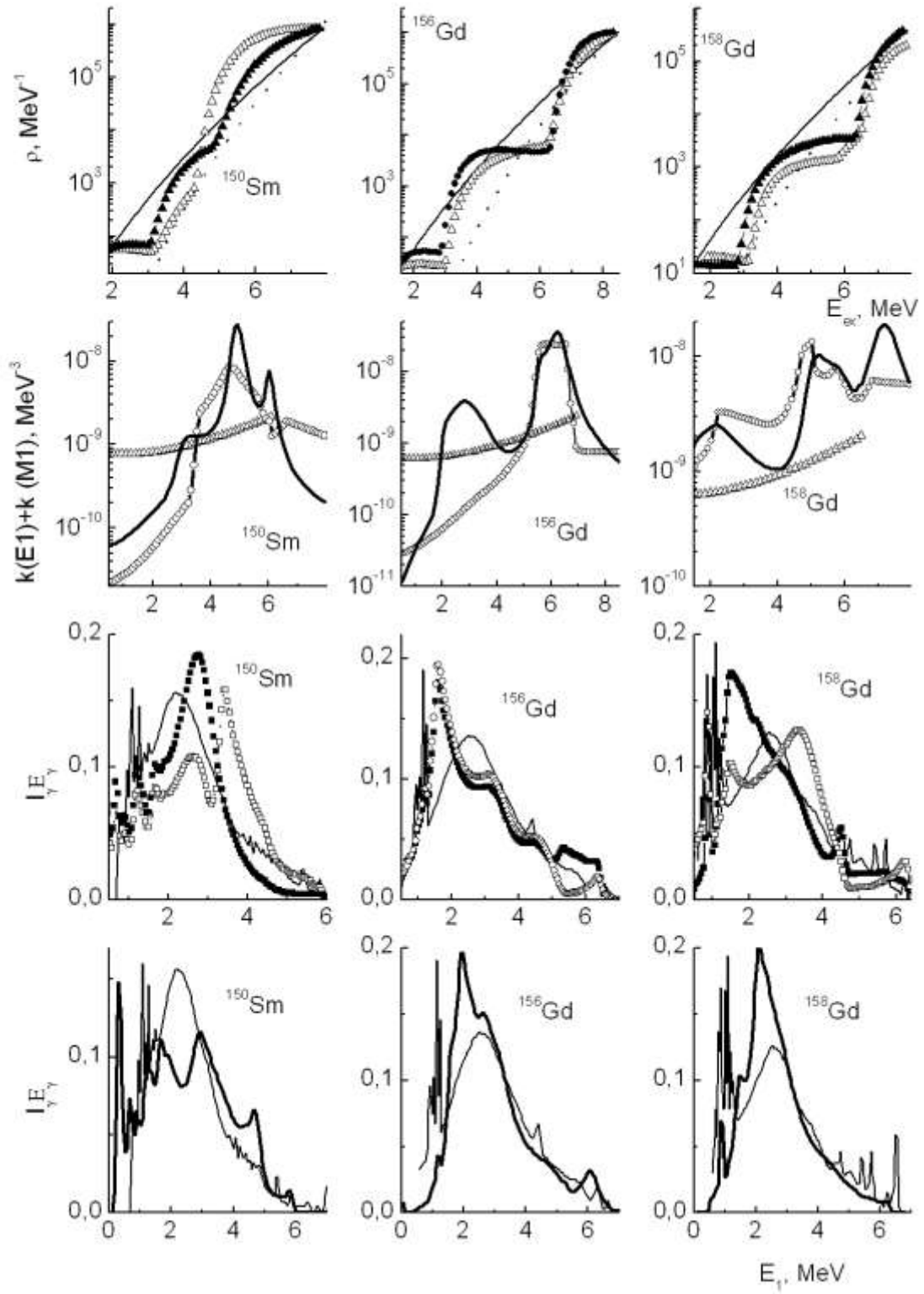


Fig. 4. The same as in Fig.3 for ^{150}Sm and $^{156,158}\text{Gd}$.

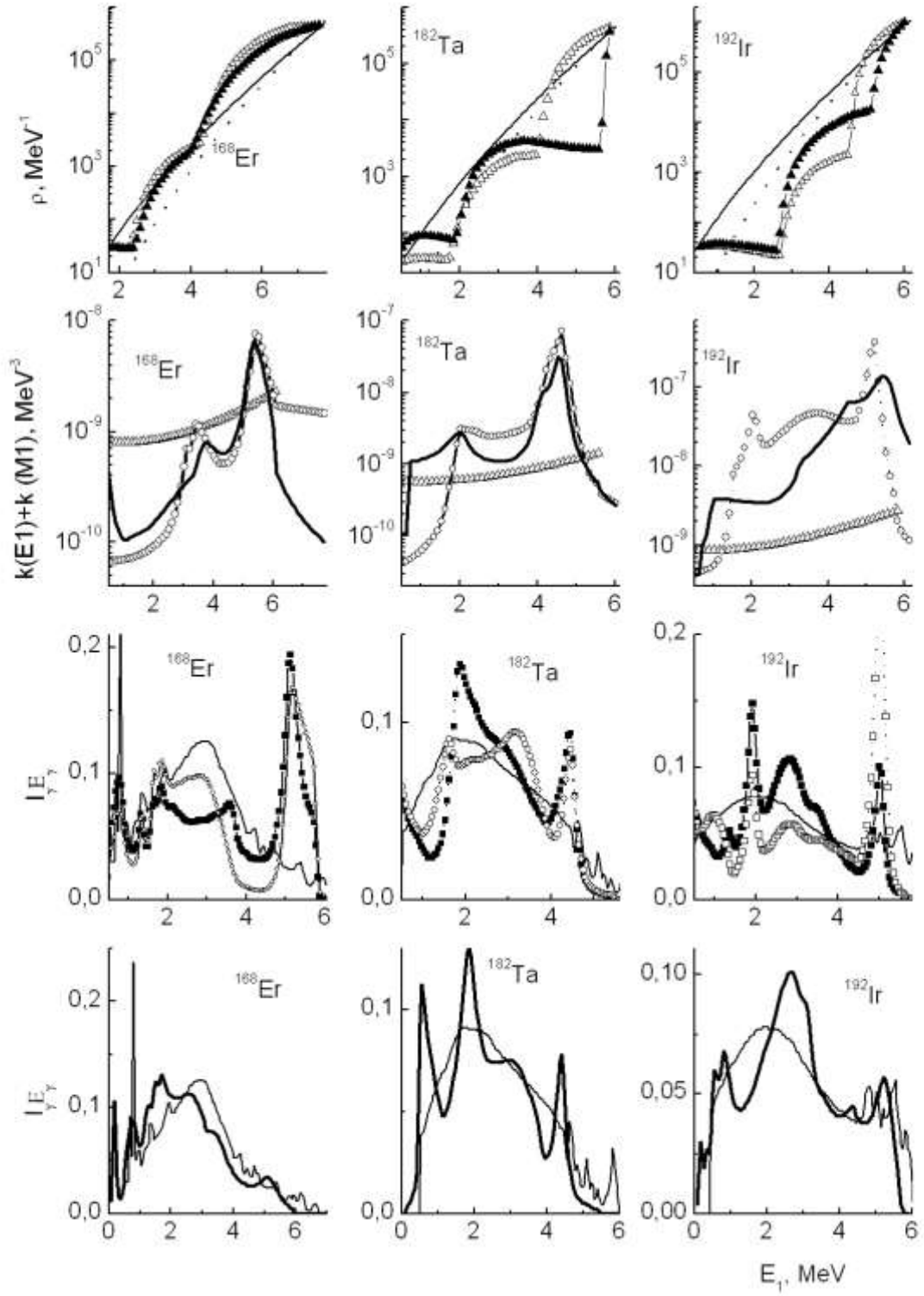


Fig. 5. The same as in Fig. 3 for ^{168}Er , ^{182}Ta , and ^{192}Ir .

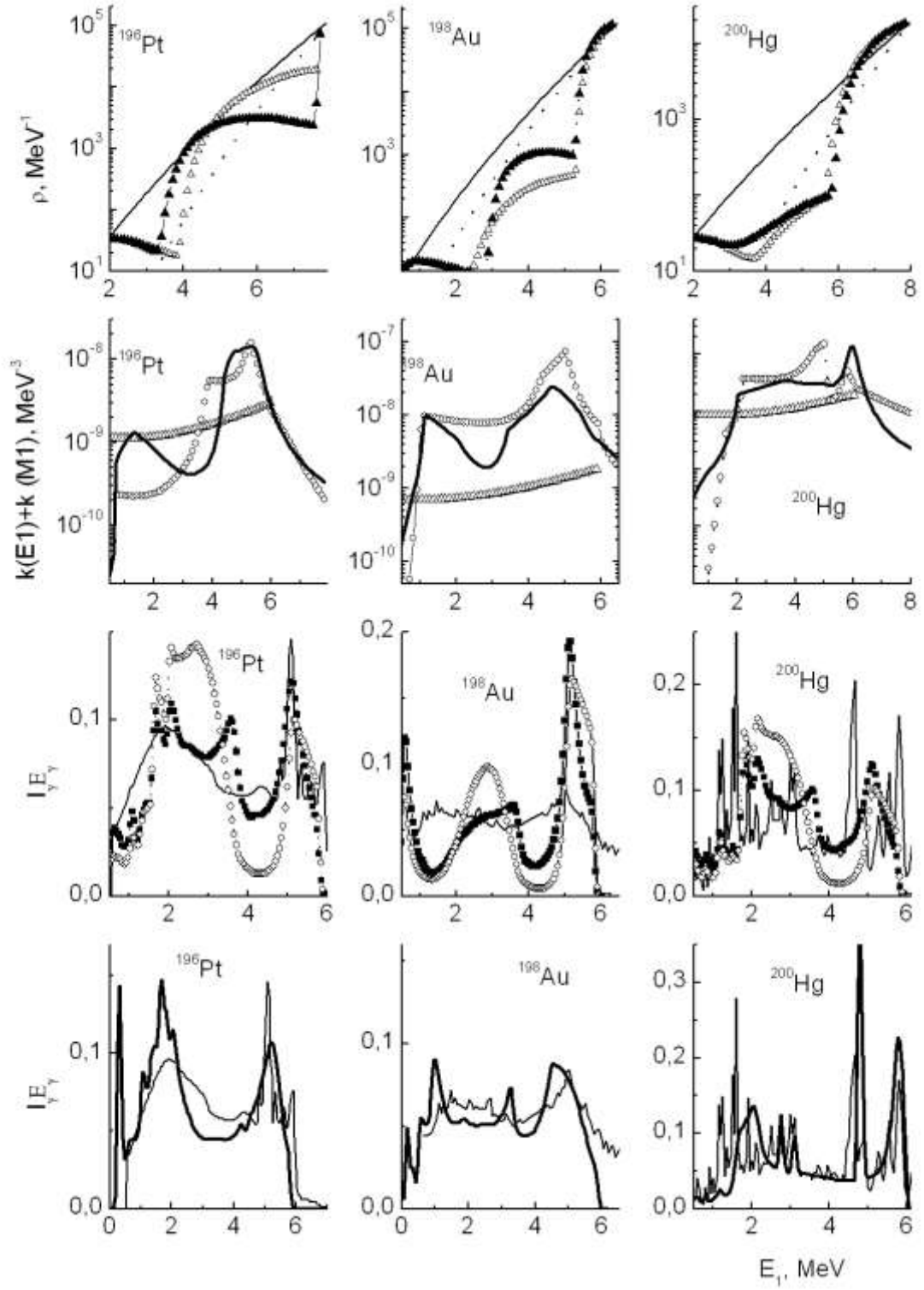


Fig. 6. The same as in Fig. 3 for ^{196}Pt , ^{198}Au , and ^{200}Hg .

Representation of the Radiative Strength Functions in the Practical Model of Cascade Gamma-Decay

Vu D.C.^{1,3}, Sukhovej A.M.¹, Mitsyna L.V.¹, Zeinalov Sh.¹, Jovancevic N.²,
Knezevic D.², Krmar M.², Dragic A.⁴

¹*Joint Institute for Nuclear Research, Dubna, 141980, Russia*

²*University of Novi Sad, Faculty of Science, Department of Physics, Novi Sad, Serbia*

³*Vietnam Academy of Science and Technology Institute of Physics, Hanoi, Vietnam*

⁴*Institute of Physics, Belgrade, Serbia*

Abstract

The developed in Dubna practical model of the cascade gamma-decay of neutron resonance allows one, from the fitted intensities of the two-step cascades, to obtain parameters both of level density and of partial widths of emission of nuclear reaction products. In the presented variant of the model a part of phenomenological representations is minimized. Analysis of new results confirms the previous finding that dynamics of interaction between Fermi- and Bose-nuclear states depends on the form of the nucleus. It also follows from the ratios of densities of vibrational and quasi-particle levels that this interaction exists near binding neutron energy and probably differs for nuclei with varied parities of nucleons.

Introduction

Parameters of the cascade gamma-decay of any high-lying nuclear level (see Figs. 1–3) at any excitation energy are determined only by the level density ρ and by the partial widths Γ of dipole electrical and magnet transitions. Cascade intensity with pure quadrupole transitions is negligible at the nuclear excitation energy of more than a few MeV. For levels excited by primary transitions interval of spins is $\Delta J \leq 4$ for any parity.

Investigation of the process of gamma-decay is interesting most of all for analysis of interaction dynamics of fermion and boson states of nuclear matter. Valid information is needed also for describing the process of fission more correctly. According to [1], energy is divided between excited fission fragments dependent on their level densities. As it is seen in Figs. 4–6, level densities calculated using available models [2] differ greatly from the modern experimental data.

Ordinary gamma-spectra and reaction cross sections depend on a $\rho \times \Gamma$ product and this fact completely cuts out a possibility of simultaneous determination of ρ and Γ valid values using such kind of data. This possibility is realized only in experiments on studying the cascade intensities of two sequential gamma-transitions. Two-step experiments can decrease a total error of determined ρ and Γ functions up to several dozens of percents as the intensities of two-step cascades include all information about energy of two gamma-transitions and any triplets of fixed nuclear levels.

As it is impossible to resolve all individual levels and to determine probabilities of transitions between them by available now spectrometers, information on superfluidity can be

obtained from indirect experiments only. At that, both level density ρ and partial widths Γ in any nucleus are fitting functions with a minimal as far as possible number of parameters.

1. Possibility of up-to-date experiment and its model representation

The intensities $I_{\gamma\gamma}(E_1)$ of two-step cascades between neutron resonance (or another compound-state) λ and some group of low-lying nuclear levels f through any intermediate levels i for a fixed energy E_1 of primary transition are written by a system of equations of type:

$$I_{\gamma\gamma}(E_1) = \sum_{\lambda, f} \sum_i \frac{\Gamma_{\lambda i}}{\Gamma_{\lambda}} \frac{\Gamma_{if}}{\Gamma_i} = \sum_{\lambda, f} \frac{\Gamma_{\lambda i}}{\langle \Gamma_{\lambda i} \rangle} \frac{n_{\lambda i}}{m_{\lambda i}} \frac{\Gamma_{if}}{\langle \Gamma_{if} \rangle} \frac{1}{m_{if}}, \quad (1)$$

where $m_{\lambda i}$ is a number of levels of excited primary γ -transitions in intervals from the energy of initial level λ to the energy of intermediate level i , m_{if} is a number of levels excited secondary transitions in intervals from the energy of intermediate level i to energy of the final level f , $n_{\lambda i}$ is a number of intermediate cascade levels in small energy intervals. From the system (1), which connects an unknown level number n (or m) and unknown partial widths, a set of p and q parameters of the model functions $\rho=f(p_1, p_2, \dots)$ and $\Gamma=\varphi(q_1, q_2, \dots)$ with some uncertainty is determined. The uncertainty is caused by a distortion of available theoretical representations and experimental results. Previous analysis [3] showed that a strong connection between ρ and Γ values in narrow intervals of excitation energies can be included in the model (1). In such a way from two-step cascades it is possible to determine simultaneously parameters of specified ρ and Γ functions at any densities of λ and i levels.

Analysis of the cascade intensities [4, 5] for nuclei of the region $28 \leq A \leq 200$ showed that obtained level densities cannot be described with the experimental accuracy by models, which ignore influence of boson-states of nuclear matter on ρ function.

The Dubna model is free from using any hypothesis untested by experiment (for example, Porter-Thomas hypothesis [6] about emission widths of nuclear reaction products, hypothesis of Axel-Brink [7, 8] about independency of Γ values on energy of excited level or Bohr-Mottelson hypothesis [9] about validation of the optical model used for determination of emission probability for nucleon products of reaction). The basis of our model of the cascade gamma-decay of nuclear compound-states with excitation energies $E_{ex} \approx 5-10$ MeV is the model of n -quasi-particle levels, balance of entropy and energy of quasi-particle levels [2, 10, 11] and tested model-phenomenological representations about form of energy dependency of radiative strength functions.

A systematic error in any procedure for ρ and Γ determination is always caused by large coefficients of error transfer of measured spectrum δS or cross section $\delta \sigma$ of reaction onto errors of $\delta \rho$ and $\delta \Gamma$ sought parameters. The error value strongly grows at increment of energy of decaying level. It is possible to evaluate this error and to choose a direction for correction of model representation about ρ and Γ only if to compare different model representations of $\rho=f(p_1, p_2, \dots)$ and $\Gamma=\varphi(q_1, q_2, \dots)$ functions. For example, comparing a few variants of the practical model [3, 5, 12, 13] we discovered that rate of density change for vibrational levels (given in [12, 13] phenomenologically) is partially or completely determined [5] by pairing energy Δ for the last nucleon in nucleus. Therefore, in proposed variant of our practical model in the coefficient C_{coll} of collective level density increasing [5, 11] E_{μ} and E_{ν} parameters (changes of rates of nuclear entropy and of energy of quasi-particle states, correspondingly) are replaced by united fitting parameter E_u . Thus, C_{coll} coefficient was used in a form

$$C_{coll} = A_l \exp(\sqrt{(E_{ex} - U_l)/E_u} - (E_{ex} - U_l)/E_u) + \beta, \quad (2)$$

where A_l are fitting parameters of vibrational level density above breaking point of each l -th Cooper pair, and U_l are energies of the corresponding breaking thresholds. Parameter $\beta \geq 1$ can differ from 1 for deformed nuclei.

An influence of the shell inhomogeneities of a single-particle spectrum [2, 11] on a parameter defining a dependence of level density on excitation energy

$$a(A, E_{ex}) = \tilde{a} (1 + ((1 - \exp(\gamma E_{ex})) \delta E / E_{ex})) \quad (3)$$

(and at the same time on $g = 6a/\pi^2$ parameter of density of n -quasi-particle levels near Fermi-surface [11]) was also taken into account. An asymptotic value $\tilde{a} = 0.114A + 0.162A^{2/3}$ and coefficient $\gamma = 0.054$ were taken from [11]. A shell correction δE calculated from the data of mass defect in a liquid-drop nuclear model [2] was lightly changed to keep an average distance D_λ between resonances of the tested nucleus.

2. Energy dependence of the strength functions

In the model of the cascade gamma-decay for any excited levels and energies of emitted quantum, the form of energy dependence for partial radiative widths must be specified with a good accuracy.

On a base of available models for nucleus of A mass a strength function is determined as $k = \Gamma / (A^{2/3} E_\gamma^3 D_\lambda)$, where E_γ is an energy of the gamma-transition. An absolute value of sum of radiative widths for primary $E1$ - and $M1$ -transitions of cascades (total radiative width) is usually obtained from measured cross sections of the reaction. The expected form of this sum may be found using phenomenological representations or extrapolation of any models to $E_d < E_{ex} < B_n$ region of excitation (E_d is a point of transition from a set of known levels [14] to a concept of level density function, and B_n is a neutron binding energy in a nucleus).

The main summand of the functions $k(E1, E_\gamma)$ and $k(M1, E_\gamma)$ may be presented as a distribution of strength functions from models type of [15] with additional varied parameters. Variation of these parameters gives a set of functions of $E1$ - and $M1$ -transitions with a wide area of possible values (as it was done in [12, 13]).

It was experimentally established [16] that an addition to $k(E1, E_\gamma) + k(M1, E_\gamma)$ energy dependence of several peaks ensures a fine description of the cascade intensities. Form of these additional peaks may be found only by empiric way. For example, a description of each of them by two exponents (as in [5, 12]) is convenient to solve a system of nonlinear equations (1), although exponents are not used in theoretical models [2].

Usually for describing a form of peaks of $E1$ - and $M1$ -strength functions Breit-Wigner or Lorentz distributions are exploited. Asymmetrical Breit-Wigner function is used in theoretical analysis of fragmentation of quasi-particle states at varied locations relative to Fermi-surface [17]. However, variety of results is a trouble for a direct usage of these theoretical representations.

It turned out that application of an asymmetrical Lorentzian curve for description of peaks of the strength functions is simpler. Local peaks of $E1$ - and $M1$ -strength functions are written by an expression:

$$k = W_i \frac{(E_\gamma^2 + (\alpha_i(E_\gamma - E_i)/E_\gamma))\Gamma_i^2}{(E_\gamma^2 - E_i^2)^2 + E_\gamma^2\Gamma_i^2}. \quad (4)$$

Lorentzian curve parameters for each i -th peak are similar to the model [15]: location of the peak center E_i , width Γ_i , amplitude W_i , and asymmetry parameter $\alpha_i \sim T^2$ (T is a nuclear thermodynamic temperature). Parameter $\alpha_i(E_\gamma - E_i)/E_\gamma$ grows linearly when an excitation energy increases (from zero in the center of peak to maximum at B_n), and it decreases if neutron excitation energy reduces.

An essential problem of using Lorentzian curve at fitting is a strong degradation of a convergence of iteration process. As all parameters of (4) are fitted, the possibility of unlimited Γ_i decreasing appears in some fitting paths.

A necessity of phenomenological accounting an influence of sharp local change of level density on the strength functions was discovered already at model-free determination of random functions ρ and Γ [18]. A required correction was done with the help of multiplication of fitted strength functions by ratio

$$M = \rho_{\text{mod}}/\rho_{\text{exp}}, \quad (5)$$

where ρ_{exp} is the best fit for a given iteration, ρ_{mod} is a smooth model functional described both density of neutron resonances and cumulative sum of known levels with E_{ex} below E_d . For ρ_{mod} determination the back shifted Fermi-gas model was chosen. In a given variant of analysis a limitation $1 \leq \rho_{\text{mod}}/\rho_{\text{exp}} \leq 10$ [12] was used. Sums of dipole strength functions with taking into account of such correction and without it are presented in Figs.7–9.

3. Results

An ambiguity of the system (1) solving appears because of both a strong nonlinearity of the sought functions ρ and Γ and their anti-correlation. There is a noticeable probability of falling into a false minimum of χ^2 what can lead to an essential systematic error of ρ and Γ values. It is possible to evaluate and minimize this uncertainty only if to compare results of different variants of the practical model with various functional ρ and Γ dependences.

A comparison of the results of a given model variant with previous ones showed that a good accuracy is achieved in describing a density of intermediate levels of cascades. The most distortion of density values were found only for ^{137}Ba and ^{182}Ta . At that, for ^{137}Ba the previous variant of fitting [5] most likely gives a large uncertainty. And breaking thresholds of the second and the third pairs for ^{182}Ta in presented variant are 1.6 and 5.8 MeV, but in [5] they are 1.6 and 4.0 MeV, respectively. It means that obtained data on the level density even at the worst case of ^{182}Ta give a picture where principle errors are caused only by ambiguity of the up-to-date representations about gamma-decay process.

A larger accuracy and adequacy of the results would be achieved if not less than $\approx 99\%$ of intensity of primary transitions is separated in experiment from all gamma-cascades of compound-state decay. But a comparison of the breaking thresholds for 3 – 4 Cooper pairs determined from (1) using different functional ρ and Γ dependencies showed that a reliable information about the most probable level density and the strength functions of dipole gamma-transitions can be extracted even from a convolution of spectrum of primary products of decay of compound-state and dependency of gamma-transitions branches coefficients on energy of intermediate level. The obtained results in the last variants of the practical model vary very weakly.

The level densities from back shifted Fermi-gas model [19] and from model with taking into account shell inhomogeneities of single-particle spectrum [11] are presented in Figs. 4–6. It is seen that the second model describes a dp/dE_{ex} derivative with a better accuracy than [19] model does. But the level densities calculated using [2] models strongly differ from ones extracted from (1).

In all realized variants of the practical model [5, 18, 20–22] at step-by-step reduction of number of fitted parameters a fitting accuracy is kept, and so description of $I_{\gamma\gamma}$ spectra in presented paper is practically the same as ones in [12, 13].

The radiative strength functions of $E1$ - and $M1$ -transitions and their sums presented in Figs. 7–9 and Figs. 10–12, respectively, have no principal distortions with ones published earlier. But a problem of unambiguous description for observed local peaks of electric and magnetic strength functions remains valid (using exponents [5] or modified Lorentzian curve (4) for this purpose gives closely χ^2).

It is need to append that the data of Figs. 7–12 do not demand to include to strength functions any additional “pygmy-resonances”. For a total interpretation of the gamma-decay process theoretical representations (about co-existing quasi-particle levels with vibrational ones and about fragmentation of all nuclear states at E_{ex} growing) are quite enough.

For many nuclei (Figs. 10–12) “plateau” in sum of strength functions of $E1$ - and $M1$ -transitions coincides with a sum of calculated values from [15] and $k(M1)$ value ($k(M1) = \text{const}$) normalized by $k(M1)/k(E1)$ experimental ratio. An essential decrease of $k(M1)+k(E1)$ sum for small energies of gamma-transitions is observed for all tested variants of functional dependences of strength functions. But an existence of asymptotical zero of sums of strength functions does not follow from Dubna model results. At that, a noticeable increase in strength functions of $E1$ - or $M1$ -transition near B_n and above this energy can be observed at sufficiently high energies of fragmented quasi-particle state. It means that radiative strength functions are not just an extrapolation of giant resonances (it contradicts the Axel-Brink hypothesis [7, 8] used earlier for gamma-spectra calculations).

In Fig.13, mass dependences of breaking thresholds of the second and the third Cooper pairs are presented. As these values differ for nuclei with various nucleon parities and depend on an average pairing energy Δ_0 they are shown separately and compared with B_n/Δ_0 (much as in [5]). It follows from this comparison that dependency of breaking thresholds of pairs on form of strength function is weak and real correlation between ρ and Γ values is insignificant in experiments on the two-step cascade recording.

In Fig.14, the fits of E_u parameter are shown. Jnt can see practically complete coincidence of E_u fits with Δ_0 value for ≈ 30 nuclei. Causes of E_u scatter for the rest nuclei may be

- errors of normalization of experimental intensities of two-step cascades,
- unaccounted in model [12] possibility of breaking proton pairs together or instead of neutron pairs,
- inaccuracy of phenomenological part of the model,
- variability of Δ_0 experimental values [23].

One cannot exclude also a possibility of various ratios of components of quasi-particle and phonon types in wave-function of resonance determined a capture cross section of thermal neutrons by any stable (or long-living) nucleus-target. In the up-to-date models [2], a total level density is equal to sum of densities of quasi-particle levels and collective ones. In Fig.15, the ratios of collective (practically vibrational only) level density to the total density are

presented. Near B_n these ratios are very similar for nuclei with any nucleon parity, but at E_d energy they are noticeable less for even-even nuclei than for even-odd and odd-odd ones.

All tested variants of Dubna model do not give reasons to suppose an existence of drastic changes of nuclear structure in $E_{ex} = B_n$ energy point. Therefore, the data of Fig.15 allow to believe that neutron resonances can keep a different type of structure (with a dominance of quasi-particle or phonon components) of wave-functions and that they belong to some various distributions of reduced neutron resonance widths and total radiative ones.

In [24], an approximation of reduced neutron widths and total radiative widths of neutron resonances was done. At analysis it is supposed that experimental set of these widths is represented by a sum of distributions (from 1 to 4) with varied widths and positions of maximums of neutron amplitudes. For total radiative widths in nuclei with a number of resonances ≥ 170 average parts of two the most intensive distributions are 44 and 34% of overall distribution of total radiative widths (it is close to 40%-part of vibrational levels).

Thus, two completely independent methodically experiments show that structure of the wave-functions differs for contiguous levels in a wide range of stable nuclei-targets up to B_n energy (and even at some higher energies).

The existence of non-principal distortion between the values of $E1$ - and $M1$ -strength functions (Fig. 10–12) and results of [5] are caused most likely by different degree of influence on χ^2 of various energy dependences (forms) of partial widths for peaks (4) at energy region of small functional values. At that, form variations for sums of $E1$ - and $M1$ -strength functions (Figs. 7–9) observed in different nuclei can be interpreted as existence of levels of various structures at excitation energy of 5–10 MeV.

Conclusions

Direct experimental information on dynamics of breaking 3 – 4 Cooper pairs of nucleons has been obtained. Systematic uncertainty of determination of breaking thresholds is not more than ~ 1 MeV for a majority of available studied nuclei.

The data extracted with the use of

1. model of n -quasi-particle level density [10] for description of sequential 3 – 4 Cooper pair breaking at energies below 5–10 MeV from Fermi-surface,
2. phenomenological representations (2) about energy dependence of density of vibrational levels at the same energy range,
3. and composition of phenomenological and/or theoretical representations about form of energy dependences of widths of gamma-quanta emission

allow us to suppose that dynamics of interaction between fermion and boson states of nuclear matter depends on the form and parity of nucleon number of studied nucleus.

References

- [1] K.H. Schmidt and B. Jurado, Phys. Rev. C **92**, 014607 (2011).
- [2] *Reference Input Parameter Library RIPL-2, Handbook for calculations of nuclear reaction data*, IAEA-TECDOC (2002).
- [3] N. Jovancevich, A.M. Sukhovoij, W.I. Furman, and V.A. Khitrov, in *Proceedings of XX International Seminar on Interaction of Neutrons with Nuclei, Dubna, May 2012*, Preprint № E3-2013-22 (Dubna, 2013), p. 157; <http://isinn.jinr.ru/past-isinns.html>.

- [4] Sukhovoĵ A.M., Mitsyna L.V., Jovancevic N. in *Proceedings of XXIII International Seminar on Interaction of Neutrons with Nuclei, Dubna, May 25-29, 2015, JINR*, Preprint № E3-2016-12 (Dubna, 2016), p.299.
- [5] A.M. Sukhovoĵ, L.V. Mitsyna, N. Jovancevich, *Phys. Atom. Nucl.* **79**, 153(2016).
- [6] C.F. Porter and R.G. Thomas, *Phys. Rev.* **104**, 483 (1956).
- [7] P. Axel, *Phys. Rev.* **126**, 671 (1962).
- [8] D.M. Brink, Ph. D. Thesis (Oxford University, 1955).
- [9] *A. Bohr, and B.R. Mottelson, Nuclear Structure, Vol. 1 (W.A. Benjamin, New York; Amsterdam, 1969).*
- [10] V.M. Strutinsky, in *Proceedings of the International Congress on Nuclear Physics, Paris, France, 1958*, p. 617.
- [11] V. Ignatyuk, Report INDC-233(L), IAEA (Vienna, 1985).
- [12] A.M. Sukhovoĵ, *Phys. Atom. Nucl.* **78**, 230 (2015).
- [13] L.V. Mitsyna, A.M. Sukhovoĵ, in *Proceedings of XXII International Seminar on Interaction of Neutrons with Nuclei, Dubna, May 2014*, Preprint № E3-2015-13 (Dubna, 2015), p. 245; <http://isinn.jinr.ru/past-isinns.html>.
- [14] <http://www-nds.iaea.org/ENDSF>.
- [15] S.G. Kadmsky, V.P. Markushev, and W.I. Furman, *Sov. J. Nucl. Phys.* **37**, 165 (1983).
- [16] A.M. Sukhovoĵ, W.I. Furman, V.A. Khitrov, *Phys. At. Nucl.*, **71**, 982(2008).
- [17] L.A. Malov and V.G. Soloviev, *Sov. J. Nucl. Phys.* **26**, 384 (1977).
- [18] E.V. Vasilieva, A.M. Sukhovoĵ, and V.A. Khitrov, *Phys. Atom. Nucl.* **64**, 153 (2001).
- [19] W. Dilg, W. Schantl, H. Vonach, and M. Uhl, *Nucl. Phys. A* **217**, 269 (1973).
- [20] A.M. Sukhovoĵ and V.A. Khitrov, Preprint No. E3-2005-196, JINR (Dubna, 2005).
- [21] A.M. Sukhovoĵ and V.A. Khitrov, *Phys. Part. Nucl.* **36**, 359(2005).
- [22] A.M. Sukhovoĵ and V.A. Khitrov, *Phys. Part. Nucl.* **37**, 899(2006).
- [23] V.A. Kravtsov, Atomic Masses and Binding energy of Nuclei (Atomizdat, Moscow, 1965) [in Russian].
- [24] A.M. Sukhovoĵ and V.A. Khitrov, *Phys. Atom. Nucl.* **76**, 68 (2015).

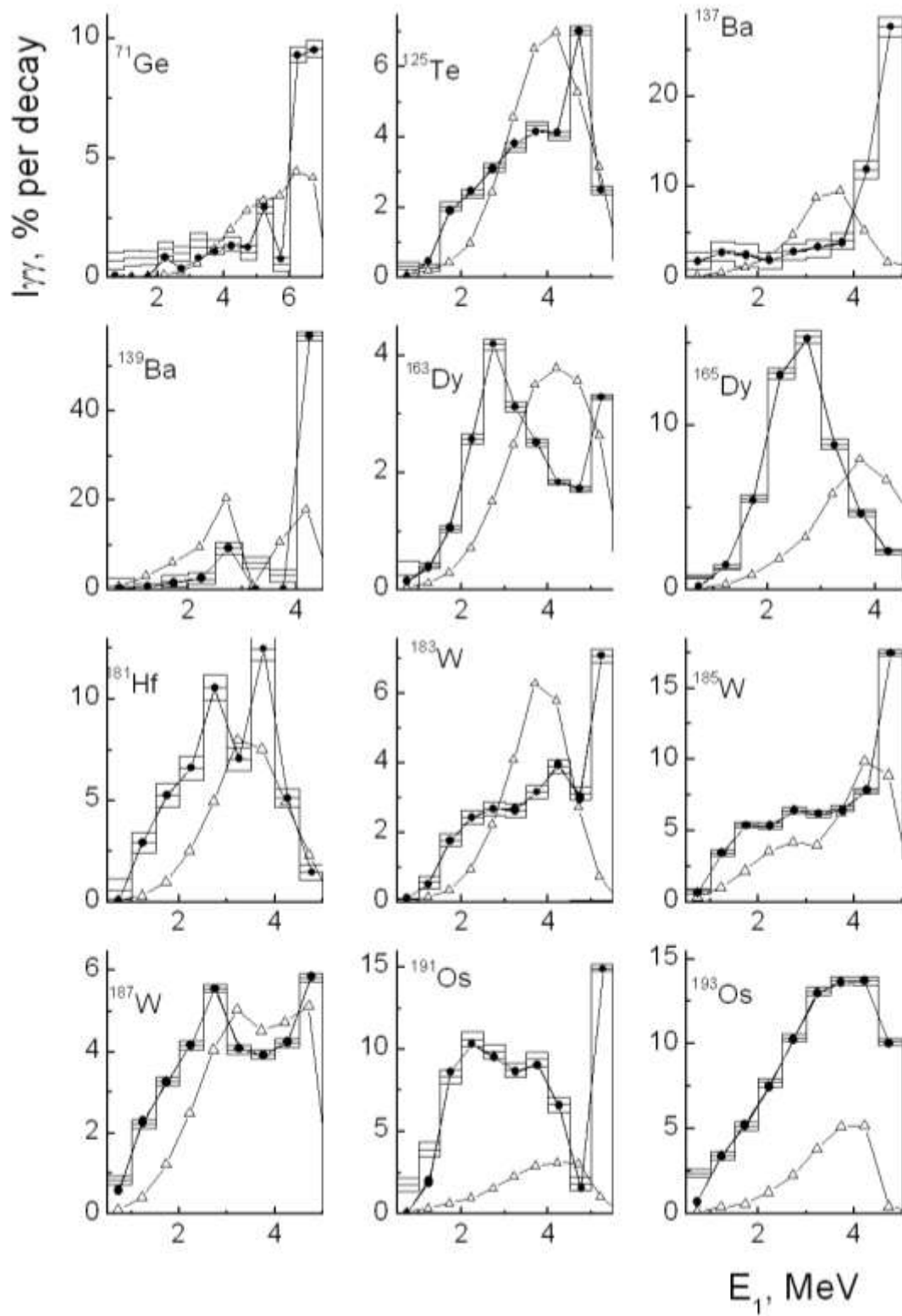


Fig. 1. Dependencies of the experimental intensities (histogram with experimental errors) and their best approximations (points) on the energy of primary transition. Triangles are the results of calculations based on statistical model.

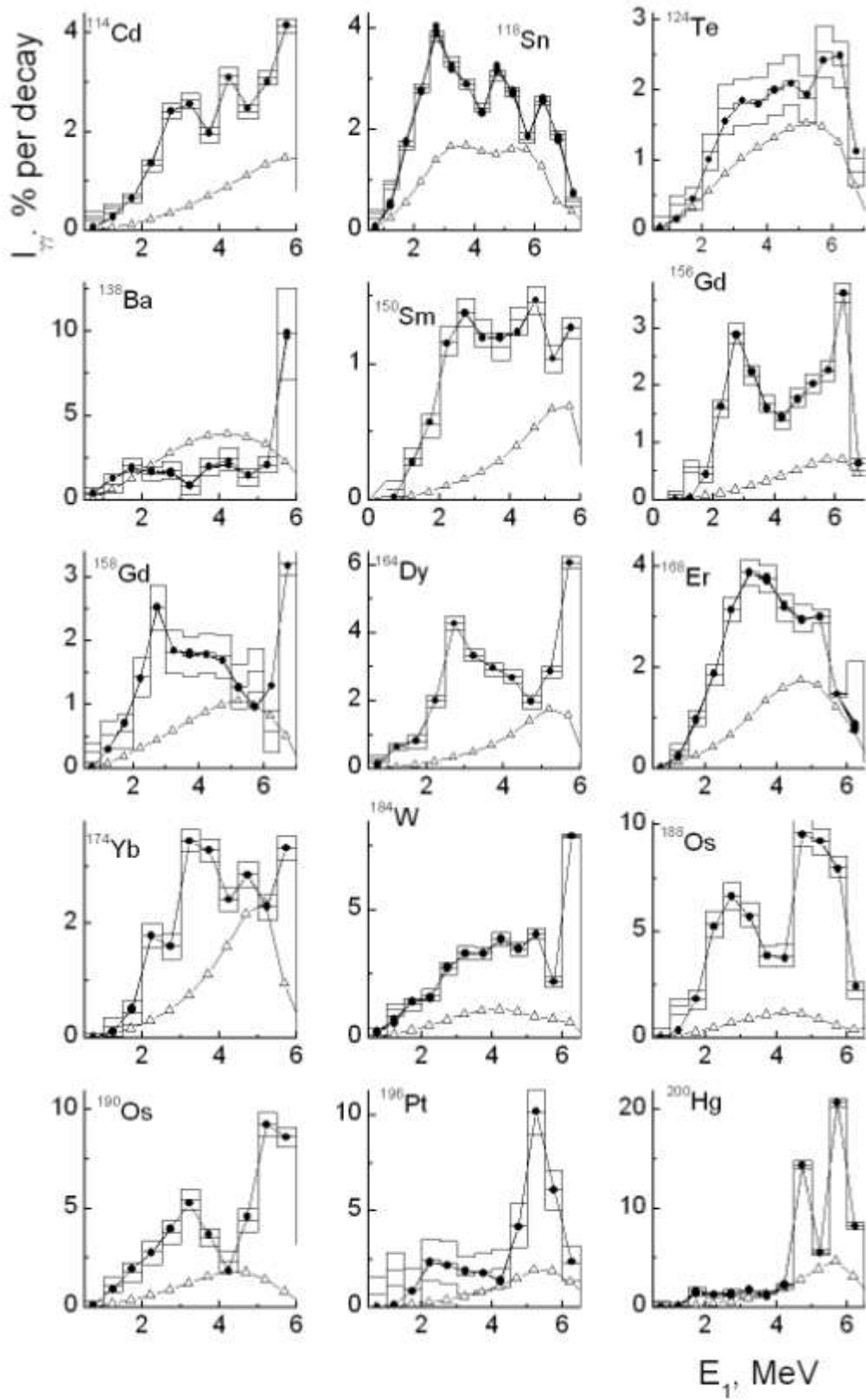


Fig. 2. The same (as fig. 1) for in for even-even nuclei.

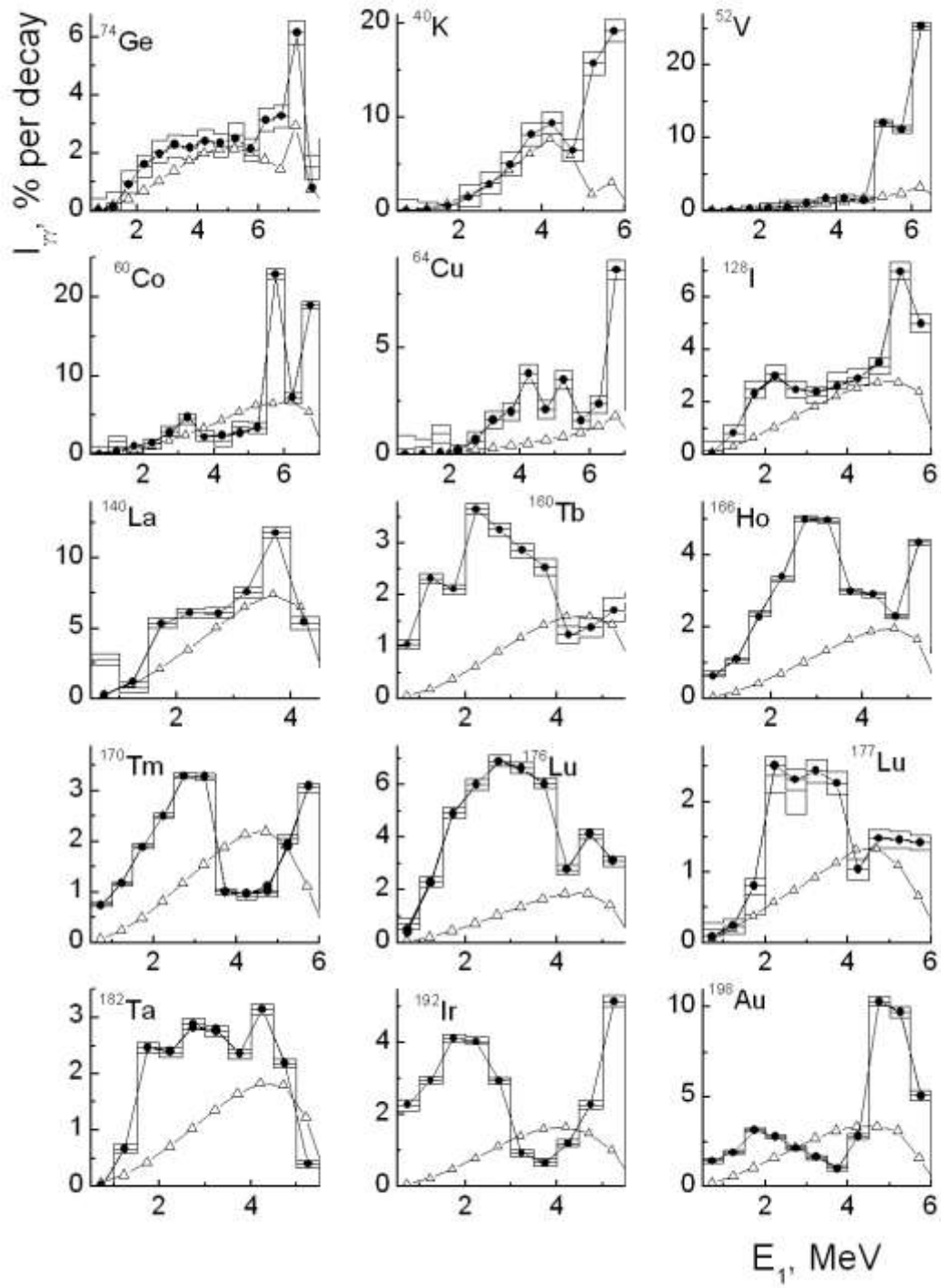


Fig. 3. The same (as fig. 1) for ^{74}Ge , ^{177}Lu and odd-odd nuclei.

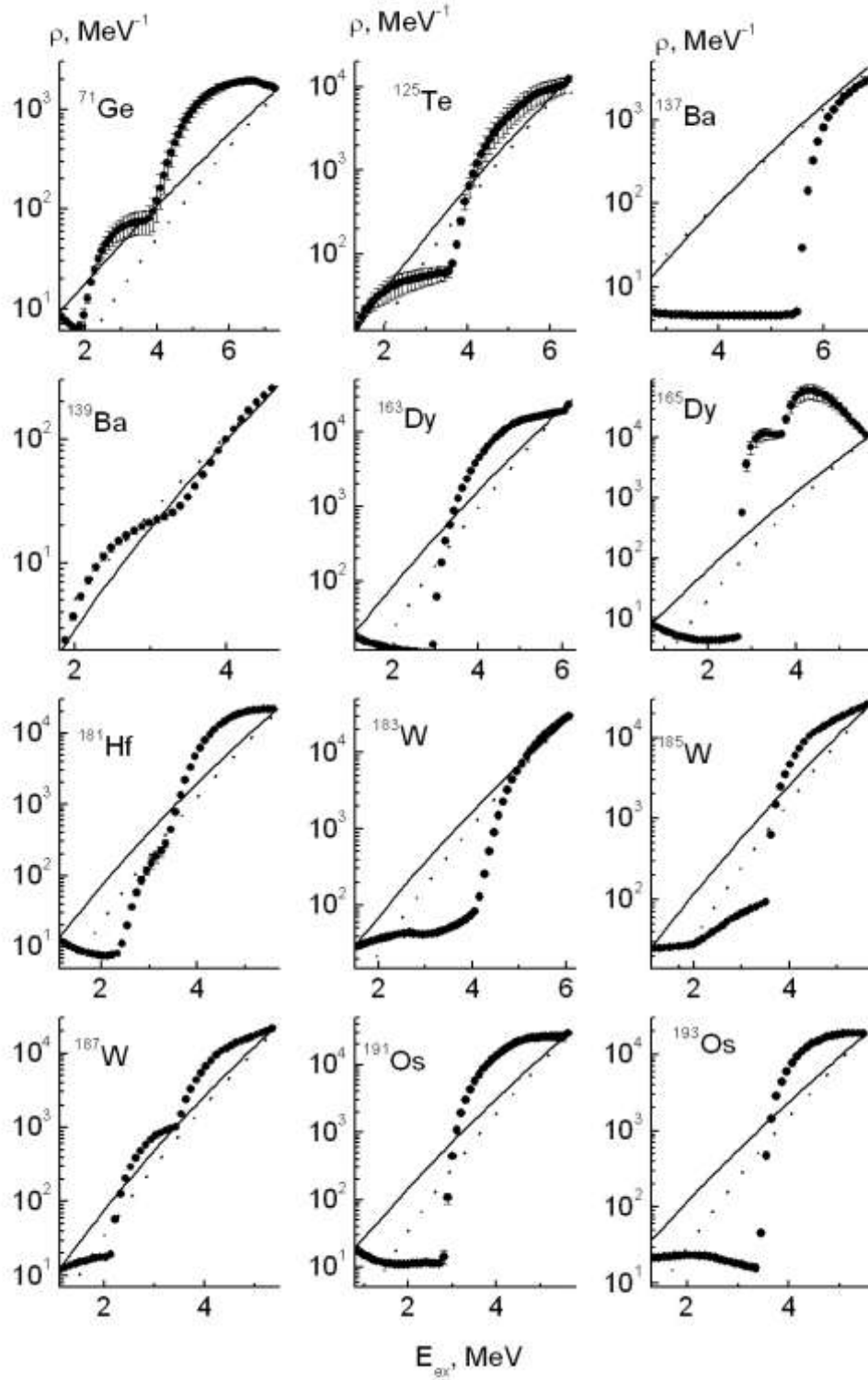


Fig. 4. Average densities of intermediate levels of two-step cascades (points with errors) for even-odd nuclei (fits of the smallest χ^2) depending on the excitation energy. Lines are the data of [19], dotted lines are calculations by model taken into account shell inhomogeneities of single-particle spectrum [11].

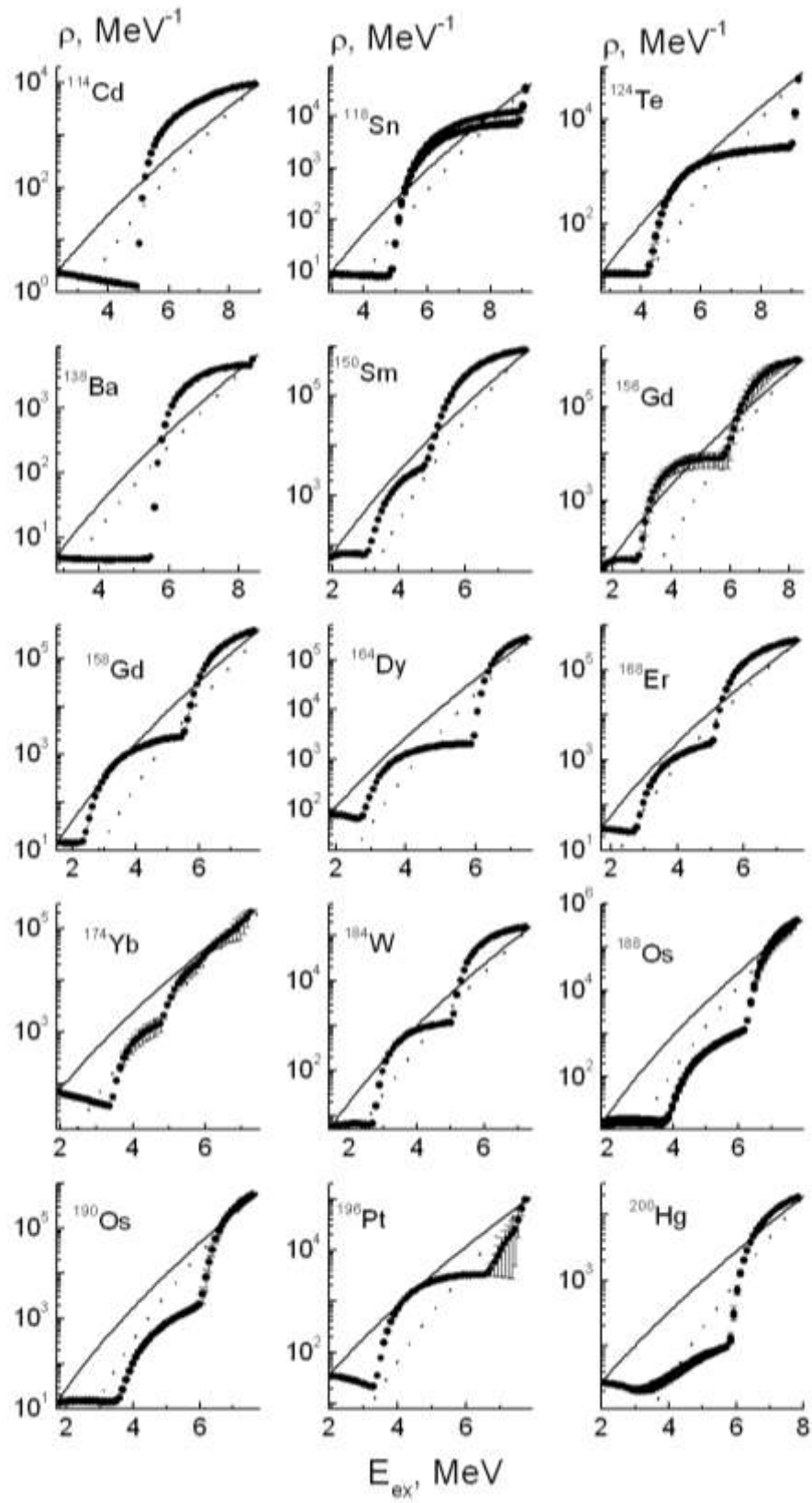


Fig. 5. The same (as fig. 4) for in for even-even nuclei.

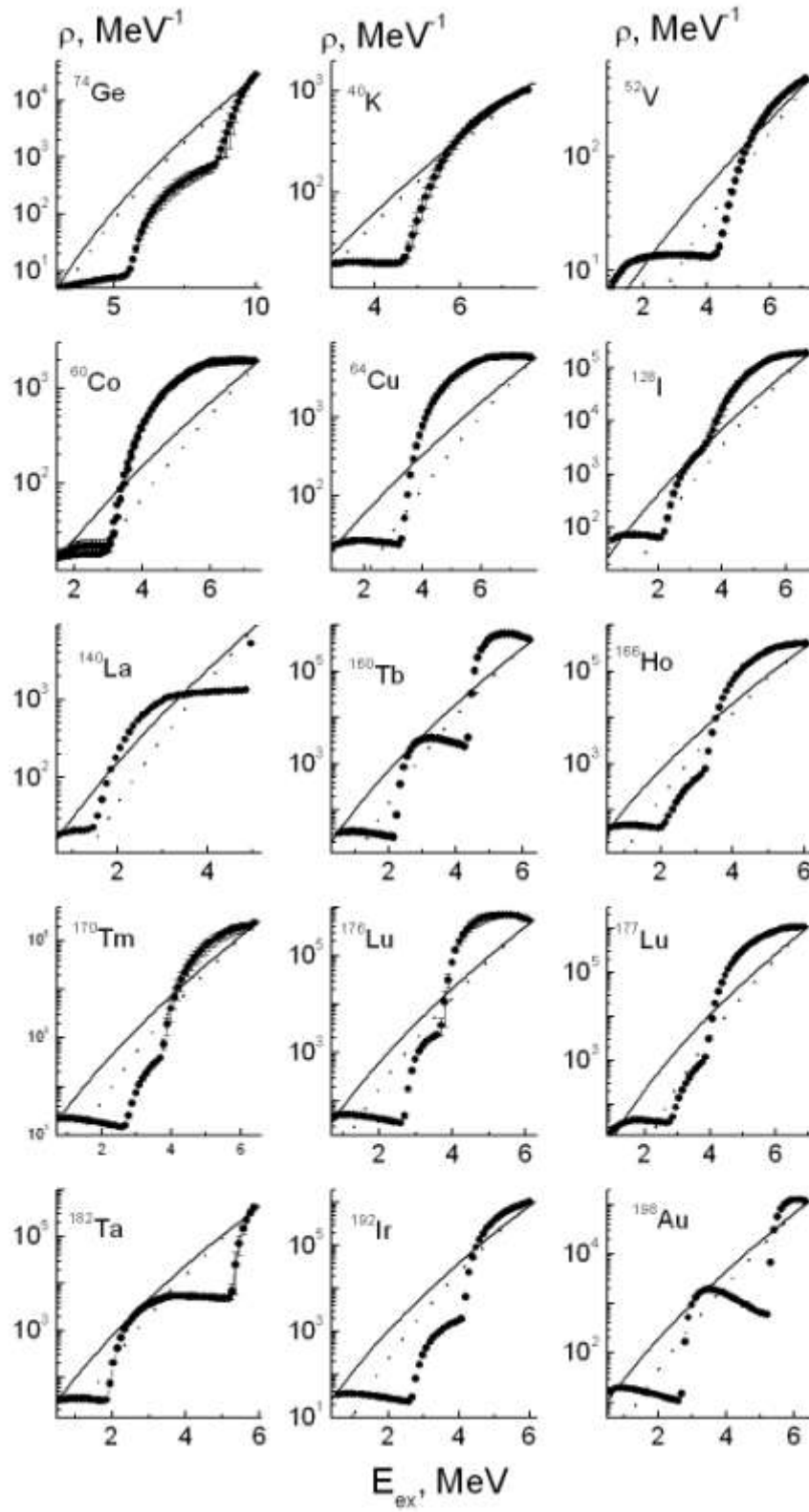


Fig. 6. The same (as fig. 4) for ⁷⁴Ge, ¹⁷⁷Lu and odd-odd nuclei.

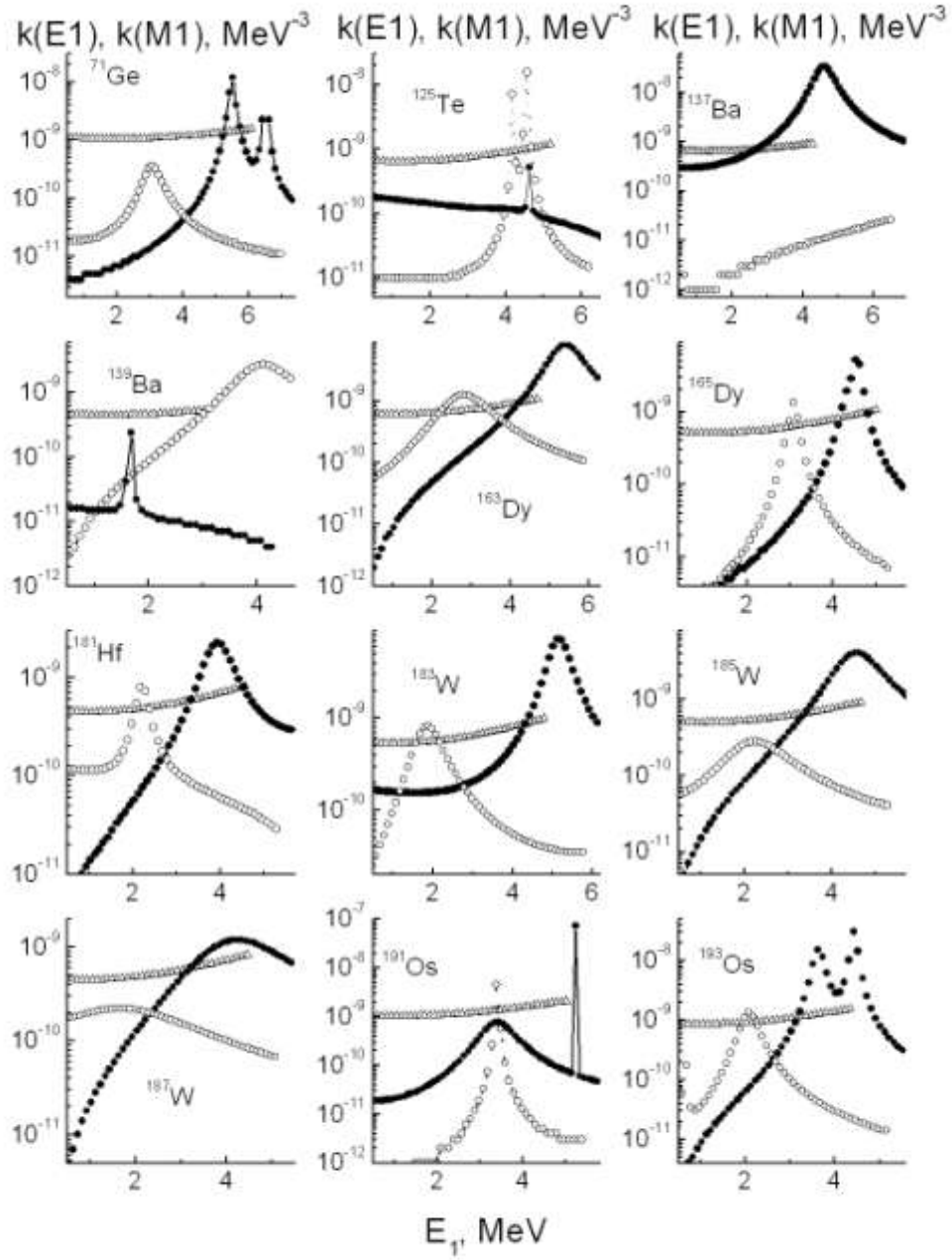


Fig.7. Strength functions of $E1$ -transitions (black points) and of $M1$ -transitions (open points) for even-odd nuclei. Triangles are calculations by model [KMF] adding $k(M1)=\text{const}$ in $0 < E_1 \leq B_n - E_d$ energy range.

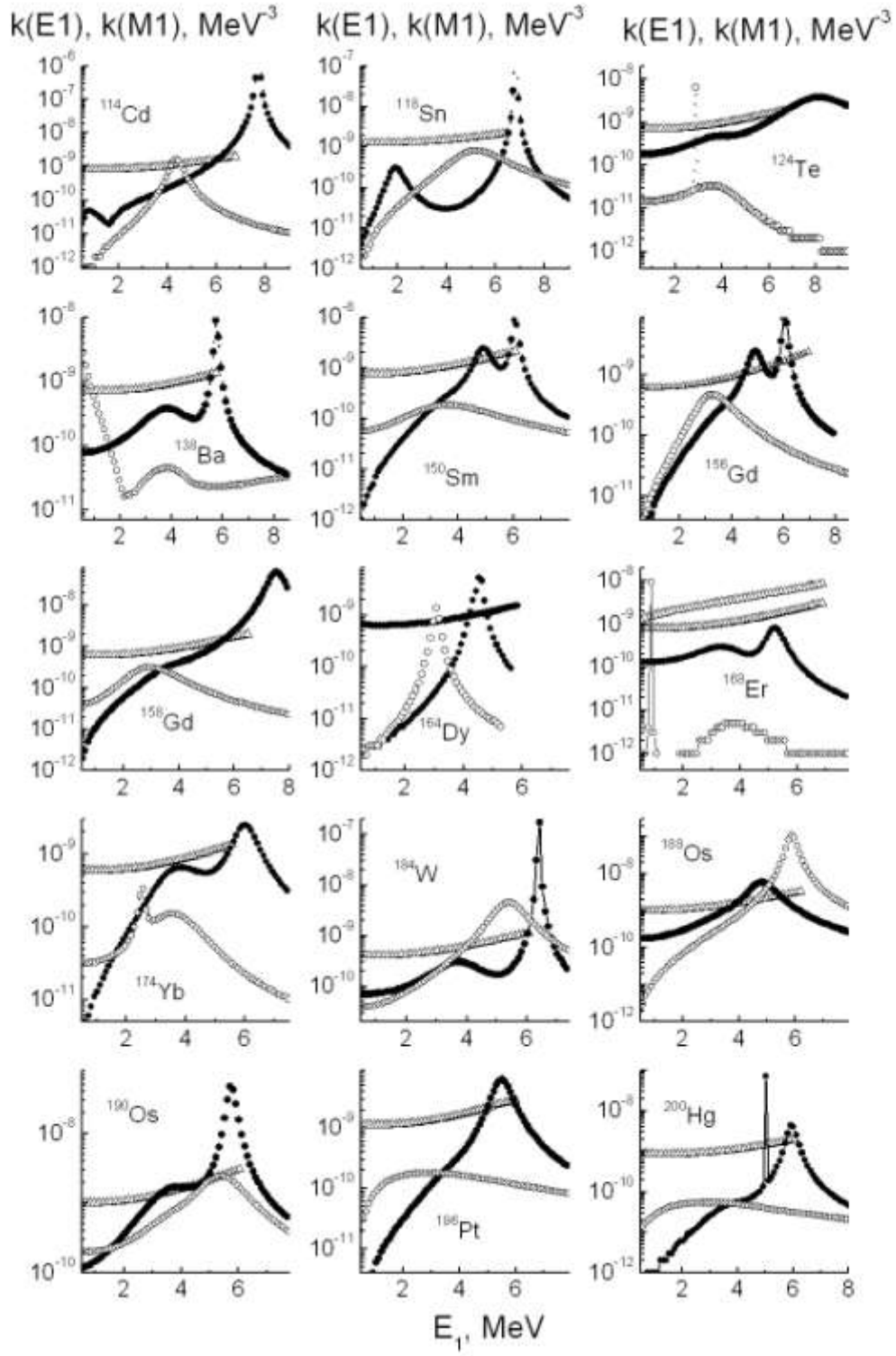


Fig. 8. The same (as fig. 7) for even-even nuclei.

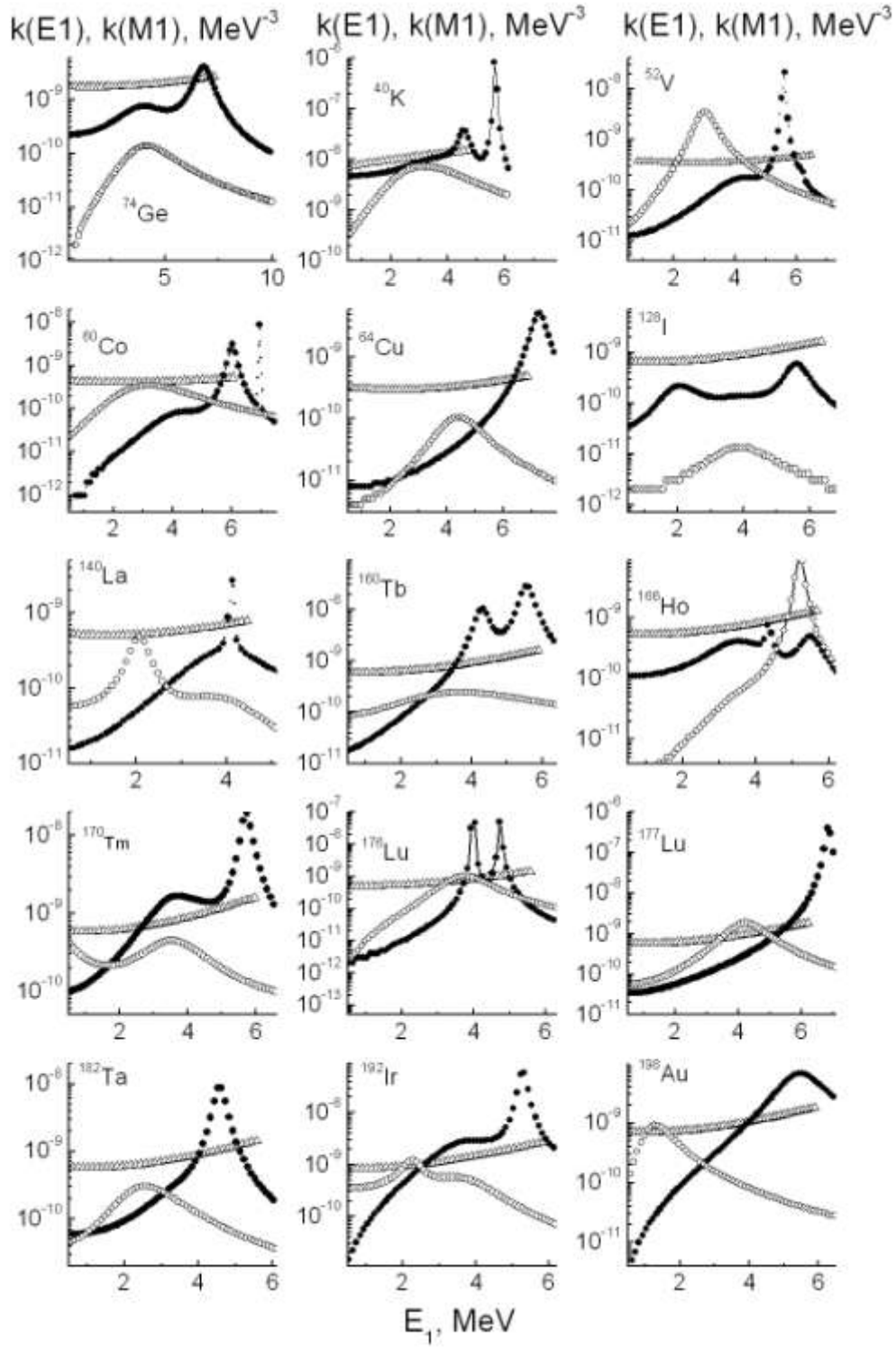


Fig. 9. The same (as fig. 7) for ^{74}Ge , ^{177}Lu and odd-odd nuclei.

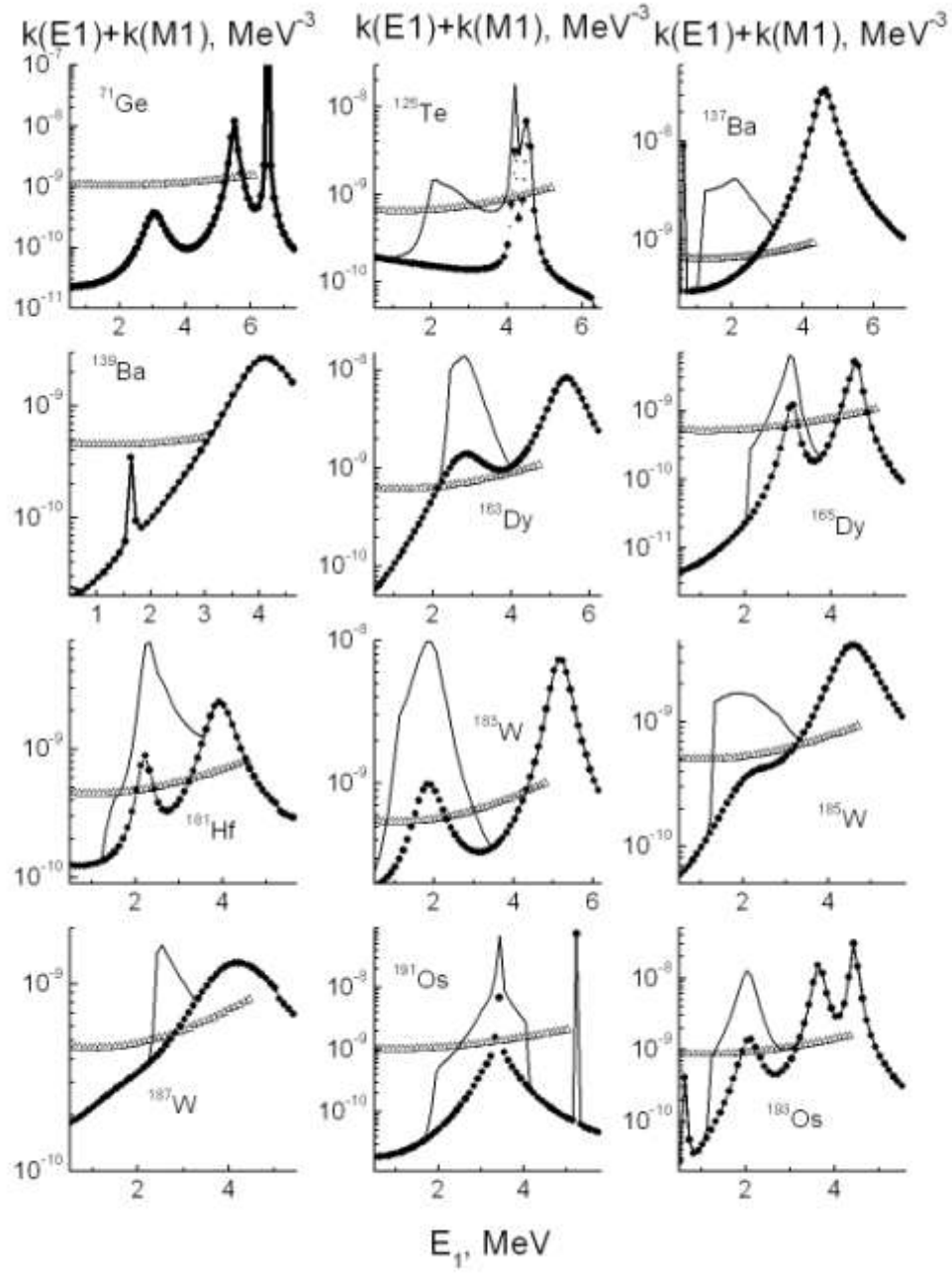


Fig. 10. Sums of strength functions of $E1$ - and $M1$ -transitions (black points) for even-odd nuclei depending on the energy of primary transition. Lines are fits with taking into account the correction (5). Triangles are calculations by model [15] adding $k(M1)=\text{const}$ for $0 < E_1 \leq B_n - E_d$ energy range.

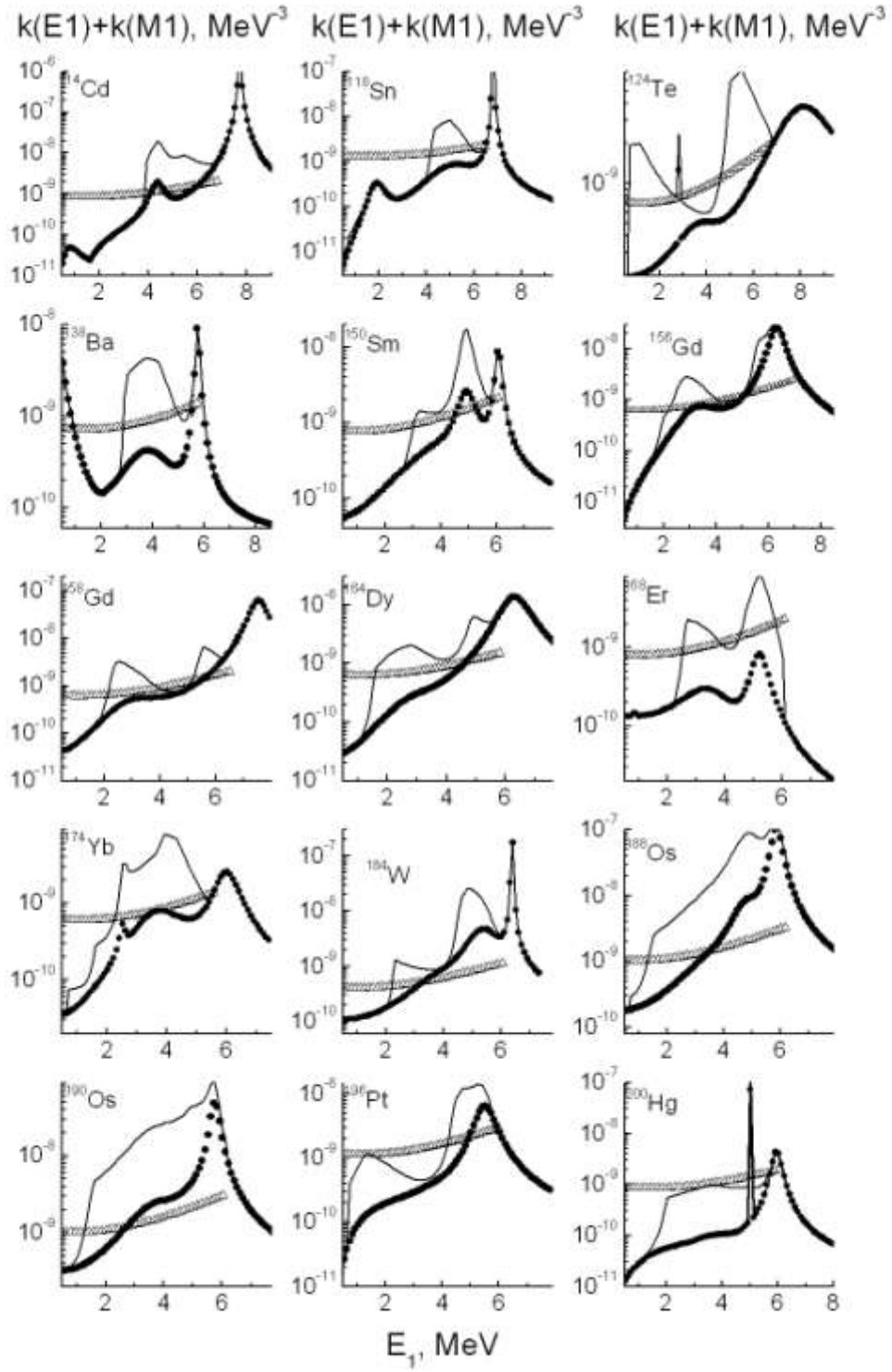


Fig. 11. The same (as fig. 10) for ^{74}Ge , ^{177}Lu and odd-odd nuclei.

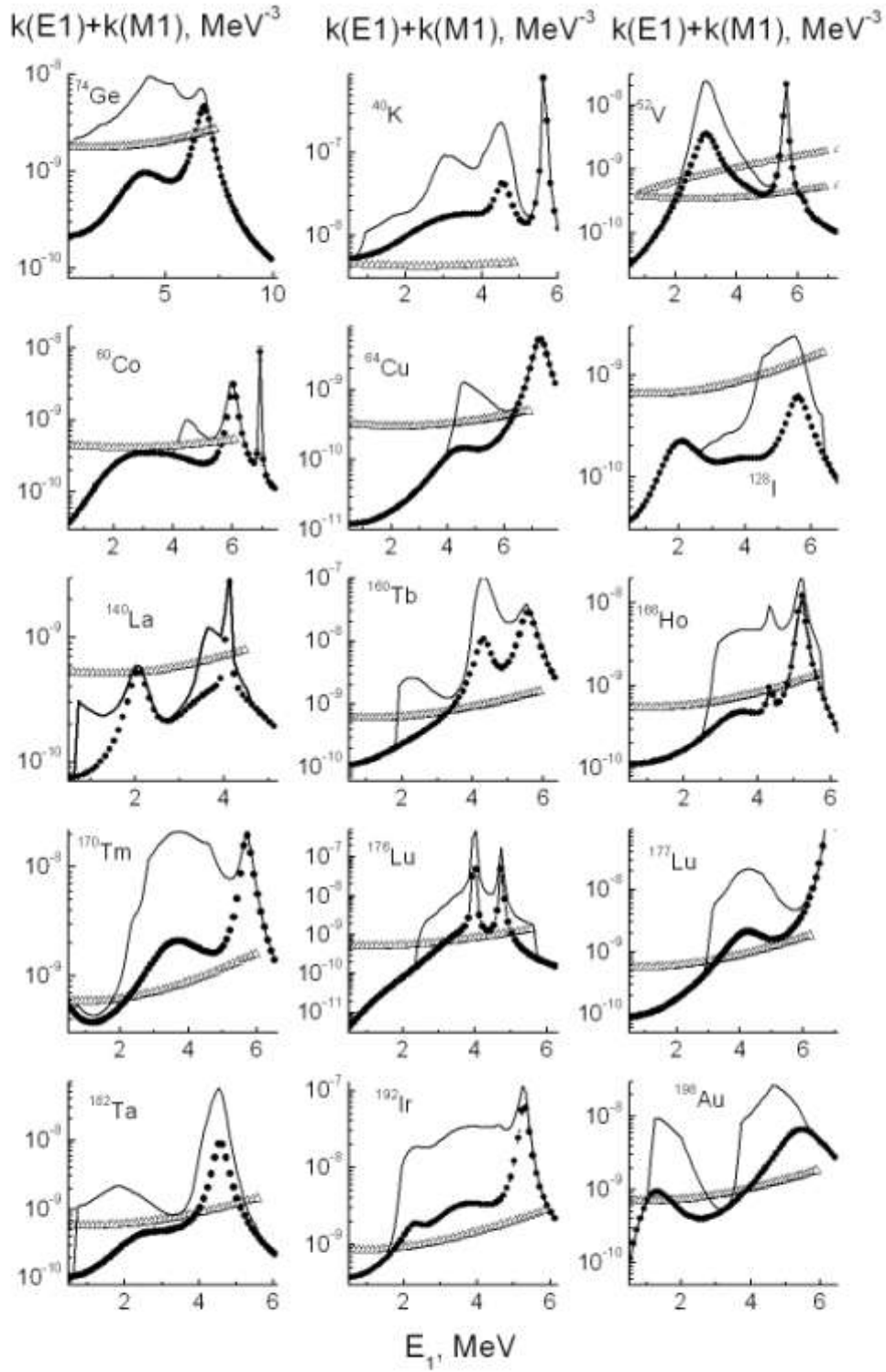


Fig. 12. The same (as fig. 7) for ^{74}Ge , ^{177}Lu and odd-odd nuclei.

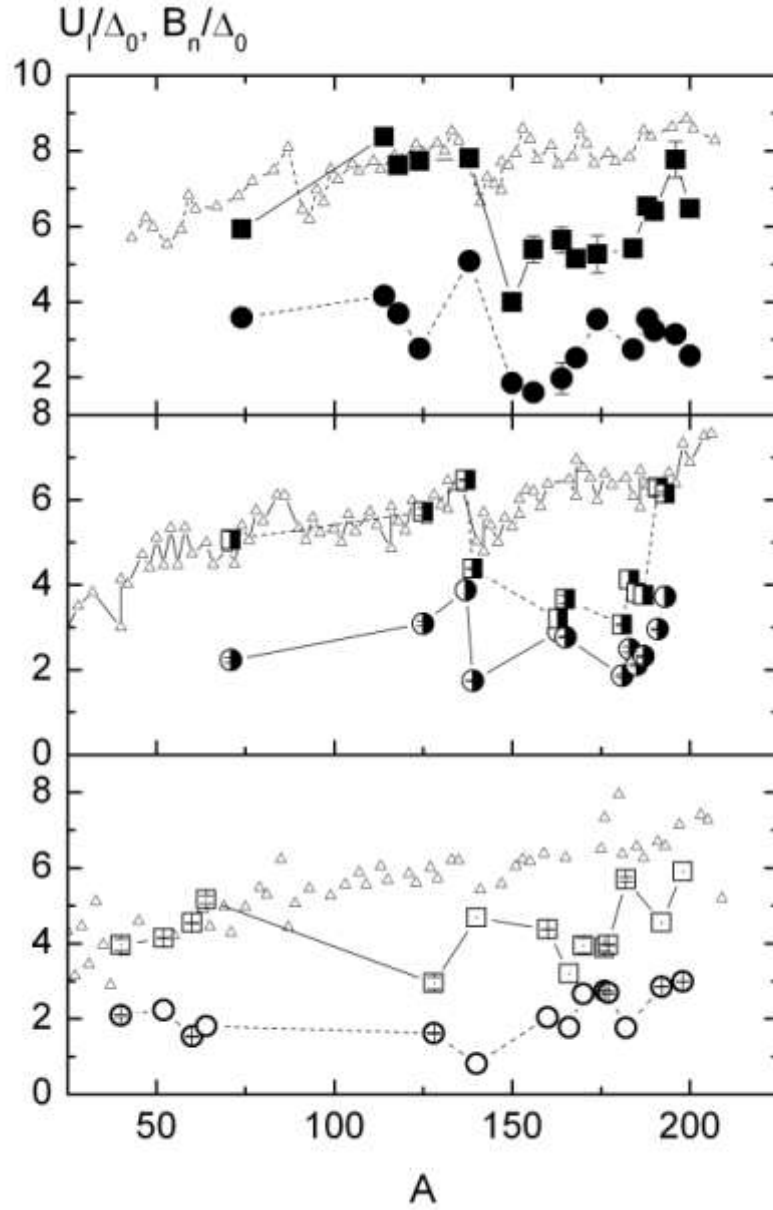


Fig. 13. Mass dependencies of breaking thresholds of the second (points) and of the third (squares) Cooper pairs. Black points – even-even nuclei, half-open points – even-odd nuclei, open points – odd-odd compound- nuclei. Triangles are mass dependencies of B_n/Δ_0 .

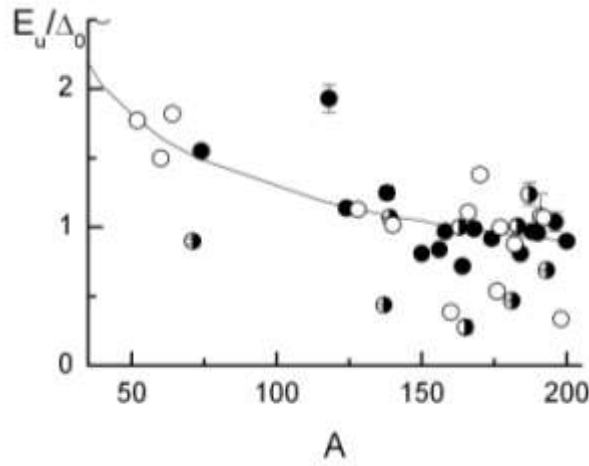


Fig. 14. Dependencies of E_u parameter (2) on nuclear mass A . Black points – even-even nuclei, half-open points – even-odd nuclei, open points – odd-odd compound-nuclei.

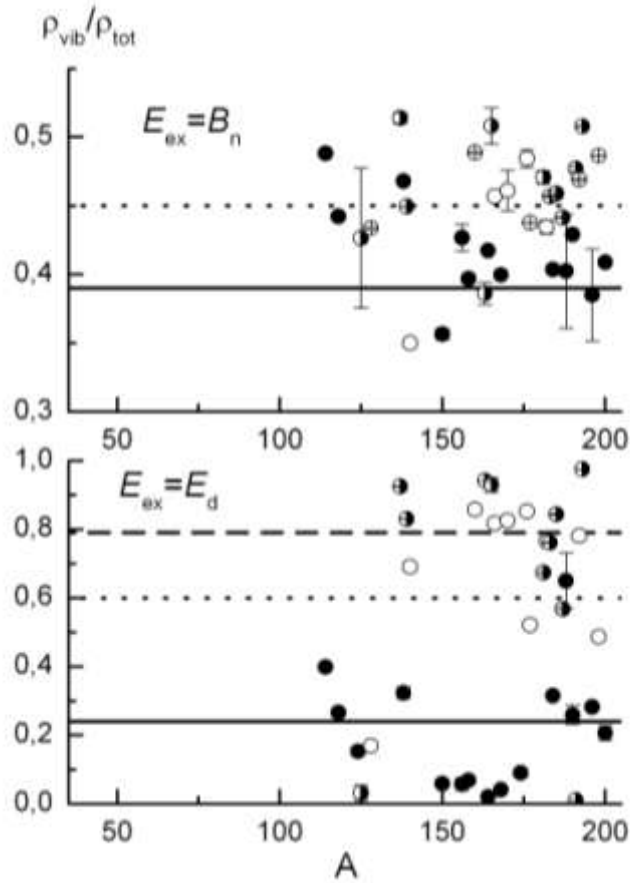


Fig. 15. Mass dependencies of the ration of vibrational level density to the total one near B_n energy (upper picture) and for E_d energy point (bottom picture). Lines – the average of these ratios for even-even nuclei, dashed lines – for even-odd nuclei and dot lines – for odd-odd nuclei.

**ДРУШТВО ЗА ЗАШТИТУ ОД ЗРАЧЕЊА
СРБИЈЕ И ЦРНЕ ГОРЕ**



ЗБОРНИК РАДОВА

**XXIX СИМПОЗИЈУМ ДЗЗСЦГ
Сребрно језеро
27- 29. септембар 2017. године**

**Београд
2017. године**

**SOCIETY FOR RADIATION PROTECTION OF
SERBIA AND MONTENEGRO**



PROCEEDINGS

XXIX SYMPOSIUM DZZSCG

Srebrno jezero

27- 29. September 2017

**Belgrade
2017**

ЗБОРНИК РАДОВА

XXIX СИМПОЗИЈУМ ДЗЗСЦГ
27-29.09.2017.

Издавачи:

Институт за нуклеарне науке „Винча“
Друштво за заштиту од зрачења Србије и Црне Горе

За извршног издавача:

Др Борислав Грубор

Уредници:

Др Јелена Станковић Петровић
Др Гордана Пантелић

ISBN 978-86-7306-144-3

©Institut za nuklearne nauke „Vinča“

Техничка обрада:

Јелена Станковић Петровић, Гордана Пантелић

Штампа:

Институт за нуклеарне науке ”Винча”, Мике Петровића Аласа 12-14, 11351
Винча, Београд, Србија

Тираж:

150 примерака

Година издања:

Септембар 2017.

**XXIX СИМПОЗИЈУМ ДРУШТВА
ЗА ЗАШТИТУ ОД ЗРАЧЕЊА
СРБИЈЕ И ЦРНЕ ГОРЕ**
Сребрно језеро, од 27.09. до 29.09.2017. године

Организатори:

ДРУШТВО ЗА ЗАШТИТУ ОД ЗРАЧЕЊА СРБИЈЕ И ЦРНЕ ГОРЕ

ИНСТИТУТ ЗА НУКЛЕАРНЕ НАУКЕ „ВИНЧА“

Лабораторија за заштиту од зрачења и заштиту животне средине „Заштита“

Организациони одбор:

Председник: Гордана Пантелић

Чланови:

Маја Еремић Савковић, Агенција за заштиту од јонизујућих зрачења и
нуклеарну сигурност, Београд
Вера Спасојевић Тишма, Нуклеарни објекти Србије, Београд
Иван Кнежевић, Нуклеарни објекти Србије, Београд
Данијела Аранђић, Институт за нуклеарне науке „Винча“, Београд
Јелена Станковић Петровић, Институт за нуклеарне науке „Винча“, Београд
Милица Рајачић, Институт за нуклеарне науке „Винча“, Београд
Сандра Ђеклић, Институт за нуклеарне науке „Винча“, Београд
Наташа Сарап, Институт за нуклеарне науке „Винча“, Београд
Предраг Божовић, Институт за нуклеарне науке „Винча“, Београд
Никола Кржановић, Институт за нуклеарне науке „Винча“, Београд

Редакциони одбор:

др Невенка Антовић, Природно математички факултет, Подгорица
др Перко Вукотић, Природно математички факултет, Подгорица
др Софија Форкапић, Природно математички факултет, Нови Сад
др Душан Мрђа, Природно математички факултет, Нови Сад
др Миодраг Крмар, Природно математички факултет, Нови Сад
др Драгослав Никезић, Природно математички факултет, Крагујевац
др Ненад Стевановић, Природно математички факултет, Крагујевац
др Јелена Ајтић, Факултет ветеринарске медицине, Београд
др Владимир Удовичић, Институт за физику, Земун, Београд
др Драгана Тодоровић, Институт за нуклеарне науке „Винча“, Београд
др Ивана Вуканац, Институт за нуклеарне науке „Винча“, Београд
др Јелена Крнета Николић, Институт за нуклеарне науке „Винча“, Београд
др Марија Јанковић, Институт за нуклеарне науке „Винча“, Београд
др Милош Живановић, Институт за нуклеарне науке „Винча“, Београд
др Оливера Цирај-Бјелац, Институт за нуклеарне науке „Винча“, Београд
др Србољуб Станковић, Институт за нуклеарне науке „Винча“, Београд

Организацију су помогли:

Институт за нуклеарне науке „Винча“, Лабораторија за заштиту од зрачења и заштиту животне средине

Излагачи:

Canberra Packard Central Europe GmbH.

Wienersiedlung 6

2432 SCHWADORF, Austria

Phone: +43 (0)2230 3700-0

Fax: +43 (0)2230 3700-15

Web: <http://www.cpce.net/>

LKB Vertriebs GmbH, Представништво Београд

Цвијићева 115

11120 Београд, Србија

Тел: +381 (0)11 676 6711

Факс: +381 (0)11 675 9419

Веб: www.lkb.eu

ТИМ Цо.

Јована Рајића 5ц

11000 Београд,

Тел: +381 11 2836-786, 2836-787

Факс: +381 11 2833-342

Веб: <http://www.timco.rs/>

Овај Зборник је збирка радова саопштених на XXIX Симпозијуму Друштва за заштиту од зрачења Србије и Црне Горе који је одржан од 27. до 29.09.2017. године на Сребрном језеру. Радови су разврстани по секцијама. Мада су сви радови у Зборнику рецензирани од стране Редакционог одбора, за све изнесене тврдње и резултате одговорни су сами аутори.

Југословенско друштво за заштиту од зрачења основано је 1963. године у Порторожу, а од 2005. године носи име Друштво за заштиту од зрачења Србије и Црне Горе.

Ове године Друштво обележава 54 године организоване заштите од зрачења на простору бивше Југославије. Симпозијум Друштва за заштиту од зрачења Србије и Црне Горе је јединствена прилика да кроз стручни програм предочимо напредак у области заштите од зрачења, анализирамо досадашње резултате и актуелна дешавања, разменимо искуства са колегама из земље и региона, али и да сретнемо старе и упознамо нове пријатеље.

Организациони одбор се захваљује ауторима и коауторима научних и стручних радова на доприносу и уложеном труду. Посебно се захваљујемо спонзорима који су помогли одржавања Симпозијума.

Организациони одбор

CIP - Каталогизација у публикацији
Народна библиотека Србије, Београд

502:504.5]:539.16(082)(0.034.2)
614.875/.876(082)(0.034.2)
539.16.04(082)(0.034.2)
539.1.074/.08(082)(0.034.2)
577.1:539.1(082)(0.034.2)

ДРУШТВО за заштиту од зрачења Србије и Црне Горе (Београд). Симпозијум (29 ; 2017 ; Сребрно језеро)

Зборник радова [Електронски извор] / XXIX симпозијум ДЗЗСЦГ [Друштва за заштиту од зрачења Србије и Црне Горе], Сребрно језеро 27- 29. септембар 2017. године ; [организатори] Друштво за заштиту од зрачења Србије и Црне Горе [и Институт за нуклеарне науке "Винча", Лабораторија за заштиту од зрачења и заштиту животне средине Заштита ; уредници Јелена Станковић Петровић, Гордана Пантелић]. - Београд : Институт за нуклеарне науке "Винча" : Друштво за заштиту од зрачења Србије и Црне Горе, 2017 (Београд ; Институт за нуклеарне науке "Винча"). - 1 USB флеш меморија : текст ; 2 x 2 x 14 cm (у задњем делу оловке)

Системски захтеви: Нису наведени. - Насл. са насловне стране документа. - Радови на срп. и енгл. језику. - Текст ћир. и лат. - Тираж 150. - Библиографија уз већину радова. - Abstracts. - Регистар.

ISBN 978-86-7306-144-3

а) Заштита од јонизујућег зрачења - Зборници б) Животна средина - Загађење радиоактивним материјама - Зборници с) Радиоактивно зрачење - Штетно дејство - Зборници д) Нејонизујуће зрачење - Штетно дејство - Зборници е) Радиобиологија - Зборници ф) Дозиметри - Зборници
COBISS.SR-ID 245691404

UTICAJ PROMENA MIONSKOG FLUKSA NA NIVO FONSKA AKTIVNOSTI U NISKOFOONSKIM GAMA SPEKTROMETRIJSKIM MERENJIMA

Nikola JOVANCEVIĆ¹, David KNEŽEVIĆ¹, Miodrag KRMAR¹, Jovana NIKOLOV¹, Nataša TODOROVIĆ¹, Strahinja ILIĆ²

1) Univerzitet u Novom Sad, Prirodno-matematički fakultet, Departman za fiziku, Novi Sad, Republika Srbija, nikola.jovancevic@df.uns.ac.rs

2) Fakultet tehničkih nauka, Novi Sad, Republika Srbija

SADRŽAJ

Mioni predstavljaju glavnu komponentu kosmičkog zračenja na nivou mora, zbog čega su značajan izvor fonske aktivnosti u gama spektrometrijskim merenjima. Fonsku aktivnost mioni mogu proizvoditi interakcijama sa detektorom i okolnim materijalima. Tom prilikom nastali neutroni daju takođe značajan doprinos vrednosti fonske gama aktivnosti. U ovom radu su predstavljeni rezultati merenja korišćenjem HPGe detektora sa gvozdnom i olovnom pasivnom zaštitom u dva okruženja, kada je iznad detektora bila prisutna različita debljina pokrovnog betonskog sloja. Monitoring prisustva miona je vršen korišćenjem plastičnog scintilacionog detektora. Određene su vrednosti inteziteta gama pikova koji se javljaju usled neutronske reakcije i upoređeni su sa promenom prisustva miona u okruženju detektora. Dobijeni rezultati mogu poslužiti za unapređenje projektovanja zaštite prilikom niskofonskih gama spektrometrijskih merenja.

1. UVOD

Mioni su jedna od glavnih komponenta kosmičkog zračenja na nivou mora [1]. Putem različitih interakcija oni daju bitan doprinos odbroju fonskog zračenja u različitim niskofonskim gama spektroskopskim merenjima [2-6]. Jedan od načina na koji mioni utiču na detekciju fonskih događaja je njihova interakcija sa detektorom i okolnim materijalima, prvenstveno materijalima zaštite detektora. Tom prilikom pre svega putem zahvata miona na materijalima velike gustine i visokog rednog broja može doći do produkcije neutrona [6-8]. Na ovaj način kreirani neutroni interaguju sa detektorom i okolnim materijalima. Ove interakcije se pre svega odvijaju putem zahvata neutrona i njihovog rasejanja. To dovodi do toga da se u snimljenim gama spektrima detektuju gama pikovi koji prate deekscitaciju jezgara pobuđenih u ovim procesima [9,10]. Detekcija ovih događaja je često neželjena tokom različitih gama spektroskopskih merenja. Zbog toga je od važnosti analizirati kako se gama aktivnost uzrokovana interakcijama fonskog neutronske spektra menja u zavisnosti od promene prisustva miona u okruženju detektora [11-17]. Treba napomenuti da se doprinos miona fonskom zračenju otklanja izgradnjom dubokih podzemnih laboratorija ili korišćenjem različitih aktivnih zaštita [18, 19]. Međutim, u ovom radu biće razmatran ovaj doprinos u nadzemnim laboratorijama sa malom debljinom pokrovnog sloja.

Da bi se analizirala korelacija između prisustva miona i gama aktivnosti indukovane neutronske interakcijama u ovom radu su vršena merenja sa dva HPGe detektora koja su bila prisutna u dva različita okruženja. U prvom slučaju iznad detektora je bio tanji pokrovni sloj u vidu jedne betonske ploče, dok je u drugom slučaju debljina pokrovnog

sloja bila četiri betonske ploče. Monitoring prisustva miona je izvršen merenjima pomoću plastičnog scintilacionog detektora. Treba napomenuti i da su HPGe detektori imali dve različite zaštite, olovnu i gvozdenu, te je na taj način analiziran i uticaj promene mionskog fluksa na produkciju neutrona u ovim materijalima.

Snimljeni gama spektri su analizirani i utvrđeni su intenziteti gama pikova koji potiču od neutronske reakcije i njihova promena je upoređena sa varijacijama prisustva miona u okruženju detektora. Ovakva analiza može poslužiti za buduće projektovanje i izgradnju niskofonskih gama spektroskopskih laboratorija.

2. EKSPERIMENTALNA POSTAVKA I MERENJA

Gama spektrometrijska merenja su izvršena na Departmanu za fiziku, PMF, Novi Sad. Tom prilikom su korišćena dva germanijumska poluprovodnička detektora (HPGe) [10, 12, 14].

Prvi detektorski sistem se sastojao od HPGe detektora proizvođača Canberra. Detektor je koaksijalni n-tipa, sa U-tipom kriostatske konfiguracije. Relativna efikasnost ovoga detektora je 100 % i aktivna zapremina mu je 380 cm^3 . Detektor je postavljen u kućište sa prednjim prozorom od karbon fibera visoke čistoće sa debljinom od 0.89 mm, što omogućava visoku efikasnost za detekciju zračenja i sa energijama manjim od 20 keV. Detektor se nalazio u pasivnoj zaštiti izrađenoj od olova (Canberra model 777B). Ukupna masa zaštite je 1633 kg. Debljina zaštite je 15 cm s tim što je 125 cm spoljašnjeg sloja zaštite izgrađeno od običnog niskoaktivnog olova a unutrašnji sloj od 25 cm je od posebno namenjenog olova koje sadrži koncentraciju aktivnosti ^{210}Pb od 20 Bq/kg. Zaštita takođe sadrži i sloj bakra debljine 1.5 mm i kalaja debljine 1 mm [10].

Drugi detektorski sistem je HPGe detektor relativne efikasnosti 22.3% i zapremine 119 cm^3 (Canberra model G.C.2525-7600). Detektor je bio smešten u gvozdenoj zaštiti zidova debljine 25 cm i mase od oko 20 tona [10]. Zaštita je proizvedena od gvožđa izlivenog pre Drugog svetskog rata zbog čega ne sadrži radioaktivnu kontaminaciju prouzrokovanu nuklearnim probama i havarijama na nuklearnim postrojenjima. Gvozdena zaštita je oblika kocke i ima korisnu zapreminu od oko 1 m^3 što omogućava postavljanje u zaštitu detektora zajedno sa Djuardovim sudom.

Monitoring prisustva miona je vršen korišćenjem plastičnog scintilatora. Ovaj detektor je dimenzija 50cm·50cm·5cm. Proizvođač detektora je Sconix Holland BV a tip detektora je R500*50 N 500/2P+VD 10-E2-X. Ova vrsta detektora je prvenstveno namenjena za izgradnju aktivnih zaštita germanijumskih detektora prilikom niskofonskih gama spektrometrijskih merenja.

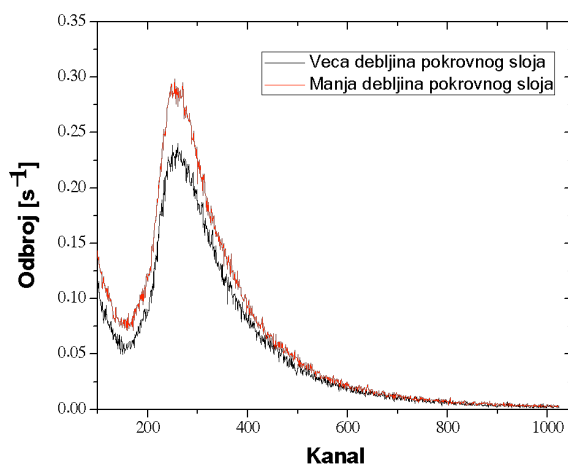
Merenja u ovom radu sa dva germanijumska sistema i detektorom za praćenje prisustva miona su vršena na dve lokacije. Na prvoj lokaciji debljina pokrovnog sloja je bila od jedne betonske ploče debljine oko 20 cm dok je na drugoj lokaciji debljina pokrovnog sloja bila četiri betonske ploče (oko 80 cm). Mogućnost za ova merenja se javila usled preseljenja Laboratorije za gama spektroskopiju na Departmanu za fiziku u Novom Sadu. Na ovaj način je bilo moguće izvršiti analizu promene prisustva miona u dva različita okruženja i takođe analizirati promene u snimljenim gama spektrima.

Za potrebnu analizu su izvršena snimanja vremenski dugih fonskih spektara sa vremenom merenja od 252237 s do 2473816 s. Takođe na obe lokacije su vršena merenja i sa scintilacionim detektorom pri čemu su vremena merenja bila oko 2 h. To vreme merenja je bilo dovoljno da prikupljen broj događaja bude zadovoljavajući za statističku analizu podataka.

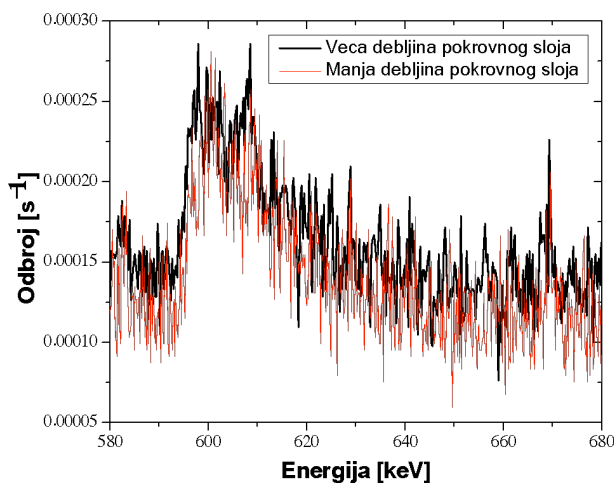
3. REZULTATI

Na slici 1 prikazani su snimljeni spektri sa scintilacionim detektorom na dve lokacije. U spektrima se uočava karakterističan pik od interakcije miona sa detektorom. Određen je ukupan odbroj ispod mionskog pika i vrednosti za dva data merenja su upoređene. Dobijeni rezultati si prikazani u tabeli 1.

Svi snimljeni gama spektri sa germanijumskim detektorima su analizirani pri čemu je posebna pažnja posvećena analizi broja detektovanih gama kvanata koji se javljaju usled interakcija neutrona sa germanijumom. Posebno su zanimljiva dva gama pika. Prvi od njih je sa energijom od 139,9 keV i prati zahvat neutrona na izotopu germanijuma ^{74}Ge ($^{74}\text{Ge}(n,\gamma)^{75\text{m}}\text{Ge}$) [2]. Ovaj gama pik se standardno koristi za određivanje prisustva sporih neutrona u niskofonskim spektrometrijskim sistemima sa Ge detektorima. Na slici 3 su prikazani delovi snimljenih spektara sa uočljivim pikom energije od 139,9 keV. Drugi gama pik čiji je intenzitet analiziran, prikazan na slici 2, ima energiju od 691 keV i detektuje se usled neelastičnog rasejanja neutrona na izotopu germanijuma ^{72}Ge ($^{72}\text{Ge}(n,n')^{72}\text{Ge}$) [2]. Ovaj gama pik se standardno koristi kao indikator prisustva brzih neutrona u samom germanijumskom detektoru.



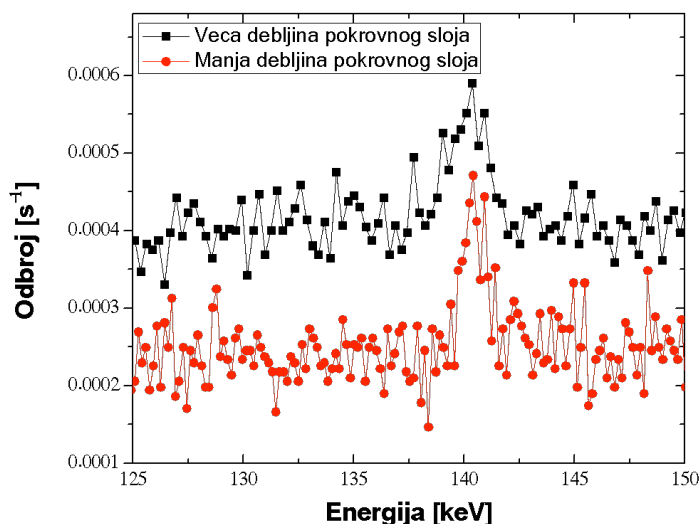
Slika 1. Snimljeni spektri sa scintilacionim detektorom na dve različite lokacije sa uočljivim pikom koji potiče od detekcije miona



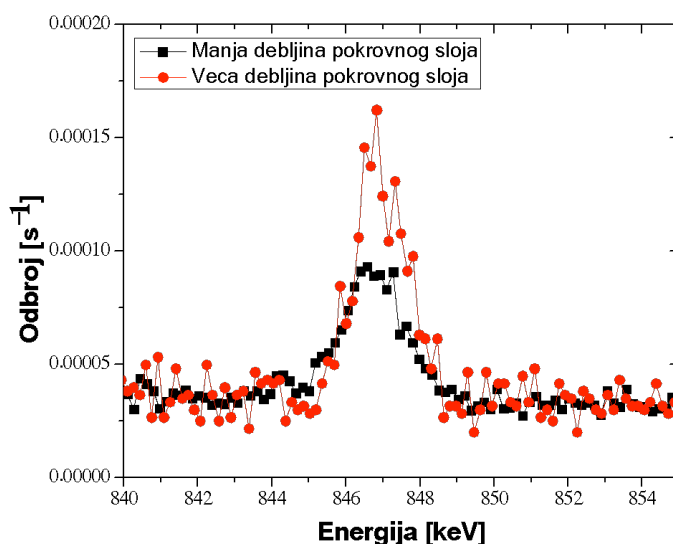
Slika 2. Deo snimljenih spektara sa HPGe detektorom u olovnoj zaštiti sa uočljivim gama pikom od 691 keV koji prati reakciju $^{72}\text{Ge}(n,n')^{72}\text{Ge}$

Intenziteti ovih pikova su određeni i upoređeni su njihovi odnosi za oba HPGe detektora na dve merne lokacije. Rezultati su prikazani u tabeli 1.

Za analizu prisustva brzih neutrona u gvozdenoj zaštiti posebno može poslužiti gama pik energije od 846,8 keV koji prati reakciju $^{56}\text{Fe}(n,n')^{56}\text{Fe}$. Zbog toga su i intenziteti ovoga pika analizirani i predstavljeni u tabeli 1, dok je deo spektra koji sadrži ovaj pik prikazan na slici 4.



Slika 3. Deo snimljenih spektara sa HPGe detektorom u olovnoj zaštiti sa uočljivim gama pikom od 139 keV koji prati reakciju $^{74}\text{Ge}(n,\gamma)^{75\text{m}}\text{Ge}$



Slika 4. Deo snimljenih spektara sa HPGe detektorom u gvozdenoj zaštiti sa uočljivim gama pikom od 846.8 keV koji prati reakciju $^{56}\text{Fe}(n,n')^{56}\text{Fe}$

Tabela 1. Detektovani intenziteti i odnosi gama pikova koji potiču od neutronske interakcije sa Ge detektorom i detektovani intenziteti mionskih događaja. Pozicija 1 - manja debljina pokrovnog sloja, Pozicija 2 - veća debljina pokrovnog sloja

	Pozicija 1	Pozicija 2	I_1/I_2
	$I_1[s^{-1}]$	$I_2[s^{-1}]$	
Odbroj mionskih događaja	56,51(28)	46,63(23)	1,212(8)
139,9 keV $^{72}\text{Ge}(n,\gamma)^{73}\text{Ge}$ HPGe sa Pb zaštitom	0,00128(7)	0,00088(5)	1,47(11)
139,9 keV $^{72}\text{Ge}(n,\gamma)^{73}\text{Ge}$ HPGe sa Fe zaštitom	0,00134(5)	0,000618(16)	2,18(8)
691 keV $^{74}\text{Ge}(n,n')^{74}\text{Ge}$ HPGe sa Pb zaštitom	0,00463(14)	0,00338(9)	1,37(5)
691 keV $^{74}\text{Ge}(n,n')^{74}\text{Ge}$ HPGe sa Fe zaštitom	0,0008(1)	Nije detektovano	-
846,8 keV $^{56}\text{Fe}(n,n')^{56}\text{Fe}$	0,00119(4)	0,000710(17)	1,69(7)

4. DISKUSIJA I ZAKLJUČAK

U ovom radu analiziran je uticaj promene prisustva miona na fonske događaje generisane neutronske reakcijama sa germanijumskim detektorima u olovnoj i gvozdenoj zaštiti. Monitoring mionskog fluksa sa scintilacionim detektorom je pokazao da je na lokaciji sa manjim pokrovnim slojem prisutan oko 20% veći broj miona. Što je i očekivan rezultat usled veće atenuacije miona u većoj debljini materijala.

Rezultati pokazuju da smanjenje broja miona prati i smanjenje broja detektovanih odbroja u gama pikovima koji potiču od neutronske reakcije. To je posledica manje produkcije neutrona u materijalu zaštite detektora usled manjeg broja miona koji stižu do detektora u slučaju veće debljine pokrovnog sloja. Međutim, smanjenje broja neutrona je različito za detektore sa olovnom i gvozdenom zaštitom. Uočava se da je promena broja neutrona mnogo manja u olovnoj nego u gvozdenoj zaštiti (tabela 1). Smanjenje broja sporih neutrona (poređenje intenziteta gama linije od 139,9 keV) je u olovu oko 47% dok je u gvožđu značajno veće, čak više od dva puta. Isti trend se zapaža i za brze neutrone (gama linija od 691 keV). Broj brzih neutrona procenjen na osnovu neutronske interakcije sa Ge je za oko 40% veći u slučaju manje debljine pokrovnog sloja. U slučaju Ge detektora u gvozdenoj zaštiti gama pik od 691 keV nije detektovan i neophodno je izvršiti fonsko merenje sa većim periodom merenja da bi se mogao utvrditi intenzitet ovoga pika. Odnosi detektovanih intenziteta gama pika od 846 keV upućuju na smanjenje broja brzih neutrona od oko 70% u gvozdenoj zaštiti.

Ovde prikazani rezultati će biti osnova za dalju analizu uticaja promene mionskog fluksa na produkciju neutrona u različitim materijalima koji su prisutni u okruženju germanijumskih detektora tokom niskofonskih gama spektroskopskih merenja. Ova analiza takođe može pružiti i informacije značajne za buduće projektovanje i izgradnju niskofonskih laboratorija za gama spektrometriju.

5. LITERATURA

- [1] In: Povinec, P.P. (Ed.), Analysis of Environmental Radionuclides. Elsevier, Amsterdam, pp. 209–239. S. Niese, 2008. Underground laboratories for low-level radioactivity measurements.
- [2] G.P. Škoro et al., Environmental neutrons as seen by a germanium gamma-ray spectrometer, Nucl. Instr. and Meth. A 316 (1992) 333-336.
- [3] G. Fehrenbacher et al., Fast neutron detection with germanium detectors: computation of response functions for the 692 keV inelastic scattering peak, Nucl. Instr. and Meth. A 372 (1996) 239-245.
- [4] G. Heusser, Cosmic ray interaction study in low-level Ge spectrometry, Nucl. Instr. And Meth. A 369 (1996) 539-543.
- [5] R. Wordel et al., Study of neutron and muon background in low-level germanium gamma-ray spectrometry, Nucl. Instr. And Meth. A 369 (1996) 557-562.
- [6] W.V. Scroder et al, Z. Phys. 239 (1974) 57.
- [7] E. Gete et al., Neutron-induced peaks in Ge detectors from evaporation neutrons, Nucl. Instr. And Meth. A 388 (1997) 212-219.
- [8] T. Siiskonen and H. Toivonen, A model for fitting peaks induced by fast neutrons in an HPGe detector, Nucl. Instr. And Meth. A 540 (2005) 403-411.
- [9] M. Krmar et al., A method to estimate a contribution of Ge(n,n') reaction to the low-energy part of gamma spectra of HPGe detectors, Nucl. Instr. And Meth. A 709, (2013) 8-11.
- [10] N. Jovancevic and M. Krmar, Analysis of Neutron Induced Gamma Activity in Lowbackground Ge – Spectroscopy Systems, Physics Procedia, 31, (2012) 93-98.
- [11] M. Krmar et al., Measurement of ^{56}Fe activity produced in inelastic scattering of neutrons created by cosmic muons in an iron shield, Applied Radiation and Isotope, 70(1), (2012), 269-273.
- [12] N. Jovančević and M. Krmar, Neutrons in the low-background Ge-detector vicinity estimated from different activation reactions, Applied Radiation and Isotopes, 69, (2011), 629-635.
- [13] N. Jovančević et al., Neutron induced background gamma activity in low-level Ge-spectroscopy systems, Nucl. Instr. And Meth. A 612, (2009), 303-308.
- [14] I. Bikit et al., Production of X-rays by cosmic-ray muons in heavily shielded gamma-ray spectrometers, Nucl. Instrum. Methods A 606, (2009), 495-500.
- [15] S. Croft et al., The specific total and coincidence cosmic-ray-induced neutron production rates in materials, Nucl. Instrum. Methods A 505, (2003), 536–539.
- [16] Da Silva et al., Neutron background for a dark matter experiment at a shallow depth site, Nucl. Instrum. Methods Phys. Res. A 354, (1995), 553-559.
- [17] Y. Feige et al., Production rates of neutrons in soils due to natural radioactivity, J. Geophys. Res. 73, (1968), 3135–3142.
- [18] G. Heusser, 1994. Background in ionizing radiation detection. In: Garcia-Leon, M., Gracia-Tenorio, R. (Eds.), Low-Level Measurements of Radioactivity in the Environment. Word Scientific, Singapore, pp. 69–112.
- [19] G. Heusser, Low-radioactivity background techniques, Annu. Rev. Nucl. Part. Sci. 45, (1995), 543–590.

**INFULECE OF MUON FLUX VARIATIONS TO LEVEL OF
BACKGROUND ACTIVITY DURING LOW-BACKGROUND
GAMMA SPECTROMETRIC MEASUREMENTS**

**Nikola JOVANČEVIĆ¹, David KNEŽEVIĆ¹, Miodrag KRMAR¹, Jovana
NIKOLOV¹, Nataša TODOROVIĆ¹, Strahinja ILIĆ²**

- 1) *University of Novi Sad, Faculty of Science, Department of Physics, Novi Sad,
Republic of Serbia, nikola.jovancevic@df.uns.ac.rs*
2) *Faculty of Technical Sciences, Novi Sad, Republic of Serbia*

ABSTRACT

Muons are one of the main components of cosmic radiation on the sea level and there are significant source background activities during gamma spectroscopic measurements. Background activity can be produced by muon interactions with detector and surrounding materials. On this way created neutrons also have high influence on detection of background events. In this work there are presented the results of measurements by use of HPGe detectors with iron and lead shields. The detectors were located in two different environments where the different thicknesses of covering concrete layer were present. The monitoring of muons presence was done by measurements with plastic scintillation detector. The levels of neutron induced gamma activates were determinated and compared with changing of muon flux in detectors environment. The results can be used for improving of new detector shield in gamma spectrometry measurements.

ODREĐIVANJE ENERGETSKOG SPEKTRA NEUTRONA PRISUTNOG U GAMA SPEKTROMETRIJSKIM MERENJIMA SA GERMANIJUMSKIM DETEKTORIMA

Nikola JOVANCEVIĆ¹, David KNEŽEVIĆ^{1,2}, Miodrag KRMAR¹, Jovana NIKOLOV¹, Nataša TODOROVIĆ¹, Jovana PETROVIĆ¹

1) *Univerzitet u Novom Sadu, Prirodno-matematički fakultet, Departman za fiziku, Novi Sad, Republika Srbija, nikola.jovancevic@df.uns.ac.rs*

2) *Institut za fiziku, Univerzitet u Beogradu, Republika Srbija*

SADRŽAJ

Određivanje prisustva neutrona tokom niskofonskih gama spektrometrijskih merenja je od posebne važnosti. Zbog toga je u ovom radu analiziran način određivanja energetskog spektra neutrona prisutnog u merenjima sa HPGe detektorima. Ovaj metod se zasniva na korišćenju metoda dekonvolucije. Za to je neophodno poznavati gama aktivnost indukovanu neutronske reakcijama sa različitim izotopima germanijuma kao i efikasne preseke za date neutronske reakcije. Ovaj pristup je testiran merenjima sa fisionim izvorom neutrona ²⁵²Cf koji je bio postavljen u blizini HPGe detektora. Dobijeni rezultati pokazuju da ovaj metod može pružiti pouzdane podatke o obliku energetskog spektra neutrona tokom gama spektrometrijskih merenja.

1. UVOD

Neutronske reakcije sa Ge-detektorom i okolnim materijalima mogu da proizvedu merljivu gama aktivnost putem reakcija zahvata i rasejanja [1]. Kako su neutroni jedan od primarnih izvora fona u gama spektrometriji, analiziranje neutronske prisustva je od velikog značaja u niskofonskim eksperimentima, kao i u različitim promptnim neutronske aktivacionim eksperimentima [2]. Analiza neutronske interakcija, shodno tome, je bila predmet mnogih istraživanja [1-10]. Međutim, i dalje ostaje problem određivanja neutronske spektra u Ge-detektoru tokom gama spektrometrijskih merenja [11-13]. U prethodnim istraživanjima koristili smo proceduru dekonvolucije za procenu neutronske spektra koji potiče od kosmičkog zračenja u germanijumskom detektoru [14]. Ova procedura polazi od početnog (pretpostavljenog) spektra, koji se određuje na osnovu eksperimentalno ili teorijski određenih dostupnih podataka. Postupak dekonvolucije modifikuje početni spektar tako da se dobije najbolje slaganje između izmerenih vrednosti gama aktivnosti (u našem slučaju germanijumskih izotopa nakon interakcije sa neutronima) i izračunatih vrednosti gama aktivnosti korišćenjem dekonvolucijom dobijenog neutronske spektra i dostupnih podataka za efikasne preseke za nuklearne reakcije koje su od interesa. Ovaj metod bi trebao da bude univerzalan i primenjiv u svim merenjima kada su u okruženju germanijumskih detektora prisutni neutroni, kao na primer u slučaju promptnih neutronske aktivacionih merenja. U ovom radu smo uporedili izmerene aktivnosti germanijumskih izotopa i uporedili ih sa vrednostima dobijenim računom, pri čemu je kao izvor neutrona korišćen ²⁵²Cf.

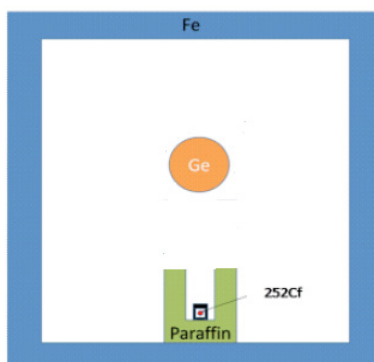
Poređenje ovih vrednosti je neophodno da bi se dobio preliminarni rezultat koji će se koristiti u postupku dekonvolucije za dobijanje neutronske spektra prilikom merenja sa fisionim izvorom neutrona ²⁵²Cf [15, 16]. Poređenjem izračunatih i izmerenih vrednosti

gama aktivnosti moguće je doći do informacija koje će poboljšati početni spektar koji se onda može koristiti za procedure dekonvolucije.

2. ЕКСПЕРИМЕНТАЛНА ПОСТАВКА

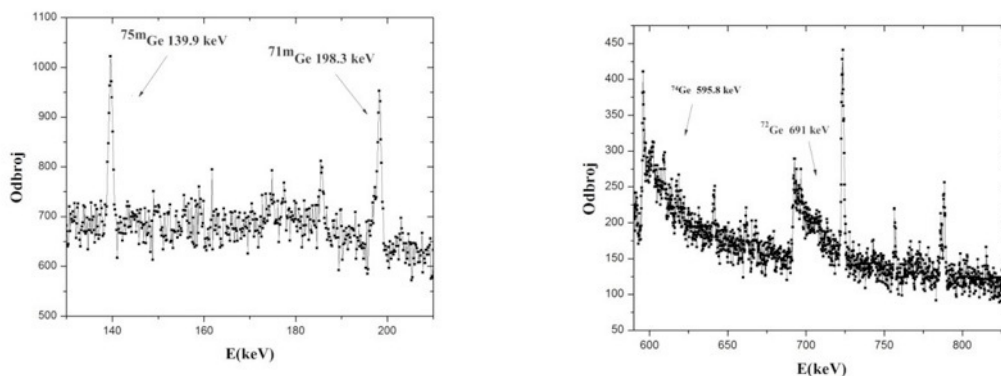
Merenje je izvršeno u Laboratoriji za gama spektroskopiju, Katedre za nuklearnu fiziku, u okviru Departmana za fiziku, Prirodno-matematičkog fakulteta u Novom Sadu. Za merenje gama aktivnosti indukovane neutronima, korišćen je HPGe detektor proizvođača Canberra, serijskog broja G.C.2520-7600. Detektor je n-tipa, relativne efikasnosti 22.3% i aktivne zapremine 119 cm³. Detektor se tokom merenja nalazio unutar gvozdene zaštite zapremine 1 m³ sa zidovima debljine 25 cm i mase oko 20 t.

Izvor neutrona u ovom eksperimentu je bio, kao što je ranije pomenuto, ²⁵²Cf aktivnosti 4,5 · 10³ n/s u 4π sr. ²⁵²Cf ima dva moguća kanala raspada: alfa raspad (96,9%) i spontanu fisiju (3,2%). Period poluraspada za spontanu fisiju je T_{1/2}=2,645 godina i prilikom svake spontane fisije emituje se u proseku 3,77 neutrona.



Slika 1. Šematski prikaz eksperimenta

²⁵²Cf se nalazio u Marineli posudi obloženoj parafinom sa svih strane osim sa strane koja je usmerena ka HPGe detektoru, kao što je prikazano na slici 1. Kako bi se apsorbovalo gama zračenje koje potiče od raspada fisionih potomaka nakupljenih u ²⁵²Cf, izvor je prekriven gvozdenom pločicom debljine 8 mm. Merenje je trajalo 151367 s, što je omogućilo zadovoljavajuću statistiku detektovanih gama kvanata nastalih prilikom interakcije neutrona sa jezgrima germanijuma.



Slika 2. Delovi spektra sa detektovanim neutronima indukovanim gama pikovima koji potiču od (n,γ) reakcija (leva slika) i (n,n') reakcija (desno)

3. REZULTATI

3.1. DETEKTOVANE AKTIVNOSTI

Na slici 2 prikazani su delovi spektra sa karakterističnim gama pikovima koji potiču od neutronske interakcije sa izotopima germanijuma [9, 17]. Identifikovane gama linije, njihovo poreklo i intenziteti su prikazani u tabeli 1. Od svih detektovanih linija izabrane su one sa najboljom statistikom [9]. Za intenzitete standardnih spektroskopskih pikova Gausovskog oblika (139 keV $^{74}\text{Ge}(n,\gamma)^{75\text{m}}\text{Ge}$ i 198 keV $^{70}\text{Ge}(n,\gamma)^{71\text{m}}\text{Ge}$) korišćen je programski paket GENIE2000. Intenzitet asimetričnih (n,n') gama pikova (691,0 keV $^{72}\text{Ge}(n,n')^{72}\text{Ge}$ i 595,8 keV $^{74}\text{Ge}(n,n')^{74}\text{Ge}$), određen je korišćenjem funkcije za fitovanje [4,17]:

$$C(E) = a_0 \text{ERFC} \left[-\frac{E-E_0}{\sigma_0} \right] \cdot \text{Exp} \left[-\frac{E-E_0}{\Delta} \right] + \sum_{i=1}^n a_i \cdot \text{Exp} \left[-\frac{1}{2\sigma_i^2} (E-E_i)^2 \right] + F \quad (1)$$

Tabela 1. Opšte informacije o detektovanim gama linijama i odgovarajućim vrednostima intenziteta

Energija [keV]	Nuklid	Reakcije	Intenzitet [s ⁻¹]
139,9	$^{75\text{m}}\text{Ge}$	$^{74}\text{Ge}(n,\gamma)^{75\text{m}}\text{Ge}$ $^{76}\text{Ge}(n,2n)^{75\text{m}}\text{Ge}$	0,0136(8)
198,3	$^{71\text{m}}\text{Ge}$	$^{70}\text{Ge}(n,\gamma)^{71\text{m}}\text{Ge}$ $^{72}\text{Ge}(n,2n)^{71\text{m}}\text{Ge}$	0,0159(8)
595,8	^{74}Ge	$^{74}\text{Ge}(n,n')^{74}\text{Ge}$	0,0559(27)
691,3	^{72}Ge	$^{72}\text{Ge}(n,n')^{72}\text{Ge}$	0,068(5)

U jednačini (1), prvi član opisuje oblik Ge(n,n') gama pika. U drugom članu, izraz unutar sume je Gausova funkcija koja odgovara simetričnim gama linijama u regionu koji se fituje. Ove linije mogu biti Ge(n,γ) gama linije ili bilo koje druge linije koje pripadaju fonu. Parametar F označava fonski kontinuum za koji se prilikom fitovanja pretpostavlja da je linearna funkcija. Parametri fita su a_0 , a_i , E_0 , E_i , σ_0 , σ_i i Δ . U ovom slučaju E_0 i E_i predstavljaju energije detektovanih gama linija; a_0 i a_i su maksimalne amplitude ovih linija. Parametri σ_0 i σ_i su određeni širinom linije na polovini maksimuma i odgovaraju energetske rezoluciji detektora. Parametar Δ određuje karakteristike eksponencijalnog repa Ge(n,n') linija. Varijacijom parametara fita linija i fona, kao i varijacijom energetskog opsega unutar kojeg je izvršeno fitovanje dobijeni su optimalni rezultati [4]. Za fitovanje je korišćen ROOT softver za analizu podataka [18]. Pomoću ovog fita obrađen je i intenzitet gama pika germanijuma energije od 595,8 keV-a koji nastaje i usled (n,γ) i (n,n') reakcija, tj. interakcijama i sporih i brzih neutrona. Ovo je omogućilo razdvajanje ove linije za potrebe analize na simetričnu gama liniju koja potiče od zahvata i asimetričnu gama liniju koja potiče od neelastičnog rasejanja [19].

Nakon određivanja intenziteta gama linija od interesa, saturacione aktivnosti određenih germanijumskih izotopa po atomu prirodnog germanijuma su izračunate kao [9, 12]:

$$A_k = \frac{C \cdot M}{t \cdot p \cdot (\varepsilon + \alpha) \cdot m \cdot N_A} \quad (2)$$

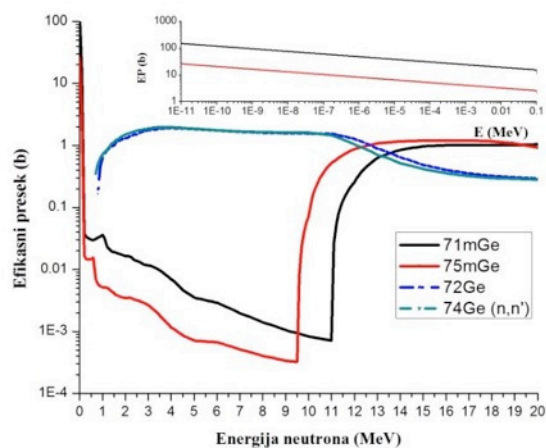
gde C predstavlja detektovani odbroj gama linije, t je vreme merenja, p je verovatnoća emisije gama linije, α je konverzioni koeficijent, ε je efikasnost u piku pune absorpcije (izračunata pomoću GEANT4 softverskog paketa), M je molarna masa germanijuma, m je masa germanijumskog kristala i N_a Avogadrova konstanta. Aktivnosti dobijene korišćenjem jednačine (2), A_k , su prikazane u tabeli 2.

3.2. RAČUNATE AKTIVNOSTI

Metod za računanje aktivnosti germanijumskih izotopa se zasniva na činjenici da je neutronima indukovana aktivnost za aktivirani radionuklid, k , proporcionalna proizvodu efikasnog preseka za proizvodnju određenog radionuklida i neutronskog fluksa [20]:

$$A_k = \sum_i \sigma_{ik} \Phi_i ; i = 1, 2, 3 \dots c; \quad k = 1, 2, 3 \dots m \quad (3)$$

gde su σ_{ik} odgovarajuće funkcije efikasnog preseka, a Φ_i je neutronski fluks za energijski prozor E_i . Indeks k prolazi kroz brojeve korišćenih radionuklida, a m predstavlja ukupan broj radionuklida. Maksimalna vrednost indeksa i , c , označava broj energijskih prozora u neutronskom spektru i funkciji efikasnog preseka. Iz jednačine (3), moguće je proceniti očekivane vrednosti za aktivnosti germanijumskih izotopa. U ovom radu, aktivnosti od interesa, A_k , predstavljaju aktivnosti izotopa germanijuma koje su indukovane različitim neutronskim reakcijama. Vrednosti σ_{ik} za reakcije od interesa su preuzete iz ENDF baze podataka za efikasne preseke, preciznije iz ENDF/B-VII.1 biblioteke [21], kao što je prikazano na slici 3.



Slika 3. Funkcije efikasnih preseka za proizvodnju Ge izotopa putem neutronskih reakcija (sa uvećanim niskoenergetskim delom)

Za neutronski spektar je korišćen spektar ^{252}Cf čiji je oblik dobro poznat, bez ikakvih modifikacija njegovog oblika, iako je realno za očekivati da je u našoj eksperimentalnoj postavci spektar neutrona u detektoru drugačiji od spektra koji emituje izvor. Ovo je urađeno upravo iz razloga da bi se poređenjem merenih i izračunatih vrednosti aktivnosti izotopa germanijuma moglo zaključiti kakve modifikacije treba izvršiti nad spektrom ^{252}Cf tako da on realnije opisuje spektar neutrona unutar samog detektora. Vrednosti ovako dobijenih aktivnosti su prikazani u tabeli 2. Treba napomenuti da je prilikom

izračunavanja aktivnosti izotopa germanijuma korišćen faktor normiranja koji treba da omogući poređenje izmerenih i izračunatih vrednosti jer je prilikom računanja ukupan fluks neutrona normiran na jediničnu vrednost.

4. DISKUSIJA I ZAKLJUČAK

U tabeli 2 prikazane su izmerene i izračunate aktivnosti, kao i njihovi odnosi. Uočava se da se za izotope germanijuma ^{71m}Ge i ^{72}Ge izračunate vrednosti relativno dobro slažu sa izmerenim vrednostima, dok su kod ^{74}Ge i ^{75m}Ge izmerene vrednosti veće oko 2,5 i 4 puta od izračunatih, respektivno. Odstupanja računatih i izmerenih vrednosti za izotop ^{75m}Ge upućuju na mogućnost značajnijeg uticaja interakcija brzih neutrona na intenzitet gama pika od 139,9 keV, što je i bio predmet naše prethodne studije [19]. Neslaganje izmerenih i računatih vrednosti za ^{74}Ge može biti objašnjeno značajnijim doprinosom $^{73}\text{Ge}(n,\gamma)^{74}\text{Ge}$ detektovanom odbroju gama pika energije od 595,8 keV. Ova odstupanja postavljaju i pitanje validnosti dostupnih efikasnih preseka za korišćene neutronske reakcije.

Ovde prikazani rezultati upućuju na to da promptni fisioni neutronske spektar ^{252}Cf ne može na najbolji način objasniti prisutan spektar neutrona tokom izvršenog merenja. To može biti posledica usporavanja i termalizacije neutrona u materijalima prisutnim u okruženju detektora. Takođe, za dalju analizu neophodno je u račun uključiti i druge neutronske reakcije sa izotopima germanijuma i izvršiti proveru validnosti dostupnih podataka za efikasne preseke za interakciju neutrona sa jezgrima germanijuma.

Tabela 2. Intenziteti, izmerene i računate aktivnosti za reakcije od interesa, kao i odnosi izmerenih i računatih vrednosti

Izotop	Izmerena aktivnost [10^{-26} Bq]	Računata aktivnost [10^{-26} Bq]	Odnos aktivnosti (I/R)
^{71m}Ge	0,506(27)	0,63	0,80
^{72}Ge	1,31(9)	1,57	0,83
^{74}Ge	7,1(3)	1,74	4,08
^{75m}Ge	0,288(16)	0,112	2,57

5. LITERATURA

- [1] G. Heusser, Nucl. Instrum. Methods Phys. Res. A 369 (1996) 539.
- [2] A. Dragić, et al., Phys. Procedia 59 (2014) 125.
- [3] R. Wordel, et al., Nucl. Instrum. Methods Phys. Res. A 369 (1996) 557.
- [4] E. Gete, et al., Nucl. Instrum. Methods Phys. Res. A 388 (1997) 212.
- [5] N. Jovančević, M. Krmar, Phys. Procedia 31 (2012) 93–98.
- [6] Y. Feige, et al., J. Geophys. Res. 73 (1968) 3135–3142.
- [7] G.P. Škoro, et al., Nucl. Instrum. Methods Phys. Res. A 316 (1992) 333.
- [8] N. Jovančević, M. Krmar, Appl. Rad. Isot. 69 (2011) 629–635.
- [9] N. Jovančević, et al., Nucl. Instrum. Methods Phys. Res. A 612 (2009) 303–308.
- [10] G. Heusser, Background in ionizing radiation detection, in: M. Garcia-Leon, R. Gracia-Tenorio (Eds.), Low-Level Measurements of Radioactivity in the Environment, Word Scientific, Singapore, 1994, pp. 69–112.

- [11] C. Chund, Y.R. Chen, Nucl. Instrum. Methods Phys. Res. A 301 (1991) 328–336.
- [12] J.E. Naye, Nucl. Instrum. Methods Phys. Res. A 368 (1996) 832–846.
- [13] G. Fehrenbacher, et al., Nucl. Instrum. Methods Phys. Res. A 372 (1996) 239.
- [14] D. Knežević, N. Jovančević, M. Krmar, J. Petrović, Modeling of neutron spectrum in the gamma spectroscopy measurements with Ge-detectors, Nucl. Instrum. Methods Phys. Res. A, 833 (2016), p. 23–26.
- [15] C.W. Reich, W. Mannhart, T. England, IAEA Technical Report INDC(NDS)220/L, p.305, IAEA, Vienna (1989).
- [16] International Reactor Dosimetry and Fusion File, IAEA Data, <https://www-nds.iaea.org/IRDF>.
- [17] T. Siiskonen, H. Toivonen, Nucl. Instrum. Methods Phys. Res. A 540 (2005) 403.
- [18] ROOT cern, (<https://root.cern.ch>).
- [19] B. Anđelić, D. Knežević, N. Jovančević, M. Krmar, J. Petrović, A. Toth, Ž. Medić, J. Hansman, Presence of neutrons in the low-level background environment estimated by the analysis of the 595.8 keV gamma peak, Nucl. Instrum. Methods Phys. Res. A, 852 (2017), p. 80–84.
- [20] A. Trkov, V. Radulović, J. Radioanal. Nucl. Chem. 304 (2015) 763–778.
- [21] The ENDF, Evaluated Nuclear Data File, (<https://www-nds.iaea.org/exfor/endl.htm>).

DETERMINATION OF NEUTRON ENERGY SPECTRA PRESENCE IN GAMMA SPECTROSCOPIC MEASUREMENTS USING GE-DETECTORS

Nikola JOVANČEVIĆ¹, David KNEŽEVIĆ^{1,2}, Miodrag KRMAR¹, Jovana NIKOLOV¹, Nataša TODOROVIĆ¹, Jovana PETROVIĆ¹

1) University of Novi Sad, Faculty of Sciences, Department of Physics, Novi Sad, Serbia, nikola.jovancevic@df.uns.ac.rs

2) Institute of Physics, Pregrevica 118, University of Belgrade, Belgrade, Serbia

ABSTRACT

Determination of neutron spectra in the Ge-detector during low-level gamma spectroscopy measurements is of great importance. Thus, in this paper we analyzed the method for the determination of neutron energy spectra present during measurements with HPGe detectors. This method is based on using the deconvolution procedure. It requires the knowledge of neutron induced gamma activities of Ge isotopes and the cross section data for the neutron reactions of interest. This approach was tested with measurements that used the fission neutron source ²⁵²Cf placed in proximity of the HPGe detector. Results show that this method can provide reliable data about the shape of neutron energy spectrum during gamma spectroscopy measurements.

Representation of Radiative Strength Functions within a Practical Model of Cascade Gamma Decay

D. C. Vu^{1),2)*}, A. M. Sukhovej^{1)**}, L. V. Mitsyna^{1)***}, Sh. Zeinalov^{1)****},
N. Jovancevic^{3)*****}, D. Knezevic^{3)*****}, M. Krmar^{3)*****}, and A. Dragic^{4)*****}

Received June 14, 2016; in final form, August 24, 2016

Abstract—A practical model developed at the Joint Institute for Nuclear Research (JINR, Dubna) in order to describe the cascade gamma decay of neutron resonances makes it possible to determine simultaneously, from an approximation of the intensities of two-step cascades, parameters of nuclear level densities and partial widths with respect to the emission of nuclear-reaction products. The number of the phenomenological ideas used is minimized in the model version considered in the present study. An analysis of new results confirms what was obtained earlier for the dependence of dynamics of the interaction of fermion and boson nuclear states on the nuclear shape. From the ratio of the level densities for excitations of the vibrational and quasiparticle types, it also follows that this interaction manifests itself in the region around the neutron binding energy and is probably different in nuclei that have different parities of nucleons.

DOI: 10.1134/S1063778817020260

INTRODUCTION

At any excitation energy, parameters of the cascade gamma decay of an arbitrary high-lying nuclear level are determined exclusively by the level density ρ and the partial widths Γ with respect to electric and magnetic dipole transitions. The intensity of cascades that involve purely quadrupole transitions is negligible at nuclear-excitation energies above several MeV units. For either parity, the spins of levels that are excited by primary transitions lie in the range of $2 \leq \Delta J \leq 4$. Investigation of the gamma-decay process is of interest, first of all, for studying the dynamics of interaction of fermion and boson states

of nuclear matter. Reliable information on the subject is also necessary for more precisely describing the fission process. According to [1], the distribution of the energy between excited fission fragments depends on their level densities. However, the level densities calculated on the basis of existing models [2] deviate strongly from the most recent experimental data [3]. The reason behind this discrepancy may only be that experiments that detect the cascade of reaction products provide more information than any procedure for obtaining spectra of single gamma rays or nucleon products without employing a coincidence mode.

Since one-step gamma-ray spectra and reaction cross sections depend on the product $\rho \times \Gamma$, it is absolutely impossible to determine simultaneously reliable values of ρ and Γ from such data. This was done only in experiments that study cascades involving two sequential gamma transitions whose intensities carry information both about the nuclear excitation energy and about the energy of the emitted photon (nucleon). Only such experiments may reduce the total error in the values determined for ρ and Γ to a few tens of percent.

Since all individual levels and probabilities for transitions between them cannot be determined with the aid of modern spectrometric detectors, information about nuclear superfluidity is extractable from indirect experiments exclusively. In that case, both the level density ρ and the partial widths Γ are unknown functions in any nucleus.

¹⁾Joint Institute for Nuclear Research, ul. Joliot-Curie 6, Dubna, Moscow oblast, 141980 Russia.

²⁾Institute of Physics, Vietnam Academy of Science and Technology, 10 Dao Tan, Ba Dinh, Ha Noi, Viet Nam.

³⁾Department of Physics, Faculty of Sciences, University of Novi Sad, Trg Dositeja Obradovića 3, 21000 Novi Sad, Republic of Serbia.

⁴⁾Institute of Physics Belgrade, Pregrevica 118, 11080 Zemun, Republic of Serbia.

*E-mail: vuconghnue@gmail.com

**E-mail: sukhovej@nf.jinr.ru

***E-mail: mitsyna@nf.jinr.ru

****E-mail: zeinal@nf.jinr.ru

*****E-mail: nikola.jovancevic@df.uns.ac.rs

E-mail: david.knezevic@df.uns.ac.rs

E-mail: krmar@df.uns.ac.rs

E-mail: dragic@ipb.ac.rs

1. POTENTIAL OF THE PRESENT-DAY EXPERIMENT AND OF ITS MODEL SIMULATION

At a fixed primary-transition energy E_1 , the intensities $I_{\gamma\gamma}(E_1)$ of two-step cascades connecting a neutron resonance (or some other compound state) λ and some group f of low-lying nuclear levels and proceeding through arbitrary intermediate levels i are described by the set of equations

$$I_{\gamma\gamma}(E_1) = \sum_{\lambda,f} \sum_i \frac{\Gamma_{\lambda i} \Gamma_{if}}{\Gamma_{\lambda} \Gamma_i} \quad (1)$$

$$= \sum_{\lambda,f} \frac{\Gamma_{\lambda i}}{\langle \Gamma_{\lambda i} \rangle m_{\lambda i}} n_{\lambda i} \frac{\Gamma_{if}}{\langle \Gamma_{if} \rangle m_{if}},$$

where $m_{\lambda i}$ is the number of levels excited by primary transitions in the ranges between the energy of the initial level λ and the energy of an intermediate level i , m_{if} is the number of levels excited by secondary gamma transitions in the ranges between the energy of an intermediate level i and the energy of the final level f , and $n_{\lambda i}$ is the number of intermediate levels of cascades in narrow ranges of primary-transition energies. From the set of Eqs. (1), which relates the unknown number of levels, n (or m), to unknown partial widths, Γ , one determines the set of parameters p and q of the model functions $\rho = f(p_1, p_2, \dots)$ and $\Gamma = \varphi(q_1, q_2, \dots)$ with an error originating from the inconsistency of the existing theoretical ideas with experimental results. The analysis performed earlier in [4] revealed that one can even include in the model the possible relation between the values of the level density and strength functions in some narrow excitation-energy interval. Thus, we see that, at any densities of the levels λ and i , one can determine parameters of the sought functions ρ and Γ from the spectra of two-step cascades.

The analysis in [3] of experimental data on cascade intensities over the mass-number range of $28 \leq A \leq 200$ showed that experimental level densities could not be reproduced to an experimental precision on the basis of models that ignore the existence of bosonic branches of nuclear-matter states (on the basis of those where the inclusion of this branch was insufficiently correct).

The procedure developed by our group does not require invoking hypotheses not tested experimentally (such as the Porter–Thomas hypothesis [5] on the distribution of widths with respect to the emission of nuclear-reaction products, the Axel–Brink hypothesis [6, 7] that radiative-width values are independent of the energy of an excited level, or the Bohr–Mottelson hypothesis [8] on the correctness of employing the optical model of the nucleus to determine the probability for the emission of nucleon reaction

products). The Dubna model of the cascade gamma decay of compound nuclear states whose excitation energies lie in the range of $E_{\text{ex}} \approx 5\text{--}10$ MeV is based on a model of the density of n -quasiparticle levels, the balance of the changes in the entropy and energy of quasiparticle levels [2, 9, 10], and tested ideas about the shape of the energy dependence of radiative strength functions.

The systematic error of any experimental procedure for obtaining the functions ρ and Γ is always determined by large coefficients of the transfer of the errors in the measured spectrum, δS , or in the reaction cross section, $\delta\sigma$, to the errors $\delta\rho$ and $\delta\Gamma$ in the parameters being determined. The error in question may grow sizably upon the increase in the energy of the level that decays in the reaction under study. This error and the direction in which the model concepts of $\rho = f(p_1, p_2, \dots)$ and $\Gamma = \varphi(q_1, q_2, \dots)$ should be corrected can only be estimated by comparing various versions of the description of the level densities and radiative strength functions. For example, a comparison of several versions of our practical model [3, 11, 12] made it possible to reveal that the rate of the change in the vibrational level density specified phenomenologically in [11, 12] is determined partly or fully by the pairing energy Δ_0 of the last nucleon in the nucleus being considered. In all of the implemented versions of the practical model, the accuracy of the approximation of intensities remains unimpaired as one gradually reduces the number of fitted parameters; therefore, we do not present here the ultimate approximations of the spectra $I_{\gamma\gamma}$.

In contrast to what was done in [3], the proposed model version employs, instead of two parameters (the rate of the change in the nuclear entropy and the rate of the change in the energy of quasiparticle states) in the phenomenological expression for the coefficient of the collective level-density enhancement, C_{coll} [3, 10], only one fitted parameter, E_u ; that is,

$$C_{\text{coll}} = A_l \exp(\sqrt{(E_{\text{ex}} - U_l)/E_u}) - (E_{\text{ex}} - U_l)/E_u + \beta, \quad (2)$$

where A_l are the parameters of the vibrational level density above the point of break of each l th Cooper pair and U_l are the energy thresholds for the break of Cooper pairs. For deformed nuclei, the parameter $\beta \geq 1$ may differ from unity.

The effect of shell inhomogeneities in the single-particle spectrum [2, 10] was taken into account in terms of the excitation-energy-dependent level-density parameter a ,

$$a(A, E_{\text{ex}}) = \tilde{a}(1 + ((1 - \exp(\gamma E_{\text{ex}}))\delta E/E_{\text{ex}})), \quad (3)$$

or in terms of the parameter $g = 6a/\pi^2$ for n -quasiparticle states in the vicinity of the Fermi surface [9]. The asymptotic value of $\tilde{a} = 0.114A + 0.162A^{2/3}$ and the value of $\gamma = 0.054$ were taken from [2, 10]. The shell correction δE calculated [2] on the basis of mass-defect data within the liquid-drop model of the nucleus was slightly modified for the mean spacing between resonances, D_λ , to remain unchanged [3].

2. ENERGY DEPENDENCE OF STRENGTH FUNCTIONS

In the model of cascade gamma decay, the shape of the energy dependence of partial radiative widths should be specified to a high degree of precision for any excited levels and energies of emitted gamma rays.

On the basis of existing models, the strength function for a nucleus of mass number A is defined as $k = \Gamma/(A^{2/3}E_\gamma^3 D_\lambda)$, where E_γ is the gamma-transition energy. The absolute value of the sum of radiative widths for primary $E1$ and $M1$ cascade transitions (total radiative width) can usually be determined from measured reaction cross sections. The most probable form of this sum can be obtained from purely phenomenological considerations or from an extrapolation of some theoretical models to the excitation-energy range of $E_d < E_{\text{ex}} < B_n$ {here, E_d is the point of transition in Eq. (1) from known levels [13] to the level-density concept, while B_n is the neutron binding energy in the nucleus}.

It was found experimentally that a precise reproduction of cascade intensities leads to supplementing the energy dependence of the function $k(E1, E_\gamma) + k(M1, E_\gamma)$ with several peaks that have various areas, positions of the center, and shape asymmetries. But the main term in this energy dependence can be represented by a smooth distribution of strength functions from models of the type in [14] but with allowance for additional parameters whose variation generates a set of functions describing $E1$ and $M1$ transitions and taking values over a broad region (see [11, 12]). The shape of the extra peaks can be revealed and specified only empirically. For example, a description of each such peak in terms of two exponentials (as in an earlier version of our model [3, 11, 12]) is convenient in solving the set of nonlinear equations in (1), even though these exponentials are not used in the model formalism based on theoretical concepts [2].

In order to describe the shape of the peaks in the $E1$ and $M1$ strength functions, Breit–Wigner or Lorentzian functions are used. An asymmetric Breit–Wigner function was applied in theoretically analyzing the regularities of fragmentation of quasiparticle

states for their various positions with respect to the Fermi surface [15]. In employing this function, we were unfortunately unable to choose a set of parameters that would be appropriate for approximating the most probable values of $\rho = f(p_1, p_2, \dots)$ and $\Gamma = \varphi(q_1, q_2, \dots)$.

The use of an asymmetric Lorentzian curve in describing local peaks in the strength functions proved to be more straightforward. For each i th peak its parameters, such as the position of the center, E_i ; the width, Γ_i ; the amplitude, W_i ; and the asymmetry parameter, $\alpha_i = CT^2$, are similar to their counterparts in the model employed in [14]. The expression $\alpha_i(E_\gamma - E_i)/E_\gamma$ increases linearly as the excitations energy $B_n - E_i$ grows from zero at the center of the respective peak to the maximum value at B_n and decreases as the nuclear excitation energy becomes lower. Thus, the peaks of the $E1$ and $M1$ strength functions are represented in the form

$$k = W \frac{(E_\gamma^2 + (\alpha_i(E_i - E_\gamma)/E_\gamma))\Gamma_i^2}{(E_\gamma^2 - E_i^2)^2 + E_\gamma^2\Gamma_i^2}. \quad (4)$$

In approximating Lorentzian functions that describe the decay of a highly excited level, the convergence of the respective iterative process sharply becomes poorer, which creates a serious problem. Upon fitting all parameters of the functions in Eq. (4), the widths Γ_i decrease indefinitely within some segments of the iterative-process trajectory.

The need for taking into account the effect of a sharp local change in the level density on strength functions was revealed at the stage of a model-free determination of the set of random functions ρ and Γ [16]. For this purpose, the strength functions to be determined were multiplied in [4] by the ratio

$$M = \rho_{\text{mod}}/\rho_{\text{exp}}, \quad (5)$$

where ρ_{exp} is the best approximation for the iteration being considered and ρ_{mod} is a smooth model dependence that reproduces both the density of neutron resonances and the cumulative sum of known levels for which E_{ex} is lower than E_d . In order to determine ρ_{mod} , we have chosen the back-shifted Fermi gas model. In the present version of our analysis, we have employed the constraint $1 \leq \rho_{\text{mod}}/\rho_{\text{exp}} \leq 10$ [11].

3. RESULTS

Difficulties in solving the set of Eqs. (1) arise both because of a strong nonlinearity of the sought functions ρ and Γ and because of their anticorrelation. There is a probability for arriving at a spurious minimum of χ^2 , and this may lead to a sizable systematic error in the resulting values of ρ and Γ .

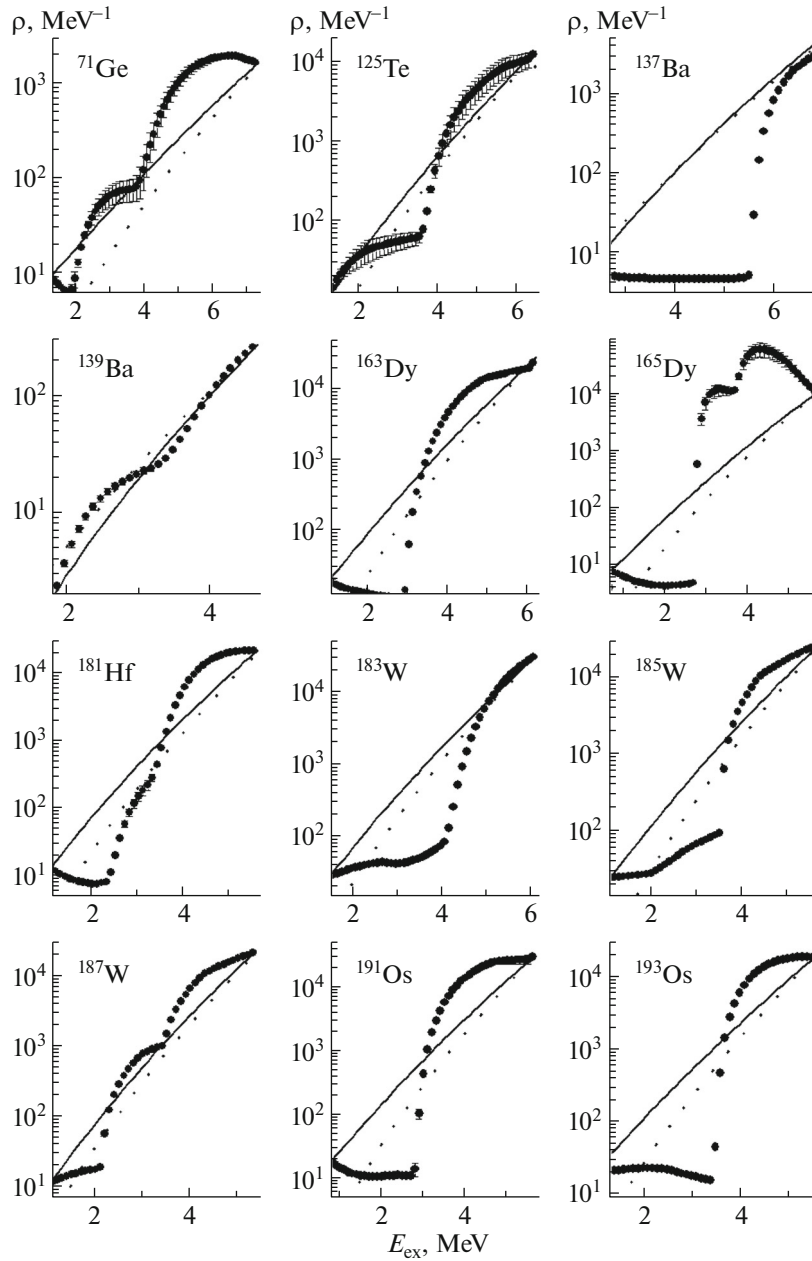


Fig. 1. Excitation-energy dependence of the mean densities of intermediate levels in two-step cascades (points with error bars) for even-odd nuclei (lowest χ^2 fits): (solid lines) data calculated in [17] and (dotted lines) results of the calculations based on the model proposed in [10].

A comparison of the results obtained within the present version of our model and within its earlier versions showed that we reached a fairly high accuracy in describing the densities of intermediate cascade levels. The discrepancies are the greatest for ^{137}Ba and ^{182}Ta . Most likely, a large error for ^{137}Ba stems from the preceding approximation version [3]. For ^{182}Ta , the energy thresholds for the break of the second and third Cooper pairs are 1.6 and 5.8 MeV within the present version; in [3], the values of the same

thresholds are 1.6 and 4.0 MeV. It follows that, even in the worst case of ^{182}Ta , the data obtained for the level density yield a picture where the uncertainties are due to the imperfections in the present-day ideas of the gamma-decay process.

One can reach the highest accuracy and reliability of the results on the basis of experiments where it is possible to single out not less than about 99% of the intensities of primary transitions among the whole array of gamma-ray cascades of the decay of the

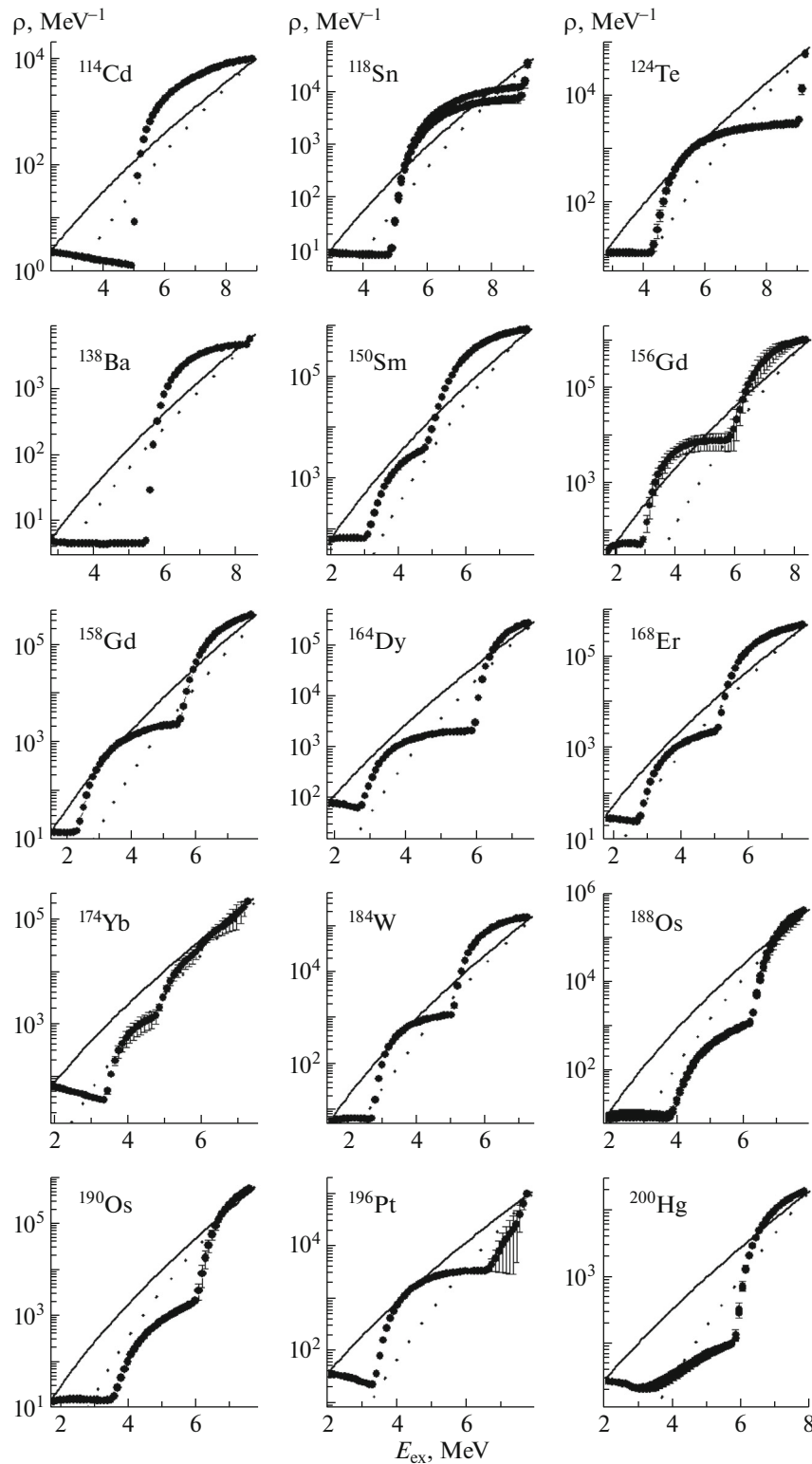


Fig. 2. As in Fig. 1, but for even-even nuclei.

compound state of any nucleus. Nevertheless, reliable information about the most probable level density and about strength functions for dipole gamma transi-

tions can be extracted even from the convolution of the spectrum of primary products of the decay of the compound state and the gamma-transition branching fractions depending on the energy of the interme-

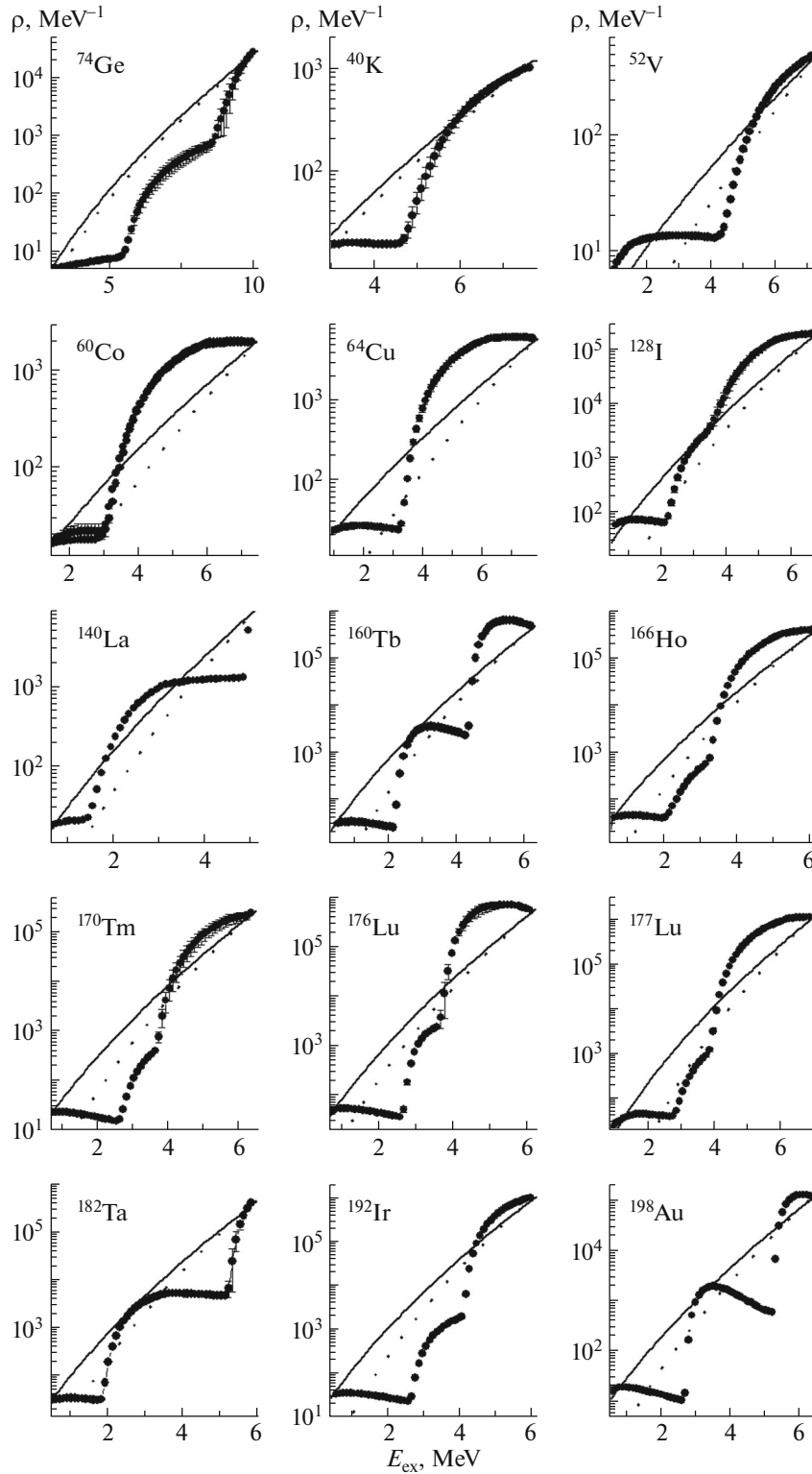


Fig. 3. As in Fig. 1, but for ^{74}Ge , ^{177}Lu , and odd–odd nuclei.

diate cascade level. This follows from a comparison of the thresholds determined for the break of three to four Cooper pairs by employing different versions of the energy dependence of ρ and Γ . In the most recent

versions of the practical model, these results change only slightly.

The level densities from the back-shifted Fermi gas model [17] and those from the model that takes

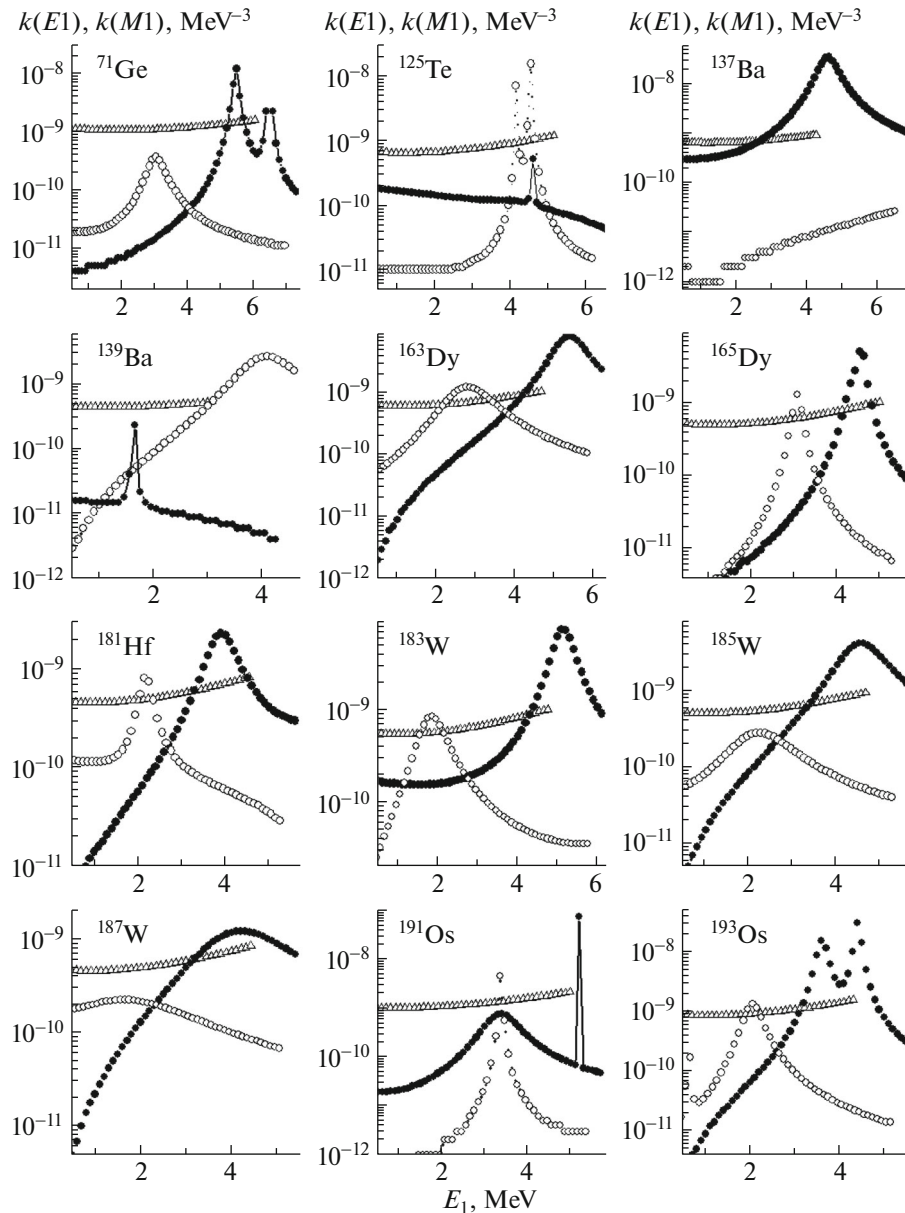


Fig. 4. Strength functions for $E1$ (closed circles) and $M1$ (open circles) transitions for even-odd nuclei versus the primary-transition energy. The open triangles stand for the sum of the values calculated on the basis of the model used in [14] and $k(M1) = \text{const}$ in the energy range of $0 < E_1 < B_n - E_d$.

into account the shell-inhomogeneities in the single-particle spectrum [10] are given in Figs. 1–3. One can see that the model from [10] reproduces the derivative $d\rho/dE_{\text{ex}}$ to a higher degree of precision than the model from [17]; however, the level densities calculated on the basis of both models deviate markedly from the respective experimental results.

The results presented for the $E1$ and $M1$ radiative strength functions (Figs. 4–6) and their sums (Figs. 7–9) do not exhibit drastic distinctions from those published earlier in [18–20], but there remains the unresolved problem of unambiguously describing

the shape of the observed peaks in the electric and magnetic strength functions in those cases where the use of exponential functions [3] and the modified Lorentzian function (3) leads to close values of χ^2 .

It is worth noting that the data in Figs. 4–9 do not require including any additional pygmy resonance in the strength functions being considered. In order to interpret the process in question, it is sufficient to develop theoretical ideas of the coexistence of vibrational and quasiparticle levels in any nucleus and their fragmentation as E_{ex} grows.

In many nuclei (see Fig. 7–9), the sum of the

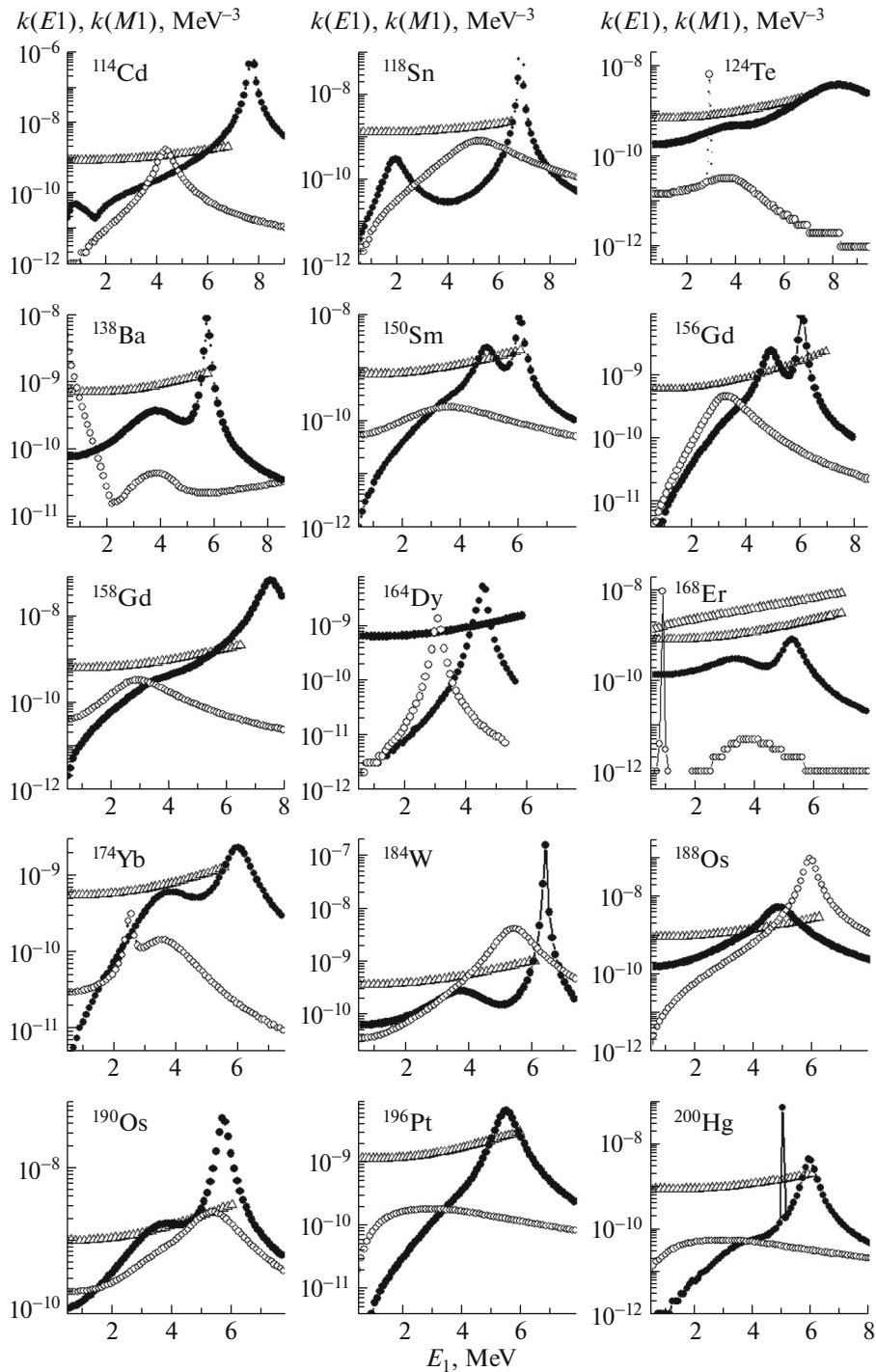


Fig. 5. As in Fig. 4, but for even–even nuclei.

strength functions for $E1$ and $M1$ transitions develops a plateau that agrees with the sum of the values calculated within the model used in [14] and $k(M1) = \text{const}$ normalized to the experimental ratios $k(M1)/k(E1)$. The strength functions for primary transitions whose energy lies in the range of $E_1 < 0.5B_n$ decrease regularly as the energy becomes lower. A significant decrease in the

sum $k(M1) + k(E1)$ for moderately small gamma-transition energies is observed for all versions of the description of radiative strength functions. At the same time, there are no asymptotic zero values of the sums of strength functions [14]. We cannot rule out the possibility of a sizable increase in the $E1$ or $M1$ strength functions in the vicinity of and above B_n because of the fragmentation of n -quasiparticle nu-

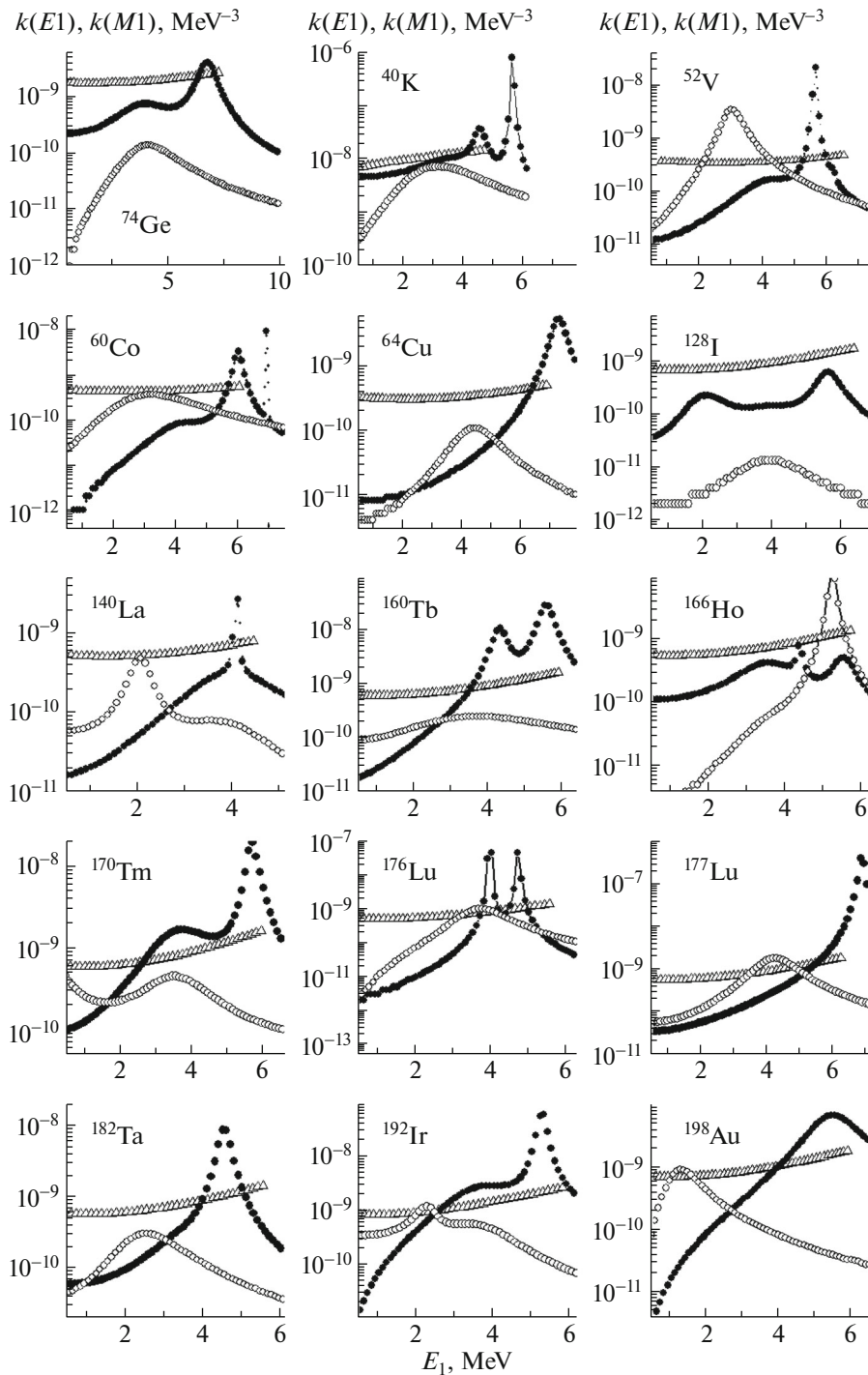


Fig. 6. As in Fig. 4, but for ^{74}Ge , ^{177}Lu and odd-odd nuclei.

clear states if the threshold for the break of a Cooper pair lies in the region of the neutron binding energy. Therefore, the radiative strength functions cannot be a mere extrapolation of giant resonances. This contradicts radically the Axel-Brink hypothesis [6, 7], which is used in dealing with gamma spectra.

Figure 10 gives the mass-number dependence of

the energy thresholds for the break of the second and third Cooper pairs. Since these quantities are different for nuclei in which the numbers of nucleons have different parities and depend on the mean pairing energy, they are shown separately in this figure and are compared with B_n/Δ_0 (in just the same way as in [3]). One can see that the thresholds for the break of

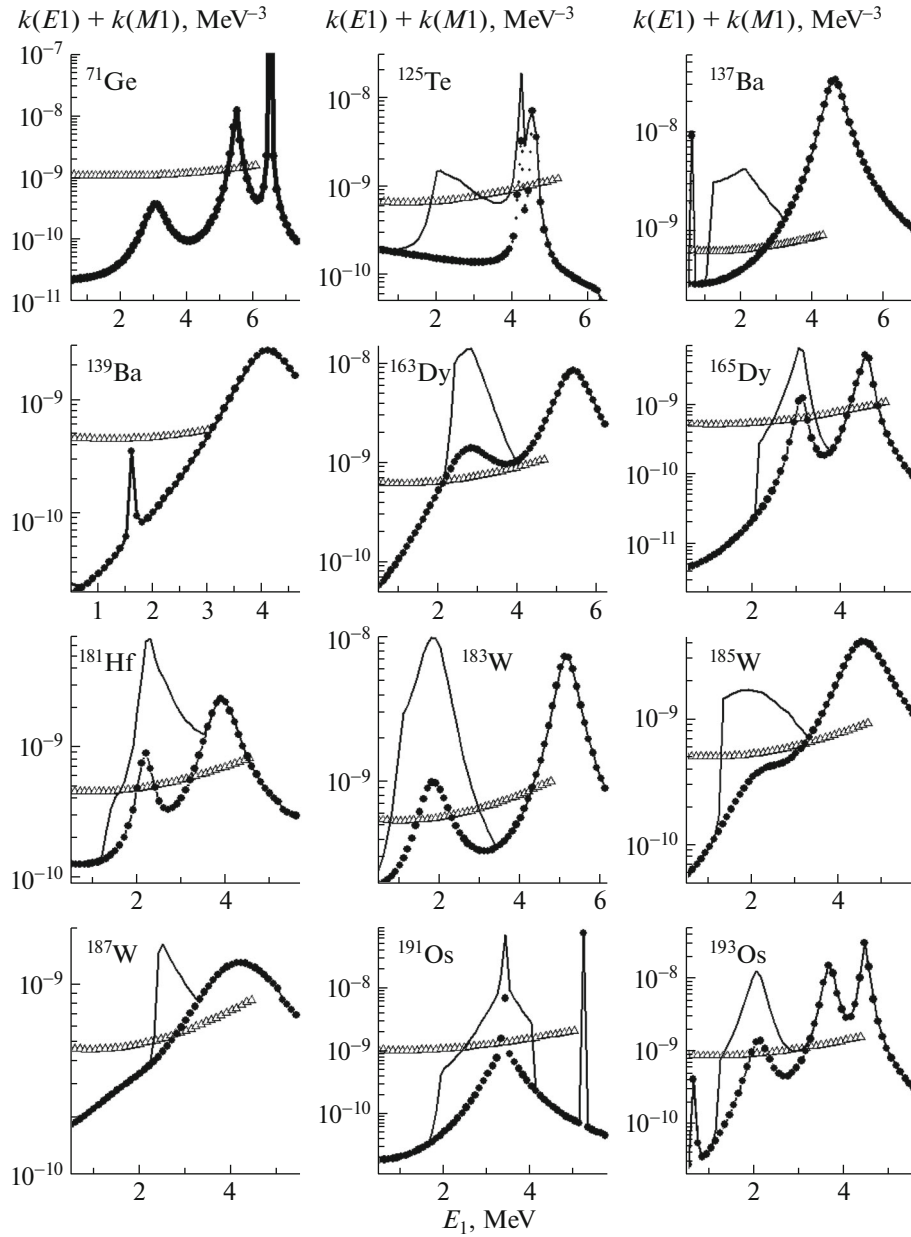


Fig. 7. Sums of strength functions for $E1$ and $M1$ transitions (closed circles) for even-odd nuclei versus the primary-transition energy. The solid lines represent the results fitted with allowance for the correction in Eq. (5). The open triangles stand for the sum of the values calculated on the basis of the model used in [14] and $k(M1) = \text{const}$ in the energy range of $0 < E_1 < B_n - E_d$.

pairs depend only slightly on the shape of the strength functions. This means that, in experiments detecting two-step cascades, the actual correlation of ρ and Γ is insignificant.

Figure 11 shows the results obtained by approximating the parameter E_u . Its values almost perfectly comply with the mean pairing energy Δ_0 of the last nucleon for approximately 30 nuclei. The spread of the remaining values of E_u may be due to the errors in the normalization of experimental values of $I_{\gamma\gamma}$ because of the fact that the model used in [11, 12]

disregards the possibility of the break of proton pairs simultaneously with or instead of the break of neutron pairs, the inaccuracy of the phenomenological part of the model, or fluctuations of the experimental values of Δ_0 [21]. In addition, we cannot rule out the possibility of different weights of quasiparticle and phonon components in the wave function for the resonance that determines the cross section for thermal-neutron capture by any stable (long-lived) target nucleus.

In currently used models [2], the total level density is represented as the sum of the level densities for

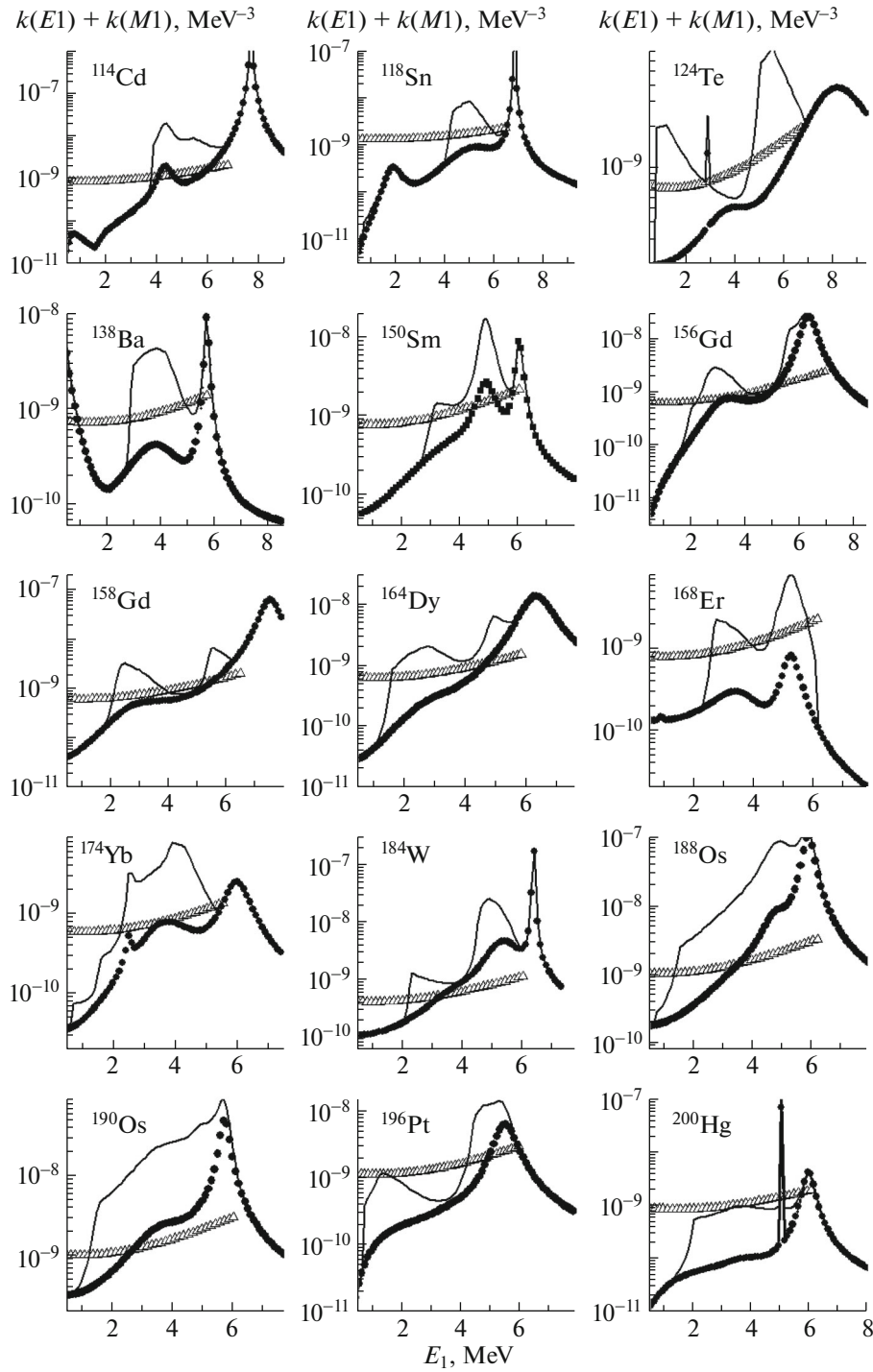


Fig. 8. As in Fig. 7, but for even–even nuclei.

quasiparticle and collective excitations. Figure 12 gives the ratio of the collective (only vibrational in actual practice) level density to the total level density. In the region around B_n , this ratio has close values for nuclei in which the numbers of nucleons have different parities, but, at the energy E_d , the ratio in question is substantially smaller for even–even nuclei than

for even–odd and odd–odd ones. No version of the Dubna model gives grounds to assume the presence of sharp changes in the nuclear structure at the point $E_{ex} = B_n$. On the basis of the data in Fig. 12, it would be legitimate to assume that neutron resonances may preserve various types of the wave-function structure (dominated by quasiparticle or phonon components)

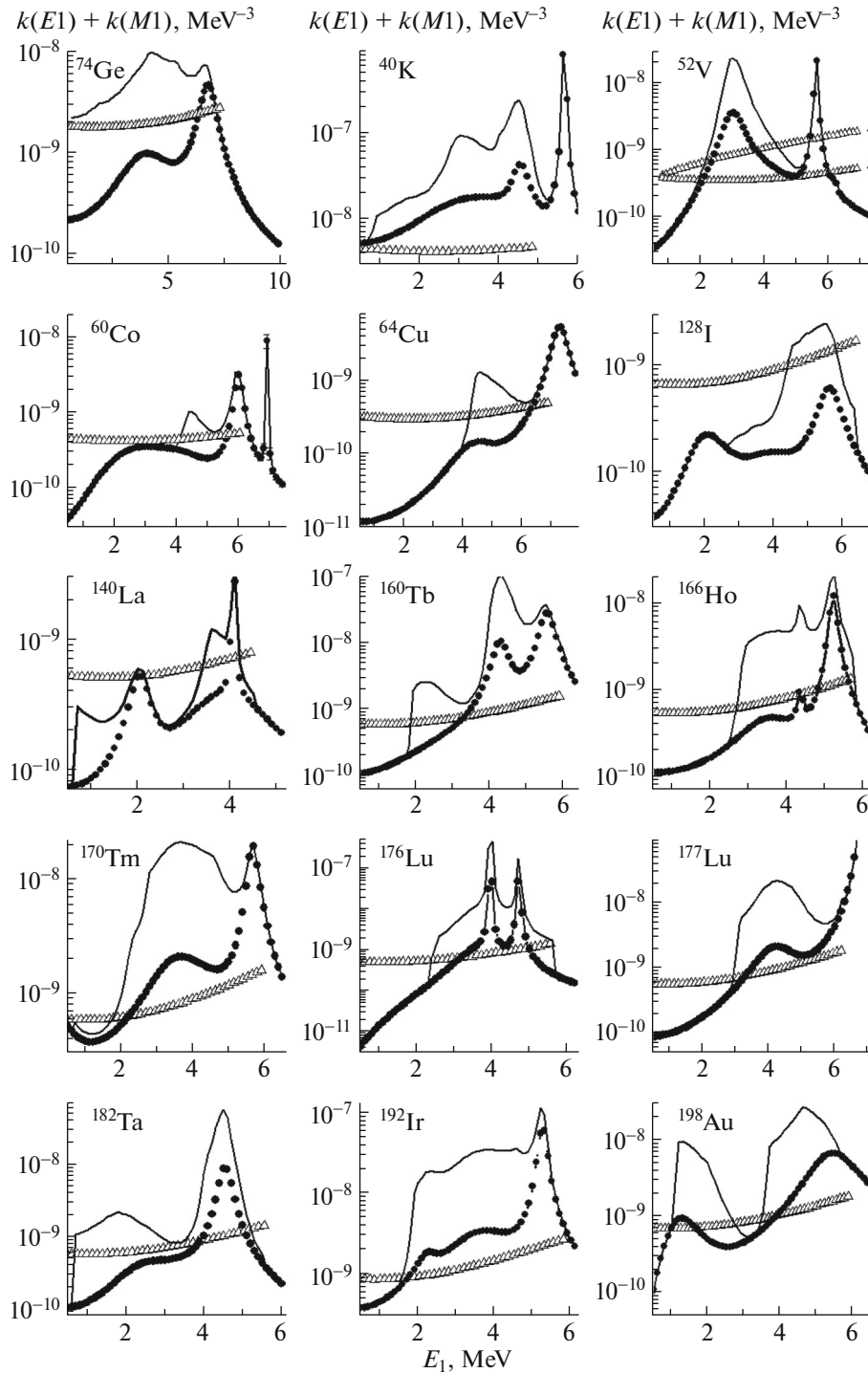


Fig. 9. As in Fig. 7, but for ^{74}Ge , ^{177}Lu , and odd–odd nuclei.

and belong to several different distributions of reduced neutron and total radiative resonance widths.

The distribution of reduced neutron and total radiative widths of neutron resonances were approximated in [22]. In the respective analysis, it is assumed that the experimental set of these widths is represented as the sum of several (up to four) distributions

whose widths and peak positions are varied. For the total radiative widths in nuclei featuring not less than 170 resonances, the mean fractions of two distributions that are the most intense are 44 and 34% of the summed distribution of total radiative widths (this is close to a 40% fraction of vibrational levels). Thus, two experiments that are methodologically indepen-

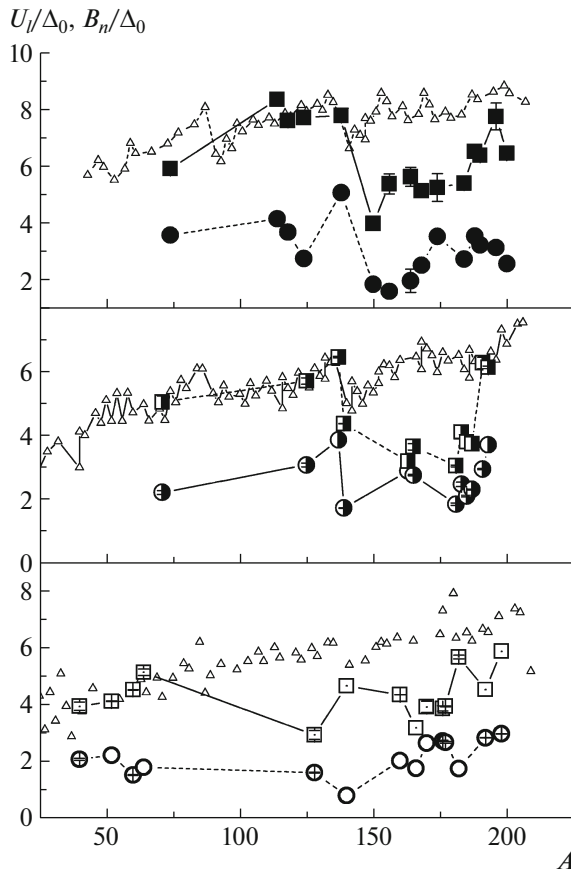


Fig. 10. Mass-number dependence of the energy thresholds for the break of the (circles) second and (boxes) third Cooper pairs. The closed, half-closed, and open symbols represent these results for, respectively, even–even, even–odd, and odd–odd compound nuclei. The open triangles correspond to the mass-number dependence of B_n/Δ_0 .

dent are indicative of the difference in the structure of the wave functions for neighboring levels over a broad range of stable target nuclei up to an energy of or somewhat higher than B_n .

There is some discrepancy between the values obtained here for the $E1$ and $M1$ strength functions (see Fig. 4–9) and the results reported in [3], which is due most likely to different degrees of the effect that the shape of the partial widths of the additional peaks (4) in the strength functions exert on χ^2 values in the region of small values of the energy dependences used. The observed variations in the shape of the sums of $E1$ and $M1$ strength functions (see Fig. 7–9) cannot be interpreted as their unquestionable distinction without ruling out the possible existence of levels of different structure at excitation energies of about 5 to 10 MeV.

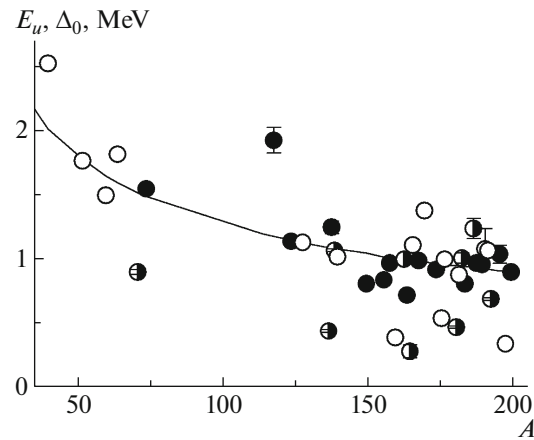


Fig. 11. Mass-number (A) dependence of the parameter E_u (2) for (closed circles) even–even, (half-closed circles) even–odd, and (open circles) odd–odd compound nuclei. The curve represents the mean pairing energy Δ_0 of the last nucleon in a nucleus of mass number A [21].

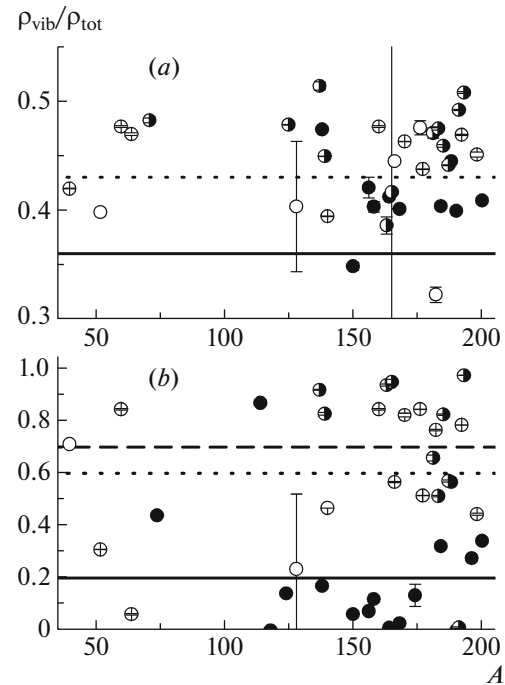


Fig. 12. Ratio of the vibrational level density to the total level density in the region around the neutron binding energy B_n (a) and at the point E_d (b). The closed, half-open, and open circles represent these results for, respectively, even–even, even–odd, and odd–odd nuclei. The solid, dashed, and dotted lines stand for the mean values in, respectively, even–even, even–odd, and odd–odd nuclei.

4. CONCLUSIONS

We have obtained experimental information about the dynamics of the break of three to four Cooper pairs of nucleons. The systematic error in determining the

break thresholds does not exceed a value of about 1 MeV for the bulk of nuclei that are accessible to study.

The set of data obtained by employing (i) the model of the density of n -quasiparticle levels from [9] for describing the sequential break of three to four Cooper pairs at an energy not higher than 5 to 10 MeV above the ground state of the nucleus being considered; (ii) the phenomenological concepts specified by Eq. (2), which concern the energy dependence of the vibrational level density in the same energy range; and (iii) combinations of phenomenological and/or theoretical ideas of the shape of the energy dependences of widths with respect to gamma-ray emission gives sufficient grounds to assume that the dynamics of the interaction of fermion and boson nuclear-matter states depends on the shape of the nucleus being studied.

REFERENCES

1. K. H. Schmidt and B. Jurado, Phys. Rev. C **83**, 014607 (2011).
2. *Reference Input Parameter Library RIPL-2, Handbook for Calculations of Nuclear Reaction Data*, IAEA-TECDOC (IAEA, 2002).
3. A. M. Sukhovej, L. V. Mitsyna, N. Jovancevic, Phys. At. Nucl. **79**, 313 (2016).
4. N. Jovancevic, A. M. Sukhovej, W. I. Furman, and V. A. Khitrov, in *Proceedings of the 20th International Seminar on Interaction of Neutrons with Nuclei, Dubna, May 2012*, Preprint JINR No. E3-2013-22 (Joint Inst. Nucl. Res., Dubna, 2013), p. 157. <http://isinn.jinr.ru/past-isinns.html>.
5. C. F. Porter and R. G. Thomas, Phys. Rev. **104**, 483 (1956).
6. P. Axel, Phys. Rev. **126**, 671 (1962).
7. D. M. Brink, PhD Thesis (Oxford Univ., Oxford, 1955).
8. A. Bohr and B. R. Mottelson, *Nuclear Structure*, Vol. 1: *Single-Particle Motion*, (Benjamin, New York, 1969).
9. V. M. Strutinsky, in *Proceedings of the International Congress on Nuclear Physics, Paris, France, 1958*, p. 617.
10. A. V. Ignatyuk, Report INDC-233(L) (IAEA, Vienna, 1985).
11. A. M. Sukhovej, Phys. At. Nucl. **78**, 230 (2015).
12. A. M. Sukhovej and L. V. Mitsyna, in *Proceedings of the 22nd International Seminar on Interaction of Neutrons with Nuclei, Dubna, May 2014*, Preprint JINR No. E3-2015-13 (Joint Inst. Nucl. Res., Dubna, 2015), p. 245. <http://isinn.jinr.ru/past-isinns.html>.
13. <http://www-nds.iaea.org/ENDSF>.
14. S. G. Kadenskii, V. P. Markushev, and V. I. Furman, Sov. J. Nucl. Phys. **37**, 165 (1983).
15. L. A. Malov and V. G. Solov'ev, Sov. J. Nucl. Phys. **26**, 384 (1977).
16. E. V. Vasilieva, A. M. Sukhovej, and V. A. Khitrov, Phys. At. Nucl. **64**, 153 (2001).
17. W. Dilg, W. Schantl, H. Vonach, and M. Uhl, Nucl. Phys. A **217**, 269 (1973).
18. A. M. Sukhovej and V. A. Khitrov, Preprint JINR No. E3-2005-196 (Joint Inst. Nucl. Res., Dubna, 2005).
19. A. M. Sukhovei and V. A. Khitrov, Phys. Part. Nucl. **36**, 359 (2005).
20. A. M. Sukhovej and V. A. Khitrov, Phys. Part. Nucl. **37**, 899 (2006).
21. V. A. Kravtsov, *Atomic Masses and Nuclear Binding Energies* (Atomizdat, Moscow, 1965) [in Russian].
22. A. M. Sukhovej and V. A. Khitrov, Phys. At. Nucl. **76**, 68 (2013).

Testing the modified dependence of the radiative strength function on different excitation energies in the light nucleus ^{28}Al

¹D. Knezevic, N. Jovancevic¹, A. M. Sukhovej², L.V. Mitsyna²

¹University of Novi Sad, Faculty of Science, Department of Physics, Novi Sad, Serbia

²Joint Institute for Nuclear Research, Dubna, 141980, Russia

E-mail: nikola.jovancevic@df.uns.ac.rs

Received: December 29, 2017

Abstract

The spectrum of random functions of level density as well as radiative strength functions of dipole E1- and M1-transitions of ^{28}Al were determined. Obtained functions can reproduce very precisely the intensity of the two-step cascade following the radiative capture of thermal neutrons for a given energy of the primary transitions. The density of the observed intermediate levels can be reproduced correctly using the mean value of these functions. In this work we proposed a new hypothesis about the dependence of radiative strength functions for gamma-transitions in heated nucleus on the energy of excited levels. The results provide a solid basis that this new hypothesis allows to get realistic estimation on the parameters of nuclear structure in any nucleus, including the light ones.

Key words: Neutron resonance, two step gamma cascades, level density, radiative strength function.

1. Introduction

The determination of accurate values for the excited nuclei level density and radiative strength functions is one of the most important tasks in low energy nuclear physics. Trustable experimental values of these parameters are necessary for the study of the fundamental properties of the nuclear structure. For example, the step-like structure in the level density provides information about the phase transitions in heated nuclei and the influence of different type of resonance wave functions on radiative strength function for the γ decay process. Moreover, accurate experimental values of the level density and the radiative strength function are very important for applications as the analysis of astrophysical reactions, the production of medical isotopes, reactor technology, the production of rare isotope beams, etc.

The development of theoretical models needs a set of experimental information for the excited levels density (with given quantum numbers) and for the values of the partial radiative widths of all possible decay channels. If those data are available, the theoretical calculations can give a correct interpretation of the dynamics of the nuclear transitions, in a broad variety from the simple low-lying levels (e.g., quasiparticle or phonon structure) to the very complex compound-states.

The quality of the model-based description of all the parameters for the neutron resonance gamma-decay, for example, depends entirely on the precision of the experimental data. Hence, it is very important to minimize the overall experimental uncertainty and, accordingly, to minimize the possible misrepresentation in analysis of the observed process, mostly as a result of the use of certain assumptions and the related hypothesis. The ability to get an accurate solution substantially increases when in the measurement are employed nuclear spectrometers, having $FWHM \ll D_\lambda$ for all energy spaces D between the initial nuclear levels λ .

In this situation a fundamental experimental problem is to search for the connection between the emission probability Γ of the reaction product and the excited levels densities ρ . The sum of the branching ratios B_r ($B_r = \Gamma_{\lambda i}/\Gamma_\lambda$) for partial $\Gamma_{\lambda i}$ and total widths Γ_λ (if there are no competing processes) is equal to one and does not depend on the absolute values of the levels density ρ and the partial widths Γ . However, branching ratios of any level are determined by the sum of the partial widths and consequently they are dependent on the level density. So, to give an accurate description of the dependence between the measured values (intensity of the emitted spectrum of particles observed in the reaction), the excited levels density and the partial radiative widths is one of the most important tasks in the process of estimation of those parameters values.

In this work we proposed a new and a modified form of the dependence for the radiative strength function of the excited level density, based on the analysis of the experimental data and the existing models of the level density as well as the partial gamma-widths. This new approach was tested experimentally by the estimation of the most probable mean values of the level density and the radiative strength function of ^{28}Al compound-state gamma-decay. To accomplish this task, the Dubna two-step gamma cascade method was used [1, 2].

2. Theoretical considerations

2.1. Current state of the experiments designed for the determination of Γ and ρ

The information about the properties of the excited nuclei can be extracted only by the measurement of the spectra (cross-sections) S of the observed reaction product, and the subsequent analysis based on some existing functional dependencies between S and the parameters Γ and ρ ($S = \Psi(\Gamma, \rho)$). Such experiment can be performed measuring the reaction products spectra with a single detector (“one-step” reaction [3]), or by coincidences between two detectors (“two-step” reaction [4, 5]).

The first of these two experimental techniques was used up to now for the analysis of the spectra and the cross-sections of evaporative nucleons [3, 6] and full gamma spectra [7, 8]. The second one was applied in the spectroscopy measurements of two photons [3, 4] successively emitted after the neutron capture. Comparison of the Γ and ρ values obtained in the analysis of the experimental data collected in one- and two-step reactions, makes

possible to identify the main sources of the systematic experimental uncertainties, to estimate the uncertainty values and to compare them if different methods were applied in the study of the same nucleus.

2.1.1. Spectra of evaporative nucleons

The level density can be obtained from the evaporative nucleons spectra by the use of this method only if the value of Γ is known. The numerical value of the parameter Γ was calculated until now from the relatively rudimentary optical model. The agreement between the calculated cross-section and the experimentally determined one can be used for the validation of the obtained results. However, this method does not take into consideration that the experimentally measured cross-section (spectrum) is determined only by the absolute value of the product $\Gamma \cdot \rho$, and not by the absolute values of the individual terms Γ and ρ . One of the consequences (as can be seen comparing the data measured by this method [3, 8] with the two-step reaction analysis [4, 5]), is that the obtained values for the level density in the energy range around the threshold of the second gap for nucleons Cooper pairs are overestimated at least by 5-10 times [9].

2.1.2. Spectra of the primary quanta of cascades depopulating different energy excited states

The total intensity of the spectra of the first generation of cascade quanta [7] does not depend on the absolute values of Γ and ρ . Moreover, the absolute value of the function describing the dependence of the mentioned parameters Γ and ρ on the energy of the gamma-quanta and the energy of the excited level has no significant influence on the total gamma spectra (the sum of the gamma energies of cascade photons depopulating some level is absolutely independent from Γ and ρ). The mean quadratic variation of the different forms of the full gamma-spectra calculated employing various realistic representations of $\Gamma = f(E_\gamma)$ and $\rho = \varphi(E_{ex})$ does not exceed 30 %, in the best case, [10] (where E_{ex} is the excited level energy).

Fig. 1 shows the gamma rays spectra [11] following the inelastic scattering of ^3He on the ^{45}Sc isotope. The intensive and well-resolved low energy peaks registered in the “first generation” and the in “higher-generation” spectrum are produced, in most cases, only by second or higher cascade quanta [11]. These gamma peaks appear in the “first generation” spectra only due to an error of the specific techniques used. Specifically, this is a consequence of the non-compliance of the basic condition of the used technique [7]. The spectrum of the gamma radiation emitted after the decay of the levels for a given excitation energy is initialized by the beam of the charged particles and described by the one particular set of quantum numbers. This spectrum should be exactly the same as the spectrum measured in the experiment where observed levels are populated by the transitions from the high-lying energy levels. As a result, the systematic error of the “first generation” spectra can exceed 100 % in low energy photon region. The increase of E_γ can reduce this error by some unknown degree. This fact is not mentioned in the evaluation [12] of the error appearing in this approach [8].

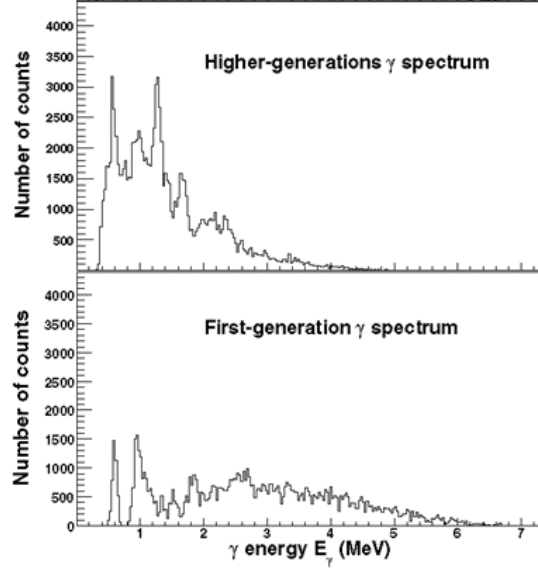


Figure 1: Gamma-ray spectra in the $^{45}\text{Sc}(^3\text{He}, ^3\text{He}\gamma)^{45}\text{Sc}$ reaction [11] for the first and next cascade quantum.

2.1.3. Two-step cascade quanta

The absolute intensity of the cascades $I_{\gamma\gamma} = \Psi(\Gamma, \rho)$, which can be measured by ordinary HPGe-detectors for a limited number of final levels, is defined by the inverse absolute value of the level density and by the form of the strength function $K = f(E_\gamma)$ [13]. Thereby, the relationship between the experimental values of $I_{\gamma\gamma}$ and the unknown functions Γ and ρ is always nonlinear, for all intervals of the excitation energy. The current experimental methods allow to determine only an interval for the possible values of Γ and ρ reproducing the measured intensity of the cascades $I_{\gamma\gamma}$. Even in the limit of zero statistical errors of the experimental values, Γ and ρ could not be unequivocally determined [14].

All the methods listed above have also common sources of systematic errors.

1. There is no practical model of the decay of the nuclear excited levels, for both nucleon and radiation channel, suitable for the analysis of the experiment. Such a model should be able to take into account explicitly the coexistence and the interactions of the boson and the fermion components of the nuclear matter.

2. It is necessary that the model considers the dependence of the partial widths Γ on the wave function for both the initial and the final level when the reaction product of a specified energy is emitted.

All the three techniques listed above, without exception, requires an additional, methodically independent, experiment. That experiment should produce a non-degenerate system of equations which can describe the relation between the measured spectrum and the values of the parameters Γ and ρ .

The influences of the mentioned sources of systematic errors, which are most significant for one-step reactions, can be essentially reduced in the two-step reaction experiment. Therefore, it is necessary to develop a modern model able to describe and predict possible changes of the nuclear properties caused by different excitation energies. This model would

require data from two-step reaction experiments.

2.2. Status of the current models of the level density and the partial gamma-widths

In modern theoretical views, for example for the quasiparticle-phonon model of the nucleus, the partial emission width is determined by the coefficients of the wave function components for both decayed and excited level [15]. The actual values of the partial widths are specified by the degree of the fragmentation for the different nuclear states with a fixed number of quasiparticles and phonons. The level density directly determines it, since the ρ value is defined by the degree of the fragmentation of all the possible states of the nucleus having energy lower than the excitation one.

Currently, the radiation strength function of the dipole gamma transitions for a nucleus with mass A can be expressed as:

$$k_{standard} = \Gamma_{\lambda i} / (E_{\gamma}^3 A^{3/2} D_{\lambda}) \quad (1)$$

where E_{γ} is the energy of the emitted gamma quanta, A is the atomic mass, D_{λ} is the density of the decaying level and $\Gamma_{\lambda i}$ represents the partial width of the nucleus transition from the λ to the i -th level.

The expression above takes into account the dependence of the partial radiative widths only from the density $\rho_{\lambda} = D_{\lambda}^{-1}$ of the decayed high-energy levels, such as the neutron resonances. However, the possibility that the partial radiative widths can be a function of the density of the intermediate levels of the heated nucleus having sufficiently high energy is not taken into consideration by Eq. 1. The modern two-step reaction $(n_{th}, 2\gamma)$ experiment revealed the existence of such a kind of dependence [16].

It was observed the smooth form of the function describing the energy spectra of the evaporated nucleons for the composite ^{181}W nucleus for several different initial excitation energies [17]. But, analysis [18] indicates that in the excitation energy near the threshold of the second gap of the Cooper pair of nucleons, the partial widths of the nucleon emission increase many times, compared with the partial widths in neighboring excitation energies of the residual nucleus. This tendency does not change (or shows just a moderate variation) when the energy of the incident protons in the (p, n) reaction is changed [18]. This can be explained only if the partial width of a nucleon emission is strongly dependent on the excitation energy of the residual nucleus and if the Strutinsky model for the level density [19] is used for the reproduction of the evaporate spectra. The set of parameters in the Strutinsky model approximation for the masses $40 \leq A \leq 200$ is derived from the level density obtained by $(n_{th}, 2\gamma)$ reaction. This means that, even for the different excitation energies of the produced nucleus ^{182}W , the product $\Gamma \cdot \rho$ preserves its form. Moreover, in the case of (p, n) reactions the wave function of the excited levels of the target nucleus (neutron resonance) changes significantly through the decay when evaporated neutron appears.

Therefore, it is possible to obtain the correct form of the energy dependence of the $\Gamma \cdot \rho$ product and, accordingly, the cross-section, for fixed nucleus excitation energy and for different energies of charged particles beam, even if the calculated values of Γ and ρ

are not correct.

2.3. Principles of the proposed modified model of radiation strength functions

In the previous section we mentioned the effect on dependence of the partial width for a nucleon emission on the excitation energy of the residual nucleus. This effect opens a possibility for a modification of the standard form of the relation between the radiative strength function and the excited level density. The modified expression Eq. 1 describing the radiation strength of the gamma transitions between an arbitrary compound state λ and any low-lying level i , can be written in the following form [20]:

$$k_{modif} = k_{standard}/D_i = (\Gamma_{\lambda i}/(E_{\gamma}^3 A^{3/2} D_{\lambda}))/D_i \quad (2)$$

This modification takes into account the fact that the radiative strength function is dependent on the average spacing D_i between the low-lying levels i .

In practice, in order to maintain continuity with Eq. 1, the following modification is suitable:

$$k_{modif} = k_{standard} \frac{D_{asim}}{D_i} = \frac{\Gamma_{\lambda i}}{E_{\gamma}^3 A^{3/2} D_{\lambda}} \frac{D_{asim}}{D_i} \quad (3)$$

In Eq. 3 D_{asim} is the asymptotic spacing between the levels of a heated nucleus treated as a pure fermion system (defined, for example, by non-interacting Fermi gas model) and D_i is the maximum possible expected space between the intermediate levels for a given excitation energy. The specific value D_i is the outcome of the coexistence and the interaction of the quasiparticle and the phonon types of excitations in the nucleus. Considering that the degree of fragmentation of some nuclear states is minimal at it's initial energy and grows up with energy increase [21], it can be expected that $D_{asim} \leq D_i$ and $k_{modif} \geq k_{standard}$ for the highest number of gamma transitions.

3. Measurement of the two-step gamma cascade intensity of ^{28}Al

The ^{28}Al compound state gamma decay was measured in order to test the new modified model describing the dependence of the radiative strength function on the level density. The two-step gamma cascade method was used for this purpose.

It is commonly believed that the mechanism of neutron capture in light nuclei, for example, is significantly more dependent on the structure of the wave function of the excited level than in the neutron capture reaction in medium and heavy mass nuclei. Therefore, there is a modest practical interest for the average parameters of cascade gamma decay of neutron resonance in light nuclei. However, it can be important for the estimation of the reliability of the radiation strength functions for the gamma transitions between the levels of the heated nucleus obtained by the use of modified model Eqs. 2 and 3.

The spectroscopic analysis data were already published and all details can be found in reference [22]. In this paper we present just a short description of the measurement procedure and the analysis of the spectroscopic information.

3.1. Experimental set-up

The two-step cascades emitted after thermal neutrons capture in the ^{27}Al target were measured at the LWN-15 reactor in Rež, Czech Republic. Gamma-gamma coincidences were registered by two HPGe detectors with 28 % and 25 % relative efficiency, respectively, which have the standard energy resolution for this type of detectors. The time resolution was better than 10 ns. The optimal count rate for the gamma-gamma coincidence detection of the ordinary fast-slow coincidences scheme was $100 - 200 \text{ s}^{-1}$. This count rate is a trade-off between two demands: to get the maximal possible values of the photopeak underlying background intensity ratios and to collect at least several tens of thousand events for the most intensive peaks. The required result can be achieved if the duration of the experiment is about several days at least and if the mass of the target ranges from hundreds of milligrams to several grams.

3.2. Spectroscopic information

The coincidence events were analyzed with the standard method [1, 2] based on the sum coincidence principle. Fig. 2 presents the most informative part of the measured spectrum.

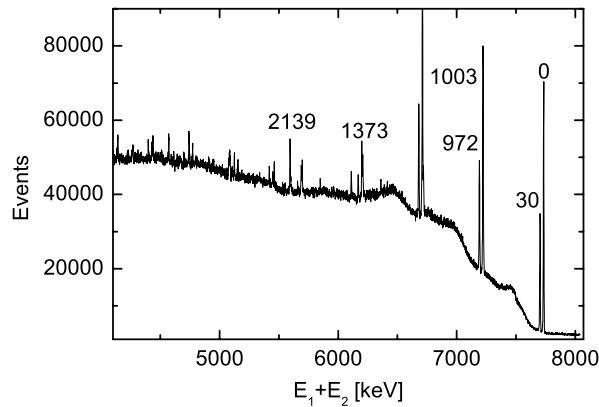


Figure 2: The main part of the sum coincidence spectrum of ^{28}Al . Full-energy peaks are labeled with the energy (in keV) of the final cascades levels.

Using the procedure described in [23], the intensity distributions of the cascades were obtained for some selected primary transition energy. For example, Fig. 3 shows the half of the measured intensity spectra of the cascades with energy of 7.725 MeV populating the ground state of the ^{28}Al nucleus (for $E_\gamma < 0.5B_n$). The other half is mirror symmetric [24]. The transition energy and the intensity of about 250 cascades were obtained using 13 collected spectra, similar to the one presented in Fig. 2. The positions and the area of the peaks in the spectrum are uniquely identified by the cascade parameters.

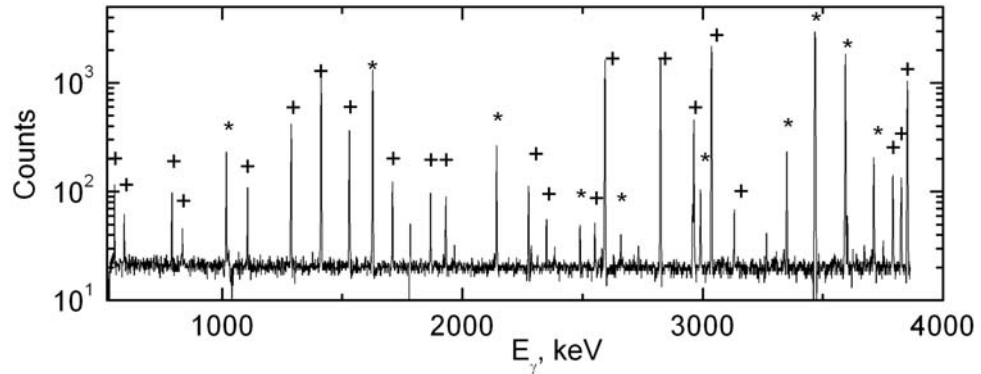


Figure 3: Half of the intensity distribution of the two-step cascades with energy 7.725 MeV populating the ground state. The primary transition of the ^{28}Al cascades are marked by crosses, whereas asterisks are the secondary one's. (The spectrum is shifted up to 20 counts due to the logarithmic scale.)

The order of the quanta in the cascades was determined by an algorithm [25]. This algorithm is based on a fact: the primary gamma transition has some energy in different two-step cascades and the second cascade photon energies have shifted on a difference for the final cascade level energies.

After the quanta sequence and the intermediate level energy were determined, almost all detected cascades were exactly placed into the decay scheme up to the energy of $\approx B_n - 520 \text{ keV}$. This method of two-step gamma cascades gives the possibility to provide the most complete level scheme for an investigated nucleus. The total number of levels observed with this method in ^{28}Al is close to hundred; file of evaluated data [26] contains about 45 levels identified up to now. It should be emphasized that in the two-step cascade spectrum registered after the thermal neutron capture, the number of observed excited levels is always noticeably higher than the number of levels found in any other nuclear spectroscopy method.

In order to extract the values of the level density and of the radiative strength function by the analysis of the experimental data, it is required to transform the relative intensities of the resolved peaks into absolute values (in % per decay). This was done by normalization to the absolute intensities i_1 [27] of some primary transitions, multiplied by the branching ratios B_r of the corresponding secondary transitions. B_r was determined from the standard data treatment of the same measurement set of $\gamma - \gamma$ coincidence.

The dependence of the absolute intensity of the two-step gamma cascades on the energy of the primary gamma transition, was obtained as final spectroscopic result. This result is crucial for the determination of the level density and of the radiative strength function. Fig. 4 presents the absolute intensity of the two-step gamma cascades on the two first excited levels and the ground level [22]. The values of the level density and of the radiative strength function for ^{28}Al were obtained by the fitting procedure described in references [2, 20] and the spectroscopic results are presented on Fig. 4.

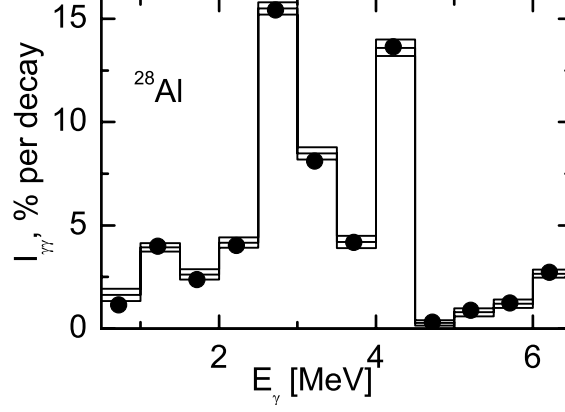


Figure 4: Histogram - distribution of the intensity of the two - step gamma cascades of the ^{28}Al to the ground, the first and the second excited level as functions of their primary transition energy. The approximated values $I_{\gamma\gamma}$ obtained by one of the variants defining the random radiative strength and the level density functions are noted by dots.

3.3. The levels density and the radiation strength functions of the ^{28}Al nucleus

The unambiguous determination of ρ and Γ from the measured spectra is impossible, even in principle, because the functional dependence of the two-step gamma cascade intensity on the level density and on the radiative strength function is nonlinear and degenerated:

$$I_{\gamma\gamma}(E_1) = \sum_{\lambda,f} \sum_i \frac{\Gamma_{\lambda i} \Gamma_{if}}{\Gamma_{\lambda} \Gamma_i} = \sum_{\lambda,f} \frac{\Gamma_{\lambda i}}{\langle \Gamma_{\lambda i} \rangle m_{\lambda i}} n_{\lambda i} \frac{\Gamma_{if}}{\langle \Gamma_{if} \rangle m_{if}} \quad (4)$$

where $\Gamma_{\lambda i}$ and Γ_{if} are the partial radiative widths corresponding to the primary and to the secondary transition; $n_{\lambda i} = \rho_{\lambda} \Delta E_i$ is the number of the excited intermediate levels in a certain interval of the excitation energy ΔE_i ; $\langle \Gamma_{\lambda i} \rangle$ and $\langle \Gamma_{if} \rangle$ are the average values of the corresponding intervals of the nucleus excitation energy widths; $m_{\lambda i}$ and m_{if} are the number of levels in the same intervals.

However, the form of the functional relation for the parameters appearing in Eq. 4 limits the region of their possible parameter values. For this reason N values of the experimental cascade intensities always can be converted in $\sim 2N$ values of ρ and Γ , satisfying the conditions:

$$\begin{aligned} \rho_1 &\leq \rho \leq \rho_2 \\ \Gamma_1 &\leq \Gamma \leq \Gamma_2. \end{aligned} \quad (5)$$

With the use of an iterative technique it is possible to obtain a random function of the level density and of the radiative strength function which can reproduce, with high precision, the experimental values of $I_{\gamma\gamma}$. Hence the measurement of the two-step gamma cascades provides a good possibility to determine the most probable values for these parameters.

The approximated values of the measurement $I_{\gamma\gamma}$ (obtained by the iterative method based on Eq. 4) are presented by the dots in Fig. 4. These values correspond to any of the single random functions of the level density and of the radiative strength function. In Fig. 5 the thin lines represent the obtained random functions for the level density and by the dots are shown the average value of these random functions. The most probable region of the level density is presented on Fig. 6.

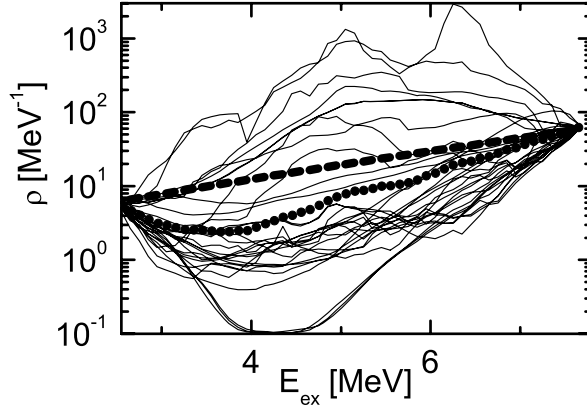


Figure 5: A set of random functions describing level densities able to reproduce data presented on Fig. 4 with a very close and small χ^2 values (thin lines). The average value of the entire set of random functions is presented by dots. Dashed line - model value for ρ [29].

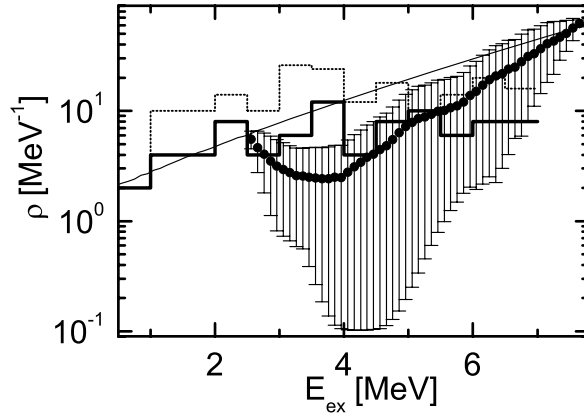


Figure 6: Thick line - model value for ρ [29]. Solid histogram presents density of the ^{28}Al levels from [26], dotted histogram - from processing spectra [22] similar to those shown in Fig. 1. Dots with error bars are the results of this study (same as in Fig. 5).

Two different forms of the radiative strength function dependence on the level density (Eq. 1 and 3) were used in the fitting procedure. In this way, the modified dependence in

Eq. 3 is tested in comparison with the standard one in Eq. 1 on the set of experimental data presented in Fig. 4. In Figs. 7 and 8 are presented the obtained random functions and the most probable region of the radiation strength function when using Eq. 1. The same results are shown in Figs. 9 and 10, but here Eq. 3 was used. The difference between the obtained values of the radiative strength function, as presented in Figs. 8 and 10, provides the information about the influence of the collective enhancement for the level density on the radiative strength function.

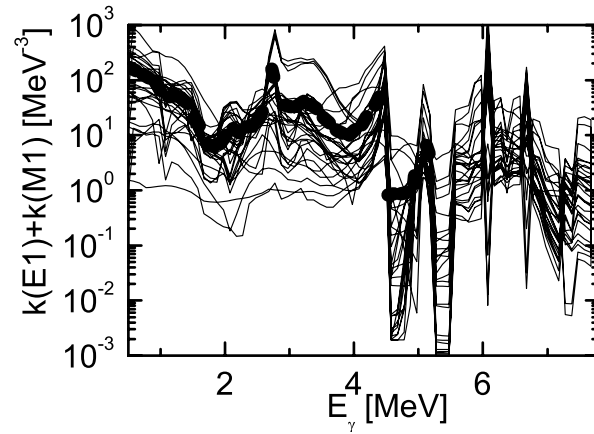


Figure 7: Thin lines - set of random functions (obtained by iterative process) describing the radiation strength function in standard definition Eq. 1 able to reproduce data presented on Fig. 4. Dotted line - average for sum of strength function E1- and M1- transition.

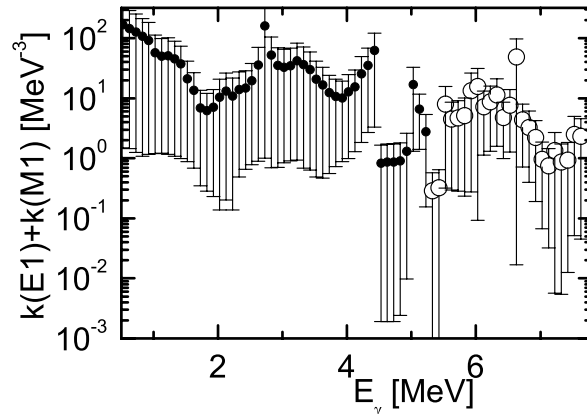


Figure 8: Values for the radiation strength function in standard definition Eq. 1. Dark dots - sum of M1- and E1-transition. Open dots - data only for M1-transition.

The values of the radiative strength functions for the $E1 + M1$ transition (dotted line) and the values for only the $M1$ -transition are presented in Figs. 7 and 8. In the energy region above 3.465 MeV are present only $M1$ - transitions. The positive parity

of the ^{28}Al neutron resonances and of all the known low-lying levels define practically only $M1$ multiplicities of the primary transitions. Hence, the information on the $E1$ radiative strength functions for $E_\gamma > 4260\text{ keV}$ cannot be obtained from the two-step cascade intensity.

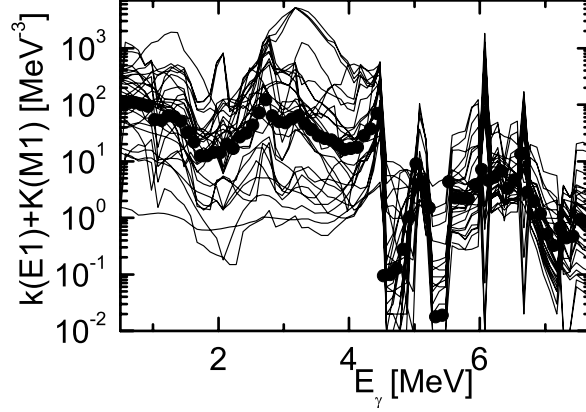


Figure 9: The same as in Fig. 7 for the modified model of the radiation strength function Eq. 3. Dotted line is average values.

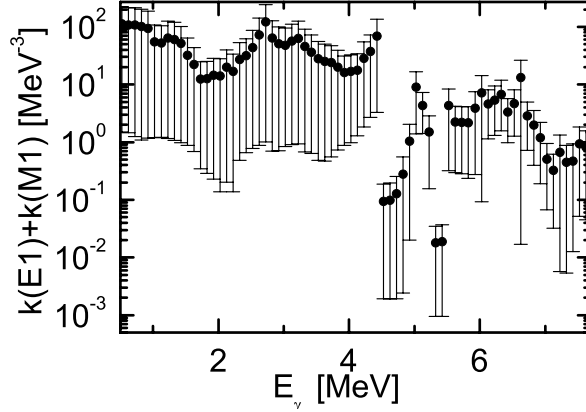


Figure 10: Average values of radiation strenght function with error bars in case of modified model Eq. 3.

The thermal neutrons capture cross sections for this nucleus is determinated by the resonances with spins 2 and 3. The dominant dipole type of the primary gamma-transitions limits the spin window for the intermediate levels to the interval $1 \leq J \leq 4$. The level density in this spin interval, calculated from the schemes evaluated from file [26, 27] in Fig. 5 is compared with similar data obtained from the two-step cascades. The corresponding data, together with the density of the neutron resonances are always used for the normalization of the relative level density in both the one- and the two-step reactions. Unfortunately,

the independent analysis [18] of the accuracy for the values D_λ showed that the possible systematical error may underestimate the density of the neutron resonances, even by one order of magnitude.

The influence of the mentioned error of the level density in all excitations can be accounted by a simple change of the normalization parameters for the set of random chosen functions describing the level density and the radiative strength. However, no data related to the real errors on the neutron resonances densities, identified in [28], are available in the literature until now.

4. Discussion

The unknown values of Γ and ρ correspond to each interval of the excitation energy for the intermediate levels (two-step cascades, in particular). In the general case, the inequality of the radiative strength functions for the primary and the secondary gamma transitions should be taken into account, even if they have the same energy and multipolarity. In principle, these circumstances make degenerated any system of nonlinear equations which connect the spectra intensity and unknown gamma-decay parameters. However, even in such case it can be defined a region Eq. 5 of the possible values for the level density and for the radiation strength functions. Authors of [2] showed that this can be done with acceptable precision if a sufficiently large set of values of the random functional dependencies for ρ and Γ on the energy gamma-transition are provided for excitation of nuclei. This is true in the frame of the postulate that the difference between the average of the random values and true unknown real value always tends always to minimum. Therefore, the value obtained in the two-step gamma cascades experiment [2] can be considered as a valid results, with the corresponding uncertainty of the level density and the radiation strength functions values.

The very significant difference of the ^{28}Al low-lying levels density in the region from $\rho \approx 4 \text{ MeV}^{-1}$ up to $\rho \approx 20 \text{ MeV}^{-1}$ (Fig. 5, solid and dotted histogram), can explain the skepticism related to the contemporary experiment. This includes as well the occurrence of the possible methodical errors in the determination of the values of Γ and ρ . However, the hypothesis in Eq. 3 can be taken as a first approximation of the model description for the radiative strength functions in any heated nucleus. As a special case, this hypothesis includes the existing assumption that the radiative strength functions and the level density for any nucleus are independent from the structure of the excited levels. This possibility should be checked on a large set of experimental data.

The practical absence of the negative-parity levels below 3.3 MeV does not allow to obtain the strength function of the $E1$ -transition in this interval for ^{28}Al excitation energies. It is also not possible to obtain a satisfactory approximation for the intensity distribution in the range of the primary cascade energies from $E_1 \approx 0.5 \text{ MeV}$ to $E_1 \approx 1 \text{ MeV}$. The increase of the strength functions in this interval, which can be observed in Fig. 8 and 10, can be explained as a consequence of the absence of secondary cascade transitions enhancement in this interval of energies. The corresponding increase in the strength functions can be qualitatively explained only by the presence of the collective type of primary transitions in the region of B_n and the corresponding vibration enhancement of the level density. This might be possible if the breaking threshold of the next Cooper pair falls randomly in the region of nuclear excitation near B_n .

In Fig. 11, we show the potential effectiveness of the technique presented in this work. In Fig. 11a, the level density was determined by model [29], whereas in Fig. 11b the level density was obtained with the approximation similar to the one presented on Fig. 5 but assuming equality of ρ for the levels of positive and negative parity. The main result of this exercise is to show that an independent experiment, able to determine the level density, will make possible to obtain a precise information on the radiation strength function. In the same way an experiment designed to determine the radiative strength function can provide the values of the level density.

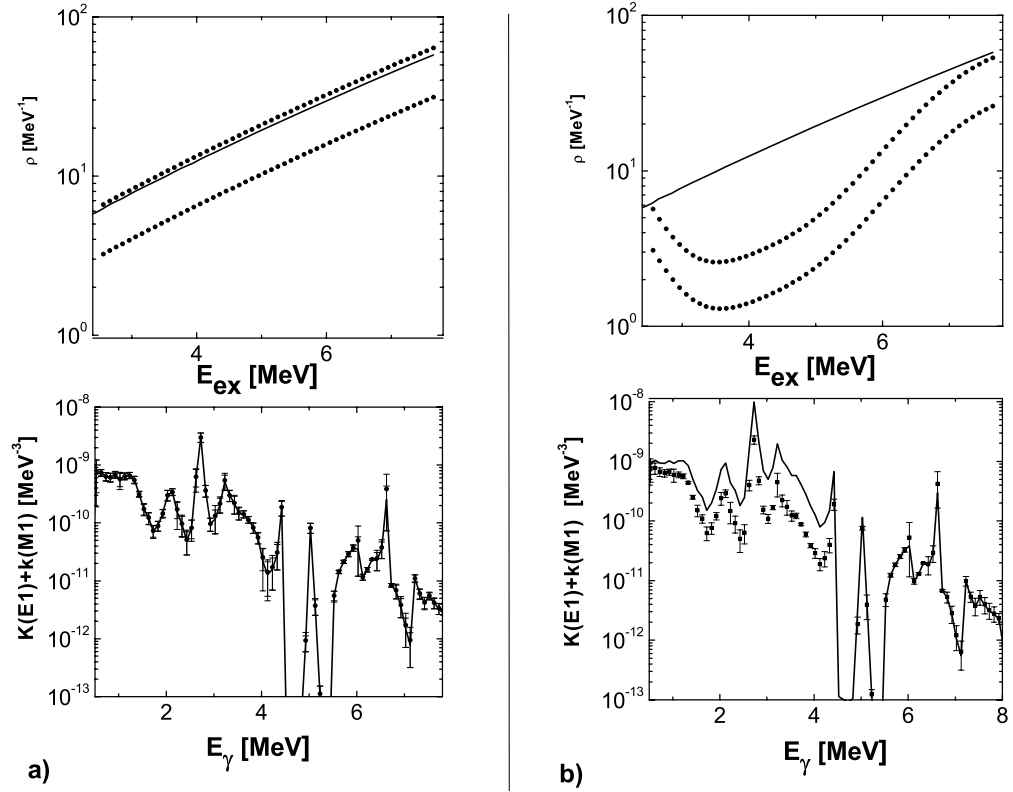


Figure 11: a) Top row: fixed to the level density of ^{28}Al (dots and line) from model [29]. Bottom row: the best approximation of the radiative strength functions for fixed level density. Points with error bars: standard presentation of the radiation strength function; line: strength function in the Eq. 3. b) Top row: level density from model [29] (line) and approximated level density (dots). Bottom row: points with error bars: standard presentation of the radiation strength function; line: strength function in the Eq. 3.

Searching the solution of a degenerate nonlinear systems of equations can always give as a result both the real function and a local maximum likelihood function. Methods good enough to identify and solve such systems have already been developed. The data in Fig. 4, presenting the worst version for the fitting process of the experimental data at $I_{\gamma\gamma}$, has been used to determine Γ and ρ . Hence, the number of iterations required to achieve a minimum disagreement between the experimental and the approximation values for the cascade gamma decay of the neutron resonances on ^{27}Al nucleus usually exceeds 10^5 for

each variant of the calculation. Here, as in many other cases, it is convenient that the first iteration includes in source data specific values of the strength functions for the most intensive gamma-transition “spread” under appropriate intervals of the primary gamma-transition energy.

5. Conclusion

In this work we proposed Eqs. 2 and 3 as new hypothesis for the energy dependence form of the radiative strength function for the excited level density of the residual nuclei. This hypothesis was experimentally tested on the light nuclei ^{28}Al . The spectrum of the random functions for the level density as well as the radiative strength functions of the dipole $E1$ - and $M1$ -transitions were determined for ^{27}Al . The obtained functions can reproduce very precisely the intensity of the two-step cascade following the radiative capture of thermal neutrons for a given energy of primary transitions. The density of the intermediate levels corresponding to all the energetically resolved cascades observed (including those firstly established in reaction($n_{th}, 2\gamma$)) can be reproduced correctly using the mean value of the obtained functions for the level density. In this work, for the first time, we obtained the information about the influence of the collective enhancement of the level density on the radiative strength function.

The results of the ^{28}Al two-step cascades experiment show that the hypothesis given by Eq. 2 can ensure the maximum precision for the description of the spectra and of the cross sections in a broad region of nuclear masses [20] (including light nuclei). Unfortunately, the determination of the density for the low-lying levels and the neutron resonances in a custom nucleus, with acceptable precision, still remains an unsolved problem. For this reason the dynamic model of the interaction of superfluid and normal states of nuclei, in the transition region from levels with a simple wave function to extremely complex compound-states, can not be identified and described correctly.

Further experiments are indispensable to accomplish this task. This can be done through the implementation of multi-step reactions. The most promising technique is the measurement of the intensity for a sequence of three or more cascade photons [30] in the radiation capture of nucleons and light nuclei reactions, as well as measuring the intensities of the cascades, containing nucleon products of nuclear reactions [9], in coincidences with photons.

The improvement of the process for the determination of the radiative strength function and the level density can be achieved also by the development of new models. These models should introduce the dependence of both the radiative strength function and the level density on the same fitting parameters. The first of all these parameters should be the threshold gap for the Couper pair and the mutually connected coefficients for vibration and collective enhancement of the levels density. This should be done for the radiative strength functions at decay of the levels with large enough components of the phonon type in the structure of their wave functions. For example, it can be expected that the models of this type will be able to easily reproduce the intensity of the cascades primary transition in the $\approx 0.5 - 1$ MeV energy range (Fig. 2) for ^{28}Al , as well as, for large number of other nuclei. Under favorable conditions (a small number of parameters), it can be expected a rather uniquely determination of the radiative strength functions and of the level density

even without fixing one of those parameters.

References

- [1] S. T. Boneva, E. V. Vasileva, Yu. P. Popov, A. M. Sukhovoij and A. Khitrov, *Sov. J. Part. Nucl.* **22**, 232 (1991).
- [2] S. T. Boneva, E. V. Vasileva, Yu. P. Popov, A. M. Sukhovoij and V.A. Khitrov, *Sov. J. Part. Nucl.* **22**, 698 (1991).
- [3] H. Vonach, *Phys. Rev. C* **38**, 2052–2062 (1988).
- [4] E. V. Vasilieva, A. M. Sukhovoij and V. A. Khitrov, *Phys. At. Nucl.* **64**, 153 (2001).
- [5] A. M. Sukhovoij and V. A. Khitrov, *Phys. Particl. and Nuclei* **36**, 359 (2005).
- [6] B. V. Zhuravlev, *Bull. Rus. Acad. Sci. Phys.* **63**, 123 (1999).
- [7] G. A. Bartholomew, E. D. Earle, A. J. Ferguson, J. W. Knowles and M. A. Lone, *Advances in nuclear physics* **7**, 229 (1973).
- [8] A. Schiller, L. Bergholt, M. Guttormsen, E. Melby, J. Rekstad and S. Siem, *Nucl. Instrum. And Methods A* **447**, 498 (2000).
- [9] A.M. Sukhovoij and V. A. Khitrov, *Nucl. Instrum. Phys. At. Nucl.* **73**, 1635 (2010).
- [10] A. M. Sukhovoij and V. A. Khitrov, In *Proc. of the XVII International Seminar on Interaction of Neutrons with Nuclei*, Dubna (2009).
- [11] A. C. Larsen, M. Guttormsen, R. Chankova, F. Ingebretsen, T.Lomnroth, S. Messelt, J. Rekstad, A. Shiller, S. Siem, N. U .H. Syed and A. Voinov, *Phys. Rev. C* **76**, 044303 (2007).
- [12] A. C. Larsen, M. Guttormsen, M. Krtcka, A. Betak, A. Burger, A. Gorgen, H. T. Nyhus, J. Rekstad, A. Schiller, S. Siem, H. K. Toft, G. M. Tveten, A. V. Voinov and K.Wikan, *Phys. Rev. C* **83**, 034315 (2011).
- [13] A. M. Sukhovoij, V. A. Khitrov and W. I. Furman, *Phys. At. Nucl.* **72**, 1759 (2009).
- [14] V. A. Khitro,v and Li Chol and A. M. Sukhovoij, *Proceedings of the XII International Seminar on Interactions of Neutrons with Nuclei*, Dubna, **E3-2004-9**, (2004).
- [15] V. G. Soloviev, *Sov. Phys. Part. Nuc.* **3**, 390 (1972).
- [16] A. M. Sukhovoij and V. A. Khitrov, *Phys. Particl. and Nuclei* **37**, 899 (2006).
- [17] V. G. Pronyaev et al., *Sov. J. Nuc. Phys.* **30**, 310 (1979).
- [18] A. M. Sukhovoij and V.A. Khitrov, *Phys. At. Nucl.* **73**, 1507 (2010).

- [19] V. M. Strutinsky, Proceedings of the International Congress on Nuclear Physics, Paris, 617 (1958).
- [20] N. Jovancevic, A. M. Sukhovej, W. I. Furman and V. A. Khitrov, Proc. XX International Seminar on Interaction of Neutrons with Nuclei, Alushta (2012).
- [21] L. A. Malov and V. G. Solovev, Yad. Phys. **26**, 729 (1977).
- [22] J. Honzatko, V.A. Khitrov, A.M. Sukhovej and I. Tomandl, Fizika B **12**, 299 (2003).
- [23] S. T. Boneva, V. A. Khitrov and A. M. Sukhovej, Nucl. Phys. A **12**, 199 (1995).
- [24] A. M. Sukhovej and V. A. Khitrov, Instrum. Exp. Tech. **27**, 1071 (1984).
- [25] Yu. P. Popov et al., Bull. Acad. Sci. USSR Phys. Ser. **48**, 53 (1984).
- [26] NNDC, *Evaluated Nuclear Structure Data File* (2013), URL <http://www.nndc.bnl.gov/nndc/ensdf>
- [27] IAEA, *Evaluated Gamma-ray Activation File* (2013), URL <http://www-nds.iaea.org/pgaa/egaf.html>
- [28] A. M. Sukhovej and V.A. Khitrov, XVIII International Seminar on Interaction of Neutrons with Nuclei, Dubna (2011).
- [29] W. Dilg, W. Schantl, H. Vonach and M. Uhl, Nucl. Phys. A **217**, 269 (1973).
- [30] K. Furutaka, M. Oshima, A. Kimura, Y. Toh, M.Koizumi, T. Kin and J.Goto, In Proceedings of the International Conference on nuclear data for science and technology 2007, Nice, 517 (2007).

Gamma-2 Scientific Workshop on the Emission of Prompt Gamma Rays in Fission and Related Topics

Studies of the low-energy gamma background

K. Bikit, D. Mrđa*, I. Bikit, J. Slivka, M. Veskovc, D. Knezevic

Department of Physics, Faculty of Sciences, University of Novi Sad, Trg Dositeja Obradovica 4, 21 000 Novi Sad, Serbia

Abstract

The investigations of contribution to the low-energy part of background gamma spectrum (below 100 keV) and knowing detection efficiency for this region are important for both, a fundamental, as well as for applied research. In this work, the components contributing to the low-energy region of background gamma spectrum for shielded detector are analyzed, including the production and spectral distribution of muon-induced continuous low-energy radiation in the vicinity of high-purity germanium detector. In addition, the detection efficiency for low energy gamma region is determined using the GEANT 4 simulation package. This technique offers excellent opportunity to predict the detection response in mentioned region. Unfortunately, the frequently weakly known dead layer thickness on the surface of the extended-range detector, as well as some processes which are not incorporated in simulation (e.g. charge collection from detector active volume) may limit the reliability of simulation technique. Thus, the 14, 17, 21, 26, 33, 59.5 keV transitions in the calibrated ^{241}Am point source were used to check the simulated efficiencies.

© 2014 The Authors. Published by Elsevier B.V. This is an open access article under the CC BY-NC-ND license (<http://creativecommons.org/licenses/by-nc-nd/3.0/>).

Selection and peer-review under responsibility of Guest Editor: Mr. Stephan Oberstedt - stephan.oberstedt@ec.europa.eu

Keywords: background gamma spectrum; low-energy spectral region; Compton scattered events; X-ray fluorescence; cosmic-ray muons; Bremsstrahlung; nuclei recoils

* Corresponding author: Tel.: +381 21 485 2815.
Email-address: mrdjad@df.uns.ac.rs.

1. Introduction

Some of the examples in fundamental and applied research, where the exploration of background events in low-energy gamma region is necessary, are given below:

- The predicted weakly-interacting massive particles (WIMPs), which are the best candidates for dark matter, should cause nuclei recoils in detector active volume of up to 100 keV (Sisti; 1999)
- Weak low-energy nuclear transitions
- Many radionuclides in environmental samples (^{238}U , ^{210}Pb) emit gamma rays with energies of several tens of keV, which are used for determination of their activity concentrations

In order to obtain quantitative results of measurements, the efficiency calibration of gamma detector should be performed. However, the determination of the low-energy efficiency of high-purity germanium (HPGe) detectors is the most difficult task in detector calibration.

2. The contributing components to the low-energy gamma background

The contribution of environmental radioactivity to the low-energy spectral part of gamma spectra can be significantly reduced by passive shielding of germanium detector with dense materials, such as lead. In Fig.1, the comparison between low-energy parts of gamma spectra (below 500 keV) for unshielded and lead-shielded HPGe detector (100% relative efficiency, 380 cm³ of detector active volume) is presented (Mrđa et al., 2007).

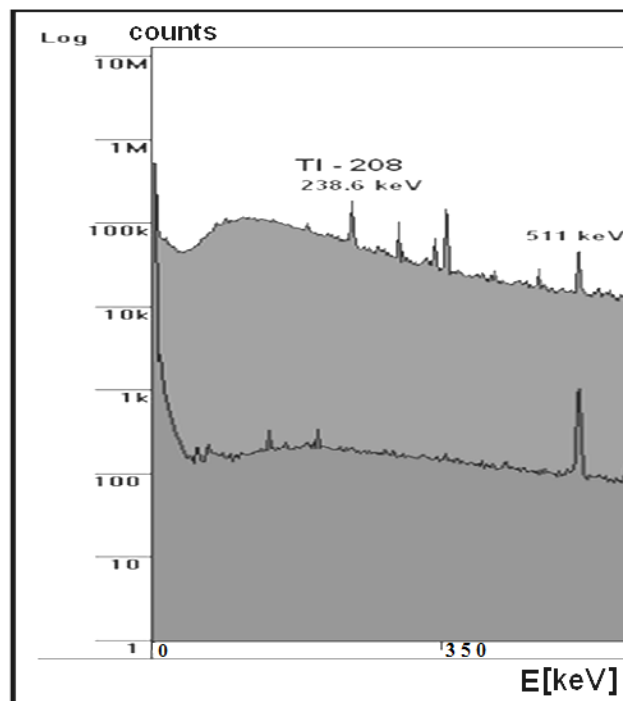


Fig. 1. The low-energy regions of unshielded (upper spectrum) and lead shielded HPGe detector (lower spectrum). The ratio of spectral intensities for the energy interval 20 keV-350 keV is about 380.

Several components contribute to the low-energy region of background gamma spectrum for the shielded detector:

- The Compton scattered events of high-energy gamma rays (^{40}K , ^{208}Tl)
- X-ray fluorescence from materials in detector vicinity (Bikit et al., 2009)
- Continuous radiation distribution induced by cosmic-ray muons in materials from detector surroundings (active shielding necessary for further background reduction)
- Bremsstrahlung from ^{210}Pb present in detector lead-shield
- Nuclei recoils in detector active volume due to elastic and inelastic neutron scattering

2.1. The Compton scattered events

The expected effects of Compton scattering of 2.6 MeV gamma rays emitted outside of lead shield, on detected gamma spectrum are presented in Fig. 2. In order to avoid all other contributions, which can be involved in real experimental conditions, this spectrum is obtained by GEANT4 simulation toolkit (Geant 4 Collaboration, 2012). As a result of Compton scattered high-energy gamma rays within lead shield and gamma detector, the approximately uniform distribution of deposited energies over wide energy interval is obtained, including the low-energy interval.

2.2. Pb X-ray fluorescence

The intensity of $K\alpha$ and $K\beta$ X-fluorescence rays from lead can be very strong if appropriate inner lining for lead shield is not applied. Very often the cadmium layer with 1 mm thickness is used as a lining material. However, since Cd has a relatively high cross section for thermal neutron capture, the corresponding gamma lines from $^{113}\text{Cd}(n,\gamma)^{114}\text{Cd}$ reaction may be present in background spectrum (558.4 keV, 805.9 keV). The other possibility is to use tin and copper layers. In figure 3 the reduction of Pb X-rays by a 1 cm thick Cu layer is shown for an “extended range” HPGe detector.

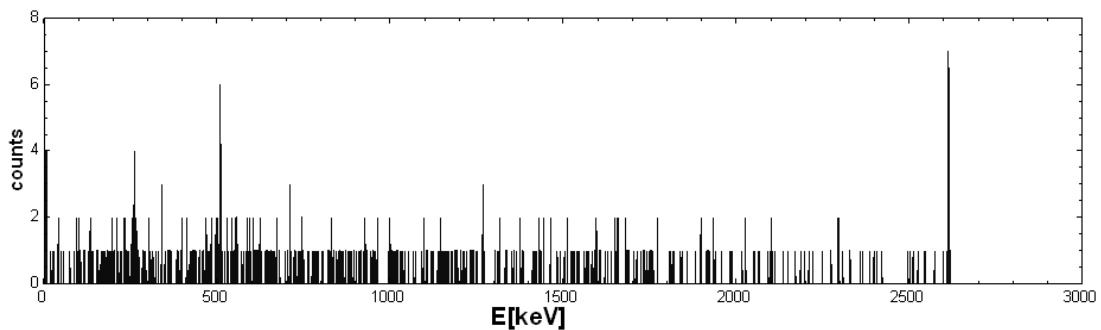


Fig. 2. The simulated gamma spectrum of events registered by the detector as a consequence of mono-energetic 2.6 MeV gamma rays emitted outside of a 10 cm thick lead shield.

2.3. Continuous radiation distribution induced by cosmic-ray muons

Although the presence of thick layers of materials in the vicinity of HPGe detector (such as thick copper layer) is efficient for Pb X-ray fluorescence reduction, this also causes the increase in intensity of low-energy continuous radiation, produced by cosmic ray muons. The coincidence measurements based on plastic scintillation detectors and germanium detector can be used for investigation of mentioned continuous spectral distribution arising from detector surrounding material, including determination of effective cross-sections for low-energy continuum production (Bikit et al., 2013).

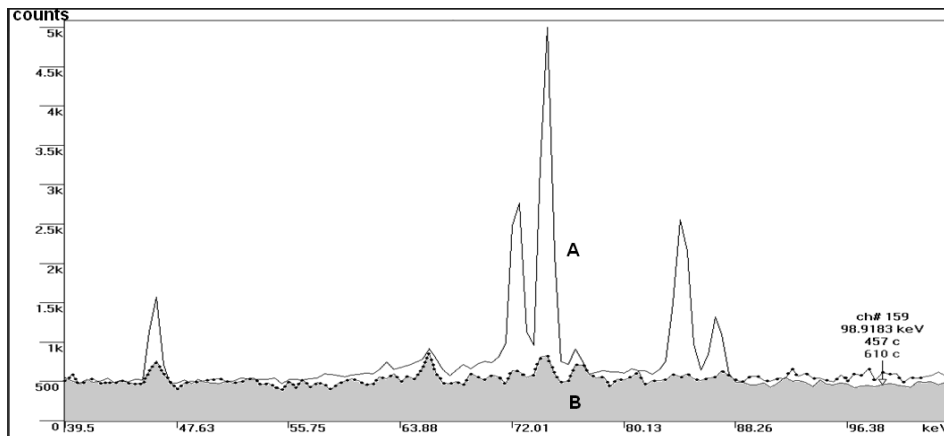


Fig. 3. The low energy regions of background gamma spectra (A- without inner lining of lead shield, B- with 1cm thick Cu lining)

2.4. Bremsstrahlung induced by ^{210}Pb in lead shield

The isotope ^{210}Pb emits only a weak (4.05%) low energy γ -ray at 46.5 keV, while its daughter ^{210}Bi is an almost pure β -emitter ($E_{\beta\text{max}} = 1.16$ MeV). We used a semi-empirical method, for the estimation of bremsstrahlung intensity, induced by ^{210}Pb , in the background of the GMX type “ORTEC” HPGe spectrometer with nominal efficiency of 32%. The ^{210}Pb content in the lead shield is measured to be 25 ± 5 Bq/kg. In figure 4 the calculated bremsstrahlung distribution compared with the measured background spectrum is presented.

We found that the bremsstrahlung contribution to the spectral intensity in the region up to 500 keV is about 20% for our surface based detector (Mrđa D. et al. 2007).

2.5. Nuclei recoils in detector active volume

As an example of inelastic scattering of neutrons in germanium crystal, the 68.7 keV line from $^{73}\text{Ge}(n, n')$ ^{73}Ge is analysed by coincidence circuit of germanium detector and plastic scintillator. The changes in the intensity and shape of the 68.7 keV line for different selected intervals of the time spectrum were observed. Thus, the fine broadening of the selected time interval toward faster events led to a more prominent tail of this line, due to the fact that faster neutrons (i.e., more energetic neutrons) cause larger recoils of germanium nuclei (Mrđa et al., 2013).

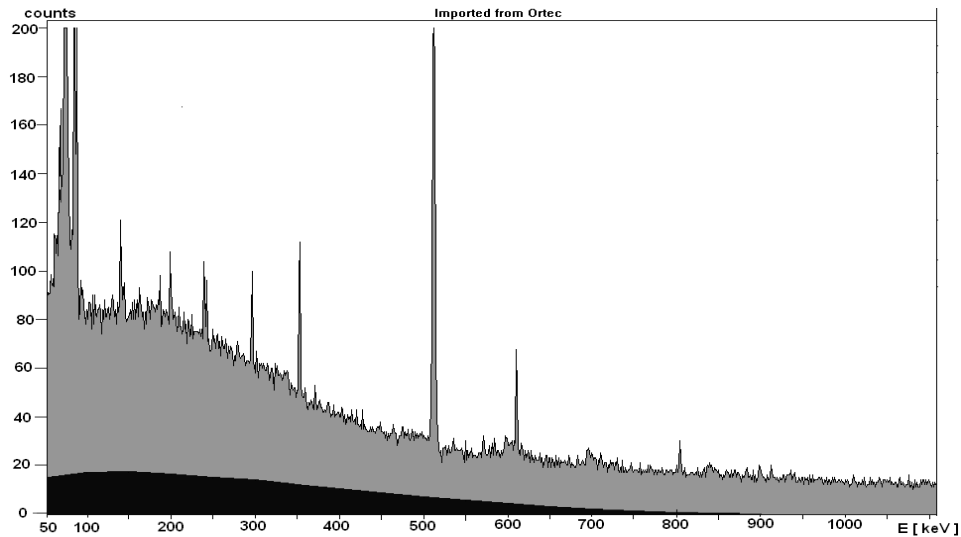


Fig. 4. The bremsstrahlung contribution (black area) to the measured background spectrum

3. Determination of detection efficiency for low-energy region

We compared the results of efficiency calibration (below 60 keV) for extended range HPGe detector, obtained by experimental approach (using ^{241}Am point source), with efficiencies determined by GEANT4 simulation software. The schematic view of experimental setup for determination of detection efficiency and the corresponding source-detector geometry from GEANT-4 simulation are given in Fig. 5.

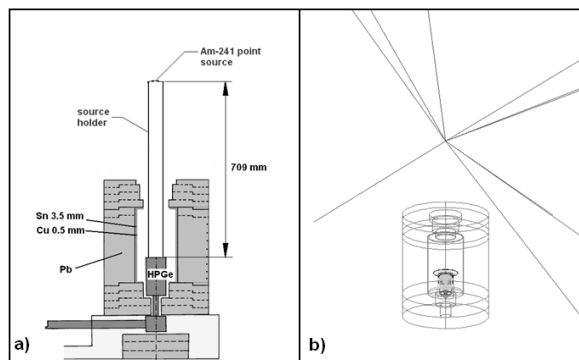


Fig. 5. The experimental setup (a) and source-detector geometry from GEANT-4 simulation (b), for determination of detection efficiency for low-energy region

The 13.9, 17.6, 21.0, 26.3, 59.5 keV transitions in the calibrated 432(15) kBq activity ^{241}Am point source were used to check the simulated efficiencies. The comparison of experimental data with GEANT4 results is

presented in Fig. 6, while the relative differences between measured and simulated efficiency values are summarized in Tab. 1.

The possible origin of these differences can be caused by the fact that the manufacturer not exactly specified the layer thicknesses, necessary for simulating the detector. However, our efficiency simulations for other detectors (which are not of extended-range type), do not show such discrepancies compared to experimental values.

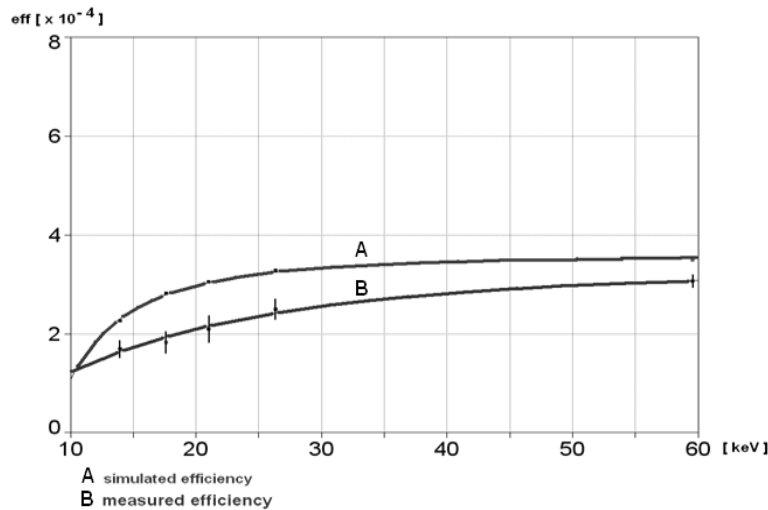


Fig. 6. Comparison of the detector efficiency obtained from experiment and using GEANT4 simulation software

Table 1. The relative differences between measured and simulated efficiencies for low-energy region

Energy [keV]	Relative differences
13.9	34
17.6	55
21.0	46
26.3	31
59.5	14

4. Concluding remarks

Many factors influence the low-energy background in gamma spectrometry and their contributions should be carefully analyzed for each specific situation (experiment). The reduction of low-energy spectral contribution can be achieved by selecting the proper surrounding materials for gamma detector, as well as by active shielding.

Monte-Carlo simulations in combination with measured results are the most effective approach for investigation of low-energy background components.

The determination of detection efficiency for low-energy region is a difficult task in case of various source types and source-detector geometries. Thus the significant discrepancies can be expected between measured and simulated results.

Acknowledgements

The authors acknowledge the financial support of the Ministry of Education, Science and Technological Development of Serbia, within the projects No.171002 and No.43002.

References

- Bikit I., Mrda D., Anicin I., Veskovic M., Slivka J., Krmar M., Todorovic N., Forkapic S., Nucl. Inst. and Meth. A606 (2009) 495
- Bikit K., Mrda D, Bikit I., Veskovic M., 2013. Investigation of cosmic-ray muon induced processes by MIREDO facility, ICRM 2013: 19th International Conference on Radionuclide Metrology and its Applications , Antwerp, Belgium , P-156
- Geant4 Collaboration, 2012. Geant4 User's Guide for Application Developers, Version: geant4 9.6.0, <http://geant4.web.cern.ch/geant4/UserDocumentation/UsersGuides/ForApplicationDeveloper/html/>
- Mrda D., Bikit I., Veskovic M., Forkapic S., Todorovic N., Harissopulus S., J. of Res. in Phys. 31, No. 2 (2007) 157.
- Mrda D., Bikit I., Vesković M., Forkapić S., Nucl. Inst. and Meth. A572 (2007) 739.
- Mrda D. et al., Astropart. Phys. 42 (2013) 103-
- Sisti M., 1999, CRESST - a Cryogenic Experiment for Dark Matter Search, Hieronymus, München, ISBN 3-89791-050-0, p.12

Study of Nuclear Structure Parameters by Using the $(n_{th}, 2\gamma)$ Reaction

N. JOVANČEVIĆ*

*University of Novi Sad, Faculty of Science, Department of Physics,
Trg Dositeja Obradovica 3, 21000 Novi Sad, Serbia*

L. V. MITSYNA and A. M. SUKHOVOJ

Joint Institute for Nuclear Research, Dubna, 141980, Russia

D. KNEŽEVIĆ

*University of Novi Sad, Faculty of Science, Department of Physics,
Trg Dositeja Obradovica 3, 21000 Novi Sad, Serbia and
Institute of Physics Belgrade, Pregrevica 118, 11080 Zemun, Serbia*

M. KRMAR and J. PETROVIĆ

*University of Novi Sad, Faculty of Science, Department of Physics,
Trg Dositeja Obradovica 3, 21000 Novi Sad, Serbia*

S. OBERSTEDT

*European Commission, Joint Research Centre, Institute for Reference
Materials and Measurements (IRMM), Retieseweg 111, B-2440 Geel, Belgium*

A. DRAGIĆ

Institute of Physics Belgrade, Pregrevica 118, 11080 Zemun, Serbia

F. -J. HAMBSCH

*European Commission, Joint Research Centre, Institute for Reference
Materials and Measurements (IRMM), Retieseweg 111, B-2440 Geel, Belgium*

V. D. CONG

*Joint Institute for Nuclear Research, Dubna, 141980, Russia and
Vietnam Atomic Energy Institute, Vietnam*

(Received 22 January 2019, in final form 11 March 2019)

The empirical Dubna model for investigating of the cascade gamma-decay of the neutron resonance allows a simultaneous determination of the level density and radiative strengths in a region up to the binding neutron energy for any nucleus. Data can be obtained by determining the intensities of two-step cascades between a decaying compound-state and a group of low-lying levels of the nucleus and describing these intensities by using the most appropriate models prescribed parametrically. For evaluation and minimization of systematical errors of the models used for the level density and radiative strengths for primary gamma transitions spectroscopic information about quanta sequence for observed resolved cascades must be obtained and at least two different sets of models must be used for verification of derivable nuclear parameters. The step-wise structure, which was observed in the energy dependence of the level density for more than 40 investigated nuclei, shows that the structure of a nucleus modifies by excitation.

PACS numbers: 27.30.+t, 21.10.Ma, 21.10.Pc, 21.60.Cs, 23.20.Lv, 28.20.Np

Keywords: Neutron capture, Two-step gamma cascades, Level density, Radiative strength function

DOI: 10.3938/jkps.75.100

*E-mail: nikola.jovancevic@df.uns.ac.rs

I. INTRODUCTION

A study of the process of step-by-step gamma emission requires experimental technique, that would allow on investigation of the properties of any nucleus at its excitation from the ground-state energy up to the energy of gamma emission when a neutron is captured [1–8]. All experiments that investigate the structure of an excited nucleus are based on measuring the spectra, *i.e.*, the cross sections. For a complete and reliable study of gamma-decay processes, the experiment has to allow both the level density, ρ , and the emission widths for products of the nuclear reaction Γ to be obtained, for all excited levels from the measured intensities of the spectra [9]. The present practical model for describing cascade gamma decay of neutron resonances makes possible the simultaneous determination of the ρ and Γ parameters, from an approximation of the intensities of two-step cascades [10–14].

If an emission spectrum is to be obtained, the total energy of gamma transitions must be recorded using multi-detector systems (calorimeters). As for a majority of stable isotopes, a capture reaction is usually accompanied by a wide spectrum of gammas, and the best calorimeters for this type of the experiment are HPGe detectors with high efficiency. In the analysis of total gamma-spectrum, problems and difficulties always exist owing to extracting the required nuclear parameters from the data from an indirect experiment. An acceptable model representation of the required nuclear parameters is always needed to obtain the values of ρ and Γ from a description of the experimental intensity gamma-spectrum. At that, a careful examination of the relation between the relative uncertainties of the experimental spectra δS and the errors of the determined parameter $\delta\rho$ and $\delta\Gamma$, which can be an order of magnitude greater than δS , is necessary.

Objective information about ρ and Γ can be obtained only from the data on a gamma spectrum of $M = 2$ multiplicity. At present, establishing a gamma-quantum sequence in the cascade experimentally and obtaining the nuclear parameters for all decaying levels is not possible, as no suitable experimental equipment is available. This is due to the absence of spectrometers with an energy resolution $FWHM < D_i$ (for any spacing D_i between intermediate levels), and with picosecond time resolution for any excitation energy of the investigated nucleus. Because of these limitations only an average number of excited levels and an average value of the partial widths in fixed energy intervals can be measured. Moreover, if the two-step cascade has only two variants of the quanta sequence, then for three quanta $3! = 6$ sequence variants exist. That is, at this time, obtaining reliable information about gamma decay from spectra with multiplicities $M \leq 3$ is not possible.

At that, one should take into account that even in the spectrum of two-step gammas, two sequences of gamma-quanta are possible, one of which is false and must be

removed from the analysis. When solving the nonlinear system of equations, that connect the strongly correlated ρ and Γ values with the experimental two-step cascade intensity, the intensifying of both primary and secondary transitions have an infinite number of solutions. That means that the two-step cascade intensity can be described with the same accuracy by using an infinite number of pairs of essentially different ρ and Γ functions. However, a solution region of the system of equations for the intensity of only primary transitions is bounded for any chosen pair of ρ and Γ model functions. Then, if reliable nuclear parameters are to be obtained, secondary transitions must be removed from the spectrum of the cascade intensity of all gamma transitions.

As the level density (the number of levels in the energy interval δE) increases, on average, exponentially when the nuclear excitation energy goes up, the wave functions of each level must be considered individually in the process of constructing the level-density function. The components of the wave function for each nuclear level increase in number with increasing excitation energy while the absolute values of these components decrease [15,16]. This effect is explained in the theory of the nucleus in the framework of the quasi-phonon model [17–19]. Undoubtedly, this effect plays the leading role when investigating the behavior of nuclear matter.

Thus, in the proposed analysis, for any pair of parametrical representations of the ρ and the Γ values, the most probable parameters of these two functions are determined describing the experimental sum of the intensities of primary transitions of the cascade with the use of the likelihood method. At present, our analysis is based on a modern model of the density of n -quasiparticle levels [31], the balance of the changes in the entropy and excitation energy of quasiparticle levels [9], the level density of collective (vibrational) states [32], and tested ideas about the shape of the energy dependence of the radiative strength functions.

1. Methods for determination of the nuclear parameters

Nuclear parameters extracted from the measured spectra describe the process of emission of the reaction products. Two different procedures usually named as “one-step” [20–25] and “two-step” reactions [1–8], are used for the studying the nuclear structure.

In the case of the one-step reaction, any gamma quanta (or nucleon) of the compound-state decay is recorded irrespective of the energy of the excited level (the total energy of all reaction products is equal to the compound-state excitation energy). In the two-step reaction, a coincidence of two gamma-quanta of the same cascade is recorded. For that, the secondary gamma transitions of the cascade to a group of low-lying levels (including the ground state of the nucleus) are also recorded. Only in

the two-step experiment is information about the energies of intermediate levels included in the data treatment process.

The fundamental difference between one-step and two-step experiments becomes evident when the level density is obtained from the evaporated spectra. As the correlations of the level density and the penetrability coefficients on the wave function of excited level are not taken into account in the one-step experiment, only the product of the ρ and the Γ functions can be determined. Additionally, because of the strong anti-correlation of the ρ and the Γ functions, an unknown systematic uncertainty of their determination appears.

Only in two-step experiments can the uncertainties in the ρ and the Γ determinations be reduced, as they are described by appreciably different functions. A decrease in the methodical errors occurs due to the fact that the intensity $I_{\gamma\gamma}(E_1)$ as a function of the primary transition energy E_1 is, in essence, a convolution of two practically independent experiments; *i.e.*, we can consider the spectrum of primary transitions and the branching ratio distribution of secondary transitions as independent distributions.

An increase the quality of the data from the two-step experiments is obtained by using the following procedures: (1) digital improvement of the energy resolution without any reduction in the efficiency of the cascade recording [3] and (2) an algorithm for determining a sequence of the resolved cascade quanta in any given interval of energies of their primary transitions by using the methods and the results of nuclear spectroscopy [4]. For the first time, procedure to extract the level density and the partial widths of γ -emission from the $(n, 2\gamma)$ reaction investigation was developed in Dubna, Refs. 6,7. From the measured spectrum of the two-step cascade, the intensity $I_{\gamma\gamma}(E_1)$, which links the neutron resonance λ (with the excitation energy E_{ex}) to the group of final levels f via intermediate levels i by dipole transitions, is determined. This can be represented by the following equation:

$$I_{\gamma\gamma}(E_1) = \sum_{\lambda, f} \sum_i \frac{\Gamma_{\lambda i} \Gamma_{i f}}{\Gamma_{\lambda} \Gamma_i} = \sum_{\lambda, f} \sum_j \frac{\Gamma_{\lambda j}}{\langle \Gamma_{\lambda j} \rangle m_{\lambda j}} n_j \frac{\Gamma_{j f}}{\langle \Gamma_{j f} \rangle m_{j f}} \quad (1)$$

where the sum of partial widths of primary transitions $\Sigma_i \Gamma_{\lambda i}$ to $M_{\lambda i}$ intermediate levels i is $\langle \Gamma_{\lambda i} \rangle M_{\lambda i}$, and this sum for secondary transitions to $m_{i f}$ intermediate levels is $\langle \Gamma_{i f} \rangle m_{i f}$ (as $\langle \Gamma_{\lambda i} \rangle = \Sigma_i \Gamma_{\lambda i} / M_{\lambda i}$ and $\langle \Gamma_{i f} \rangle = \Sigma_i \Gamma_{i f} / m_{i f}$). The sums of intermediate levels in small energy intervals ΔE_j are $n_j = \rho \Delta E_j$. The branching ratios for primary $[\Gamma_{\lambda j} / (\langle \Gamma_{\lambda j} \rangle M_j)]$ and secondary $[\Gamma_{j f} / (\langle \Gamma_{j f} \rangle m_{\lambda j})]$ transitions are fixed for each ΔE_j .

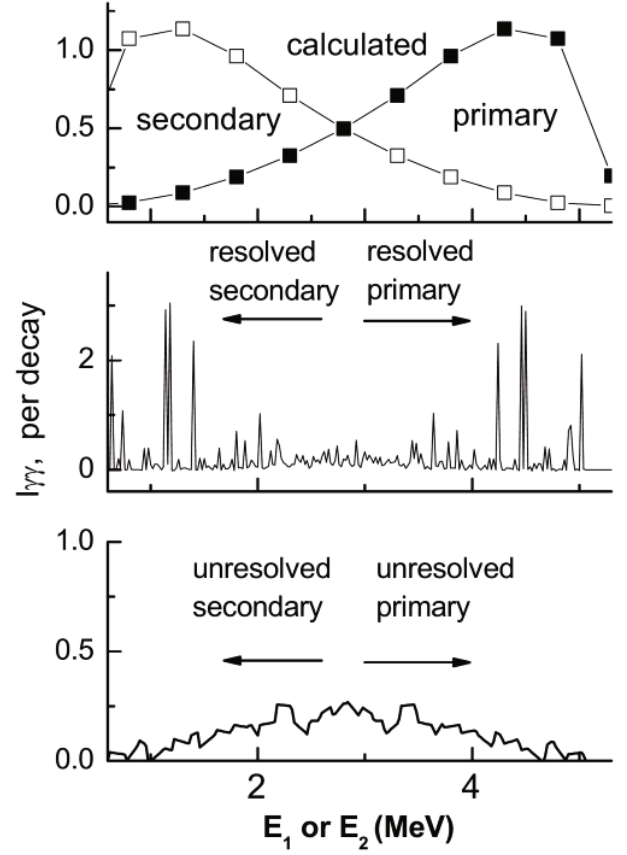


Fig. 1. Distribution of the intensity of the 5731 keV cascade for ^{185}W calculated by using the models (top picture) in Refs. 26,27, with a 500 keV averaging energy interval. Experimental distribution of resolved peaks of the cascade transitions (middle picture) and unresolved continuum (bottom picture; the average energy interval is 10 keV).

2. The $I_{\gamma\gamma}(E_1)$ spectra preparation

The division of the experimental spectra into two mirror distributions (dependent on the energies of only primary, E_1 , and only secondary, E_2 , cascade gamma-quanta) is performed using spectroscopic information. The dividing procedure [6] is based on two facts: (1) the shapes of the intensity dependencies on energy for primary and secondary transitions in the same cascade are mirror - symmetrical and (2) the resolved peaks of the intensity spectrum of the two-step cascade contain no less than half of the total intensity (this fact was confirmed experimentally for all investigated nuclei).

Figure 1 illustrates the possibility of such a division of the spectra of intensity. In the top panel of Fig. 1, the calculated intensity distribution of the cascade with the total energy $E_1 + E_2 = 5731$ keV for ^{185}W [5] is presented, as an example. For our calculations, we used the back shift Fermi-gas model [27] and the model presented in Ref. 26. The calculated intensity shows a division of the spectrum into two parts. As can be seen, the peaks

of the primary and the secondary γ -transitions of the cascade are located symmetrically in opposite parts of the interval E_γ for all γ -quanta energies (for example see Fig. 2).

The experimental distribution of the intensities of resolved peaks and the continuum of unresolved peaks are shown in Fig. 1 in the middle and the bottom panels, respectively. A combination of “primary resolved” and “primary unresolved” parts of the cascade intensity is just the desired $I_{\gamma\gamma} = f(E_1)$ distribution. The determination of the “unresolved” spectrum, where primary transitions are located, was done based on the fact that the total level density increases with the increasing excitation energy.

The calculated intensity of this cascade is about 5% per decay, and the corresponding experimental value is about 11%; thus, resolved peaks account for 8.4% of the experimental intensity, and the unresolved continuum contains 2.6% of the intensity. In addition to that, the shape of the experimental distribution noticeably differs from the calculated one; *i.e.*, description of the intensity spectrum by the statistical model is not satisfactory. As in the center of the experimental spectrum (near half the neutron binding energy $0.5B_n$), the intensity is noticeably smaller than it is for the calculated spectrum, we have a good reason to believe that the separation of $I_{\gamma\gamma}(E_1)$ from the experimented spectrum was performed with a higher accuracy than could have been expected in the framework of the statistical model of the nucleus. The experiment modeling shows that a methodical error of this dividing procedure is caused only by the inaccurate allocation of some cascades (when $E_2 > E_1$) near $0.5B_n$, but this does not change the sum of intensities.

3. Location areas of nuclear parameters

The system of nonlinear equations, Eq. (1), designed for the search of unknown functions $\rho = f(E_{ex})$ and $\Gamma = \Phi(E_1)$ is completely degenerate. Nevertheless, these functions can be defined, but only as possible values in some finite areas. Because of the nonlinearity of these functions, their values cannot be infinite. When the procedure for extracting the ρ and the Γ values was created [7], a set of possible functions, $\rho = f(E_{ex})$ and $\Gamma = \Phi(E_1)$, that describe the $I_{\gamma\gamma}$ intensity with practically zero uncertainty, had already been specified. At an arbitrary choice of the initial ρ and Γ values for fitting the system in Eq. (1), we used, in particular, the model of the Fermi gas and the extrapolation of the tail of the Giant dipole resonance. Small, local distortions of the ρ and the Γ functions were made in each iteration step in order to get a minimal χ^2 . In such a way, this reusable procedure was implemented with different independent initial ρ and Γ values and deviations of the random components of the correction vector until χ^2 minimization was reached. This approach is rather stable, when any

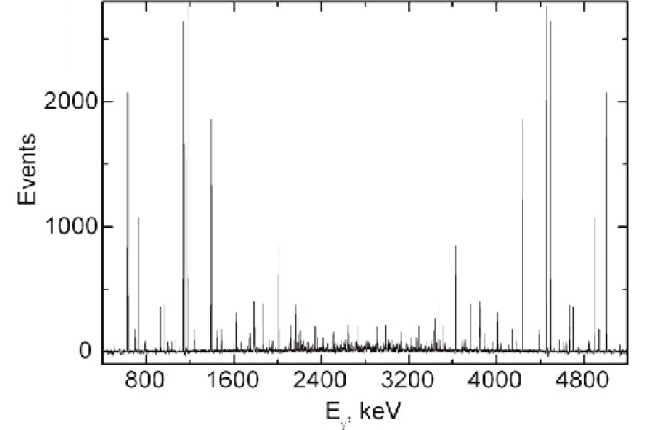


Fig. 2. Experimental distribution of intensities of two-step cascades between a neutron resonance and the first excited state of ^{185}W taking into account the detector efficiency. The spectrum is normalized to the sum of recorded events [5].

noticeable anti-correlation between the ρ and the Γ values is absent, which is ensured by the branching coefficient for the second step of the cascade, which, in turn, depends on the ratio of the partial width Γ_{if} of the secondary transition to the total gamma-width Γ_i of the decayed intermediate levels i (see Eq. (1)). Different energy dependencies for the spectra of primary quanta and the secondary ones, with the branching coefficients, allow us to bound the area of random ρ and Γ functions. A well-defined step-like structure of the level density [7, 8] has resulted from fittings with any initial parameters.

Such a step-like structure of the level density (it can be explained by the breaking of nucleon Cooper pairs in the nucleus) nowise contradicts the smoothness of the experimental spectra obtained from the nucleon reactions, when the ρ and the Γ values are connected and their product is a smooth function. Nevertheless, in this case, the location areas of the ρ and the Γ functions (for an accurate description of the experimental intensity) become bigger, as shown in Ref. 30.

The relative uncertainties, $\delta\rho/\rho$ and $\delta\Gamma/\Gamma$, always exceed $\delta I_{\gamma\gamma}/I_{\gamma\gamma}$. For the lowest energies of the primary transitions of cascades, such an excess may even reach several orders of magnitude. However, the real transfer coefficients of the uncertainties of the functions $\rho = f(E_{ex})$ and $\Gamma = \Phi(E_1)$ to the $I_{\gamma\gamma}(E_1)$ uncertainty must be analyzed. When the accuracy of the $I_{\gamma\gamma}(E_1)$ description is about a few percent, as has resulted from our analysis (see Figs. 3, 5, 6, 7, 8), the accuracies of the ρ and the Γ determinations will be a few tens of percent. The reader should note that the small number of bins in Figs. 3, 6, 7, 8 is the result of averaging multiple bins in order to show graphically the dynamics of the change in the nuclear structure. The actual bin size for the calculation was 50 keV.

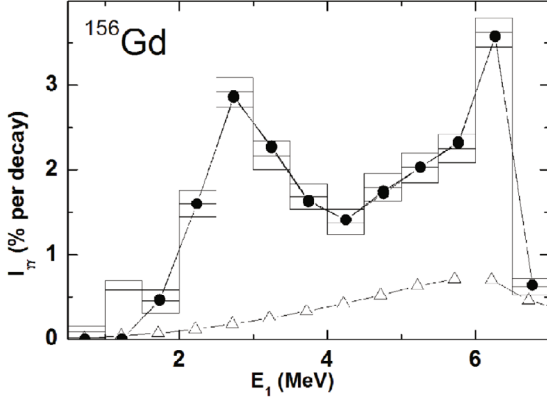


Fig. 3. Measured $I_{\gamma\gamma}(E_1)$ with uncertainties (histogram) for ^{156}Gd . Points - the fit for the practical model; triangles - $I_{\gamma\gamma}$ calculated by using the models in Refs. 26, 27. The threshold for recorded cascade gammas is $E_{\gamma} = 520$ keV.

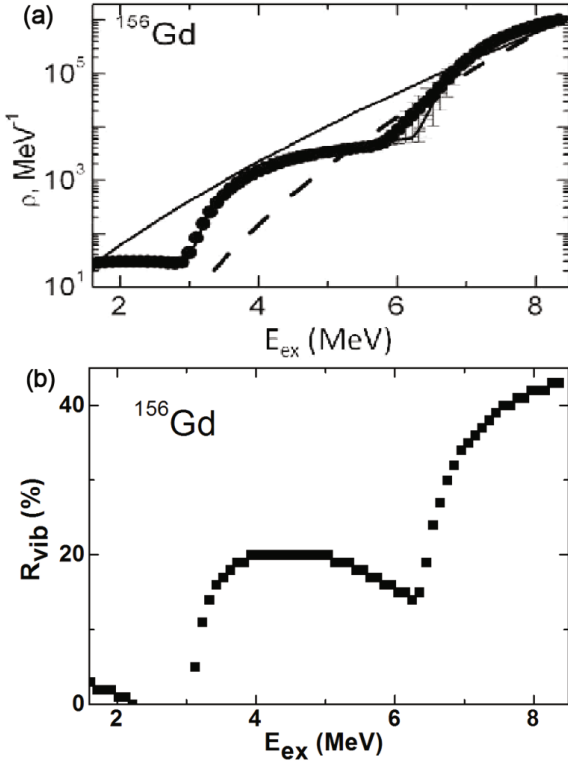


Fig. 4. Level density of ^{156}Gd . (a) Points are the fit for level density (uncertainties are scatters of fits in the case of different sets of initial parameters); dashed and solid lines are the level densities obtained from the model of Ref. 27 with the shell correction $\delta E(6)$ and without δE , respectively. (b) The ratio of collective levels density to the total level density.

II. BASIS OF THE PROPOSED MODEL

The development and the refinement of the model presented in Ref. 7 was done at the Frank Laboratory of Neutron Physics (FLNP), JINR [10–14]. We present here the basic idea and improvement of the model.

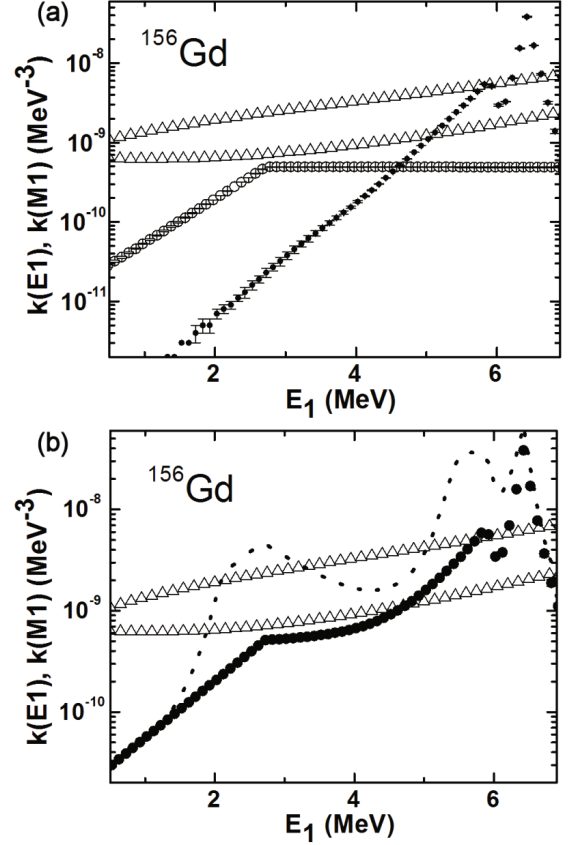


Fig. 5. Radiative strength function for ^{156}Gd . (a) Solid points are the fit of the radiative strength function for $E1$ - transitions; open points are the fit of the radiative strength function for $M1$ - transitions. (b) Solid points are the sum of $E1$ - and $M1$ - radiative strength functions. The dash line is the sum of radiative strength functions multiplied by the $\rho_{\text{mod}}/\rho_{\text{exp}}$ ratio [27]. Lower triangles are the calculations using the model of Ref. 26 with $k(M1) = \text{const}$; upper triangles are the calculations using the model of Refs. 28, 29 with $k(M1) = \text{const}$.

1. The level density

An expression for the density ρ_l for fermionic-type levels was described by using the model [31] of the density Ω_n of n -quasi-particle states:

$$\rho_l = \frac{(2J+1) \cdot \exp\left(- (J+1/2)^2 / 2\sigma^2\right)}{2\sqrt{2\pi}\sigma^3} \cdot \Omega_n(E_{\text{ex}}),$$

$$\Omega_n(E_{\text{ex}}) = \frac{g^n (E_{\text{ex}} - U_l)^{n-1}}{\left(\left(\frac{n}{2}\right)!\right)^2 (n-1)!},$$
(2)

where E_{ex} is the excitation energy, $g = 6a/\pi^2$ is the density of single-particle states near the Fermi surface (a is a parameter from the model of a back-shifted Fermi

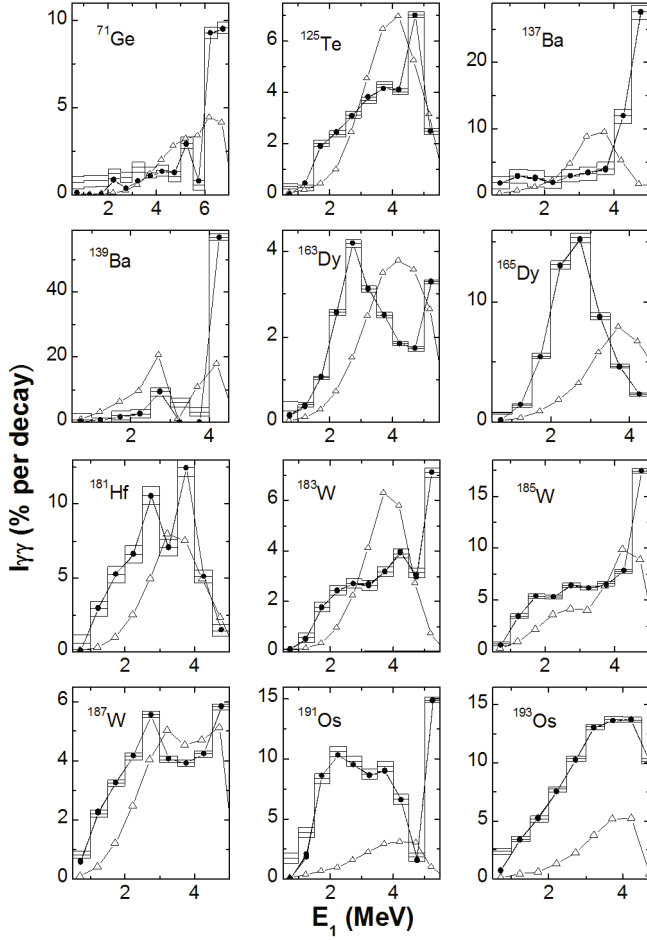


Fig. 6. Histograms are the sums of the measured cascades's intensities with their small errors in 0.5 MeV bins for even-odd nuclei. Solid points are the best fits and triangles are the spectra calculated using the models from Refs. 26,27 with $k(M1) = \text{const.}$

gas [31,32]), U_l is the energy for the l -th Cooper pair breaking threshold. The cut-off factor σ of the spin J for the excited state of a compound nucleus above the maximal excitation energy E_d of the “discrete” level area is also taken from the model of Fermi gas.

For a given E_{ex} , the coefficient of the collective enhancement of the vibrational level density (or both vibrational and rotational ones in the case of a deformed nucleus) C_{col} , was obtained from the theoretical description in Ref. 9. This description gives the following equation:

$$C_{\text{col}} = A_l \cdot \exp \left(\sqrt{(E_{\text{ex}} - U_l)/E_\nu} - (E_{\text{ex}} - U_l)/E_\mu \right) + \beta. \quad (3)$$

In the above equation, A_l are parameters for the densities of the vibrational levels above the breaking point for l -th Cooper pair. The changes in the nuclear entropy and the quasi-particles excitation energies are determined by E_μ and E_ν , respectively. The parameters A_l are fitted

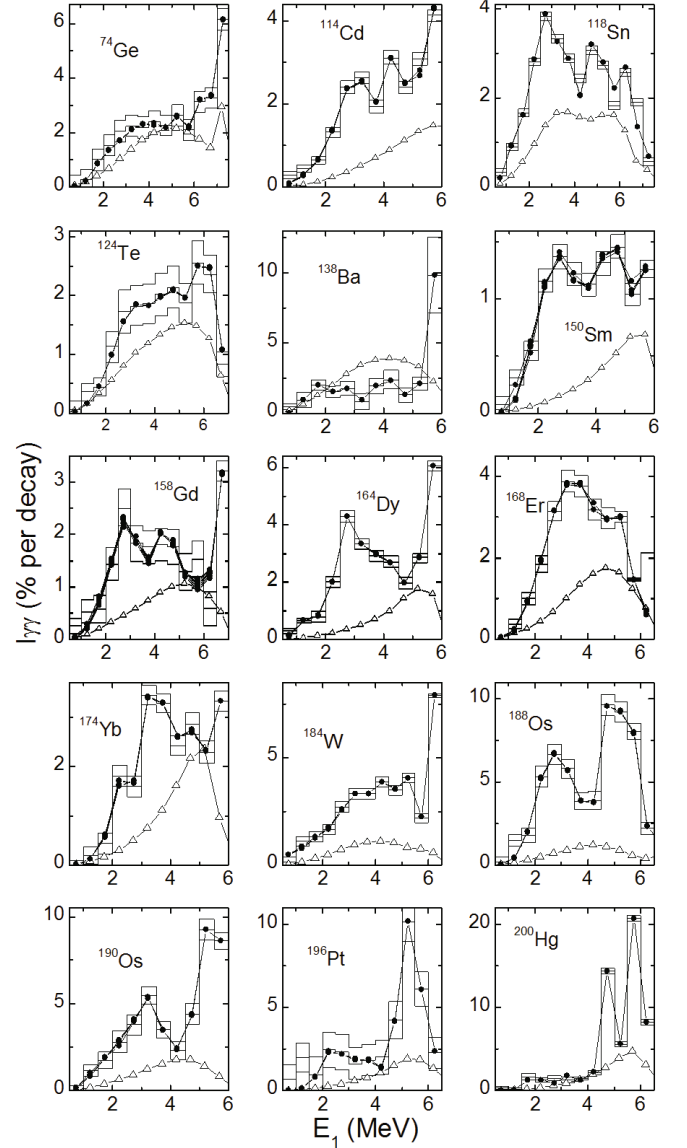


Fig. 7. Histograms are the sums of the measured cascades's intensities with their small errors in 0.5 MeV bins for even-even nuclei. Solid points are the best fits and triangles are the spectra calculated using the models from Refs. 26,27 with $k(M1) = \text{const.}$

independently for different pairs, as in Refs. 10–12. The parameter β describes for the level density of rotation levels.

2. Radiative strength function

The radiative strength functions,

$$k = \Gamma / \left(A^{2/3} E_\gamma^3 D_\lambda \right), \quad (4)$$

for $E1$ -transitions are determined in Ref. 26:

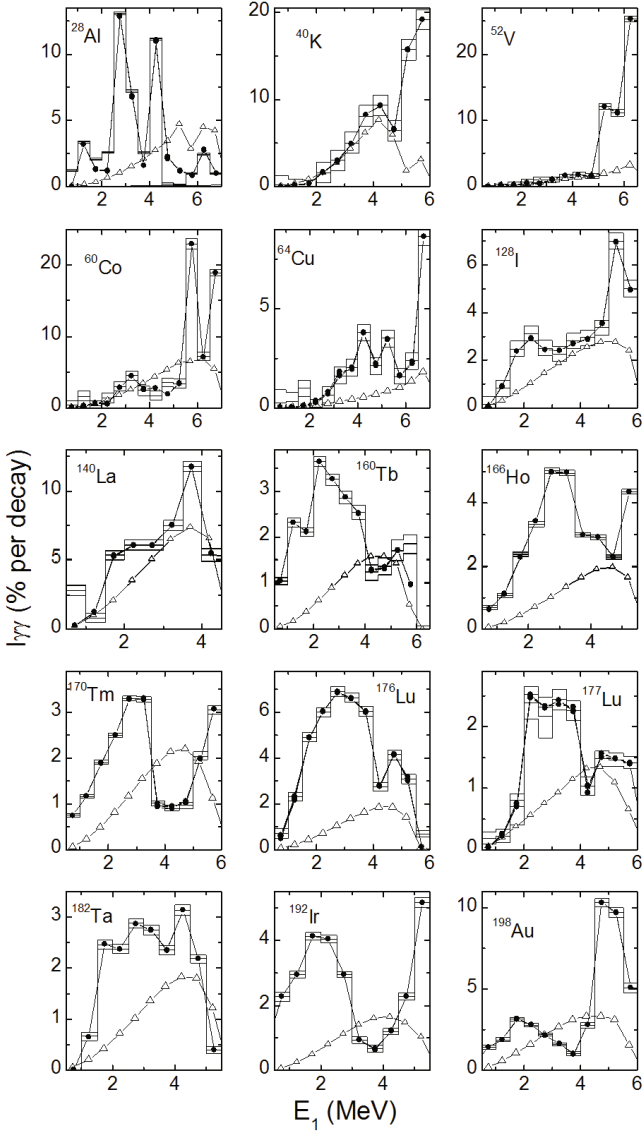


Fig. 8. Histograms are the sums of the measured cascades's intensities with their small errors in 0.5 MeV bins for odd-odd nuclei. Solid points are the best fits and triangles are the spectra calculated using the models from Refs. 26, 27 with $k(M1) = \text{const.}$

$$k(E1, E_\gamma) = w \frac{1}{3\pi^2 \hbar^2 c^2 A^{2/3}} \frac{\sigma_G \Gamma_G^2 (E_\gamma^2 + \kappa 4\pi^2 T^2)}{(E_\gamma^2 + E_G^2)^2 + E_\gamma^2 \Gamma_\gamma^2} + P\delta^- \exp(\alpha_p (E_\gamma - E_p)) + P\delta^+ \exp(\beta_p (E_p - E_\gamma)), \quad (5)$$

with the thermodynamic temperature T , the fitting normalization parameter w and the coefficient κ . Cascades with pure quadrupole transitions were not observed in our experiments, and the radiation strength functions for $M1$ -transitions were obtained for fitting in a similar manner.

The position of the giant dipole resonance E_G , its width Γ_G and its cross section σ_G in the maximum were taken from Ref. 33 for each nucleus. The results of analyses done in Ref. 34 showed the need to add peaks to the radiative strength function. We described the shape of each peak in a different ways. The presented analysis was done by using two exponential functions corresponding to the left and the right slopes of the peak, which correspond to the energies below and above the maximum, Eq. (5). E_p , the amplitude P and the slope parameters α_p and β_p are fitted for each peak independently. At $E_1 \approx B_n$, the fitted ratios Γ_{M1}/Γ_{E1} of the $E1$ - and the $M1$ - radiative strength functions were normalized to the experimental values. Their sum, Γ_λ , was normalized to the total radiation width of the resonance.

3. Parameters for fitting

The set of fitting parameters (see Eqs. (2), (3) and (5)) of all cascades in our model is as follows: the energy thresholds for breaking of Cooper pairs U_l up to $l = 4$, the E_μ and E_ν parameters, parameters A_l , parameters w , κ , β , P , E_p , α_p and β_p and the ratio of the levels density for levels with negative parity to the total level density, r . By using this set of parameters in the framework of the proposed model, we were able to describe the intensity $I_{\gamma\gamma}(E_1)$ for 43 nuclei in the mass interval $28 \leq A \leq 200$.

III. PRACTICAL MODEL IMPROVEMENTS

Significant disagreement is seen between the measured cascade intensities and the ones calculated using the statistical model [10,11]. If the most reliable information about the nuclear matter properties is to be obtained several models for ρ and Γ [32] would be combined.

The Dubna model is based on the conclusion of the theoretical analysis [35], concerning the fragmentation of different quasi-particle states in a nuclear potential, that Cooper pair breaking during nuclear excitation is a sequential process. Thus, the Dubna model allows us to examine two opposite hypotheses (the particular cases of above-mentioned theory): that the nucleus is a pure fermion system or that a phase transition to a nucleus consisting of bosons occurs at some excitation energy.

No known fully precise and correct models about the behavior of nuclear matter in excited nuclei are available. The singular verifiable hypothesis, which arose from nuclear superfluidity studies, is an increase in the total level density, which grows in a manner taken into account by the C_{col} coefficient.

At first, in our practical model [10,11], we assumed that the E_μ and the E_ν parameters of the vibrational

Table 1. Values used in the analysis (the maximal excitation energy E_d of the “discrete” level area, the energy E_{\max} of the final level of the cascade, the shell correction δE for the density of quasi-particle levels and the intensity $I_{\gamma\gamma}$ of the two-step cascade and the number of discrete levels) for the investigated nuclei.

Nucleus	E_d (MeV)	E_{\max} (MeV)	Shell correction δE (MeV)	I (%)	Spins of state λ	Number of discrete levels
^{28}Al	2.486	0.972	−11.1	49(1)	2,3	11
^{40}K	2.985	1.64	−3.1	67(3)	1,2	21
^{52}V	0.846	0.147	−5.0	60(2)	3,4	8
^{60}Co	1.515	1.5	−5.9	71(3)	3,4	22
^{64}Cu	0.926	0.278	−3.2	30(6)	1,2	13
^{71}Ge	1.298	0.0	−3.5	32(2)	1/2	18
^{74}Ge	2.963	2.165	−3.0	36(2)	4,5	26
^{114}Cd	2.316	0.558	−1.0	26(1)	0,1	17
^{118}Sn	2.930	1.230	−1.8	31(1)	0,1	17
^{124}Te	2.702	0.603	−0.3	20(2)	0,1	23
^{125}Te	1.319	0.671	−2.3	31(1)	1/2	18
^{128}I	0.434	0.434	−1.0	33(2)	2,3	21
^{137}Ba	2.662	0.279	−6.3	59(4)	1/2	11
^{138}Ba	2.780	1.436	−8.2	26(5)	1,2	12
^{139}Ba	1.748	1.082	−6.0	81(6)	1/2	8
^{140}La	0.658	0.322	−4.0	48(2)	3,4	18
^{150}Sm	1.927	0.773	3.0	12(1)	3,4	25
^{156}Gd	1.638	0.288	2.4	23(5)	1,2	25
^{158}Gd	1.517	0.261	−0.2	19(2)	1,2	20
^{160}Tb	0.279	0.279	0.12	23(3)	1,2	21
^{163}Dy	1.055	0.250	−3.0	22(1)	1/2	18
^{164}Dy	1.808	0.242	−2.0	29(1)	2,3	26
^{165}Dy	0.738	0.184	−3.6	53(1)	1/2	16
^{166}Ho	0.522	0.522	−1.5	31(1)	3,4	24
^{168}Er	1.719	0.995	−2.3	27(4)	3,4	25
^{170}Tm	0.715	0.648	−1.3	23(2)	0,1	21
^{174}Yb	1.949	0.253	−3.5	22(1)	2,3	29
^{176}Lu	0.688	0.595	−1.8	44(1)	3,4	23
^{177}Lu	0.854	0.637	0.25	16(1)	$6\frac{1}{2}, 7\frac{1}{2}$	22
^{181}Hf	1.154	0.332	−3.1	52(4)	1/2	9
^{182}Ta	0.480	0.360	−2.4	19(1)	3,4	15
^{183}W	1.471	0.209	−4.0	28(1)	1/2	13
^{184}W	1.431	0.364	−2.4	35(1)	0,1	16
^{185}W	1.106	1.068	−0.9	62(1)	1/2	24
^{187}W	1.083	0.303	−2.6	34(1)	1/2	24
^{188}Os	1.764	0.633	−0.2	59(3)	0,1	16
^{190}Os	1.682	0.756	−0.7	49(3)	1,2	12
^{191}Os	0.815	0.815	−3.5	76(2)	1/2	27
^{192}Ir	0.415	0.415	−0.3	27(6)	1,2	30
^{193}Os	1.288	0.889	−3.8	80(1)	1/2	20
^{196}Pt	1.998	0.688	−3.7	37(5)	0,1	26
^{198}Au	0.528	0.495	−5.6	42(1)	1,2	23
^{200}Hg	1.972	0.368	−8.0	59(2)	0,1	20

level density vary for different broken Cooper pairs independently and that the density g of the single-particle

states is constant near the Fermi surface for any given nucleus. However, results from Ref. 12 showed that E_μ

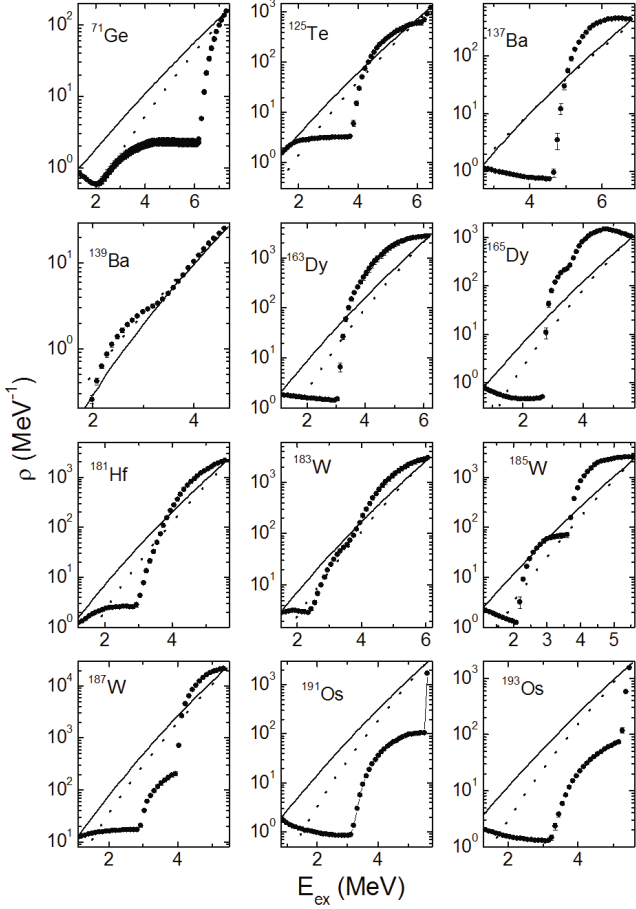


Fig. 9. Most probable densities for intermediate levels of two-step cascades (solid points) for even-odd nuclei and their variations in different fits with the lowest χ^2 . Dashed lines show the level density obtained using the model of Ref. 27 with the shell correction δE (6); solid lines show the level density obtained using the model of Ref. 27 without the shell correction δE (6).

and E_ν can be replaced by the same parameter, (*i.e.*, $E_\mu = E_\nu$), which allowed us to decrease the number of model parameters. Moreover, an analysis of scores of fittings showed that this common parameter could be taken for all broken pairs in a given nucleus. According to the results of theoretical investigations [9], an influence of the shell inhomogeneity of a single-particle spectrum on the obtained ρ and Γ values must be considered.

An interval of the approximation is specified taking into account two factors: the cascade-quantum energy must be more than 0.52 MeV and the number of levels in the bin below E_d must be less than 5. In the former case, we avoid the problem of taking into account the line shapes of annihilation peak, and, in the latter case, we diminish the strong fluctuations of the intensities of the discrete levels.

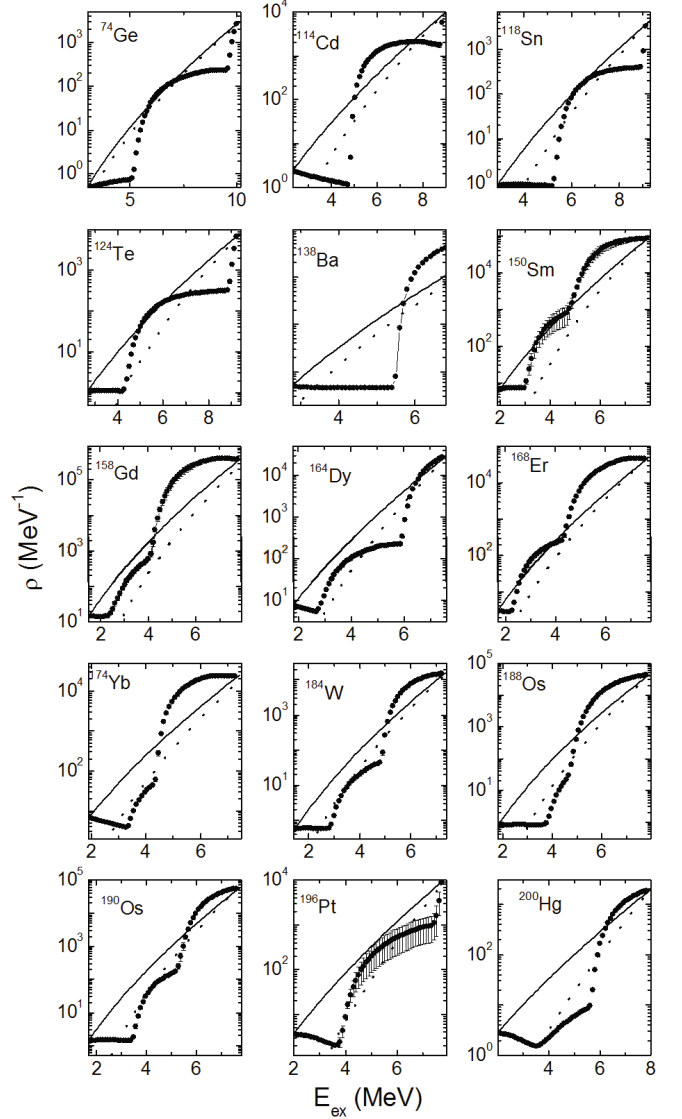


Fig. 10. Most probable densities for intermediate levels of two-step cascades (solid points) for even-even nuclei and their variations in different fits with the lowest χ^2 . Dashed lines show the level density obtained using the model of Ref. 27 with the shell correction δE (6); solid lines show the level density obtained using the model of Ref. 27 without the shell correction δE (6).

IV. CORRECTION FOR SHELL INHOMOGENEITIES

In this work, the theoretical predictions for the dependence of the density of the quasi-particle levels on the shell correction δE were tested for 43 nuclei. The testing was performed by using the parameter $a(A)$, which depended on the excitation energy, included linearly in the parameter of the single-particle density g (see Eq. (2)). $a(A)$ for a nucleus with mass A and excitation energy

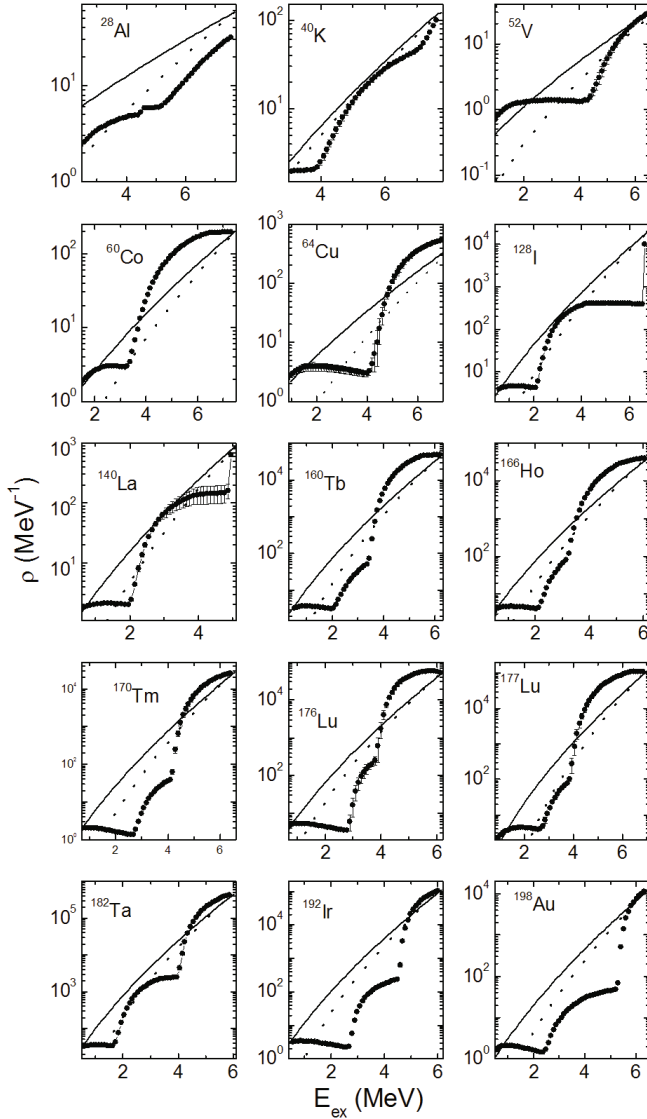


Fig. 11. Most probable densities for intermediate levels of two-step cascades (solid points) for ^{177}Lu and odd-odd nuclei and their variations in different fits with the lowest χ^2 . Dashed lines show the level density obtained using the model of Ref. 27, with the shell correction δE (6); solid lines show the level density obtained using the model of Ref. 27 without the shell correction δE (6).

E_{ex} , is given by [9]:

$$a(A) = \tilde{a} (1 + ((1 - \exp(\gamma E_{ex})) \cdot \delta E / E_{ex})) \quad (6)$$

where asymptotic value $\tilde{a} = 0.114 \cdot A + 0.162 \cdot A^{2/3}$ and $\gamma = 0.054$. For keeping and taking into account the average spacing between neutron resonances [10–12], we varied the δE values slightly relative to their calculations [9]. The shell corrections, used for fitting the parameters of the Dubna model, are presented in the Table 1.

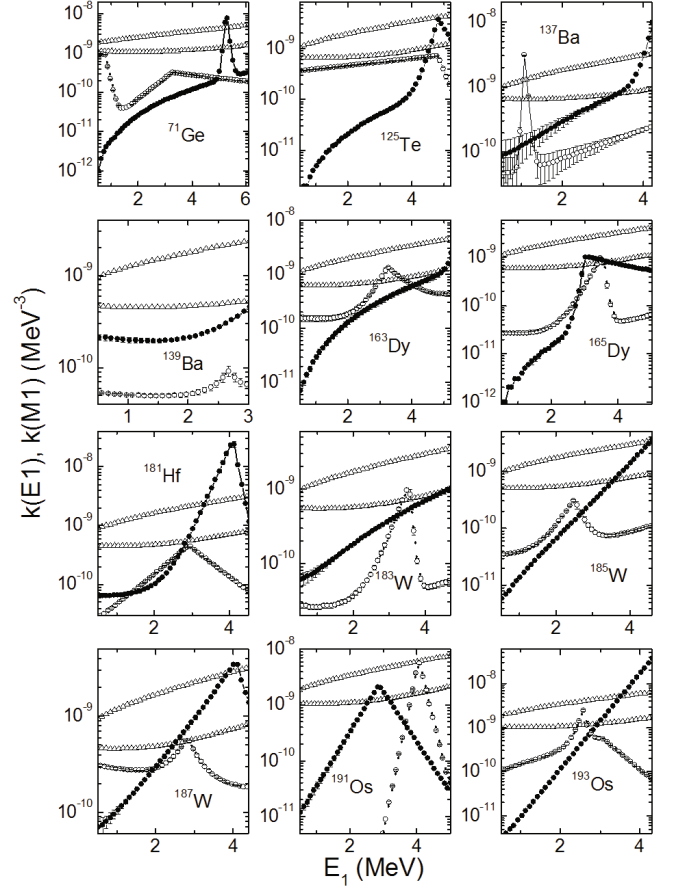


Fig. 12. Radiative strength functions of $E1$ -transitions (closed points) and of $M1$ -transitions (open points) in the case of even-odd nuclei (the best fits). The top line of triangles depicts the model calculation from Ref. 28 while the bottom line represents the model calculation of Ref. 26 in sum for $k(M1) = \text{const.}$

V. RESULTS AND DISCUSSION

The data on the energies E_{max} of the final level of the cascades and the sums of the experimental intensities are shown in Table 1. For almost half of the investigated nuclei, the intensities of the measured two-step cascades contain $\approx 50\%$ (or more) of the total intensities of all cascade transitions to the final levels. Consequently, for these nuclei the systematic uncertainties in the ρ and Γ determinations are minimized, which means that the fits for the ρ and the Γ values are the best ones. In all calculations for $E_{ex} \leq E_d$ (E_d is the maximal excitation energy of the “discrete” level area) the data on excitation energies and decay modes of low-lying levels from Ref. 36 were used. The number of discrete levels (below E_d) is presented in Table 1.

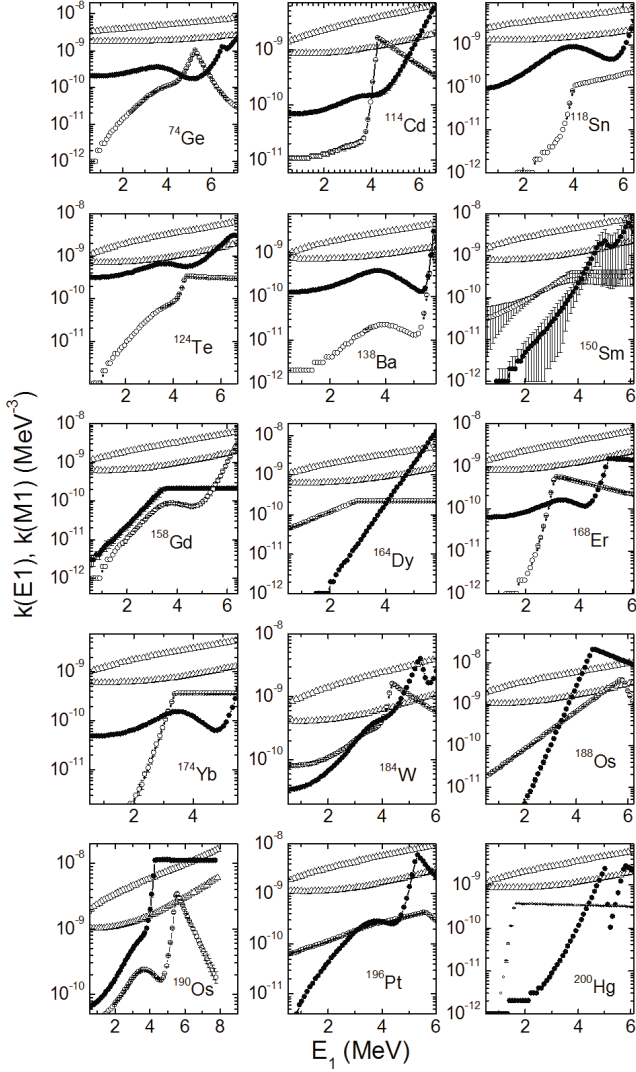


Fig. 13. Radiative strength functions of $E1$ -transitions (closed points) and of $M1$ -transitions (open points) in the case of even-even nuclei (the best fits). The top line of triangles depicts the model calculation from Ref. 28 while the bottom line represents the model calculation of Ref. 26 in sum for $k(M1) = \text{const.}$

1. Characteristics of the fitting procedure

The experimental distributions of the cascade intensities are usually measured in energy intervals with a width of 1 keV and can include from 5000 to 10000 channels (Fig. 2), for each M investigated cascade ($2 \leq M \leq 16$). The basis equations, Eqs. (2)–(5), contain on the average, ≈ 20 parameters, which are fitted for all recorded cascades of the investigated nucleus. In practice, for obtaining the fitted parameters, averaging the energy intervals of primary transitions for excitation energies over 50 keV is reasonable.

The Monte Carlo method was used to solve Eq. (1). The non-linearity of the strongly correlated equations of

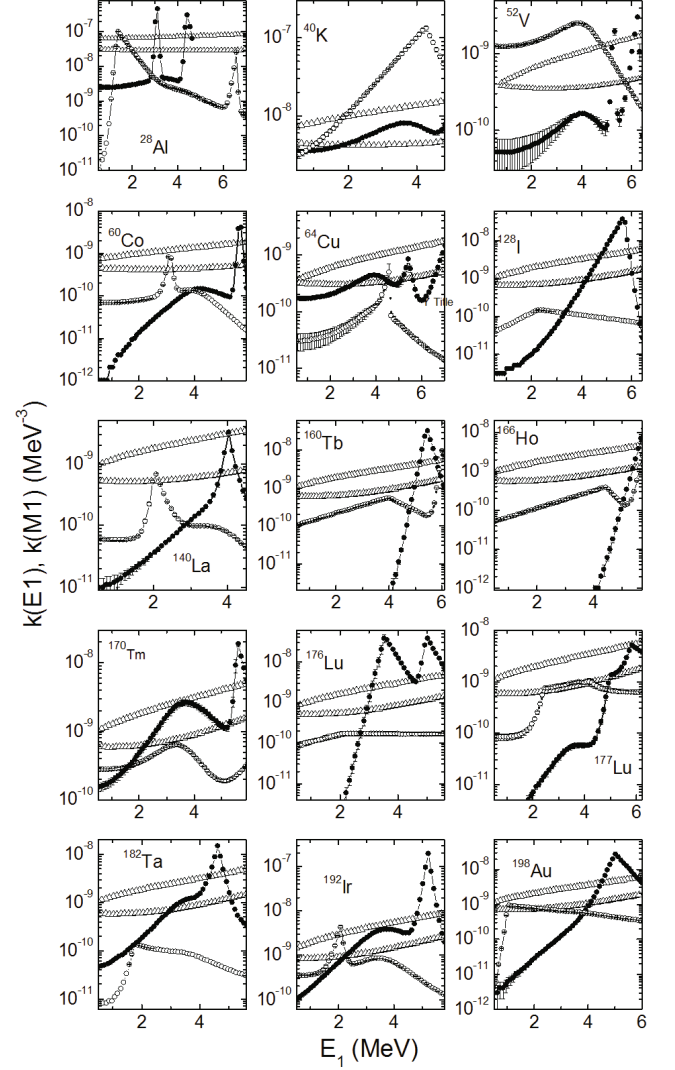


Fig. 14. Radiative strength functions of $E1$ -transitions (closed points) and of $M1$ -transitions (open points) in the case of ^{177}Lu and odd-odd nuclei (the best fits). The top line of triangles depicts the model calculation from Ref. 28 while the bottom line represents the model calculation of Ref. 26 in sum for $k(M1) = \text{const.}$

the system has an influence on the uncertainty for extracting the ρ and the Γ parameters from $I_{\gamma\gamma}$. The existence of false local minima of χ^2 is inevitable for the system of nonlinear equations in Eq. (1), and this occurrence makes a precise determination of the ρ and the Γ values harder. The probability to getting a false minimum of χ^2 sometimes amounts to 20%. Nevertheless, all accumulated data (see Table 1) provide new and very important information.

Experimental data on $I_{\gamma\gamma}(E_1)$ are usually obtained with a small total uncertainty and averaged over 500 keV energy intervals. In Figs. 3–5 the results for ^{156}Gd are presented in more detail. The best fits to $I_{\gamma\gamma}(E_1)$, the fitted level densities, and the radiative strength functions

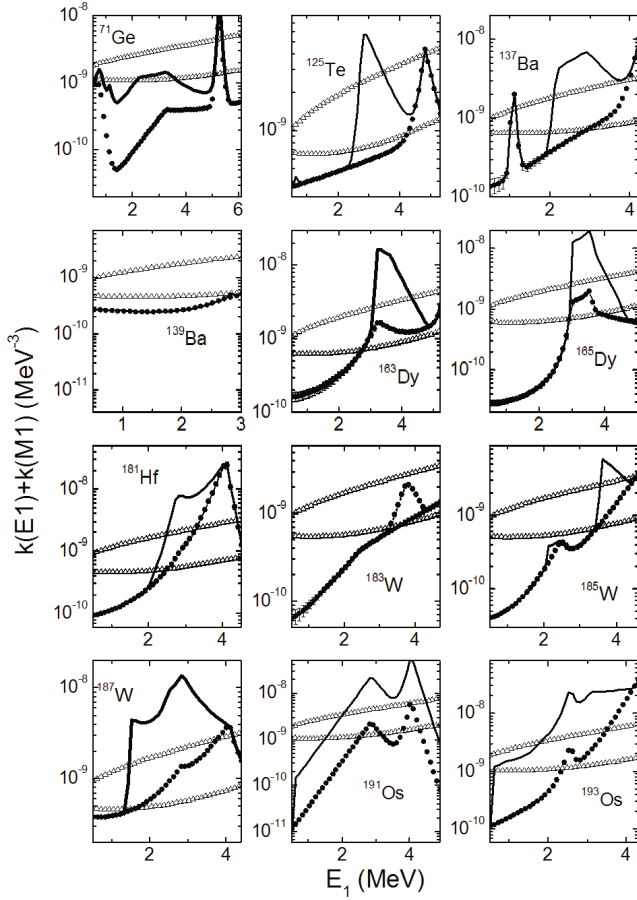


Fig. 15. Sum of radiative strength functions of $E1$ - and $M1$ -transitions (closed points) for even-odd nuclei (the best fits). The solid line is the same multiplied by $\rho_{\text{mod}}/\rho_{\text{exp}}$ [27]. The top line of triangles depicts the model calculation from Ref. 28 while the bottom line represents the model calculation of Ref. 26 in sum with $k(M1) = \text{const.}$

are compared to values obtained by using the statistical model. The results and the corresponding calculations for the rest of the investigated nuclei are presented in Figs. 6–8 (the cascade intensities), in Figs. 9–11, (the level densities), in Figs. 12–14 (the radiative strength functions of $E1$ - and $M1$ -transitions), in Figs. 15–17 (sums of the strength functions) and in Figs. 18–20 (the ratios of the density of vibrational levels to the total level density). The spectra in Figs. 3, 6–8 were calculated using functions shown as solid lines in Figs. 15–17.

2. Resulting parameters

The various shapes of the $I_{\gamma\gamma}$ distributions for different nuclei (Figs. 3, 6, 7 and 8) are most likely determined by the diverse wave functions of the exited levels. In a similar manner, for example, the very strong dependences of the neutron strength functions on nuclear mass [37] or

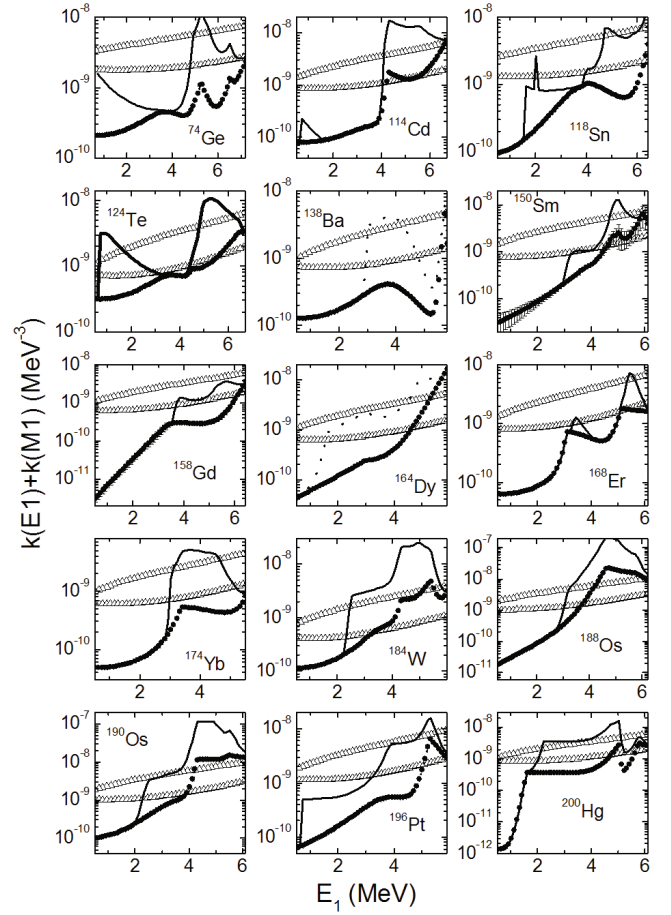


Fig. 16. Sum of radiative strength functions of $E1$ - and $M1$ -transitions (closed points) for even-even nuclei (the best fits). The solid line is the same multiplied by $\rho_{\text{mod}}/\rho_{\text{exp}}$ [27]. The top line of triangles depicts the model calculation from Ref. 28 while the bottom line represents the model calculation of Ref. 26 in sum with $k(M1) = \text{const.}$

the dependences of spectroscopic factors of reactions (d, p) and (d, t) on the locations of low-lying levels (relative to the Fermi-surface) [38] are explained.

The level densities in Figs. 4, 9, 10, and 11 demonstrate that, if the shell inhomogeneities of single-particle spectra are taken into account, the single-particle densities are noticeably reduce in comparison to the ones calculated using the hypothesis $a = \text{const.}$ Thus, level densities obtained in our model change slightly when the shell corrections are taken into account. Thus, in Figs. 4, 9, 10, and 11, the curves that describe the calculated single-particle density (using Eq. (6)) and the ones for the fitted level density, for all investigated nuclei, became closer to one another.

The main source of the large fluctuations in the radiative strength functions (see Figs. 5, 12, 13, and 14) is their anti-correlation with the level density in every energy range. Average sums of the strength functions of $E1$ - and $M1$ -transitions for $E_1 = 520$ keV are 0.80(8),

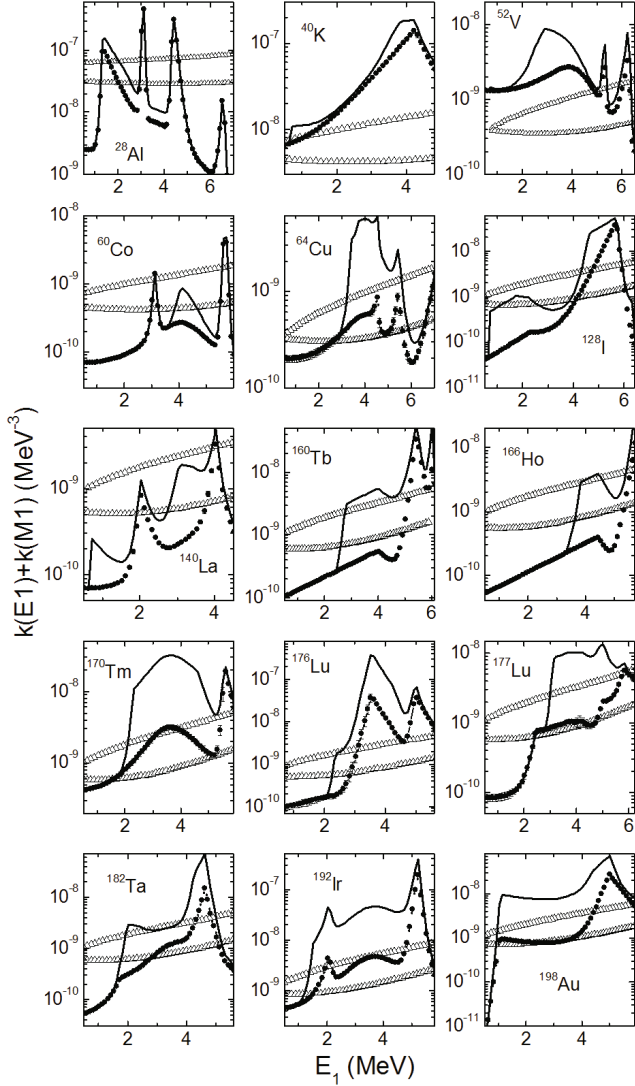


Fig. 17. Sum of radiative strength functions of $E1$ - and $M1$ -transitions (closed points) for ^{177}Lu and odd-odd nuclei (the best fits). The solid line is the same multiplied by $\rho_{\text{mod}}/\rho_{\text{exp}}$ [27]. The top line of triangles depicts the model calculation from Ref. 28 while the bottom line represents the model calculation of Ref. 26 in sum with $k(M1) = \text{const}$.

$2.1(2)$ and $2.5(3) \cdot 10^{-10} \text{ MeV}^{-3}$ for even-even, even-odd and odd-odd nuclei, respectively. Thus, the summation noticeably reduces the above-mentioned scatter and allows us to assert that the sum strength function decreases with decreasing energy of the primary transition.

The contributions of the levels of a vibrational type in the total level density (Figs. 18–20) for all nuclei decrease near the U_l points. For a majority of the nuclei the part of the vibrational levels below B_n is about 40%, which does not contradict the results of the analysis of distributions of the total radiative widths above B_n [39]. Calculations of the distributions of random deviations for the total radiative widths of s-resonances, executed in Ref. 39, showed a superposition of at least four distri-

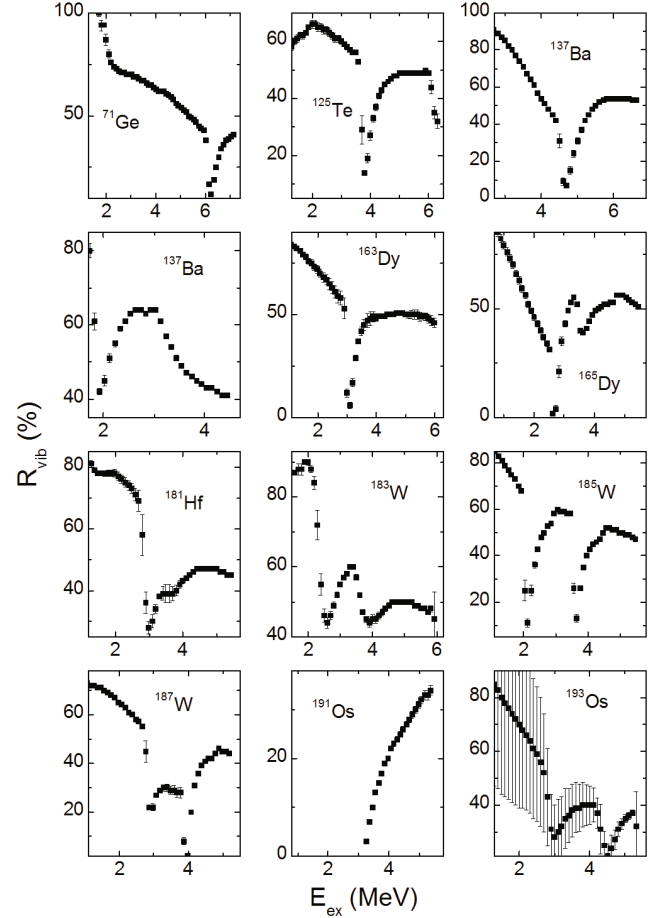


Fig. 18. Part of the vibrational levels R_{vib} in the total density of excited levels for even-odd nuclei at excitation energy E_{ex} .

butions with different averages $\langle \Gamma_\gamma \rangle$.

When the gamma-decay process is investigated, the problem of describing of special points (of the breaking of the Cooper pairs) appears. As anti-correlation between ρ and Γ values can be different to a greater or lesser extent in all excitation energy ranges, it can be maximal just at the points of breaking the Cooper pairs. A noticeable dependence of the resulting strength functions on the local jumps in the level density is seen. Then as already pointed out, in order to prevent a contradiction between the data of the two-step experiment and one-step experiment, one must take into account the connection between the ρ and the Γ values. We investigated such an anti-correlation by multiplying the phenomenological expression, Eq. (5), for the strength function by the $\rho_{\text{mod}}/\rho_{\text{exp}}$ ratio, which inserts an additional fitted correlation. Here, ρ_{exp} is taken from the best fit obtained while solving the system in Eq. (1), and ρ_{mod} was taken from the model of a back-shifted Fermi gas [27]. The function ρ_{mod} represents smoothed density for fermion-type levels and describes both a neutron resonance density and the cumulative sum of known nuclear levels at

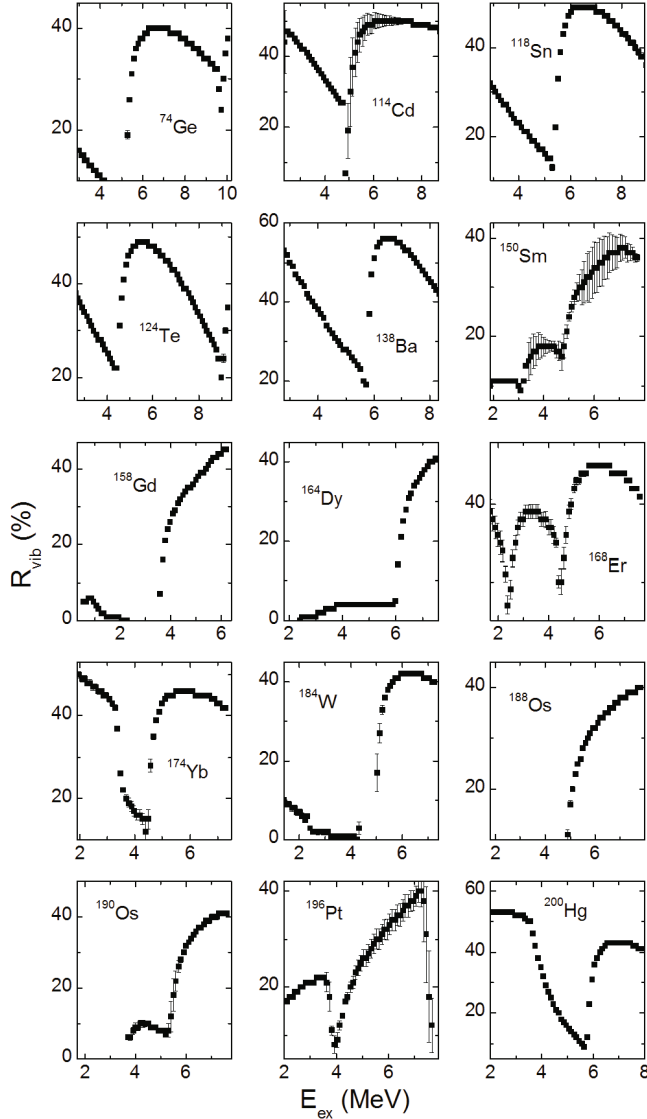


Fig. 19. Part of the vibrational levels R_{vib} in the total density of excited levels for even-even nuclei at excitation energy E_{ex} .

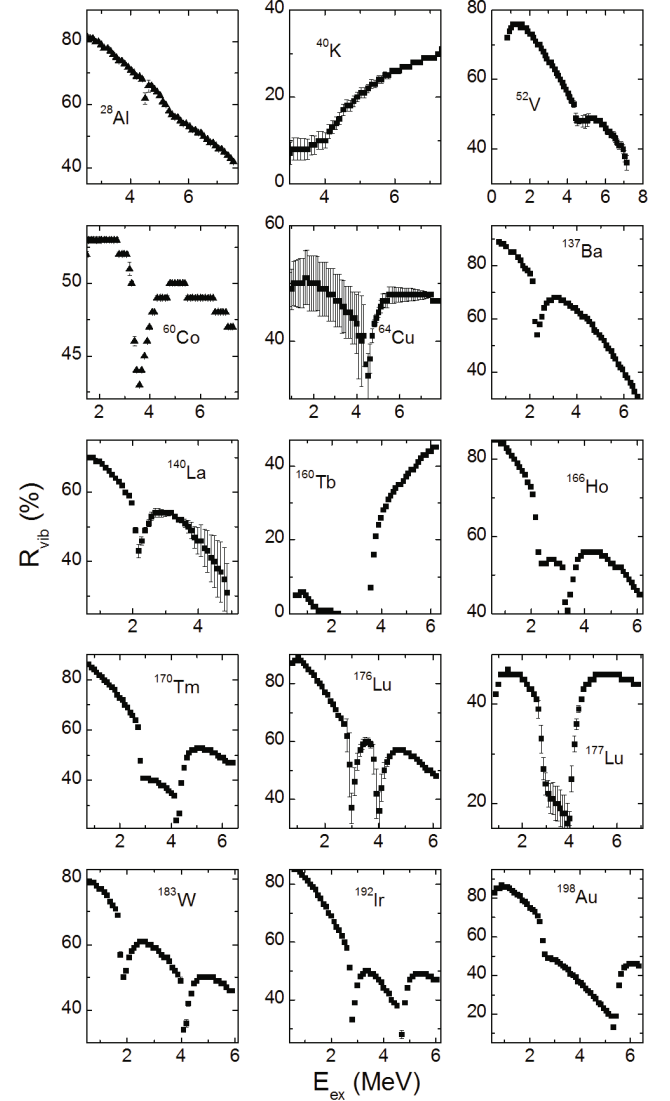


Fig. 20. Part of the vibrational levels R_{vib} in the total density of excited levels for ^{177}Lu and odd-odd nuclei at excitation energy E_{ex} .

$E_{\text{ex}} \leq E_d$ (E_d was taken from Ref. 36). The limiting condition $1 \leq \rho_{\text{mod}}/\rho_{\text{exp}} \leq 10$ from Refs. 10 and [11] was implemented in this analysis.

The coefficient $\rho_{\text{mod}}/\rho_{\text{exp}}$ was introduced to the phenomenological formula for the strength function, which makes the residual anti-correlation of the fitted ρ and Γ demonstrable, to test its influence on the shape of the strength functions of the step-like structure of fitted level density distribution. Simultaneously, it was a test of the invariability of this step-like structure.

The data in Fig. 21 show that the above-mentioned hypothesis about equality of the E_μ and E_ν parameters and about their independence from the number of breakup pairs does not make the fitting quality worse for any investigated nuclei. Therefore, the energy slope of

the vibrational level density is rather dominantly determined by the Δ_0 value. In our analysis of all investigated nuclei, that the coefficients E_μ and E_ν from Eq. (1) turn out to lie near 1 and to be randomly scatter relative to the average. Because of that, Fig. 21 is clear proof of the validity of the vibrational-increase accounting in the level density.

3. The Cooper-pairs-breaking thresholds

Our previous studies have shown the existence of a connection between the shape of the nucleus and the Cooper-pairs-breaking thresholds [11,13,14]. These results were also confirmed in this work. Figure 22 presents the dependence of the binding energy to Δ_0 on nuclei

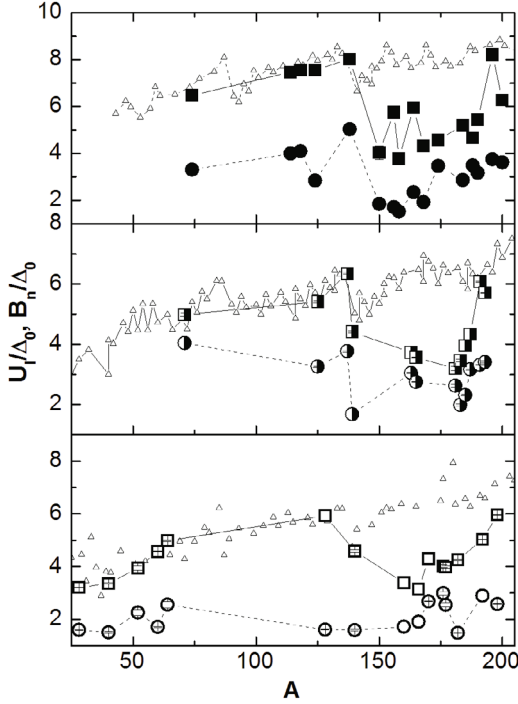


Fig. 21. Dependence of the E_μ and the E_ν (same) model parameters on the nuclear mass A . (Black points-even-even nuclei, black-white-even-odd nuclei and white points-odd-odd nuclei.)

mass and the dependencies of the ratios for the break up thresholds of the second and the third Cooper pairs to Δ_0 on nuclei mass. We should mention that the Cooper-pairs-breaking thresholds are different for nuclei with different nucleon parities and depend on the pairing energy (Δ_0) for the last nucleon. Results presented in Fig. 22 show a significant differences in the ratios U_2/Δ_0 and U_3/Δ_0 for deformed and spherical nuclei, in contrast to B_n/Δ_0 ratio.

4. Level parity

The obtained values for the ratio $r = \rho(\pi-)/(\rho(\pi-) + \rho(\pi+))$ of levels $\rho(\pi-)$ with negative parity to the total level density are presented in Fig. 23. The average values of this ratio are 0.61(22) for even-even, 0.25(28) for even-odd and 0.16(16) for odd-odd nuclei (for odd-even ^{177}Lu , it is 0.65(1)). Those results suggest that the gamma-decay process depends on various nucleon parities. The calculation of the ratio $r = \rho(\pi-)/(\rho(\pi-) + \rho(\pi+))$ was done using a linear extrapolation of the r value in the $E_d \leq E_{ex} \leq B_n$ energy region. In the B_n energy point it was used accepted assumption, that $\rho(\pi-) = 0.5 \cdot (\rho(\pi-) + \rho(\pi+))$, the $\rho(\pi-)$ value in this point was fixed, and at the E_d energy the $\rho(\pi-)$ varied.

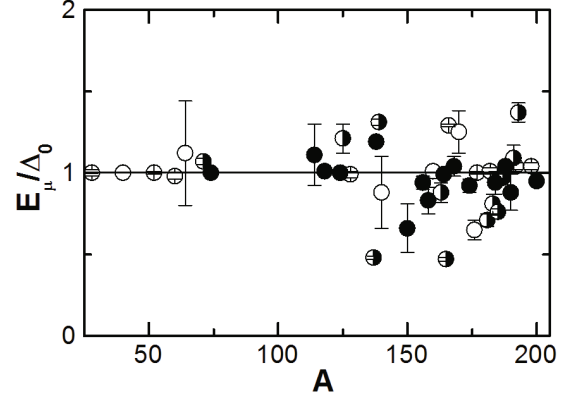


Fig. 22. Dependence of the ratios, U_l/Δ_0 , of break-up thresholds to the average pairing energy of the last nucleon on the nuclear mass A , for the second (points) and the third (squares) Cooper pairs. (Black points-even-even nuclei, black-white-even-odd nuclei and white points-odd-odd nuclei.) Triangles show the dependence of B_n/Δ_0 ratio on mass.

VI. POSSIBLE EXPERIMENTS FOR A STUDY OF SUPERFLUIDITY

Experiments on recording the cascades of two-gamma transitions of radiative capture of thermal neutrons were carried out in Dubna (Russia), Riga (Latvia), Rez (Czech Republic) and Dalat (Vietnam). Unfortunately, gamma-ray cascades at thermal neutron capture allow the determination of ρ and Γ only for a fixed area of nuclear excitations, for a certain spin interval, and for a given parity of the decaying resonance (Table 1).

Until now, in all analyses, a nucleus was usually imagined as a statistical system. The real uncertainty of this nuclear model is still unknown; therefore, new experiments (*e.g.*, as in Ref. 10) are needed. Such experiments can be carried out not only by using beams of thermal and resonance neutrons but also by utilizing any accelerators of charged particles, if provides the scattering of energies of excited levels λ in the target and the energy resolution of the HPGe - detectors are comparable.

The best approach to studying cascades of gamma transitions of decaying levels excited by gamma quanta can be achieved using any source of gamma radiation (*e.g.* ELBE [40] or S-DALINAC [41]) with a fixed energy. At fixed energy E_{max} of the gamma beam, the model of Ref. 10 can be applied in the interval of excitation energies of the decaying levels from E_{max} to $E_{max} - 511$ keV, which would allow for the cascade decay process to become clearer.

The background conditions during cascade recordings for a beam of gamma quanta are essentially better than those for neutron beams. For experiments of the types seen in Refs. 40, 41, a singular requirement is needed: detectors must be placed close to the target, in a back hemisphere relative to it. In such an experiment the ra-

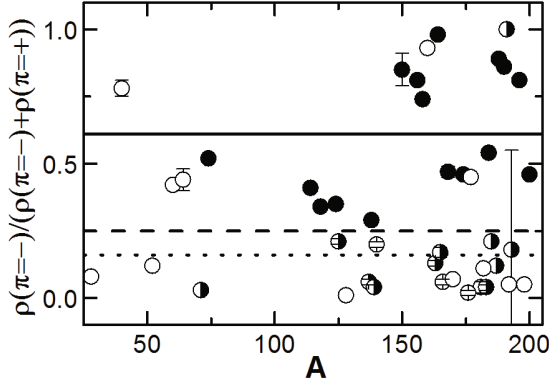


Fig. 23. Mass dependence of the ratio $r = \rho(\pi-)/(\rho(\pi-) + \rho(\pi+))$ at the upper energy border for the discrete region of levels (E_d) and their averaged values for even-even (solid lines), even-odd (dashed lines) and odd-odd nuclei (dotted lines). (Black points-even-even nuclei, black-white-even-odd nuclei and white points-odd-odd nuclei.)

diative strength functions for gamma transitions both to the ground state of the target nucleus, and to its' excited levels can be determinated separatly. The information content of such an experiment will exceed the results of $(n, 2\gamma)$ reaction investigations by at least ten times.

Unlike the cascades of gamma transitions, cascades with nucleon emission provide significant statistical improvements due to the high efficiency of recording the charged products of the reaction. Mathematically, the spectrum of primary gamma transitions of decaying levels below the emission threshold for nucleon products of the reaction and the spectrum of evaporated nucleons (light nuclei) above the binding energy are identical. Therefore, the analysis of a cascade of evaporated nucleon and gamma quanta is similar to the analysis of the cascade of two-gamma transitions. Nevertheless the intensity of a cascade of nucleon and gamma quantum to low-lying levels can be depend strongly on the orbital moment of the evaporated nucleon.

VII. CONCLUSION

In order to obtain reliable values of ρ and Γ , we used an effective practical model that takes into account the interaction of the fermion and the boson components in the nuclear matter. The need to take into account the corrections for the shell inhomogeneities of single-particle spectrum on the level density was demonstrated when comparing the parameters obtained under two different conditions: at a constant density of single-particle states near the Fermi surface and at $g \neq \text{const}$. The results obtained using the shell corrections were closer to the existing representations. Nevertheless, we cannot describe the cascade intensities without taking into account the strong influence of the nuclear superfluidity on

the gamma-decay process. The results about the Cooper pair break-up energies showed a dependence of the dynamics for interactions between superfluid and normal nuclear matter phases on the shape of nucleus. Those data were obtained with high accuracy.

Our model allows for a separate determination of the density of vibrational levels between the breaking thresholds of the Cooper pairs. In two-step gamma-decay, a common result for nuclei with different parity of nucleons is a decrease in the sum k of radiative strength functions when the energy of primary transitions decreases. When one analyzes the set of investigated nuclei, the average sums are almost equal for odd-odd and even-odd nuclei, while the k values are two times smaller for the even-even nuclei.

Unfortunately, the existence of errors for the ρ and the Γ functions is a fundamental problem. This is important for any model used for an analysis of experimental data, as well as for calculations of cross sections or spectra. The systematic uncertainties also come from fluctuations in the intensities of the gamma decay transitions in different nuclei. However, the results presented here gave a possibility for describing of the data obtained in two-step cascades experiments with a satisfactory accuracy that is higher the statistical one.

ACKNOWLEDGMENTS

We wish to express our gratitude to Dr. Petar Mali for helpful advice and discussions.

REFERENCES

- [1] S. Valenta *et al.*, Phys. Rev. C **92**, 064321 (2015).
- [2] J. Honzatko *et al.*, Nucl. Inst. Meth. A **376**, 434 (1996).
- [3] A. M. Sukhovoij and V. A. Khitrov, Instrum. Exp. Tech., **27**, 1071 (1984).
- [4] Yu. P. Popov, A. M. Sukhovoij, V. A. Khitrov and Yu. S. Yazvitsky, Bull. Acad. Sci. USSR Phys. Ser. **48**(5), 53 (1984).
- [5] V. A. Bondarenko *et al.*, Fizika B (Zagreb) **11**, 201 (2002).
- [6] S. T. Boneva, A. M. Sukhovoij and V. A. Khitrov, Nucl. Phys. A **589**, 293 (1995).
- [7] E. V. Vasilieva, A. M. Sukhovoij and V. A. Khitrov, Phys. At. Nucl. **64**, 153 (2001).
- [8] A. M. Sukhovoij and V. A. Khitrov, Phys. Part. Nucl. **36**, 359 (2005).
- [9] V. Ignatyuk, Report INDC-233(L), IAEA, Vienna (1985).
- [10] A. M. Sukhovoij, Phys. Atom. Nucl. **78**, 230 (2015).
- [11] A. M. Sukhovoij and L. V. Mitsyna, in *Proceedings of XXII International Seminar on Interaction of Neutrons with Nuclei* (Dubna, May 2014, Preprint N E3-2015-13, 2015), p. 245, <http://isinn.jinr.ru/past-isinns.html>.

- [12] A. M. Sukhovoij, L. V. Mitsyna and N. Jovancevic, in *XXIII International Seminar on Interaction of Neutrons with Nuclei* (Dubna, May 2015, JINR preprint E3-2016-12, Dubna, 2015), p. 299.
- [13] D. C. Vu *et al.*, Phys. Atom. Nucl. **80**, 237 (2017).
- [14] A. M. Sukhovoij, L. V. Mitsyna and N. Jovancevic, Phys. Atom. Nucl. **79**, 313 (2016).
- [15] V. G. Soloviev, Nucl. Phys. A **586**, 265 (1995).
- [16] V. G. Soloviev, Sov. J. Phys. Part. Nucl. **60**, 390 (1972).
- [17] V. G. Soloviev, Theory of Atomic Nuclei. Quasi-particle and Phonons, IPP, Bristol and Philadelphia, 1992.
- [18] H. A. Weidenmuller and G. E. Mitchell, Rev. Mod. Phys. **81** (2009).
- [19] F. Iachello and A. Arima, *The Interacting Boson Model* (Cambridge University Press, Cambridge, 1987).
- [20] H. Vonach, in *Proc. IAEA Advisory Group Meeting on Basic and Applied Problems of Nuclear Level Densities* (New York, 1983), INDC(USA)-092/L, p. 247.
- [21] B. V. Zhuravlev, Bull. Rus. Acad. Sci. Phys. **63**, 123 (1999).
- [22] G. A. Bartholomew *et al.*, Adv. Nucl. Phys. **7**, 229 (1973).
- [23] A. Schiller *et al.*, Nucl. Instrum. Meth. A **447**, 498 (2000).
- [24] A. C. Larsen *et al.*, Phys. Rev. **76**, 044303 (2007).
- [25] A. C. Larsen *et al.*, Phys. Rev. **83**, 034315 (2011).
- [26] S. G. Kadenskij, V. P. Markushev and W. I. Furman, Sov. J. Nucl. Phys. **37**, 165 (1983).
- [27] W. Dilg, W. Schantl, H. Vonach and M. Uhl, Nucl. Phys. A **217**, 269 (1973).
- [28] P. Axel, Phys. Rev. **126**, 671 (1962).
- [29] D. M. Brink, Ph. D. Thesis, Oxford University, 1955.
- [30] N. Jovancevic, A. M. Sukhovoij, W. I. Furman and V. A. Khitrov, in *Proceedings of XX International Seminar on Interaction of Neutrons with Nuclei* (Dubna, May 2012, Preprint N E3-2013-22, Dubna, 2013), p. 157.
- [31] V. M. Strutinsky, in *Proceedings of the International Congress on Nuclear Physics* (Paris, France, 1958), p. 617.
- [32] Reference Input Parameter Library RIPL-2, *Handbook for Calculations of Nuclear Reaction Data* (IAEA-TECDOC, 2002).
- [33] S. S. Dietrich and B. L. Berman, Atom. Data Nucl. Data Tab. **38**, 199 (1988).
- [34] A. M. Sukhovoij, V. A. Khitrov and W. I. Furman, Phys. Atom. Nucl. **71**, 982 (2008).
- [35] L. A. Malov and V. G. Soloviev, Sov. J. Nucl. Phys. **26**, 384 (1977).
- [36] <http://www-nds.iaea.org/ENDSF>.
- [37] A. Bohr and B. R. Mottelson, *Nuclear Structure* (W. A. Benjamin, New York; Amsterdam, 1969), Vol. 1.
- [38] V. A. Bondarenko *et al.*, Nucl. Phys. A **762**, 167 (2005).
- [39] A. M. Sukhovoij and V. A. Khitrov, Phys. Atom. Nucl. **76**, 68 (2013).
- [40] A. Makinaga *et al.*, Phys. Rev. C **90**, 044301 (2014).
- [41] B. Özel-Tashenov *et al.*, Phys. Rev. C **90**, 024304 (2014).

Study of gamma ray transitions and level scheme of ^{56}Mn using the $^{55}\text{Mn}(n_{th}, 2\gamma)$ reaction

David Knezevic^{a,b,*}, Nikola Jovancevic^b, Anatoly M. Sukhovoij^c,
Aleksandar Dragic^a, Liudmila V. Mitsyna^c, Zsolt Revay^d,
Christian Stieghorst^d, Stephan Oberstedt^e, Miodrag Krmar^b,
Ilija Arsenic^f, Dimitrije Maletic^a, Dejan Jokovic^a

^a University of Belgrade, Institute of Physics Belgrade, Pregrevica 118, 11080 Zemun, Serbia

^b University of Novi Sad, Faculty of Science, Department of Physics, Trg Dositeja Obradovica 3, 21000 Novi Sad, Serbia

^c Joint Institute for Nuclear Research, 141980 Moscow region, Dubna, Russia

^d Technische Universität München, Heinz Maier-Leibnitz Zentrum (MLZ), Lichtenbergstr. 1, D-85747 Garching, Germany

^e European Commission, Joint Research Centre, Directorate G – Nuclear Safety and Security, Unit G.2, Retieseweg 111, B-2440 Geel, Belgium

^f University of Novi Sad, Faculty of Agriculture, Trg Dositeja Obradovica 8, 21000 Novi Sad, Serbia

Received 20 May 2019; received in revised form 9 September 2019; accepted 12 September 2019

Available online 18 September 2019

Abstract

This work provides new data about the level scheme of ^{56}Mn studied by the $^{55}\text{Mn}(n_{th}, 2\gamma)$ reaction. The spectroscopic information were collected using the gamma-gamma coincidence spectrometer at the Technische Universität München, Heinz Maier-Leibnitz Zentrum (MLZ), Garching, Germany. The intensities, energies of primary and secondary transitions of 71 energy-resolved cascades, as well as intermediate cascade levels were determined. The updated level scheme of ^{56}Mn was obtained from analyzing the intensity spectra of the strongest cascades. The comparison with the existing data in the ENSDF database shows that 23 primary transitions, 24 intermediate cascades levels as well as 32 secondary transitions determined in this work can be recommended as new nuclear data.

© 2019 Published by Elsevier B.V.

* Corresponding author at: University of Belgrade, Institute of Physics Belgrade, Pregrevica 118, 11080 Zemun, Serbia.
E-mail addresses: davidk@ipb.ac.rs (D. Knezevic), nikola.jovancevic@df.uns.ac.rs (N. Jovancevic).

Keywords: Gamma ray spectrometry; Thermal neutron capture; Level scheme; Gamma ray cascades

1. Introduction

Accurate data about the nuclear level scheme play an important role in the understanding of the nuclear properties. They are necessary for studying nuclear reactions as well as for determining nuclear structure parameters. In this work we chose to study the level scheme of the ^{56}Mn . For that purpose, we used the two-step gamma-cascade method based on measurements of coincident prompt gamma rays following thermal neutron capture [1–4]. An advantage of this technique is a low Compton background in collected spectra owing to the use of the background-subtraction algorithm [1].

The properties of ^{56}Mn nucleus have been studied by means of thermal and resonance neutron capture [5–24] but also by other methods, such as the $^{56}\text{Cr} \beta^-$ decay [25], $^{48}\text{Ca}(^{11}\text{B}, 3n\gamma)$ [26], $^{54}\text{Cr}(^3\text{He}, p)$ [27], $^{54}\text{Cr}(\alpha, d)$ [28], $^{55}\text{Mn}(d, p)$ [29–32], $^{56}\text{Fe}(\mu^-, \nu\gamma)$ [33], $^{56}\text{Fe}(t, ^3\text{He})$ [34], $^{56}\text{Fe}(^{12}\text{C}, ^{12}\text{N})$ [35,36], $^{58}\text{Fe}(d, \alpha)$ [37]. The overview of excitation data shows the need for collecting new accurate spectroscopic data on ^{56}Mn .

In this work, we present new information on the ^{56}Mn nucleus (levels, gamma ray transition energies and their intensities per capture). The obtained results were compared with the existing ENSDF data [38]. As it is an odd-odd nucleus, the ^{56}Mn can also be interesting from a theoretical point of view, such as studying the level density and the radiative strength function. Since the two-step gamma ray-cascades method provides the possibility to estimate simultaneously the level density and radiative strength functions, in a future work, these nuclear parameters may be obtained for this nuclei as well, as it was done in [39–44] for other investigated nuclei.

2. Experimental setup and measurement

The objective of this experiment was the detection of two-step gamma ray cascades in ^{56}Mn following thermal neutron capture on ^{55}Mn , $^{55}\text{Mn}(n_{th}, 2\gamma)^{56}\text{Mn}$. The measurement was carried out at the PGAA station of Technische Universität München, Heinz Maier-Leibnitz Zentrum (MLZ), Garching, Germany [45,46].

The experimental setup consisted of two HPGe detectors with relative efficiencies of 60% and 30%. The distance between detectors was 22.5 cm (this distance is the distance between the detector cap of the 60% detector and the point on the axis of the 30% detector that lies on the line determined by the detector cap of the 60% detector and the position of the sample). Target was placed at 9 cm from the detector with a 30% efficiency (distance measured on the above mentioned line) as shown in Fig. 1. The other detector was surrounded by an active anti-Compton suppression made of bismuth germanate (BGO). The shielding against scattered neutrons consisted of a 1 mm thick boron-containing plastic tube that was built around the detectors. The detector was also surrounded by 10 cm of lead shielding to reduce background gamma ray radiation. The necessary experimental data for the analysis (energy of both detected coincident photons and time difference between their detection) were collected by a N1728B CAEN ADC digitizer. For the mono-isotopic manganese (^{55}Mn) the preparation of a high-purity target for the experiment is considerably easier compared to nuclei of more complex isotopic composition. The target was high-purity (99.9%) natural manganese powder with the mass of 50 mg. The relative efficiency of the detectors was determined from single gamma ray spectra accumulated using a PVC tar-

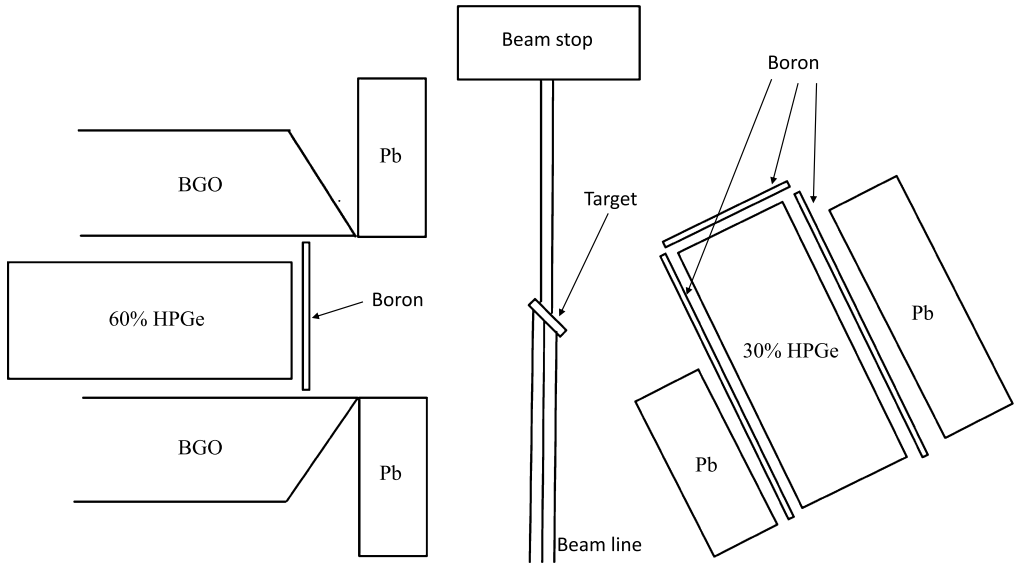


Fig. 1. Sketch of the experimental setup.

get (the $^{35}\text{Cl}(n,\gamma)^{36}\text{Cl}$ reaction) [47]. For the 30% detector the efficiency curve was $\ln(\epsilon) = -1.124210 \cdot \ln(E_\gamma) - 2.01161 \cdot \ln(E_\gamma/1022) + 0.453523 \cdot \ln^2(E_\gamma/1022)$, and for the 60% detector it was $\ln(\epsilon) = -0.751695 \cdot \ln(E_\gamma) + 0.150324 \cdot \ln(E_\gamma/1022) - 0.177287 \cdot \ln^2(E_\gamma/1022)$. Manganese two gamma ray events were recorded for 105.6 h.

3. Result and discussion

Only a short description of the applied procedure to extract the cascade events and intensities is presented here. The detailed description can be found in Ref. [1].

The most important part of the collected spectrum of sums of amplitudes for coincident pulses (SACP) is shown in Fig. 2. The five marked peaks in Fig. 2 present the two-step cascade peaks of $^{56}_{25}\text{Mn}$ for transitions from the neutron binding energy (7270.0(5) keV) to the ground state and to the first four excited states with the energies of 26.5, 110.4, 212.0 and 341.0 keV. In Table 1, the core information about these five cascade peaks is presented. The remaining unmarked peaks in the SACP spectrum correspond to background events (Fig. 2). They may come from recording of coincidences of the first with the third or fourth quantum of the multiple-step gamma ray cascades or from neutron interaction with surrounding materials. In Table 1, there is also information about part of the resolved intensity, that represents the fraction of the total intensity (% per decay) observed in the spectra $E_{\gamma,1} + E_{\gamma,2} = \text{const}$ in the form of pairs of intense energy-resolved peaks in Fig. 3 and Fig. 4. These cascades are observed in the form of pairs of standard peaks. Their intensity is given in column 4 of Table 2 in the form of $I_{\gamma\gamma}$. The concept of “part of resolved cascade intensity” is used in further analysis to determine the ratio of the sum of the intensity of only resolved peaks to the total sum of the intensities of all resolved and unresolved cascades. The total sum includes all cascades without exception, primary and secondary transitions that satisfy the rules of selection by multiplicity. The cascades to other spins and multipolarities are impossible to determine in this type of experiment.

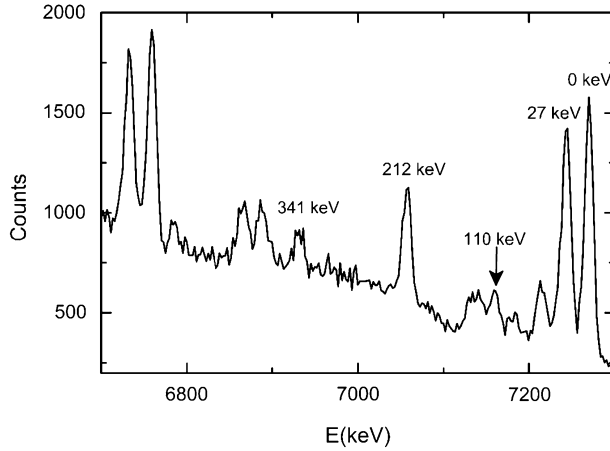


Fig. 2. Spectrum of sums of amplitudes for coincident pulses (SACP) at the radiative capture of thermal neutrons in ^{55}Mn nucleus. Peaks of the full capture of two quanta are labeled by energy of the final level of the resolved cascades.

Table 1

Information about the two-step cascades to the ground state and the first four excited states collected in the experiment. The spin values of the final levels were taken from [38].

Gamma ray cascade total energy (keV)	Final level (E_f) of the cascade (keV)	Spin of level E_f	Part of resolved cascade intensity	Full intensities % per decay
7270	0	3+	70(5)	17(3)
7243	26.5	2+	70(7)	13(3)
7160	110.4	1+	51(9)	5.0(10)
7058	212.0	4+	49(5)	16.0(20)
6929	341.0	3+	40(6)	6.0(10)
Sum of total			56(3)	57(5)

From collected SACP spectra the two-step-cascade (TSC) spectra were obtained. This was done for five energy-resolved amplitude peaks. The obtained TSC spectra represent the cascades from the initial state to the defined low-lying final levels of the $^{56}_{25}\text{Mn}$ nucleus. The elimination of Compton background and random coincidences was done by gating on the region nearby the peaks of interest in Fig. 2. Figs. 3 and 4 show examples of the obtained TSC spectra for cascade total energies of 6929 and 7058 keV. The background in the two-step-cascade (TSC) spectra of mono-isotopic manganese is practically absent.

The mirror-symmetrical peaks [2] in the TSC spectra represent primary and secondary transitions of the investigated two-step gamma ray cascade. The peaks' positions correspond to the energies, $E_{\gamma,1}$ and $E_{\gamma,2}$, of primary and secondary quanta of the cascades. The relative intensity of each peak is proportional to its area. The criteria for selecting if the structure in the TSC spectrum is a peak is based on searching for the peak structures with non zero count across multiple channels, and then verifying the existence of the peak using the fitting procedure. All energy-resolved peaks are approximated by the Gauss function, and the background is approximated by a constant or a weakly varying linear function. The ratio of the area of all peaks to the sum of the spectrum gives the value of the proportion of resolved peaks detected in the experiment. The remainder is a continuum of the unresolved cascades.

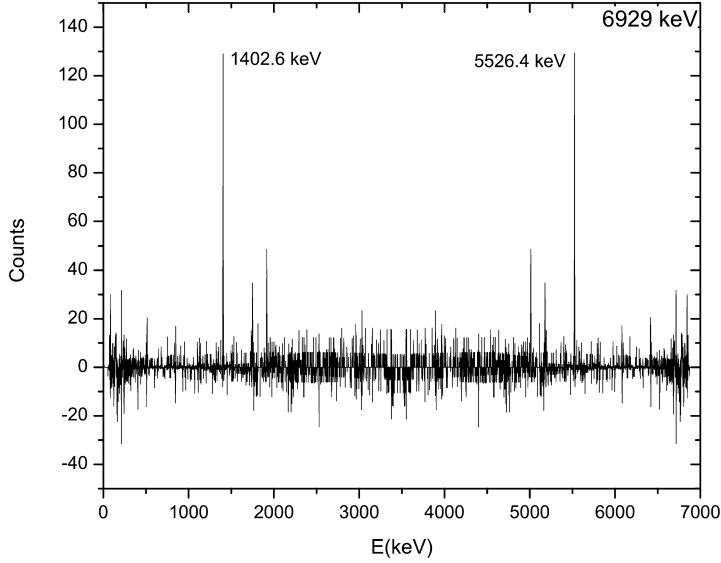


Fig. 3. Two step cascade (TSC) spectrum with the total energy of 6930 keV. The final level of the cascade is 340.957(6) keV (value taken from [38]). This spectrum represents the TSC spectrum with low number of cascades (8 pairs of gamma rays). The energies of the most intense pair of gamma rays are labeled.

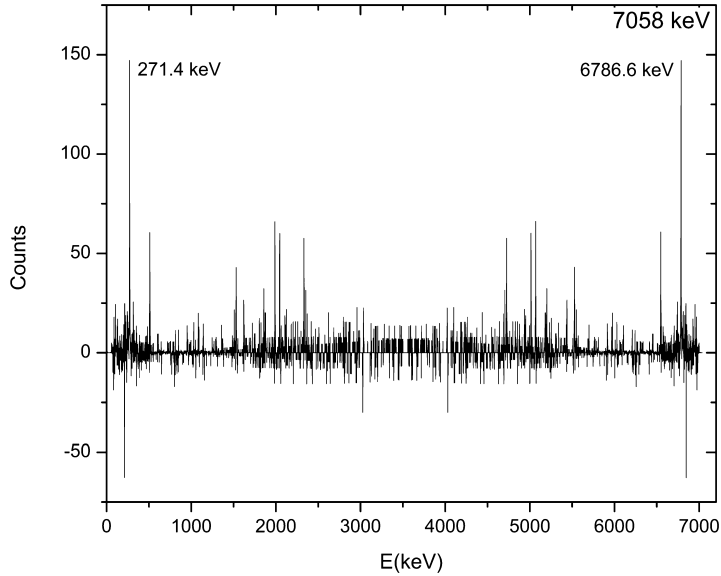


Fig. 4. Two step cascade (TSC) spectrum with the total energy of 7058 keV. The final level of the cascade is 212.004(5) keV (value taken from [38]). This spectrum represents the TSC spectrum with high number of cascades (22 pairs of gamma rays). The energies of the most intense pair of gamma rays are labeled.

Details of the method and the maximum likelihood function used to determine the energies of primary and secondary cascade transitions were presented in [1,4]. The intensities of 71 resolved cascades are determined from five TSC distributions. In all investigated cascades, primary tran-

sitions (except for 7 of them) have the higher energy in comparison with the energy of secondary quanta. All detected primary and secondary gamma ray transitions and their intensities as well as the energies of intermediate levels are presented in Table 2.

In order to compare the data of the cascade spectra (Figs. 3 and 4) with the experimental data for strongest primary transitions with $E_{\gamma,1}=7058, 7160, 6929, 6784, 5527$ and 5181 keV, the branching coefficients (Br) of their secondary transitions were obtained independently (using existing ENSDF data), which gave data of absolute intensity of the cascades for normalization of the data from Table 2.

The intensities of primary gamma transitions to individual low-lying levels i_1 are generally known. The product $i_1 \cdot Br$ is the absolute intensity of one of these cascades to the intermediate level. Then, from the proportion with three known values $i_1, i_2, i_1 \cdot Br$ and the total sum of the intensity of all transitions of the given stages $i_{\gamma\gamma} = 100\%$, we obtain the ratio $I_{\gamma\gamma} = i_1 \cdot Br \cdot i_1 i_2 / 100$. It is equal to the sum of $I_{\gamma\gamma}$ of all two-quantum cascades (resolved and unresolved energetically for the cascade with the corresponding finite level). The values of the total intensity $I_{\gamma\gamma}$ obtained in such a way (Table 1), which include both the resolved cascades and unresolved cascade continuum with sub-threshold intensity, show that, for the investigated nucleus, we have obtained in this experiment 57% of total intensity of all two-step cascades. At that, 56% of this intensity $I_{\gamma\gamma}$ falls to the share of the energy-resolved cascades (Table 2).

The data were compared with the existing ones in the ENSDF database [38]. From this comparison, 22 primary transitions that existed in the ENSDF data set were determined. 23 primary transitions, which are not included in the ENSDF library, can be therefore recommended as new data. 21 intermediate levels are identified in our experiment and already listed in the ENSDF database. However, for 24 levels observed in this study, there are no data in the ENSDF library yet. The difference between number of primary gamma rays and levels comes from the fact that in some cases, as is the case of gamma ray with energy (database value [38]) 5432.9 keV, that is identified as primary gamma-ray corresponding to experimental value of 5431.5 keV, gamma-rays exist in the database, but do not have a scheme position assigned to them, so the authors tentatively assigned the scheme position for a number of gamma rays as the primary gamma rays of the cascades. Same is the case for gamma ray with energies (database values [38]) 6019.2, 4324.1 and 3034.1 keV. In this work, we observed 32 secondary gamma ray transitions for which there is no information in the ENSDF database. 14 of these new observed secondary transitions come from the levels already in the ENSDF library, and 18 from levels determined for the first time in this work. Also, 11 secondary gamma rays observed in this study are listed in the ENSDF database, but do not have an assigned position in the decay scheme. In this paper we assigned the decay scheme positions for gamma rays with energies (database values [38]) of 1140.4, 2147.3, 2437.8, 2582.0, 2864.4, 2832.9, 2740.3, 2937.6, 3135.6, 4127.7 and 4024.5 keV.

The comparison of determined energies of levels and gamma rays with the ones from the ENSDF database shows an average deviation of about 1.5 keV. For levels and gamma rays where the deviation was larger than 2 keV, ENSDF values were in some cases assigned tentatively by the authors. This relatively large discrepancy can be explained by insufficient statistics in the present TSC spectra, as well as by the keV/Ch difference between the two detectors during measurement, which can cause uncertainty in the determination of the energy.

The level scheme of $^{56}_{25}\text{Mn}$ obtained in this work is presented in Figs. 5 and 6.

Spin of the neutron capture level is determined by the ground state spin of the capturing nuclei \pm the $1/2$ spin of the neutron. This state decays primarily via dipole transition, predominantly of electric multipolarity. As the compound-state of $^{55}_{25}\text{Mn}$ is $5/2^-$, after a capture of a thermal neutron primary gamma ray transitions can be emitted from the decay of levels with spins 2^- or

Table 2

Comparison of the experimental data with the ENSDF database. $E_{\gamma,1}$ and $E_{\gamma,2}$ are the energies of the first and second quanta of the cascade, respectively, E_i is the energy of the intermediate level and E_f are the final levels of the two step gamma ray cascade. $I_{\gamma\gamma}$ is the intensity of the cascade (per 100 decays) observed in the experiment. The experimental uncertainty of $E_{\gamma,2}$ has the same absolute values as for $E_{\gamma,1}$ (listed in the table). Values in bold are values for which there is no data in the ENSDF library.

Present work				ENSDF			
$E_{\gamma,1}$ (keV)	$E_{\gamma,2}$ (keV)	E_i (keV)	$I_{\gamma\gamma}$	E_f (keV)	$E_{\gamma,1}$ (keV)	$E_{\gamma,2}$ (keV)	E_i (keV)
7160.6(3)	82.9	109.0(6)	4.8(6)	26.516(3)	7159.7(2)	83.8990(15)	110.428(3)
7058.80(21)	211.20	211.2(5)	9.2(8)	g.s.	7057.8(2)	212.017(6)	212.004(5)
7053.1(13)	106.5	216.9(14)	0.9(4)	110.428(3)	–	104.6234(20)	215.057(3)
6925.1(12)	344.9	344.9(13)	0.10(5)	g.s.	6928.7(2)	340.990(25)	340.957(6)
6929.9(6)	313.6	340.1(8)	1.3(4)	26.516(3)	6928.7(2)	314.395(10)	340.957(6)
6786.6(7)	271.4	483.4(9)	1.3(4)	212.004(5)	6783.3(2)	271.175(9)	486.251(8)
6786.6(17)	142.4	483.4(18)	0.22(15)	340.957(6)	6783.3(2)	145.320(20)	486.251(8)
6733.0(8)	510.5	537.0(9)	0.55(17)	26.516(3)	–	–	–
6699.7(27)	229.3	570.3(27)	0.15(17)	340.957(6)	–	229.867(7)	–
6101.8(12)	1141.7	1168.2(13)	0.25(16)	26.516(3)	6103.9(2)	1140.4(10)	1166.54(21)
6101.8(9)	1057.8	1168.2(10)	0.16(5)	110.428(3)	6103.9(2)	–	1166.54(21)
6101.8(14)	956.2	1168.2(15)	0.09(4)	212.004(5)	6103.9(2)	–	1166.54(21)
6021.8(20)	1221.7	1248.2(21)	0.08(6)	26.516(3)	6019.2(8)	–	–
5919.4(15)	1324.1	1350.6(16)	0.18(11)	26.516(3)	5920.5(2)	–	1349.95(21)
5916.7(13)	1141.3	1353.3(14)	0.08(4)	212.004(5)	–	–	–
5789.8(27)	1453.7	1480.2(27)	0.09(8)	26.516(3)	–	–	–
5759.7(4)	1510.3	1510.3(6)	0.79(14)	g.s.	5760.9(2)	–	1509.55(21)
5759.7(13)	1298.3	1510.3(14)	0.07(3)	212.004(5)	5760.9(2)	–	1509.55(21)
5759.7(17)	1169.3	1510.3(18)	0.034(24)	340.957(6)	5760.9(2)	1169.71(13)	1509.55(21)
5547.5(10)	1510.5	1722.5(11)	0.10(4)	212.004(5)	–	–	–
5526.4(13)	1717.1	1743.6(14)	0.12(8)	26.516(3)	5527.4(2)	1716.63(14)	1744.3(10)
5526.4(5)	1531.6	1743.6(7)	0.46(8)	212.004(5)	5527.4(2)	–	1744.3(10)
5526.4(6)	1402.6	1743.6(8)	0.82(24)	340.957(6)	5527.4(2)	1401.7(10)	1744.3(10)
5438.7(12)	1720.9	1831.3(13)	0.07(3)	110.428(3)	5437.0(2)	–	1833.67(21)
5438.7(16)	1619.3	1831.3(17)	0.08(5)	212.004(5)	5437.0(2)	–	1833.67(21)
5431.5(24)	1626.5	1838.5(25)	0.10(7)	212.004(5)	5432.9(2)	–	–
5313.6(16)	1956.4	1956.4(17)	0.07(5)	g.s.	–	–	–
5270.3(11)	1889.3	1999.7(12)	0.17(7)	110.428(3)	–	–	–
5250.8(16)	2019.2	2019.2(17)	0.13(8)	g.s.	–	2016.5(2)	2016.39(15)
5201(3)	2042.5	2069(3)	0.12(11)	26.516(3)	–	2044.7(2)	–
5197.8(14)	1961.8	2072.2(15)	0.08(4)	110.428(3)	5199.1(2)	–	2071.39(15)
5197.8(11)	1860.2	2072.2(12)	0.17(9)	212.004(5)	5199.1(2)	–	2071.39(15)
5182.7(11)	2060.8	2087.3(12)	0.46(23)	26.516(3)	–	2063.2(2)	–
5180.6(7)	2089.7	2089.7(9)	0.54(10)	g.s.	5181.6(2)	2090.4(2)	2089.38(15)
5180.6(17)	1877.7	2089.7(18)	0.18(9)	212.004(5)	5181.6(2)	1876.2(10)	2089.38(15)
5180.6(7)	1748.7	2089.7(9)	0.49(14)	340.957(6)	5181.6(2)	1747.0(10)	2089.38(15)
5064.4(13)	2179.1	2205.6(14)	0.40(20)	26.516(3)	–	2176.6(2)	2202.73(15)
5064.4(16)	1993.6	2205.6(17)	0.22(12)	212.004(5)	–	–	2202.73(15)
5030.8(23)	2128.8	2239.2(24)	0.07(5)	110.428(3)	–	–	2235.14(21)
5013.5(9)	2044.5	2256.5(10)	0.26(13)	212.004(5)	5015.0(2)	2044.7(2)	2255.24(15)
5013.5(5)	1915.5	2256.5(7)	0.5(11)	340.957(6)	5015.0(2)	1915.2(10)	2255.24(15)
4950.9(12)	2292.6	2319.1(13)	0.31(14)	26.516(3)	4949.4(2)	2294.8(2)	2321.15(10)
4950.9(14)	2208.7	2319.1(15)	0.12(7)	110.428(3)	4949.4(2)	2211.3(2)	2321.15(10)
4907.4(11)	2252.2	2362.6(12)	0.12(7)	110.428(3)	4907.9(2)	2254.8(2)	2362.62(21)
4907.4(11)	2150.6	2362.6(12)	0.054(22)	212.004(5)	4907.9(2)	2147.3(2)	2362.62(21)

(continued on next page)

Table 2 (continued)

Present work				ENSDF			
$E_{\gamma,1}$ (keV)	$E_{\gamma,2}$ (keV)	E_i (keV)	$I_{\gamma\gamma}$	E_f (keV)	$E_{\gamma,1}$ (keV)	$E_{\gamma,2}$ (keV)	E_i (keV)
4831.9(13)	2438.1	2438.1(14)	0.23(11)	g.s.	4829.7(2)	2437.8(2)	2441.27(15)
4831.9(25)	2327.7	2438.1(25)	0.10(7)	110.428(3)	4829.7(2)	2331.2(2)	2441.27(15)
4730.2(14)	2539.8	2539.0(15)	0.14(10)	g.s.	—	—	—
4726.3(5)	2331.7	2543.7(7)	0.64(12)	212.004(5)	4725.0(2)	2331.2(2)	2545.65(20)
4659(3)	2584	2611(3)	0.17(26)	26.516(3)	—	2582.0(2)	—
4551.1(19)	2506.9	2718.9(20)	0.07(5)	212.004(5)	4550.6(2)	—	2719.96(21)
4379.0(14)	2864.5	2891.0(15)	0.15(11)	26.516(3)	4381.0(2)	2864.4(2)	2889.57(21)
4341.3(16)	2716.7	2928.7(17)	0.09(5)	212.004(5)	—	—	—
4325.1(22)	2834.5	2944.9(23)	0.05(4)	110.428(3)	4324.1(2)	2832.9(2)	—
4317.7(20)	2740.3	2952.3(21)	0.06(5)	212.004(5)	4319.5(2)	2740.3(8)	2951.07(21)
4263.3(16)	3006.9	3006.9(17)	0.17(10)	g.s.	—	3003.4(2)	—
4263.3(23)	2794.9	3006.9(24)	0.06(4)	212.004(5)	—	—	—
4224.5(16)	3045.5	3045.5(17)	0.19(10)	g.s.	4223.5(2)	3047.5(2)	3047.34(15)
4224.5(14)	2935.1	3045.5(15)	0.09(5)	110.428(3)	4223.5(2)	2937.6(8)	3047.34(15)
4134.8(22)	3135.2	3135.2(23)	0.16(10)	g.s.	—	3135.6(2)	—
3879(4)	3391	3391(4)	0.07(9)	g.s.	—	—	—
3871.6(14)	3057.4	3398.4(15)	0.09(5)	340.957(6)	3873.0(2)	3058.2(2)	3397.61
3751.1(13)	3408.5	3518.9(14)	0.22(10)	110.428(3)	3752.3(2)	—	3518.32(21)
3592.8(14)	3465.2	3677.2(15)	0.12(6)	212.004(5)	—	—	—
3035.0(11)	4124.6	4235.0(12)	0.20(7)	110.428(3)	3034.1(2)	4127.7(8)	—
3035.0(20)	4023.0	4235.0(21)	0.13(9)	212.004(5)	3034.1(2)	4024.5(10)	—
3035.0(17)	3894.0	4235.0(18)	0.13(7)	340.957(6)	3034.1(2)	—	—
2959.5(14)	4200.1	4310.5(15)	0.06(3)	110.428(3)	—	—	—
2959(5)	4098	4311(5)	0.05(6)	212.004(5)	—	—	—
2588(3)	4571	4682(3)	0.08(10)	110.428(3)	—	—	—
2179.7(9)	4878.3	5090.3(10)	0.12(4)	212.004(5)	—	—	—

3^- , exciting the levels with spins from $J=1$ to $J=4$. Cross section for the neutron resonance with a spin of 2^- is 8.36 b, for spin 3^- this cross section is 3.57 b, and for boundary resonance with cross section of 1.39 b, the spin is unknown [22]. Spin interval for the nuclear levels that are excited by secondary transitions of the cascade is from $J=0$ to $J=5$. Such limitation on the possible values of spins is due to decay of excited nucleus by mainly dipole E1- and M1-transitions, at least, if cascade energy is larger than 6930 MeV. Cascades of less total energy with $\Delta J=3$ were not observed in our experiment. A contribution of quadrupole gamma ray transitions to the total gamma ray spectrum is negligible.

Insufficient resolution of HPGe-detectors did not allow to uncouple the two-step cascades to doublets of final levels 212.026/215.128 keV and 335.529/340.989 keV. But small shift of average of total-energy sum of these doublets (7058 and 6934 keV) give us the reason to think that cascades to the final levels with the energies of 212 and 340 keV and corresponded to them spins 4^+ and 3^+ are dominated in the decay scheme.

4. Conclusion

In this paper, new spectroscopic information was obtained for $^{56}_{25}\text{Mn}$ by investigating two-step gamma ray cascades following thermal-neutron capture on $^{55}_{25}\text{Mn}$. The level scheme and gamma ray transitions for the $^{56}_{25}\text{Mn}$ nucleus were obtained. The data show good agreement with the ones from the ENSDF library. 24 new levels were observed with 23 new primary and 32 secondary

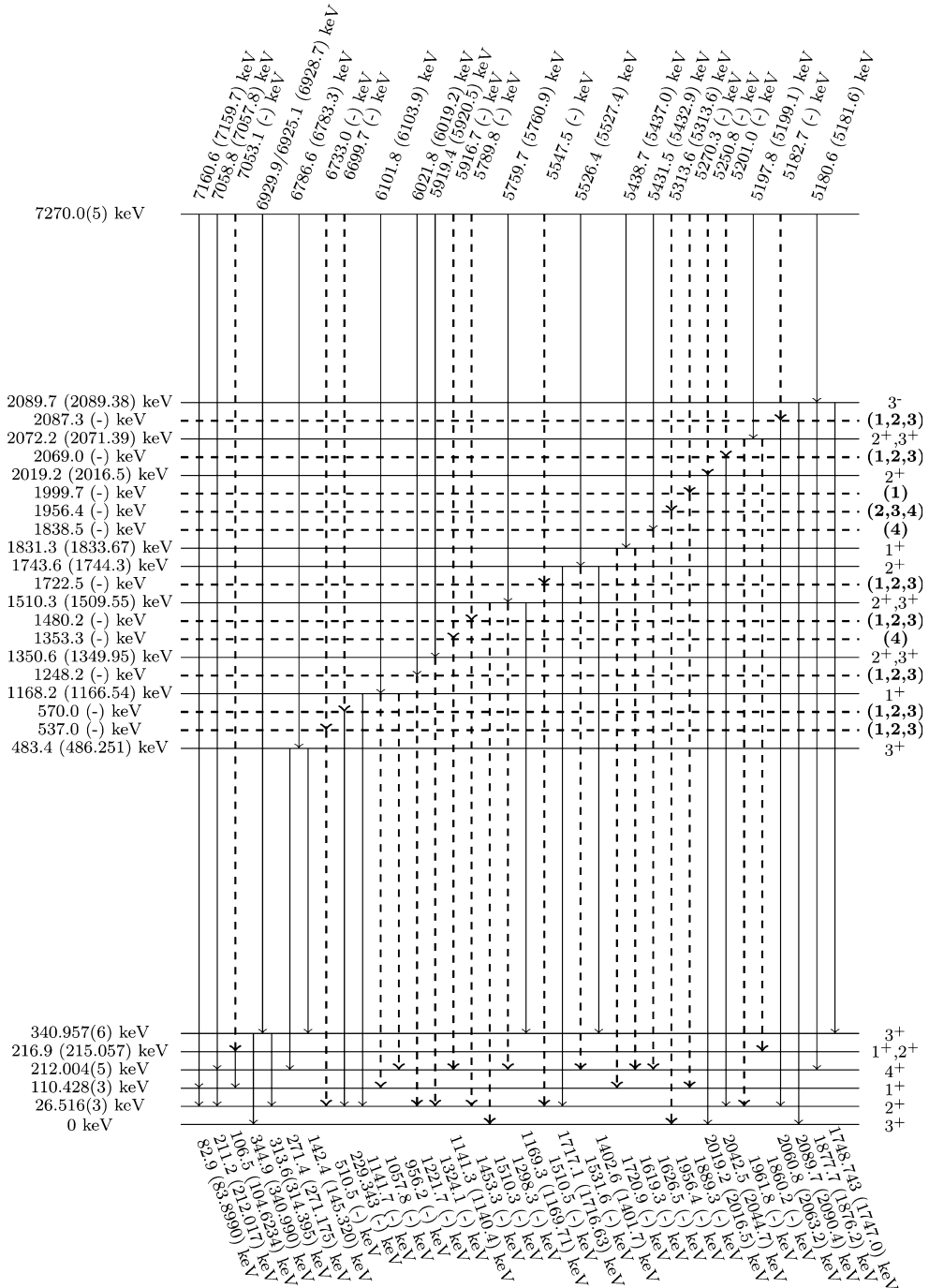


Fig. 5. Experimental level scheme of $^{56}_{25}\text{Mn}$ with intermediate level energies up to 2100 keV. Dashed lines – levels and gamma rays not found in the ENSDF library; bold spin values – values suggested by the authors for the levels without spin information in the ENSDF library. All energy values, except the energy values for the first 4 low-lying levels are given in the form: Experimental value(ENSDF value).

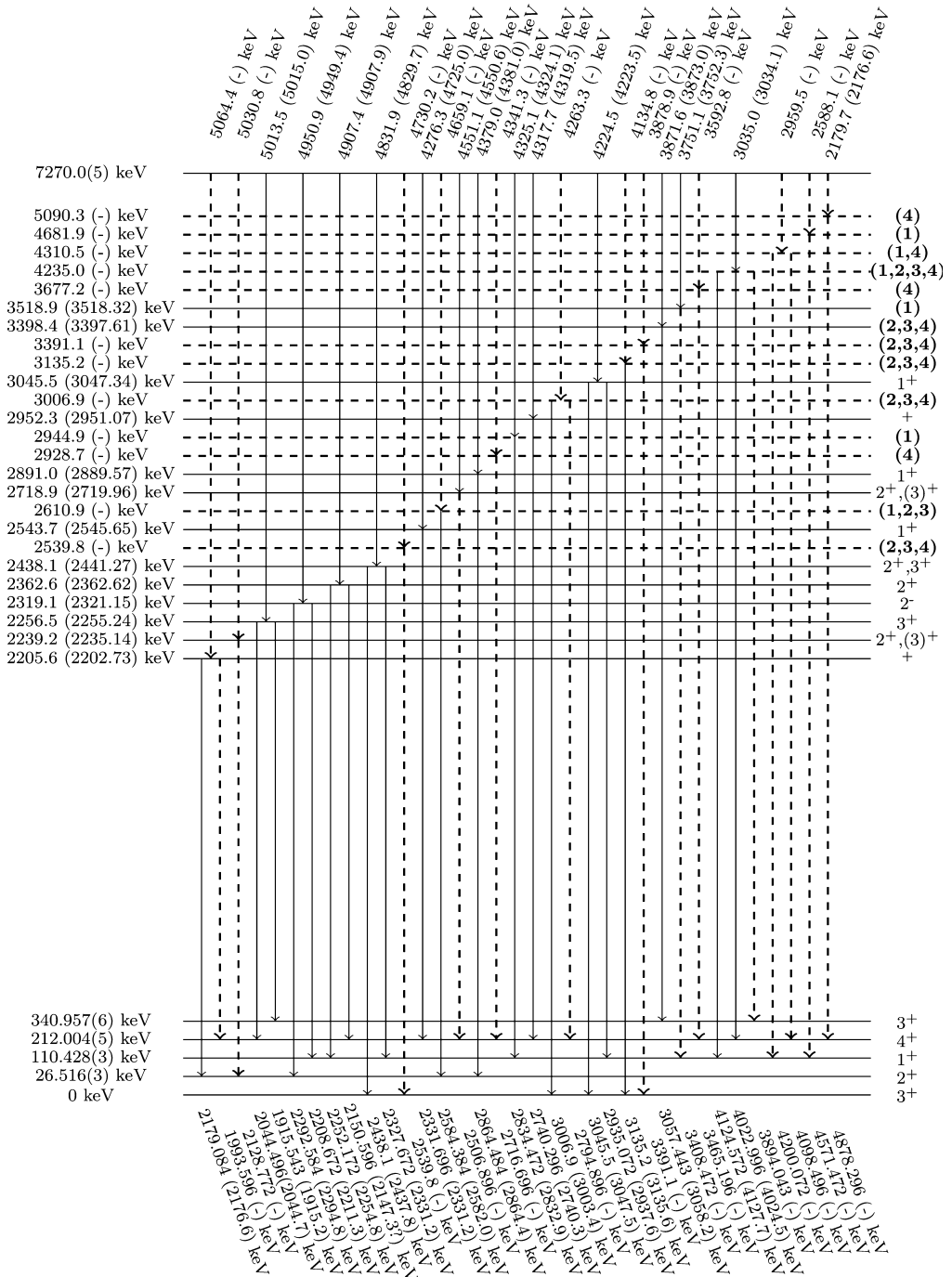


Fig. 6. Experimental level scheme of ^{56}Mn with intermediate level energies from 2200 to 5100 keV. Dashed lines – levels and gamma rays not found in the ENSDF library; bold spin values – values suggested by the authors for the levels without spin information in the ENSDF library. All energy values, except the energy values for the first 4 low-lying levels are given in the form: Experimental value(ENSDF value).

gamma ray transitions in the energy range between 0.3 MeV and 7.1 MeV. These new results can be useful for future investigations of nuclear structure parameters such as the nuclear level density and radiative strength function.

Acknowledgement

The authors gratefully acknowledge the financial support provided by the FRM II to perform the experiment at the Heinz Maier-Leibnitz Zentrum (MLZ), Garching, Germany.

References

- [1] S. Boneva, E. Vasil'eva, Y.P. Popov, A. Sukhovoï, V. Khitrov, Two-quantum cascades of radiative neutron capture I. Spectroscopy of excited states of complex nuclei in the neutron binding energy region, *Sov. J. Part. Nucl.* 22 (2) (1991) 232–248 (English Translation).
- [2] Y.P. Popov, A. Sukhovoï, V. Khitrov, Y.S. Yazvitskij, Study on the γ decay of ^{165}Dy with the help of the $(n, 2\gamma)$ reaction, *Izv. Akad. Nauk SSSR, Ser. Fiz.* 48 (5) (1984) 891–900.
- [3] A. Sukhovoï, V. Khitrov, Method of improving the amplitude resolution of the spectra of gamma-transition cascades in the computer processing of encoded coincidence data, *Instrum. Exp. Tech.* 27 (5) (1985) 1071–1074.
- [4] E. Vasilieva, A. Sukhovoï, V. Khitrov, Direct experimental estimate of parameters that determine the cascade gamma decay of compound states of heavy nuclei, *Phys. At. Nucl.* 64 (2) (2001) 153–168.
- [5] R.W. Bauer, M. Deutsch, Nuclear orientation of Mn-56, *Phys. Rev.* 117 (2) (1960) 519.
- [6] S. Du Toit, L. Bollinger, Lifetimes of energy levels in Al-28, Mn-56, Cu-64, Rh-104, and I-128 excited by slow neutron capture, *Phys. Rev.* 123 (2) (1961) 629.
- [7] I. Estulin, A. Melioransky, L. Kalinkin, Transitions between low-lying excited states of Mn-54 and Ho-166, *Nucl. Phys.* 24 (1) (1961) 118–125.
- [8] P. Carlos, H. Nifenecker, J. Fagot, J. Matuszek, Étude de cascades γ — γ dans la capture thermique de neutrons par les isotopes ^{55}Mn , ^{56}Fe , ^{59}Co , ^{199}Hg , *J. Phys.* 25 (11) (1964) 957–960.
- [9] L. Hughes, T. Kennett, W. Prestwich, A study of the $^{55}\text{Mn}(n, \gamma)^{56}\text{Mn}$ reaction, *Nucl. Phys.* 80 (1) (1966) 131–144.
- [10] D. Dorioman, M. Popa, M. Cristu, Gamma Rays from Thermal Neutron Capture in Manganese, Germanium, and Iridium Nuclei, *Tech. Rep., Inst. of Atomic Physics, Bucharest*, 1967.
- [11] R. Alves, J. Kuchly, J. Julien, C. Samour, J. Morgenstern, Capture radiative partielle des neutrons de résonance dans le chlore, le manganèse, le fer, le cuivre, le thulium et le mercure, *Nucl. Phys. A* 135 (2) (1969) 241–280.
- [12] J. Kopecký, E. Warming, Circular polarization measurements with a Ge (Li) detector, *Nucl. Phys. A* 127 (2) (1969) 385–398.
- [13] J. Mellema, H. Postma, Investigation of nuclear level spins of ^{56}Mn by means of nuclear orientation, *Nucl. Phys. A* 154 (2) (1970) 385–406.
- [14] V. Orphan, N.C. Rasmussen, T. Harper, Line and Continuum Gamma-Ray Yields from Thermal-Neutron Capture in 75 Elements, *Tech. Rep., Gulf Energy And Environmental Systems INC San Diego CA*, 1970.
- [15] J. Boulter, W. Prestwich, Lifetimes of the 26 and 110 keV levels in ^{56}Mn , *Can. J. Phys.* 49 (23) (1971) 2911–2916.
- [16] P. Van Assche, H. Baader, H. Koch, B. Maier, U. Gruber, O. Schult, J. McGrory, J. Comfort, R. Rimawi, R. Chrien, et al., Energy levels of ^{56}Mn , *Nucl. Phys. A* 160 (2) (1971) 367–384.
- [17] F. Stecher-Rasmussen, K. Abrahams, J. Kopecky, W. Ratynski, Circular polarization of neutron-capture gamma-rays from Mn, Ni, Ga and W, *Nucl. Phys. A* 1 (1972) 250.
- [18] H. Börner, O. Schult, Resonance neutron capture in ^{55}Mn and levels in ^{56}Mn , *Z. Naturforsch. A* 29 (3) (1974) 385–388.
- [19] A. Colenbrander, T. Kennett, An investigation of the reaction $^{55}\text{Mn}(n, \gamma)^{56}\text{Mn}$, *Can. J. Phys.* 53 (3) (1975) 236–250.
- [20] P. Delheij, K. Abrahams, W. Huiskamp, H. Postma, The $^{55}\text{Mn}(n, \gamma)^{56}\text{Mn}$ reaction studied with polarized neutrons and polarized manganese nuclei, *Nucl. Phys. A* 341 (1) (1980) 45–55.
- [21] M. Islam, T. Kennett, S. Kerr, W. Prestwich, A self-consistent set of neutron separation energies, *Can. J. Phys.* 58 (2) (1980) 168–173.
- [22] S. Mughabghab, *Neutron Cross Sections: Neutron Resonance Parameters and Thermal Cross Sections, Part A: Z=1-60, vol. 1*, Elsevier, 2012.
- [23] R. Macklin, Resonance neutron capture by manganese below 2.5 keV, *Nucl. Sci. Eng.* 89 (4) (1985) 362–365.

- [24] A. Wapstra, G. Audi, The 1983 atomic mass evaluation: (i). atomic mass table, Nucl. Phys. A 432 (1) (1985) 1–54.
- [25] B. Dropesky, A. Schardt, T. Shull, Note on the decay of the new nuclide Cr-56, Nucl. Phys. 16 (2) (1960) 357–359.
- [26] A.M. Nathan, J.W. Olness, E.K. Warburton, J.B. McGrory, Yrast decay schemes from heavy ion + ^{48}Ca fusion-evaporation reactions. i. $^{54-56}\text{Mn}$, ^{56}Cr , and $^{52-53}\text{V}$, Phys. Rev. C 16 (1977) 192–214, <https://doi.org/10.1103/PhysRevC.16.192>.
- [27] T. Caldwell, D. Pullen, T. Mulligan, O. Hansen, (tau, p) reactions on Cr. ii. ^{54}Cr (tau, p), ^{56}Mn , Tech. Rep., Univ. of Pennsylvania, Philadelphia, 1971.
- [28] U. Fister, R. Jahn, P. von Neumann-Cosel, P. Schenk, T. Trelle, D. Wenzel, U. Wienands, Stretched proton-neutron configurations in fp-shell nuclei:(i). experimental results of the (α , d) reaction, Nucl. Phys. A 569 (3) (1994) 421–440.
- [29] J. Green, A. Smith, W. Buechner, M. Mazari, Excited states in Mn 56, Phys. Rev. 108 (3) (1957) 841.
- [30] J. Bjerregaard, P. Dahl, O. Hansen, G. Sidenius, Energy levels from (p, p'), (d, p) and (d, α) reactions on the stable isotopes between Sc-45 and Ni-58, Nucl. Phys. 51 (1964) 641–666.
- [31] J.R. Comfort, Nuclear structure of manganese-56, Phys. Rev. 177 (4) (1969) 1573.
- [32] A. Garcia, A. Lopez, F. Senent, The ^{55}Mn (d, p) ^{56}Mn reaction, An. Fis. 67 (1971) 181.
- [33] D.F. Measday, T.J. Stocki, γ rays from muon capture in natural Ca, Fe, and Ni, Phys. Rev. C 73 (4) (2006) 045501.
- [34] F. Ajzenberg-Selove, R.E. Brown, E.R. Flynn, J.W. Sunier, (t, ^3He) reactions on ^{56}Fe , ^{58}Fe , and ^{58}Ni , Phys. Rev. C 31 (1985) 777–786, <https://doi.org/10.1103/PhysRevC.31.777>.
- [35] N. Anantaraman, S.M. Austin, J. Winfield, Heavy ion reactions as probes for spin strength, Nucl. Phys. A 482 (1–2) (1988) 331–342.
- [36] S. Albergo, S. Costa, R. Potenza, J. Romanski, C. Tuvé, L. Jarczyk, B. Kamys, A. Magiera, A. Strzalkowski, R. Barna, V. D'Amico, D. De Pasquale, G. Mannino, Elastic transfer in the $^{11}\text{B}+^{12}\text{C}$ system in the c.m. energy range 5–40 MeV, Phys. Rev. C 43 (1991) 2704–2710, <https://doi.org/10.1103/PhysRevC.43.2704>.
- [37] H. Kelleter, D. Bachner, B. Schmidt, W. Seliger, Level investigation by means of the (d, α) reaction (ii). ^{52}Mn and ^{56}Mn , Nucl. Phys. A 183 (3) (1972) 509–522.
- [38] H. Junde, H. Su, Y. Dong, Nuclear data sheets for A=56, Nucl. Data Sheets 112 (6) (2011) 1513–1645.
- [39] V. Khitrov, A. Sukhovoij, New technique for a simultaneous estimation of the level density and radiative strength functions of dipole transitions at $E_{ex} < B_n - 0.5$ MeV, arXiv preprint, arXiv:nucl-ex/0110017.
- [40] A. Sukhovoij, L. Mitsyna, N. Jovancevic, Overall picture of the cascade gamma decay of neutron resonances within a modified practical model, Phys. At. Nucl. 79 (3) (2016) 313–325.
- [41] D. Vu, A. Sukhovoij, L. Mitsyna, S. Zeinalov, N. Jovancevic, D. Knezevic, M. Krmar, A. Dragic, Representation of radiative strength functions within a practical model of cascade gamma decay, Phys. At. Nucl. 80 (2) (2017) 237–250.
- [42] A. Sukhovoij, New model of the cascade gamma decay of neutron resonances for practitioners: basic concepts and attainable precision, Phys. At. Nucl. 78 (2) (2015) 230–245.
- [43] A.M. Sukhovoij, L.V. Mitsyna, The next-generation practical model of the cascade gamma-decay of neutron resonance and expected parameters for an arbitrary nucleus, in: Proceedings, 22nd International Seminar on Interaction of Neutrons with Nuclei: Fundamental Interactions and Neutrons, Nuclear Structure, Ultracold Neutrons, Related Topics (ISINN 22), Dubna, Russia, May 27–30, 2014, 2015.
- [44] S. Boneva, V. Khitrov, A. Sukhovoij, A. Vojnov, Excitation study of high-lying states of differently shaped heavy nuclei by the method of two-step cascades, Nucl. Phys. A 589 (2) (1995) 293–306.
- [45] Z. Revay, PGAA: Prompt gamma and in-beam neutron activation analysis facility, J. Large-Scale Res. Fac. JLSRF 1 (2015) 20.
- [46] Z. Révay, P. Kudějová, K. Kleszcz, S. Söllradl, C. Genreith, In-beam activation analysis facility at MLZ, Garching, Nucl. Instrum. Methods Phys. Res., Sect. A, Accel. Spectrom. Detect. Assoc. Equip. 799 (2015) 114–123.
- [47] B. Krusche, K. Lieb, H. Daniel, T. Von Egidy, G. Barreau, H. Börner, R. Brissot, C. Hofmeyr, R. Rascher, Gamma ray energies and ^{36}Cl level scheme from the reaction $^{35}\text{Cl}(n, \gamma)$, Nucl. Phys. A 386 (2) (1982) 245–268.

Study of gamma transitions and level scheme of ^{94}Nb using the $^{93}\text{Nb}(n_{th}, 2\gamma)$ reaction

David Knezevic^{a,b,*}, Nikola Jovancevic^b, Anatoly M. Sukhovoij^c, Aleksandar Dragic^a, Liudmila V. Mitsyna^c, László Szentmiklósi^d, Tamás Belgya^d, Stephan Oberstedt^e, Miodrag Krmar^b, Ilija Arsenic^f, Vu D. Cong^{c,g}

^a University of Belgrade, Institute of Physics Belgrade, Pregrevica 118, 11080 Zemun, Serbia

^b University of Novi Sad, Faculty of Science, Department of Physics, Trg Dositeja Obradovica 3, 21000 Novi Sad, Serbia

^c Joint Institute for Nuclear Research, 141980 Moscow region, Dubna, Russia

^d Centre for Energy Research, Hungarian Academy of Sciences, Budapest, Hungary

^e European Commission, Joint Research Centre, Directorate G – Nuclear Safety and Security, Unit G.2, Retieseweg 111, B-2440 Geel, Belgium

^f University of Novi Sad, Faculty of Agriculture, Trg Dositeja Obradovica 8, 21000 Novi Sad, Serbia

^g Vietnam Academy of Science and Technology, Institute of Physics, Hanoi, Viet Nam

Received 21 February 2019; received in revised form 18 March 2019; accepted 9 April 2019

Available online 17 October 2019

Abstract

In this paper, we present new spectroscopic information on ^{94}Nb from the $^{93}\text{Nb}(n_{th}, 2\gamma)$ reaction. The intensities of the two-step gamma cascades in the compound nucleus ^{94}Nb to the final levels, with excitation energies below 400 keV, were derived from experimental spectra recorded at the PGAA facility of Centre for Energy Research (MTA EK), Budapest, Hungary. The intensities, energies of primary and secondary transitions of 216 energy-resolved cascades as well as intermediate cascade levels were determined. The part of the level scheme of ^{94}Nb was obtained from analyzing the intensity spectra of the strongest cascades. The results were compared to the existing data in the ENSDF database. We concluded that 27 primary transitions, 29 intermediate cascades levels as well as 183 secondary transitions can be recommended as new nuclear data.

* Corresponding author at: University of Belgrade, Institute of Physics Belgrade, Pregrevica 118, 11080 Zemun, Serbia.
E-mail address: davidk@ipb.ac.rs (D. Knezevic).

© 2019 Elsevier B.V. All rights reserved.

Keywords: Gamma spectrometry; Thermal neutron capture; Level scheme; Gamma cascades

1. Introduction

Knowledge of the nuclear level scheme plays an important role in the understanding of the nuclear properties. In this work, the niobium nucleus (^{94}Nb) was chosen for a study, because it has been already applied in the nuclear technology and, due to niobium's high temperature resistance and relatively low cross section for a capture of thermal neutrons, it is expected to be increasingly utilized in innovative nuclear reactors. New accurate spectroscopic data on ^{94}Nb , as it is an odd-odd nucleus, can also be interesting from a theoretical point of view, for studying the level density and the radiative strength function [1–5].

The properties of ^{94}Nb nucleus have been studied using different methods, such as IT decay of ^{94}Nb [6–14], $^{93}\text{Nb}(^{16}\text{O}, ^{15}\text{O})$, $^{82}\text{Se}(^{19}\text{F}, 3n\alpha\gamma)$ and $^{92}\text{Zr}(\alpha, d)$ reactions for high-spin states [1,15,16], stripping reaction $^{93}\text{Nb}(d, p)$ [17–20], $^{93}\text{Nb}(p, n\gamma)$ reaction using protons of various energies [21–26], reactions with resonance capture of neutrons [27–31] as well as thermal neutron capture [2,18,27,31,32]. The latter reaction was used in this paper, too.

One of the most suitable techniques for determining the required nuclear parameters is the two-step gamma-cascade method based on measurements of coincident prompt gamma-rays following thermal neutron capture [33–36]. The objective of this experiment was the detection of two-step gamma cascades following thermal neutron captures on ^{93}Nb nuclei, $^{93}\text{Nb}(n_{th}, 2\gamma)^{94}\text{Nb}$. Niobium lies in the region of atomic masses suitable for a study by two-step gamma-cascades method, but is yet unexplored by it. For mono-isotopic niobium (^{93}Nb), the data analysis is simplified and, moreover, preparation of a high-purity target for the experiment is considerably easier. An advantage of the two-step gamma-cascades technique is a low Compton background in obtained spectra owing to usage of the background-subtraction algorithm [33]. The background in the two-step-cascade (TSC) spectra of mono-isotopic niobium is practically absent.

In this paper, we present new spectroscopic information for the ^{94}Nb nucleus (levels, gamma transitions and their intensities per capture) and compare the results with the existing ENSDF data [37]. As the two-step gamma-cascades method provides the possibility to estimate simultaneously the nuclear level density and radiative strength functions, in a future work, these nuclear parameters may be obtained for the ^{94}Nb as well [38–43].

2. Experimental setup and measurement

The experiment was carried out at the PGAA station of MTA EK in Budapest, Hungary [44,45]. The niobium target, with purity of 99.9%, a mass of 10.82 g and $25 \times 25 \times 2 \text{ mm}^3$ was used. The target was mounted at the plane orthogonal to the beam line. Two HPGe detectors, with relative efficiencies of 23% and 27%, were used. The detectors were placed one next to the other, facing the target. Each detector was put at an $\pm 11.6^\circ$ angle relative to the axis normal to the beam line, which passed through the target, as depicted in Fig. 1. The detectors were at 7.5 cm distance from the center of niobium target. Close geometry was used in order to record as many coincident events as possible. Both detectors were shielded from background gamma radiation

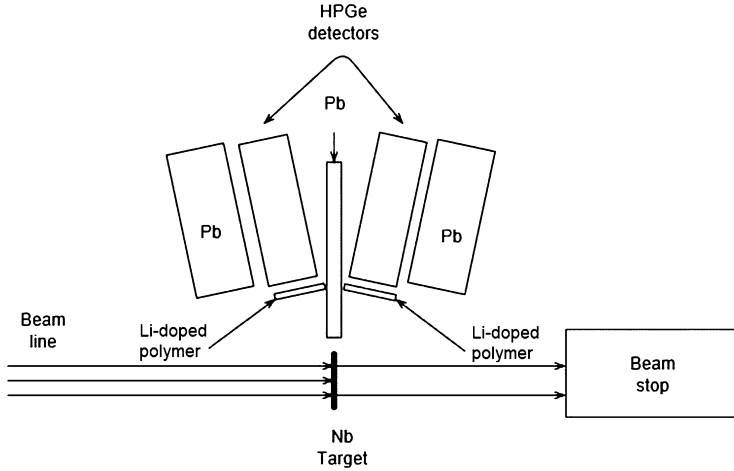


Fig. 1. Experimental setup for two-step gamma cascades measurement at the PGAA station of MTA EK, Budapest, Hungary.

with lead, and from neutrons with a 2 mm thick ^6Li doped polymer layer that was placed in front of the detector caps.

Experimental data were collected with a 4 channel CAEN N6724 digitizer [46]. The digitizer collected information on the energy and time of the gamma-coincidence events from both HPGe detectors, and stored it in list mode for offline analysis. The relative efficiency of the detectors was determined from single gamma-ray spectra accumulated using a PVC target (the $^{35}\text{Cl}(n,\gamma)^{36}\text{Cl}$ reaction) [47]. Niobium two-gamma events were recorded for 506 ks.

3. Result and discussion

The detailed procedures to extract the cascade events and intensities were described in Ref. [33], therefore, only a short description of the applied procedure will be presented here.

Fig. 2 shows the most important part of the spectrum of sums of amplitudes for coincident pulses (SACP). The coincidence time window was 40 ns. The seven marked peaks in Fig. 2 present the two-step cascade peaks of ^{94}Nb for transitions from the neutron binding energy (7227.0(5) keV) to the ground state and to the first six excited states with the energies 40.9, 58.7, 113.4, 140.3, 311.8 and 396.2 keV. Core information about these seven peaks is presented in Table 1.

The remaining unmarked peaks in SACP spectrum correspond to background events (Fig. 2). They may come from recording of coincidences of the first with the third or fourth quantum of the multiple-step gamma cascades or from neutron interaction with surrounding materials.

The next step was to obtain two-step-cascade (TSC) spectra for seven energy-resolved amplitude peaks. The obtained TSC spectra represent the cascades from the initial state to the defined final levels of the ^{94}Nb nucleus. The elimination of Compton background and random coincidences was done by gating on the region nearby the peaks of interest in Fig. 2. Figs. 3 and 4 show the examples of the obtained TSC spectra for cascade sum energies of 7087 and 7169 keV.

The mirror-symmetrical peaks [34] in the TSC spectra represent primary and secondary transitions of the investigated two-step gamma cascade. The peaks' positions correspond to the

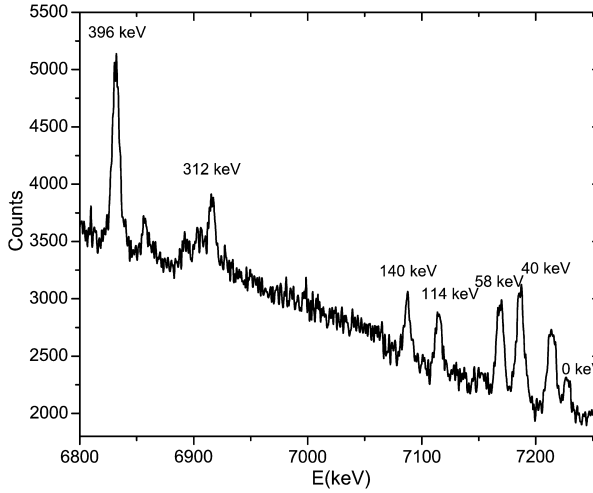


Fig. 2. Spectrum of sums of amplitudes for coincident pulses (SACP) at the radiative capture of thermal neutrons in ^{93}Nb nucleus. Peaks of the full capture of two quanta are labeled by energy of the final level of the resolved cascades.

Table 1

Information about the two-step cascades to the ground state and the first six excited states collected in the experiment.

Gamma cascade total energy (keV)	Final level (E_f) of the cascade (keV)	Spin of level E_f	Part of resolved cascade intensity	Full intensities % per decay
7227	0	6+	0.25(2)	5.4(20)
7186	40.9	3+	0.71(2)	6.2(15)
7169	58.7	(4)+	0.60(1)	7.0(11)
7114	113.4	(5)+	0.42(2)	5.3(15)
7087	140.3	(2)-	0.84(1)	2.7(9)
6916	311.8	(4,5)+	0.57(3)	3.2(10)
6831	396.2	(3)-	0.51(3)	5.4(11)
Sum of total			0.56(2)	35.2(40)

energies, E_1 and E_2 , of primary and secondary quanta of the cascades. The relative intensity of each peak is proportional to its area. The intensities of 216 resolved cascades are determined from seven TSC distributions. In all investigated cascades, primary transitions (except for 26 of them) have the higher energy in comparison with the energy of secondary quanta. Details of the method and the maximum likelihood function used to determine the energies of primary and secondary cascade transitions were presented in [36]. All detected primary and secondary gamma transitions and their intensities as well as the energy of intermediate levels are presented in Table 2.

In order to compare the data of the cascade spectra (Figs. 3 and 4) with the library data for strongest primary transitions with $E_1=5997.0, 5898.0, 5591.6, 5496.5, 5369.7, 5364.9, 5103.5$ and 5070.4 keV, the branching coefficients of their secondary transitions I_2 were obtained independently, from ENSDF database, which gave data of absolute intensity of the cascades for normalization of the data from Table 2. The values of the total intensity of two-step gamma cascades, $I_{\gamma\gamma}$, obtained in such a way (Table 1), which include both the resolved cascades and

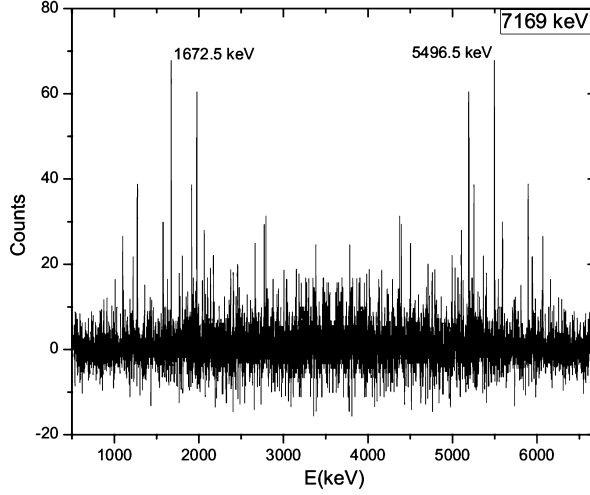


Fig. 3. TSC spectrum with the total energy of 7169 keV. The final level of the cascade is 58.708(10) keV. This spectrum represents the TSC spectrum with high number of cascades (36 pairs of gammas). The energies of the most intense pair of gammas are labeled.

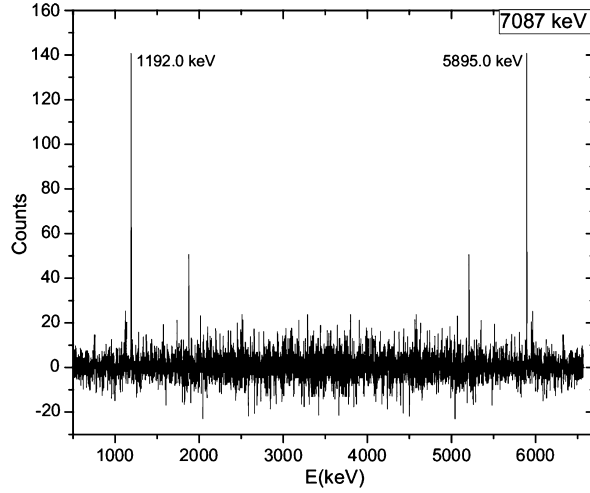


Fig. 4. TSC spectrum with the total energy of 7087 keV. The final level of the cascade is 140.298(12) keV. This spectrum represents the TSC spectrum with low number of cascades (18 pairs of gammas). The energies of the most intense pair of gammas are labeled.

unresolved cascade continuum with sub-threshold intensity, show that, for the investigated nucleus, we have obtained in this experiment 35% of total intensity of all two-step cascades. 56% of the obtained intensity $I_{\gamma\gamma}$ falls to the share of the energy-resolved cascades (Table 2).

The data was compared with the existing data from the ENSDF database [37]. From this comparison 107 primary transitions that existed in the ENSDF data set were determined. 27 primary transitions, which are not included in the ENSDF library, can be therefore considered as new data. 104 intermediate levels are identified in our experiment and already listed in the

Table 2

Comparison of the experimental data with the ENSDF database. E_1 and E_2 are the energies of the first and second quanta of the cascade, respectively, E_i is the energy of the intermediate level and E_f are the final levels of the two step gamma cascade. $I_{\gamma\gamma}$ is the intensity of the cascade (per 100 decays) observed in the experiment. The experimental uncertainty of E_2 has the same values as for E_1 (listed in the table). Values in bold are values for which there is no data in the ENSDF library.

Present work				ENSDF			
E_1 (keV)	E_2 (keV)	E_i (keV)	$I_{\gamma\gamma}$	E_f (keV)	E_1 (keV)	E_2 (keV)	E_i (keV)
6917.90(19)	251.1	309.10(21)	0.32(15)	58.708(10)	6915.73(4)	253.115(5)	311.821(10)
6835.00(15)	334.1	392.10(17)	0.26(24)	58.708(10)	6831.18(4)	337.529(8)	396.227(12)
6835.00(9)	279.1	392.1(9)	0.098(24)	113.4009(8)	6831.18(4)	–	396.227(12)
6833.9(5)	253.1	393.1(5)	2.1(3)	140.298(12)	6831.18(4)	253.113(5)	396.227(12)
6435.3(7)	751.7	791.7(7)	0.08(4)	40.892(12)	6434.78(6)	751.78(7)	792.595(16)
6410.9(10)	776.1	816.1(10)	0.05(4)	40.892(12)	6410.64(14)	775.99(6)	816.83(3)
6332.0(14)	755.0	895.0(14)	0.06(4)	140.298(12)	6331.74(7)	755.28(7)	895.650(14)
6332.0(6)	499.0	895.0(6)	0.36(14)	396.227(12)	6331.74(7)	499.426(8)	895.650(14)
6292.7(5)	894.3	934.3(5)	0.26(8)	40.892(12)	6292.19(7)	894.24(5)	936.036(20)
6271.8(6)	955.2	955.3(6)	0.11(4)	g.s.	6270.57(11)	957.34(5)	957.34(5)
6246.3(8)	867.7	980.7(8)	0.038(20)	113.4009(8)	–	–	979.29(18)
6187.3(10)	1039.7	1039.7(10)	0.050(27)	g.s.	–	–	–
6188.8(11)	642.2	1038.2(11)	0.07(5)	396.227(12)	–	–	–
6160.0(19)	954.1	1067.1(19)	0.016(11)	113.4009(8)	–	–	–
6136.0(10)	695.0	1091.0(10)	0.12(8)	396.227(12)	–	–	–
6068.9(5)	1118.1	1158.1(5)	0.14(5)	40.892(12)	6068.44(8)	1118.00(25)	1158.71(4)
6068.9(4)	1100.1	1158.1(4)	0.13(6)	58.708(10)	6068.44(8)	1100.11(15)	1158.71(4)
6058.1(7)	1055.9	1168.9(7)	0.047(23)	113.4009(8)	6058.16(9)	1056.39(15)	1169.88(6)
6050.9(10)	1176.1	1176.1(10)	0.05(3)	g.s.	–	1179.61(6)	1179.61(6)
6029.6(10)	1197.4	1197.4(10)	0.044(28)	g.s.	–	–	–
5997.0(7)	834.0	1230.0(7)	0.32(13)	396.227(12)	5995.67(9)	835.72(3)	1231.92(3)
5981.1(9)	1187.9	1245.9(9)	0.057(26)	58.708(10)	5980.20(9)	1188.3(4)	1247.26(7)
5964.3(5)	1122.7	1262.7(5)	0.17(5)	140.298(12)	5964.34(8)	1122.65(25)	1262.82(7)
5964.3(13)	866.7	1262.7(13)	0.068(27)	396.227(12)	5964.34(8)	–	1262.82(7)
5952.8(6)	1161.2	1274.0(6)	0.07(3)	113.4009(8)	5952.94(10)	1160.0(5)	1272.83(4)
5952.8(6)	878.2	1274.0(6)	0.12(8)	396.227(12)	5952.94(10)	879.75(14)	1272.83(4)
5945.3(7)	1281.7	1281.7(7)	0.11(4)	g.s.	5946.33(9)	1281.44(11)	1281.44(11)
5945.3(7)	1223.7	1281.7(7)	0.10(4)	58.708(10)	5946.33(9)	1222.98(12)	1281.44(11)
5895.00(25)	1292.0	1332.00(26)	0.38(8)	40.892(12)	5894.93(8)	1291.3(5)	1332.6(3)
5895.0(4)	1274.0	1332.0(4)	0.25(6)	58.708(10)	5894.93(8)	1273.4(5)	1332.6(3)
5895.0(9)	1219.0	1332.0(9)	0.049(24)	113.4009(8)	5894.93(8)	1220.1(5)	1332.6(3)
5895.00(21)	1192.0	1332.00(22)	0.83(11)	140.298(12)	5894.93(8)	1192.2(5)	1332.6(3)
5835.1(4)	1391.9	1391.9(4)	0.17(6)	g.s.	5834.74(11)	–	1392.73(12)
5819.9(11)	1294.1	1407.0(11)	0.028(16)	113.4009(8)	–	–	1405.0(10)
5808.6(9)	1305.4	1418.4(9)	0.058(27)	113.4009(8)	–	1304.8(5)	–
5808.6(10)	1022.4	1418.4(10)	0.13(9)	396.227(12)	–	–	–
5770.7(11)	1060.3	1456.3(11)	0.15(9)	396.227(12)	5769.77(9)	1061.45(11)	1458.12
5730.4(9)	1100.6	1496.6(9)	0.09(6)	396.227(12)	5727.98(11)	–	1499.92
5708.3(8)	1460.7	1518.7(8)	0.063(24)	58.708(10)	5708.73(11)	1459.6(14)	1519.0(10)

Table 2 (continued)

Present work				ENSDF			
E_1 (keV)	E_2 (keV)	E_i (keV)	$I_{\gamma\gamma}$	E_f (keV)	E_1 (keV)	E_2 (keV)	E_i (keV)
5708.3(9)	1405.7	1518.7(9)	0.056(28)	113.4009(8)	5708.73(11)	–	1519.0(10)
5647.4(8)	1439.6	1579.6(8)	0.038(21)	140.298(12)	5645.94(11)	–	1581.95(14)
5647.4(8)	1183.6	1579.6(8)	0.14(8)	396.227(12)	5645.94(11)	1185.1(3)	1581.95(14)
5617.0(7)	1552.0	1610.0(7)	0.059(22)	58.708(10)	–	–	1609.6(12)
5614.2(6)	1216.8	1612.8(6)	0.14(6)	396.227(12)	5612.72(11)	–	–
5607.6(7)	1307.4	1619.4(7)	0.09(4)	311.821(10)	5607(30)	1304.8(5)	1620.6(4)
5591.6(4)	1577.4	1635.4(4)	0.15(4)	58.708(10)	5591.32(10)	–	1636.14(11)
5591.6(6)	1239.4	1635.4(6)	0.29(12)	396.227(12)	5591.32(10)	1239.38(25)	1636.14(11)
5572.5(7)	1654.5	1654.5(7)	0.08(4)	g.s.	5572.33(11)	–	1655.09(17)
5572.5(7)	1541.5	1654.5(7)	0.08(4)	113.4009(8)	5572.33(11)	–	1655.09(17)
5511.6(6)	1575.4	1715.4(6)	0.09(3)	140.298(12)	5511.28(11)	–	1716.66(19)
5508.3(8)	1678.7	1718.7(8)	0.07(4)	40.892(12)	5507.80(11)	–	1720.1(3)
5496.50(27)	1672.5	1730.50(28)	0.39(6)	58.708(10)	5496.15(10)	–	1731.4(13)
5496.5(6)	1590.5	1730.5(6)	0.065(28)	140.298(12)	5496.15(10)	–	1731.4(13)
5496.5(4)	1418.5	1730.5(4)	0.23(6)	311.821(10)	5496.15(10)	1419.6(13)	1731.4(13)
5496.5(5)	1334.5	1730.5(5)	0.47(16)	396.227(12)	5496.15(10)	1334.6(5)	1731.4(13)
5453.3(10)	1461.7	1773.7(10)	0.052(29)	311.821(10)	5450.98(11)	1459.6(14)	1776.92(14)
5448.3(7)	1778.7	1778.7(7)	0.12(5)	g.s.	5447.18(13)	–	1779.72(5)
5448.3(16)	1466.7	1778.7(16)	0.029(21)	311.821(10)	5447.18(13)	–	1779.72(5)
5448.3(10)	1382.7	1778.7(10)	0.08(3)	396.227(12)	5447.18(13)	–	1779.72(5)
5414.2(9)	1772.8	1812(9)	0.06(3)	40.892(12)	5412.20(15)	–	1815.75(18)
5407.8(12)	1779.2	1819.2(12)	0.038(24)	40.892(12)	5406.92(18)	–	1821.2(7)
5369.7(9)	1545.3	1857.3(9)	0.08(4)	311.821(10)	5368.98(11)	–	1859.75(11)
5364.9(6)	1822.1	1862.1(6)	0.10(4)	40.892(12)	5363.80(11)	–	1864.13(14)
5364.9(5)	1804.1	1862.1(5)	0.12(4)	58.708(10)	5363.80(11)	–	1864.13(14)
5364.9(8)	1749.1	1862.1(8)	0.08(4)	113.4009(8)	5363.80(11)	–	1864.13(14)
5364.9(7)	1550.1	1862.1(7)	0.14(5)	311.821(10)	5363.80(11)	–	1864.13(14)
5364.9(9)	1466.1	1862.1(9)	0.10(10)	396.227(12)	5363.80(11)	–	1864.13(14)
5349.0(8)	1820.0	1878.0(8)	0.045(20)	58.708(10)	5348.56(11)	–	1879.35(14)
5349.0(8)	1738.0	1878.0(8)	0.13(5)	140.298(12)	5348.56(11)	–	1879.35(14)
5309.8(8)	1877.2	1917.2(8)	0.13(5)	40.892(12)	–	–	–
5307.3(8)	1523.7	1919.7(8)	0.11(6)	396.227(12)	5307.93(11)	–	1920.0(4)
5304.9(14)	1882.1	1922.1(14)	0.06(4)	40.892(12)	–	–	–
5300.5(10)	1886.5	1926.5(10)	0.080(28)	40.892(12)	5301.22(12)	–	1926.8(4)
5300.5(7)	1813.5	1926.5(7)	0.11(4)	113.4009(8)	5301.22(12)	–	1926.8(4)
5300.5(7)	1614.5	1926.5(7)	0.08(4)	311.821(10)	5301.22(12)	–	1926.8(4)
5284.0(6)	1885.0	1943.0(6)	0.041(19)	58.708(10)	5284.14(12)	–	1943.76(23)
5278.5(9)	1636.5	1948.5(9)	0.046(24)	311.821(10)	5277.43(19)	–	1950.4(3)
5270.4(9)	1916.6	1956.6(9)	0.044(25)	40.892(12)	5271.19(20)	–	1956.73(22)
5270.4(6)	1843.6	1956.6(6)	0.058(28)	113.4009(8)	5271.19(20)	–	1956.73(22)
5270.4(12)	1816.6	1956.6(12)	0.08(5)	140.298(12)	5271.19(20)	–	1956.73(22)
5270.4(6)	1644.6	1956.6(6)	0.08(5)	311.821(10)	5271.19(20)	–	1956.73(22)
5253.2(3)	1915.8	1973.8(3)	0.20(5)	58.708(10)	5252.51(12)	–	1975.5(4)
5212.8(6)	1702.2	2014.2(6)	0.059(26)	311.821(10)	5213.76(15)	–	2014.19(20)

(continued on next page)

Table 2 (continued)

Present work				ENSDF			
E_1 (keV)	E_2 (keV)	E_i (keV)	$I_{\gamma\gamma}$	E_f (keV)	E_1 (keV)	E_2 (keV)	E_i (keV)
5207.6(5)	1879.4	2019.4(5)	0.30(10)	140.298(12)	5207.94(12)	–	2020.0(3)
5206.8(12)	1623.4	2019.4(12)	0.05(3)	396.227(12)	5207.94(12)	–	2020.0(3)
5193.7(9)	2033.3	2033.3(9)	0.07(4)	g.s.	5193.37(12)	–	2033.6(3)
5193.7(9)	1975.3	2033.3(9)	0.36(7)	58.708(10)	5193.37(12)	–	2033.6(3)
5193.7(9)	1920.3	2033.3(9)	0.25(7)	113.4009(8)	5193.37(12)	–	2033.6(3)
5193.7(9)	1721.3	2033.3(9)	0.30(7)	311.821(10)	5193.37(12)	–	2033.6(3)
5179.9(10)	2007.1	2047.1(10)	0.042(22)	40.892(12)	5179.99(12)	–	2047.94(15)
5179.9(11)	1907.1	2047.1(11)	0.09(5)	140.298(12)	5179.99(12)	–	2047.94(15)
5179.9(7)	1651.1	2047.1(7)	0.13(5)	396.227(12)	5179.99(12)	–	2047.94(15)
5131.0(10)	1983.0	2096.0(10)	0.052(29)	113.4009(8)	5129.15(13)	–	2098.78(16)
5120.7(8)	1993.3	2106.3(8)	0.07(3)	113.4009(8)	–	–	–
5104.1(7)	2122.9	2122.9(7)	0.08(3)	g.s.	5103.33(12)	–	2124.62(15)
5104.1(6)	2082.9	2122.9(6)	0.12(4)	40.892(12)	5103.33(12)	–	2124.62(15)
5104.1(4)	2064.9	2122.9(4)	0.14(4)	58.708(10)	5103.33(12)	–	2124.62(15)
5104.1(8)	2009.9	2122.9(8)	0.12(5)	113.4009(8)	5103.33(12)	–	2124.62(15)
5104.1(7)	1726.9	2122.9(7)	0.29(13)	396.227(12)	5103.33(12)	–	2124.62(15)
5071.1(8)	2015.9	2155.9(8)	0.08(5)	140.298(12)	5070.26(12)	–	2157.67(15)
5071.1(4)	1759.9	2155.9(4)	0.26(10)	396.227(12)	5070.26(12)	–	2157.67(15)
5066.8(9)	2047.2	2160.2(9)	0.06(3)	113.4009(8)	5065.65(13)	–	2162.28(16)
5058.3(10)	2128.7	2168.7(10)	0.040(25)	40.892(12)	5059.7(3)	–	2168.2(3)
5053.8(7)	2173.2	2173.2(7)	0.11(4)	g.s.	5052.88(15)	–	2175.4(24)
5053.8(10)	2115.2	2173.2(10)	0.040(25)	58.708(10)	5052.88(15)	–	2175.4(24)
5031.8(10)	2195.2	2195.2(10)	0.07(3)	g.s.	5032.07(13)	–	2195.86(16)
5031.8(5)	2155.2	2195.2(5)	0.068(29)	40.892(12)	5032.07(13)	–	2195.86(16)
5031.8(6)	2137.2	2195.2(6)	0.13(4)	58.708(10)	5032.07(13)	–	2195.86(16)
5031.8(11)	1883.2	2195.2(11)	0.038(26)	311.821(10)	5032.07(13)	–	2195.86(16)
5019.4(10)	2167.6	2207.6(10)	0.040(22)	40.892(12)	5020.9(3)	–	2207.0(3)
5008.4(9)	2178.6	2218.6(9)	0.07(3)	40.892(12)	5006.76(22)	–	2221.16(24)
4998.3(6)	2228.7	2228.7(6)	0.14(5)	g.s.	4997.96(14)	–	2229.98(17)
4984.0(6)	2103.0	2243.0(6)	0.058(28)	140.298(12)	4982.50(13)	–	2245.3(5)
4984.0(5)	1847.0	2243.0(5)	0.13(6)	396.227(12)	4982.50(13)	–	2245.3(5)
4947.7(9)	2221.3	2279.3(9)	0.041(21)	58.708(10)	4949.72(17)	–	2278.5(7)
4890.0(12)	1941.0	2337.0(12)	0.05(3)	396.227(12)	4891.2(9)	–	2336.7(7)
4886.4(6)	2200.6	2340.6(6)	0.057(26)	140.298(12)	–	–	–
4861.6(13)	2325.4	2365.4(13)	0.05(3)	40.892(12)	4864.40(19)	–	2363.54(21)
4833.0(10)	1998.0	2394.0(10)	0.09(5)	396.227(12)	4834.8(4)	–	2393.1(4)
4827.8(10)	2341.2	2399.2(10)	0.06(3)	58.708(10)	4827.62(14)	–	2398.6(15)
4827.8(6)	2286.2	2399.2(6)	0.10(4)	113.4009(8)	4827.62(14)	–	2398.6(15)
4791.8(10)	2435.2	2435.2(10)	0.06(4)	g.s.	4791.59(14)	–	2436.5(5)
4791.8(6)	2395.2	2435.2(6)	0.15(5)	40.892(12)	4791.59(14)	–	2436.5(5)
4791.8(7)	2377.2	2435.2(7)	0.09(4)	58.708(10)	4791.59(14)	–	2436.5(5)
4760.6(14)	2426.4	2466.4(14)	0.046(29)	40.892(12)	–	–	–
4760.6(14)	2408.4	2466.4(14)	0.041(28)	58.708(10)	–	–	–
4760.6(8)	2353.4	2466.4(8)	0.051(26)	113.4009(8)	–	–	–

Table 2 (continued)

Present work				ENSDF			
E_1 (keV)	E_2 (keV)	E_i (keV)	$I_{\gamma\gamma}$	E_f (keV)	E_1 (keV)	E_2 (keV)	E_i (keV)
4760.6(9)	2070.4	2466.4(9)	0.08(3)	396.227(12)	—	—	—
4756.2(10)	2430.8	2470.8(10)	0.06(3)	40.892(12)	4756.27(15)	—	2471.68(17)
4734.7(11)	2352.3	2492.3(11)	0.048(29)	140.298(12)	—	—	—
4711.9(9)	2457.1	2515.1(9)	0.05(4)	58.708(10)	4711.62(14)	—	2516.38(18)
4711.9(6)	2203.1	2515.1(6)	0.17(5)	311.821(10)	4711.62(14)	—	2516.38(18)
4700.1(10)	2486.9	2526.9(10)	0.06(3)	40.892(12)	4699.7(4)	—	2528.3(4)
4691.5(9)	2495.5	2535.5(9)	0.051(27)	40.892(12)	4691.1(4)	—	2537.3(7)
4691.5(13)	2477.5	2535.5(13)	0.046(29)	58.708(12)	4691.1(4)	—	2537.3(7)
4682.4(12)	2486.6	2544.6(12)	0.037(23)	58.708(12)	4681.96(15)	—	2545.93(25)
4682.4(6)	2431.6	2544.6(6)	0.11(4)	113.4009(8)	4681.96(15)	—	2545.93(25)
4682.4(7)	2232.6	2544.6(7)	0.11(4)	311.821(10)	4681.96(15)	—	2545.93(25)
4674.5(9)	2512.5	2552.5(9)	0.07(4)	40.892(12)	4672.15(15)	—	2555.80(17)
4674.5(12)	2156.5	2552.5(12)	0.06(4)	396.227(12)	4672.15(15)	—	2555.80(17)
4660.8(7)	2526.2	2566.2(7)	0.07(3)	40.892(12)	4662.31(16)	—	2565.63(18)
4641.5(6)	2545.5	2585.5(6)	0.08(3)	40.892(12)	4642.2(4)	—	2585.8(4)
4635.8(18)	2591.2	2591.2(18)	0.04(5)	g.s.	4635.42(15)	—	2592.54(17)
4631.2(7)	2555.8	2595.8(7)	0.057(28)	40.892(12)	4629.89(15)	—	2598.07(17)
4631.2(8)	2537.8	2595.8(7)	0.08(3)	58.708(10)	4629.89(15)	—	2598.07(17)
4595.0(15)	2632.0	2632.0(15)	0.08(5)	g.s.	4594.44(15)	—	2633.52(17)
4595.0(10)	2592.0	2632.0(10)	0.06(3)	40.892(12)	4594.44(15)	—	2633.52(17)
4595.0(7)	2574.0	2632.0(7)	0.08(4)	58.708(10)	4594.44(15)	—	2633.52(17)
4595.0(8)	2519.0	2632.0(8)	0.07(3)	113.4009(8)	4594.44(15)	—	2633.52(17)
4560.4(11)	2626.6	2666.6(11)	0.04(8)	40.892(12)	4558.51(16)	—	2669.45(18)
4560.4(8)	2270.6	2666.6(8)	0.076(27)	396.227(12)	4558.51(16)	—	2669.45(18)
4557.0(10)	2612.0	2670.0(10)	0.045(24)	58.708(10)	4558.51(16)	—	2669.45(18)
4541.2(8)	2627.8	2685.8(8)	0.055(27)	58.708(10)	4543.2(3)	—	2685.0(4)
4512.7(8)	2714.3	2714.3(8)	0.13(6)	g.s.	—	—	—
4501.6(7)	2667.4	2725.4(7)	0.07(3)	58.708(10)	4501.41(16)	—	2726.55(18)
4428.0(7)	2799.0	2799.0(7)	0.10(5)	g.s.	—	—	—
4395.9(10)	2791.1	2831.1(10)	0.05(3)	40.892(12)	4395.05(16)	—	2832.91(18)
4395.9(11)	2773.1	2831.1(11)	0.041(26)	58.708(10)	4395.05(16)	—	2832.91(18)
4385.7(10)	2783.3	2841.3(10)	0.046(24)	58.708(10)	4384.25(18)	—	2843.73(20)
4385.7(9)	2728.3	2841.3(9)	0.07(3)	113.4009(8)	4384.25(18)	—	2843.73(20)
4363.2(9)	2823.8	2863.8(9)	0.042(25)	40.892(12)	—	—	—
4363.2(9)	2805.8	2863.8(9)	0.07(3)	58.708(12)	—	—	—
4330.9(10)	2896.1	2896.1(10)	0.08(5)	g.s.	4330.80(17)	—	2897.17(19)
4309.7(13)	2917.3	2917.3(13)	0.06(4)	g.s.	—	—	—
4304.4(11)	2922.6	2922.6(11)	0.06(4)	g.s.	4304.75(17)	—	2923.22(19)
4285.3(8)	2828.7	2941.7(8)	0.06(3)	113.4009(8)	4285.18(23)	—	2942.79(25)
4259.1(8)	2927.9	2967.9(8)	0.07(3)	40.892(12)	4260.77(17)	—	2967.3(6)
4259.1(8)	2827.9	2967.9(8)	0.10(5)	140.298(12)	4260.77(17)	—	2967.3(6)
4225.6(7)	2961.4	3001.4(7)	0.13(5)	40.892(12)	—	—	3003.6(8)
4225.6(9)	2888.4	3001.4(9)	0.06(3)	113.4009(8)	—	—	3003.6(8)
4217.3(8)	2969.7	3009.7(8)	0.058(26)	40.892(12)	4220.92(21)	—	3007.09(23)

(continued on next page)

Table 2 (continued)

Present work				ENSDF			
E_1 (keV)	E_2 (keV)	E_i (keV)	$I_{\gamma\gamma}$	E_f (keV)	E_1 (keV)	E_2 (keV)	E_i (keV)
4194.7(14)	3032.3	3032.3(14)	0.06(3)	g.s.	4196.67(18)	–	3031.21(20)
4194.7(7)	2992.3	3032.3(7)	0.07(3)	40.892(12)	4196.67(18)	–	3031.21(20)
4190.4(12)	2724.6	3036.6(12)	0.039(26)	311.821(10)	4191.04(20)	–	3036.8(3)
4154.1(8)	3032.9	3072.9(8)	0.10(4)	40.892(12)	4153.8(2)	–	3074.18(22)
4154.1(10)	2959.9	3072.9(10)	0.06(3)	113.4009(8)	4153.8(2)	–	3074.18(22)
4139.6(10)	2974.4	3087.4(10)	0.035(23)	113.4009(8)	4139.5(2)	–	3088.48(22)
4100.9(9)	3013.1	3126.1(9)	0.06(3)	113.4009(8)	4101.2(2)	–	3126.78(22)
4092.4(9)	3134.6	3134.6(9)	0.06(3)	g.s.	4090.5(2)	–	3137.6(3)
4071.7(9)	3155.3	3155.3(9)	0.06(3)	g.s.	4074.6(4)	–	3153.4(4)
4014.5(11)	3172.5	3212.5(11)	0.07(4)	40.892(12)	4015.9(2)	–	3212.09(22)
3960.5(8)	3226.5	3266.5(8)	0.06(3)	40.892(12)	3960.3(3)	–	3267.0(14)
3953.2(10)	3233.8	3273.8(10)	0.046(28)	40.892(12)	3955.7(2)	–	3272.29(22)
3947.7(10)	3239.3	3279.3(10)	0.06(4)	40.892(12)	3946.2(2)	–	3281.79(22)
3931.2(10)	3255.8	3295.8(10)	0.09(4)	40.892(12)	3931.7(2)	–	3296.29(22)
3920.8(8)	3266.2	3306.2(8)	0.09(4)	40.892(12)	3919.6(2)	–	3308.39(22)
3909.6(7)	3277.4	3317.4(7)	0.09(4)	40.892(12)	3912.7(2)	–	3315.29(22)
3891.9(6)	3295.1	3335.1(6)	0.15(6)	40.892(12)	3892.8(2)	–	3335.19(22)
3883.3(9)	3343.7	3343.7(9)	0.12(6)	g.s.	3885.9(2)	–	3342.09(22)
3867.3(10)	3319.7	3359.7(10)	0.06(3)	40.892(12)	3867.5(20)	–	3360.49(22)
2940.9(7)	4286.1	4286.1(7)	0.04(4)	g.s.	–	–	–
2940.9(7)	4246.1	4286.1(7)	0.07(3)	40.892(12)	–	–	–
2940.9(12)	4146.1	4286.1(12)	0.06(4)	140.298(12)	–	–	–
2784.6(11)	4402.4	4442.4(11)	0.05(3)	40.892(12)	–	–	–
2784.6(6)	4329.4	4442.4(6)	0.12(5)	113.4009(8)	–	–	–
2657.7(10)	4529.3	4569.3(10)	0.048(27)	40.892(12)	–	–	–
2657.7(7)	4456.3	4569.3(7)	0.07(3)	113.4009(8)	–	–	–
2412.5(11)	4765.5	4814.5(11)	0.06(3)	58.708(10)	2412.1(3)	–	–
2412.5(25)	4701.5	4814.5(25)	0.024(20)	113.4009(8)	2412.1(3)	–	–
2347.3(9)	4839.7	4879.7(9)	0.08(4)	40.892(12)	2346.3(5)	–	–
2347.3(9)	4739.7	4879.7(9)	0.06(3)	140.298(12)	2346.3(5)	–	–
2312.6(5)	4914.4	4914.4(5)	0.27(8)	g.s.	2314.32(16)	–	–
2312.6(10)	4874.4	4914.4(10)	0.05(3)	40.892(12)	2314.32(16)	–	–
2293.1(11)	4621.9	4933.9(11)	0.037(22)	311.821(10)	2291.8(10)	–	–
2293.1(7)	4537.9	4933.9(7)	0.07(4)	396.227(12)	2291.8(10)	–	–
1976.4(7)	5210.6	5250.6(7)	0.11(4)	40.892(12)	1975.41(15)	–	–
1976.4(10)	5137.6	5250.6(10)	0.07(4)	113.4009(8)	1975.41(15)	–	–
1858.3(4)	5368.7	5368.7(4)	0.21(6)	g.s.	1858.93(14)	–	–
1858.3(9)	5310.7	5368.7(9)	0.049(21)	58.708(10)	1858.93(14)	–	–
1858.3(8)	5255.7	5368.7(8)	0.07(4)	113.4009(8)	1858.93(14)	–	–
1784.5(7)	5402.5	5442.5(7)	0.11(4)	40.892(12)	–	–	–
1784.5(8)	5329.5	5442.5(8)	0.052(27)	113.4009(8)	–	–	–
1767.6(5)	5401.4	5459.4(5)	0.14(4)	58.708(10)	–	–	–
1767.6(7)	5147.4	5459.4(7)	0.052(24)	311.821(10)	–	–	–
1713.1(14)	5513.9	5513.9(14)	0.037(29)	g.s.	–	–	–
1713.1(6)	5400.9	5513.9(6)	0.10(4)	113.4009(8)	–	–	–

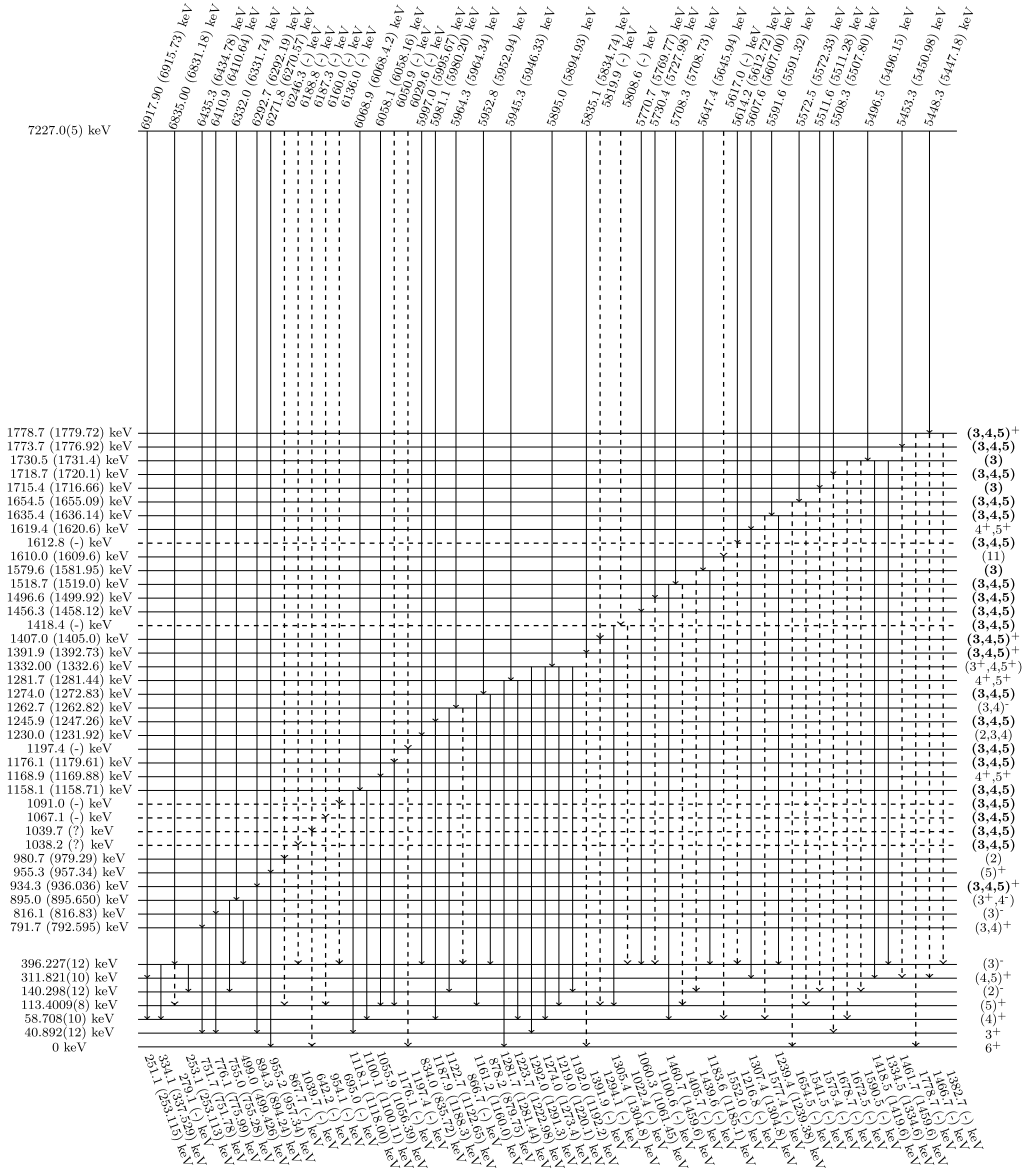


Fig. 5. Experimental level scheme of ^{94}Nb with intermediate level energies up to 1800 keV. Dashed lines - levels and gammas not found in the ENSDF library; bold spin values - values suggested by the authors for the levels without spin information in the ENSDF library. All energy values, except the energy values for the first 7 low lying levels are given in the form: Experimental value (ENSDF value).

ENSDF database. However, for 29 levels observed in this study, there is no data in the ENSDF library yet. In this work, we observed 183 secondary gamma transitions for which there is no information in the ENSDF database. 136 of these new observed secondary transitions come from the levels already in the ENSDF library, and 47 from levels determined for the first time in this work. Among secondary transitions, the ones with energies 879.75, 1061.45, 1185.1, 1304.8 and

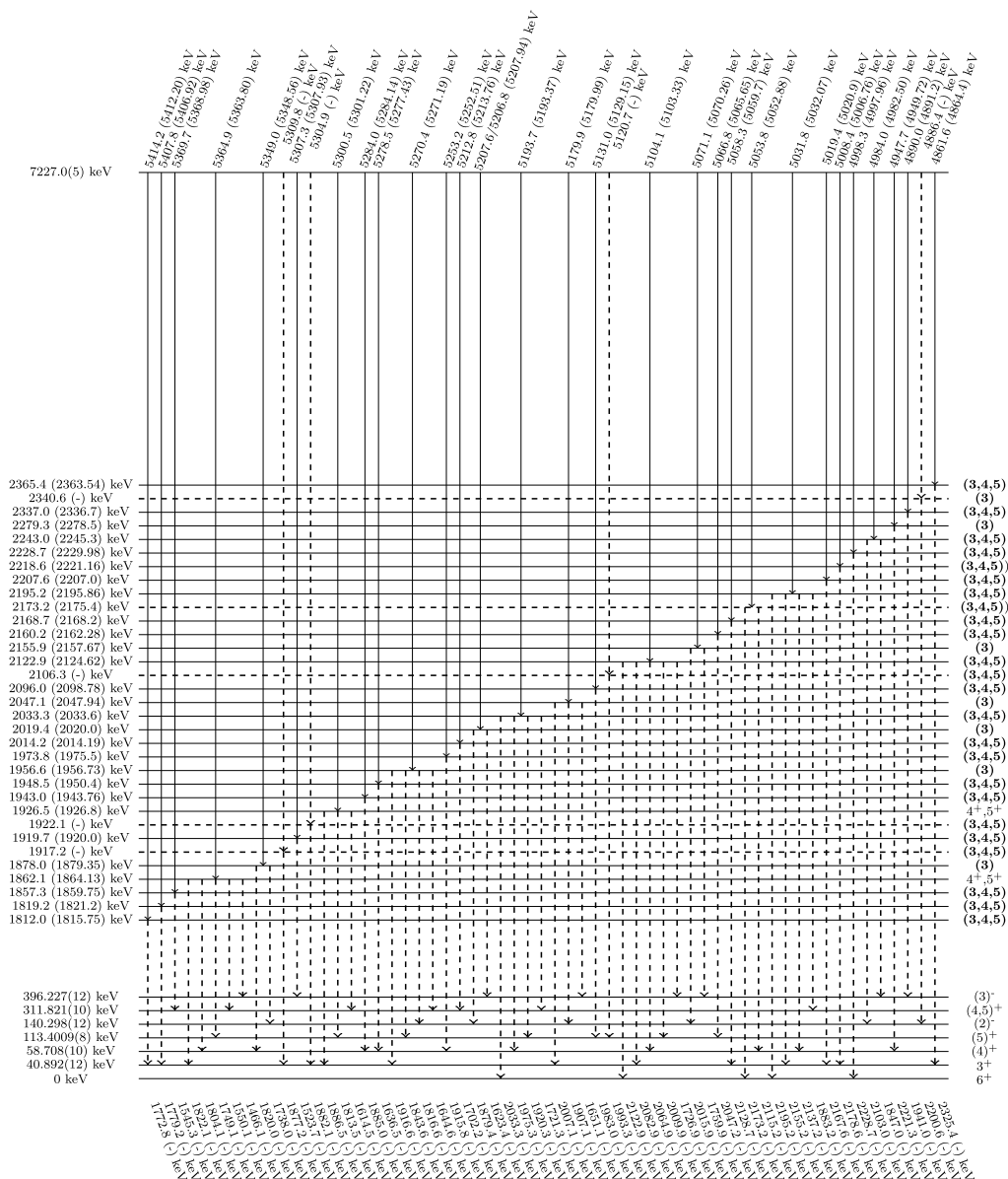


Fig. 6. Experimental level scheme of ^{94}Nb with intermediate level energies from 1800 to 2390 keV. Dashed lines - levels and gammas not found in the ENSDF library; bold spin values - values suggested by the authors for the levels without spin information in the ENSDF library. All energy values, except the energy values for the first 7 low lying levels are given in the form: Experimental value (ENSDF value).

1334.6 keV are included in the ENSDF database, but until now, they have not been placed into the decay scheme, and can also be considered as new data.

The comparison of determined energies of levels and gammas with the ones from the ENSDF database shows an average deviation of about 0.9 keV. For 104 levels and gammas, the deviation is larger than 1.5 keV. In those cases, ENSDF values were assigned tentatively by the authors.

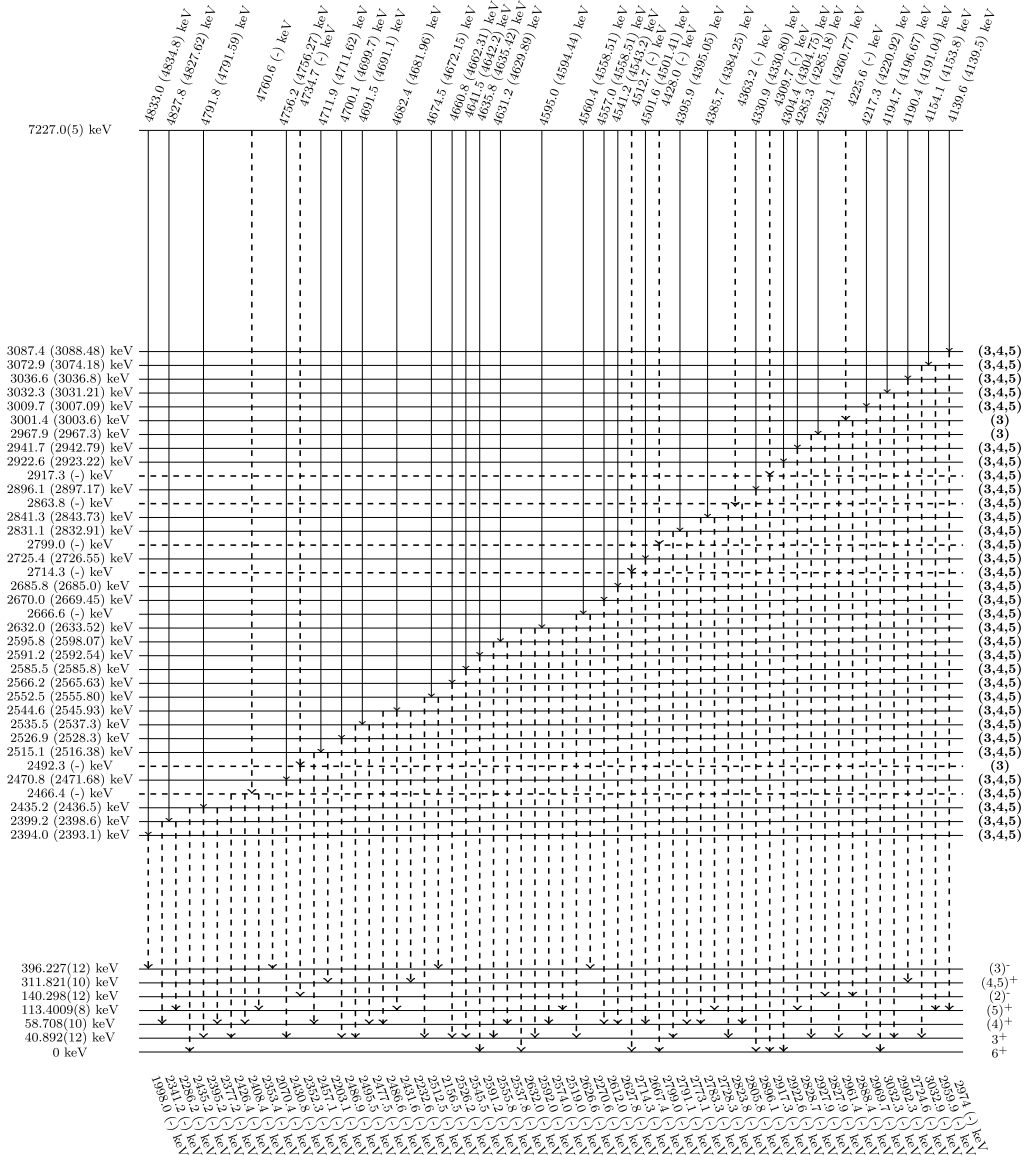


Fig. 7. Experimental level scheme of ^{94}Nb with intermediate level energies from 2390 to 3100 keV. Dashed lines - levels and gammas not found in the ENSDF library; bold spin values - values suggested by the authors for the levels without spin information in the ENSDF library. All energy values, except the energy values for the first 7 low lying levels are given in the form: Experimental value (ENSDF value).

This relatively large discrepancy can be explained by insufficient statistics in the present TSC spectra, which can cause uncertainty in the determination of the energy. For more precise data a longer time of measurements would be required.

The level scheme of ^{94}Nb obtained in this work is presented in Figs. 5 to 8. As it is known from [30], spin of the initial level of a cascade at a capture of thermal neutron in most cases

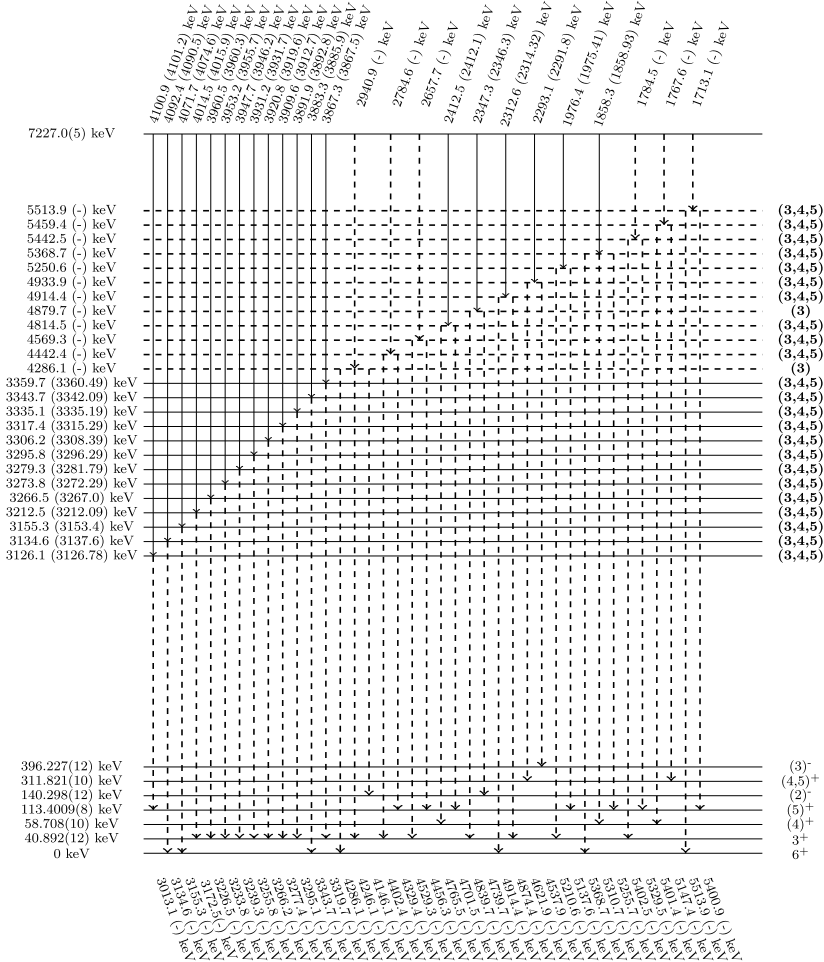


Fig. 8. Experimental level scheme of ^{94}Nb with intermediate level energies from 3100 to 5520 keV. Dashed lines - levels and gammas not found in the ENSDF library; bold spin values - values suggested by the authors for the levels without spin information in the ENSDF library. All energy values, except the energy values for the first 7 low lying levels are given in the form: Experimental value (ENSDF value).

(~96%) is 4^+ and only in some (~4%) instances $J=5^+$. Thus, spin of an intermediate cascade level can take the values of $J = 3, 4$ and 5 , with the exception of the cascade with the energy of final level $E_f = 140$ keV, for which $J = 3$ is most likely. Among the peaks presented in Fig. 2, there are no cascades with a spin difference $\delta J \geq 3$ between initial and final levels, so the nature of the major part of the cascade quanta is E1 or M1. Also, for 5 final levels of cascades with positive parity, both transitions are either magnetic or electric that can have an influence on the emission spectrum, if the investigated nucleus is to be compared with other odd-odd nuclei.

4. Conclusion

In this paper, we presented the spectroscopic information obtained by investigating two-step gamma cascades following thermal-neutron capture on ^{93}Nb . As a result, the level scheme for the

^{94}Nb nucleus was obtained. Our data are in good agreement with the data in the ENSDF library. 29 new levels were observed with 27 new primary and 183 secondary gamma transitions in the energy range between 0.2 MeV and 7 MeV. These results will be useful for future investigations of nuclear structure parameters such as level density and radiative strength function.

Acknowledgements

The authors are indebted to the CHANDA Program for funding the experiment in Budapest. Project ID: Fission-2013-4.1.2 call, grant number 605203.

References

- [1] N. Mărginean, D. Bucurescu, G. Căta-Danil, I. Căta-Danil, M. Ivaşcu, C. Ur, High-spin states in the ^{94}Nb nucleus, *Phys. Rev. C* 62 (3) (2000) 034309.
- [2] U. Gruber, R. Koch, B. Maier, O. Schult, J. Ball, K. Bhatt, R.K. Sheline, Energies and character of low-lying levels in Nb-94, *Nucl. Phys.* 67 (2) (1965) 433–442.
- [3] D. Goldberg, G. Dicker, S. Worcester, Niobium and niobium alloys in nuclear power, *Nucl. Eng. Des.* 22 (1) (1972) 124–137.
- [4] V. Likhanskii, I. Evdokimov, T. Aliev, V. Kon'kov, V. Markelov, V. Novikov, T. Khokhunova, Corrosion model for zirconium-niobium alloys in pressurized water reactors, *At. Energy* 116 (3) (2014) 186–193.
- [5] R.D. Mariani, P.G. Medvedev, D.L. Porter, S.L. Hayes, J.I. Cole, X.-M. Bai, Novel Accident-Tolerant Fuel Meat and Cladding, Tech. rep., Idaho National Laboratory (INL), 2013.
- [6] R.L. Caldwell, The internal conversion electrons of several short-lived neutron induced radioactivities, *Phys. Rev.* 78 (4) (1950) 407.
- [7] L. Ciuffolotti, C. Giori, M. Bettoni, K-conversion coefficient of the isomeric transition of nb94m, *Energia Nucleare* 8 (1961) 422.
- [8] P. Kilian, H. Langhoff, A. Flammersfeld, Der Zerfall von Nb-94m, *Z. Phys.* 169 (1) (1962) 23–31.
- [9] L. Yin, R.E. Sund, R.G. Arns, M.L. Wiedenbeck, Decay of Nb-94 and Nb-94m, *Nucl. Phys.* 34 (3) (1962) 588–592.
- [10] K. Sastry, R. Fink, P. Rao, K-conversion coefficient for 40.95-keV M3 transition in 6.3-min decay of Nb-94m, in: *Bulletin of the American Physical Society*, vol. 14, Amer. Inst. Physics Circulation Fulfillment Div., 500 Sunnyside Blvd., Woodbury ..., 1969, p. 18.
- [11] R. Gehrke, R. Lokken, Calibration of the efficiency of a Si(Li) photon spectrometer in the energy region 5 to 125 keV, *Nucl. Instrum. Methods* 97 (2) (1971) 219–228.
- [12] M. De Bruin, P. Korthoven, Low-energy gamma rays from isotopes produced by (n, γ) reactions, *J. Radioanal. Chem.* 10 (1) (1972) 125–135.
- [13] M.O. Krause, Atomic radiative and radiationless yields for k and l shells, *J. Phys. Chem. Ref. Data* 8 (2) (1979) 307–327.
- [14] H. Muller, Nuclear data sheets for A=94, *Nucl. Data Sheets (United States)* 44 (2) (1985) 277–406.
- [15] M.S. Zisman, F. Becchetti, B. Harvey, D. Kovar, J. Mahoney, J. Sherman, Heavy-ion-induced single-nucleon transfer reactions in the Zr-Mo region, *Phys. Rev. C* 8 (5) (1973) 1866.
- [16] M. Zisman, B. Harvey, High-spin levels of Nb 92, 93, 94, 95, 96 and Tc 94 populated with (α , d) and (α , t) reactions at 50 MeV, *Phys. Rev. C* 5 (3) (1972) 1031.
- [17] R.K. Sheline, R.T. Jernigan, J.B. Ball, K.H. Bhatt, Y.E. Kim, J. Vervier, The ^{93}Nb (d, p) ^{94}Nb reaction and the low-lying states of ^{94}Nb , *Nucl. Phys.* 61 (2) (1965) 342–351.
- [18] E. Jurney, H. Motz, R. Sheline, E. Shera, J. Vervier, Energy levels and configurations in ^{94}Nb , *Nucl. Phys. A* 111 (1) (1968) 105–128.
- [19] J. Moorhead, R. Moyer, Nuclear-structure studies in Mo and Nb isotopes via stripping reactions at 12 MeV, *Phys. Rev.* 184 (4) (1969) 1205.
- [20] R. Diehl, B. Cohen, R. Moyer, L. Goldman, Spectroscopic studies of molybdenum isotopes with (d, t) reactions, *Phys. Rev. C* 1 (6) (1970) 2132.
- [21] I. Fedorets, Y. Antufev, I. Zalyubovskii, A. Popov, V. Storizhko, Excited-states of Nb-94 in reaction of Zr-94 (p, n γ) Nb-94, *Izv. Akad. Nauk SSSR, Ser. Fiz.* 40 (6) (1976) 1260–1265.
- [22] E. Hagen, B. Kern, F. Snyder, D. Miracle, Low-lying levels of Nb 94, *Phys. Rev. C* 13 (2) (1976) 620.

- [23] I. Fedorets, V. Mishchenko, A. Popov, V. Storizhko, Angular correlations in the reaction $^{94}\text{Zr}(p, n\gamma)^{94}\text{Nb}$, *Bull. Acad. Sci. USSR, Phys. Ser.* 43 (5) (1979) 38.
- [24] D. Miracle, B. Kern, Multipolarities of γ -rays from 92, 94-Nb and 94, 95, 96, 97, 98Tc, *Nucl. Phys. A* 320 (2) (1979) 353–372.
- [25] H. Miska, B. Norum, M. Hynes, W. Bertozzi, S. Kowalski, F. Rad, C. Sargent, T. Sasanuma, B. Berman, Precise measurement of the charge-distribution differences of the oxygen isotopes, *Phys. Lett. B* 83 (2) (1979) 165–168.
- [26] Y. Guyash, Z. Dombradi, E. Koltai, A. Krasnakhorkai, T. Fenesh, ^{94}Nb levels excited in the reaction $^{94}\text{Zr}(p, n\gamma)^{94}\text{Nb}$, *Bull. Acad. Sci. USSR, Phys. Ser.* 44 (5) (1980) 118.
- [27] R. Chrien, K. Rimawi, J. Garg, Resonance neutron capture in Nb 93, *Phys. Rev. C* 3 (5) (1971) 2054.
- [28] R. Chrien, M. Bhat, G. Cole, Channel spin components of p-wave neutron widths in niobium, *Phys. Rev. C* 8 (1) (1973) 336.
- [29] T. Haste, B. Thomas, Investigations of resonance capture γ -ray spectra in the $^{93}\text{Nb}(n, \gamma)^{94}\text{Nb}$ reaction, *J. Phys. G, Nucl. Phys.* 1 (9) (1975) 967.
- [30] S.F. Mughabghab, *Neutron Resonance Parameters and Thermal Cross Section, Part A, Z=1-60, vol. 1*, Academic Press, 1981.
- [31] T. Kennett, W. Prestwich, J. Tsai, Energy levels of ^{94}Nb populated directly via the (n, γ) reaction, *Can. J. Phys.* 66 (11) (1988) 947–959.
- [32] M. B., et al., Low-lying states of ^{94}Nb , *Fizika (Zagreb)* 17 (1985) 219.
- [33] S. Boneva, E. Vasil'eva, Y.P. Popov, A. Sukhovo, V. Khitrov, Two-quantum cascades of radiative neutron capture 1. Spectroscopy of excited states of complex nuclei in the neutron binding energy region, *Sov. J. Part. Nucl. (English Transl.)* 22 (2) (1991) 232–248.
- [34] Y.P. Popov, A. Sukhovo, V. Khitrov, Y.S. Yazvitskij, Study on the γ decay of ^{165}Dy with the help of the $(n, 2\gamma)$ reaction, *Izv. Akad. Nauk SSSR, Ser. Fiz.* 48 (5) (1984) 891–900.
- [35] A. Sukhovo, V. Khitrov, Method of improving the amplitude resolution of the spectra of gamma-transition cascades in the computer processing of encoded coincidence data, *Instrum. Exp. Tech.* 27 (5) (1985) 1071–1074.
- [36] E. Vasilieva, A. Sukhovo, V. Khitrov, Direct experimental estimate of parameters that determine the cascade gamma decay of compound states of heavy nuclei, *Phys. At. Nucl.* 64 (2) (2001) 153–168.
- [37] <https://www.nndc.bnl.gov/ensdf/>.
- [38] V. Khitrov, A. Sukhovo, New technique for a simultaneous estimation of the level density and radiative strength functions of dipole transitions at $E_{\text{ex}} < B_n - 0.5$ MeV, arXiv preprint, arXiv:nucl-ex/0110017.
- [39] A. Sukhovo, L. Mitsyna, N. Jovancevic, Overall picture of the cascade gamma decay of neutron resonances within a modified practical model, *Phys. At. Nucl.* 79 (3) (2016) 313–325.
- [40] D. Vu, A. Sukhovo, L. Mitsyna, S. Zeinalov, N. Jovancevic, D. Knezevic, M. Krmar, A. Dragic, Representation of radiative strength functions within a practical model of cascade gamma decay, *Phys. At. Nucl.* 80 (2) (2017) 237–250.
- [41] A. Sukhovo, New model of the cascade gamma decay of neutron resonances for practitioners: basic concepts and attainable precision, *Phys. At. Nucl.* 78 (2) (2015) 230–245.
- [42] A.M. Sukhovo, L.V. Mitsyna, The next-generation practical model of the cascade gamma-decay of neutron resonance and expected parameters for an arbitrary nucleus, in: *Proceedings, 22nd International Seminar on Interaction of Neutrons with Nuclei: Fundamental Interactions and Neutrons, Nuclear Structure, Ultracold Neutrons, Related Topics*, ISINN 22, Dubna, Russia, May 27–30, 2014, 2015.
- [43] S. Boneva, V. Khitrov, A. Sukhovo, A. Vojnov, Excitation study of high-lying states of differently shaped heavy nuclei by the method of two-step cascades, *Nucl. Phys. A* 589 (2) (1995) 293–306.
- [44] L. Szentmiklósi, T. Belgia, Z. Révay, Z. Kis, Upgrade of the prompt gamma activation analysis and the neutron-induced prompt gamma spectroscopy facilities at the Budapest research reactor, *J. Radioanal. Nucl. Chem.* 286 (2) (2010) 501–505.
- [45] L. Szentmiklósi, Z. Kasztovszky, T. Belgia, Z. Révay, Z. Kis, B. Maróti, K. Gméling, V. Szilágyi, Fifteen years of success: user access programs at the Budapest prompt-gamma activation analysis laboratory, *J. Radioanal. Nucl. Chem.* 309 (1) (2016) 71–77.
- [46] <https://www.caen.it/products/n6724/>.
- [47] B. Krusche, K. Lieb, H. Daniel, T. Von Egidy, G. Barreau, H. Börner, R. Brissot, C. Hofmeyr, R. Rascher, Gamma ray energies and ^{36}Cl level scheme from the reaction $^{35}\text{Cl}(n, \gamma)^{36}\text{Cl}$, *Nucl. Phys. A* 386 (2) (1982) 245–268.

SPECTROSCOPY OF NEUTRON INDUCED REACTIONS WITH THE ν -BALL SPECTROMETER*

N. JOVANCEVIC^{a,b}, M. LEBOS^{a,b}, J.N. WILSON^{a,b}, D. THISSE^{a,b}, L. QI^{a,b}, I. MATEA^{a,b},
 F. IBRAHIM^{a,b}, D. VERNEY^{a,b}, M. BABO^{a,b}, C. DELAFOSSE^{a,b}, F. ADSLEY^{a,b},
 G. TOCABENS^{a,b}, A. GOTTARDO^{a,b}, Y. POPOVITCH^{a,b}, J. NEMER^{a,b}, R. CANAVAN^{c,d},
 M. RUDICIER^{c,d}, K. BELVEDERE^{c,d}, A. BOSO^{c,d}, P. REGAN^{c,d}, ZS. PODOLYAK^{c,d},
 R. SHEARMAN^{c,d}, M. BUNCE^{c,d}, P. INAVOV^{c,d}, S. OBERSTEDT^e, A. LOPEZ-MARTENS^f,
 K. HAUSCHILD^f, J. LJUNGVALL^f, R. CHAKMA^f, R. LOZEVA^f, P.-A. SÖDERSTRÖM^g,
 A. OBERSTEDT^g, D. ETASSE^h, D. RALET^h, A. BLAZHEVⁱ, R.-B. GERSTⁱ, G. HAFNERⁱ,
 N. CIEPLICKA-ORYŃCZAK^j, Ł.W. ISKRA^j, B. FORMAL^j, G. BENZONI^k, S. LEONI^k,
 S. BOTTONI^k, C. HENRICH^l, P. KOSEOGLOU^l, J. WIEDERHOLD^l, I. HOMM^l, C. SURDER^l,
 T. KRÖLL^l, D. KNEZEVIC^m, A. DRAGIC^m, L. CORTESⁿ, N. WARR^l, K. MIERNIK^o,
 E. ADAMSKA^o, M. PIERSA^o, K. REZYNKINA^p, L. FRAILE^q, J. BENITO GARCIA^q,
 V. SANCHEZ^q, A. ALGORA^r, P. DAVIES^s, V. GUADILLA-GOMEZ^t, M. FALLOT^t,
 T. KURTUKIAN-NIETO^u, C. SCHMITT^u, M. HEINE^u, D. REYGADAS TELLO^v, M. YAVACHOVA^w,
 M. DIAKAKI^x, F. ZEISER^y, W. PAULSON^y, D. GESTVANG^y

^aIPN Orsay, 15 rue G. Clémenceau, 91406 Orsay, France

^bUniv. Paris-Saclay, 15 rue G. Clémenceau, 91406 Orsay Cedex, France

^cDepartment of Physics, Univ. of Surrey, Guildford, GU2 7XH, UK

^dNational Physical Laboratory, Teddington, Middlesex, TW11 0LW, UK

^eEuropean Commission, Joint Research Centre, Directorate G
Retieseweg 111, 2440 Geel, Belgium

^fCSNSM Orsay, Bat. 104, 91405 Orsay, France

^gHoria Hulubei National Institute of Physics and Nuclear Engineering (IFIN-HH)
077125 Bucharest, Romania

^hLaboratoire de Physique Corpusculaire de Caen

6 Bvd. du maréchal Juin, 14050 CAEN CEDEX 4, France

ⁱInstitut für Kernphysik, Zulpicher Strasse 77, 50937 Köln, Germany

^jH. Niewodniczański Institute of Nuclear Physics, PAN
Radzikowskiego 152, 31-342 Kraków, Poland

^kDipartimentato di Fisica, Univ. degli Studi di Milano, 20133 Milano, Italy

^lInstitut für Kernphysik, TU Darmstadt, Schlossgartenstrasse 9, 64289 Darmstadt, Germany

^mInstitute of Physics Belgrade, Pregrevica 118, Belgrade, Serbia

ⁿRIKEN, 2-1 Hirosawa, Wako, Saitama 351-0198, Japan

^oUniv. of Warsaw, Faculty of Physics, 02-093 Warszawa, Poland

^pKU Leuven, 3000 Leuven, Belgium

^qUniv. Complutense de Madrid, Avda. de Séneca, 2 Ciudad Universitaria, 28040 Madrid, Spain

^rInstituto de Fisica Corpuscular, 46980 Paterna, Spain

^sThe University of Manchester, Oxford Rd, Manchester, M13 9PL, UK

^tSubatech, 4 rue Alfred Kastler — La Chantellerie — BP 20722, 44307 Nantes cedex 3, France

^uCentre d'Etudes Nucleaires de Bordeaux Gradignan

19 Chemin du Solarium CS 10120, 33175 Gradignan Cedex, France

^vUniv. of Brighton, Mithras House Lewes Road, Brighton BN2 4AT, UK

^wBulgarian Academy of Sciences, 15th November 1, Sofia, Bulgaria

^xEuropean Organization for Nuclear Research (CERN), Geneva, Switzerland

^yUniv. of Oslo, Department of Physics, P.O. Box 1048, Blindern 0316 Oslo, Norway

(Received December 19, 2018)

* Presented at the Zakopane Conference on Nuclear Physics “Extremes of the Nuclear Landscape”, Zakopane, Poland, August 26–September 2, 2018.

The ν -ball is a high-efficiency hybrid spectrometer which consists of both germanium (Ge) detectors and associated anti-Compton BGO shields, coupled to lanthanum bromide (LaBr₃) detectors. The hybrid configuration provides a combination of both excellent energy and timing resolutions. The ν -ball geometry allows the coupling with the LICORNE directional neutron source at the ALTO facility of the IPN, Orsay. This opens the possibility to perform precise spectroscopy of neutron induced reactions and was used for two experiments during the recent experimental campaign. These two experiments are described here: 1. Spectroscopy of the neutron-rich fission fragments produced in the $^{238}\text{U}(n, f)$ and $^{232}\text{Th}(n, f)$ reactions; 2. Spectroscopy above the shape isomer in ^{238}U . The $^{238}\text{U}(n, f)$ and $^{232}\text{Th}(n, f)$ reactions produce hundreds of neutron-rich nuclei on which gamma-ray spectroscopy can be performed. The main goal of the experiment aiming to populate the shape isomer in ^{238}U is the measurement of the gamma-ray and fission decay branches as well as determination of level scheme in the super-deformed minimum. The shape isomer is populated by $^{238}\text{U}(n, n')$ reaction, which gives a very advantageous population cross section over other reactions. More detailed descriptions of these two ν -ball experiments will be presented here.

DOI:10.5506/APhysPolB.50.297

1. Introduction

The ν -ball spectrometer was recently constructed at the ALTO facility of the IPN, Orsay. ν -ball is a hybrid device consisting of 24 clovers and 10 coaxial Ge detectors (and associated anti-Compton BGO shields) with excellent energy resolution and up to 20 LaBr₃ detectors with excellent timing resolution. The main goals were to perform spectroscopy of neutron-rich nuclei and fission shape isomers as well as extract information about nuclear moments or deformations with high sensitivity using fast timing techniques. The unique possibility of coupling the ν -ball spectrometer to the LICORNE (Lithium Inverse Cinematiques ORsay NEutron source) directional neutron source at the ALTO facility [1] was exploited. This opens up the possibility for detailed spectroscopic studies of neutron induced reactions. Two experiments of this type were performed: 1. Spectroscopy of the neutron-rich fission fragments produced in the $^{238}\text{U}(n, f)$ and $^{232}\text{Th}(n, f)$ reactions [2]; 2. Spectroscopy above the shape isomer in ^{238}U [3]. The $^{238}\text{U}(n, f)$ and $^{232}\text{Th}(n, f)$ reactions give a possibility for production and study of hundreds of neutron-rich nuclei, hence many different physics cases are addressed simultaneously. The main goal of the spectroscopy above the shape isomer in ^{238}U is the measurement of population and decay of this long-lived superdeformed state in a nucleus that has a significant gamma branch to the normal deformed potential minimum. The hope is to determine the level scheme in the super-deformed minimum.

2. Coupling the ν -ball spectrometer and LICORNE neutron source

The combination of LaBr₃ and Ge detectors provide excellent timing and energy resolution. The measured timing resolution of LaBr₃ detectors was ≈ 250 ps and timing resolution of Ge detectors was about ≈ 12 ns. The Ge detectors provide in average energy resolution of 2.8 keV at 1.33 MeV energy in comparison with 2.6% at 662 keV for the LaBr₃. Total efficiency was simulated and confirmed by measurements to be $\approx 6.2\%$ for Ge and $\approx 0.8\%$ for LaBr₃ detectors. One of the main characteristics of the ν -ball is full digitization of all signals from detectors including BGO detectors. The FASTER digital data acquisition system was used with a total of up to 200 channels [4]. Since the BGO detectors were used without collimation, calorimetric measurement by determination of full energy deposited in the spectrometer was possible. Calorimetric measurement in combination with the determination of gamma multiplicity is a powerful tool for selection of the events coming from different processes, for example separation of fission events and beta decay. The LICORNE neutron source [1] provides intensely focused quasi-monoenergetic neutron beams produced by the inverse kinematic reaction $p(^7\text{Li}, n)^7\text{Be}$. The neutron energy is constrained between 0.5 MeV and 4.0 MeV and is suitable for gamma-spectroscopy measurements of fast neutron induced reactions, particularly fission.

3. Spectroscopy of the neutron-rich fission fragments produced in the $^{238}\text{U}(n, f)$ and $^{232}\text{Th}(n, f)$ reactions

The collection of spectroscopic information about neutron-rich nuclei is very important for many different reasons such as the nuclear structure studies (for example, testing of different theoretical models) or better understanding of astrophysical processes in which neutron-rich nuclei can be produced. Coupling of the ν -ball spectrometer with the LICORNE neutron source gave us possibility to populate and study neutron-rich nuclei. The production mechanism was fission of ^{238}U and ^{232}Th induced by the fast neutrons of incident energy around 2 MeV. The fast fission reaction provides on average higher ratios of neutrons to protons (N/Z) in the reaction products with less emitted neutrons per fission in contrast to thermal neutron-induced fission of ^{235}U , ^{241}Pu and spontaneous fission of ^{248}Cm , ^{252}Cf . This is a clear advantages of these population mechanisms in comparison to ones used previously [5, 6]. Two targets of ^{238}U (81 g) and ^{232}Th (129 g) provide the possibility to perform cross checking of data. Many different physics cases will be studied. The first part of the experiment using the cylindrical shape ^{238}U target was performed in February 2018. The lithium primary beam energy was 16.4 MeV and pulsed with 400 ns period. The experiment lasted

for two weeks. The second part of the experiment was performed in April 2018. The target was a conical shaped aluminum shell housing 9 samples of ^{232}Th of different diameters and thickness of 0.1 mm and an average density of 1 g/cm^3 to reduce attenuation of low-energy gamma rays. The primary lithium beam energy was 16.75 MeV, again with pulsation of 400 ns period. The measurement was three weeks duration. All data were collected in triggerless mode with all gamma ray hits in the detectors stored on disk for later offline analysis. The most important task in the data analysis is to obtain very good selectivity for the particular events of interest. The pulsed neutron beam with period of 400 ns and pulse width of 2 ns, allows separation of prompt and delayed gamma rays and gives access to time correlations. In Figs. 1 and 2, the matrices of energy *versus* time for the Ge and LaBr₃ detectors are presented. Another possibility to increase selectivity comes from

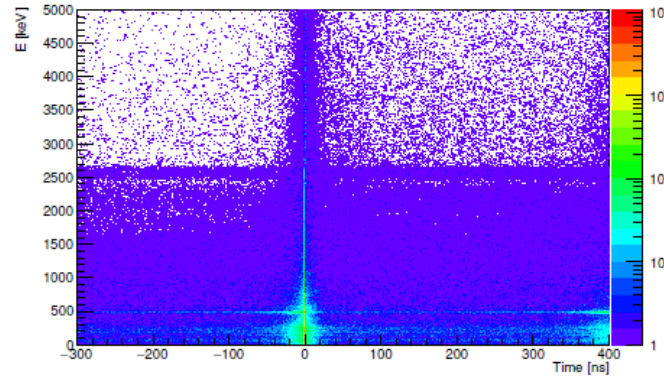


Fig. 1. Energy *versus* time for the LaBr₃ detectors during measurements with ^{232}Th target.

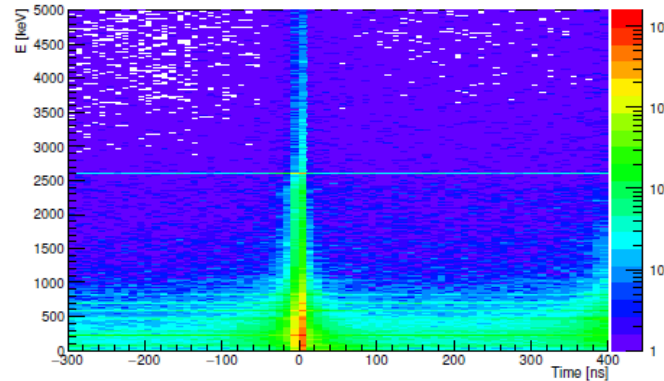


Fig. 2. Energy *versus* time for the Ge detectors during measurements with ^{232}Th target.

the fast timing of the LaBr₃ detectors as well as energy selection with excellent resolution of the Ge detectors. Finally, further selectivity is provided by calorimetric measurement. By analyzing sum-energy and gamma multiplicity (Fig. 3), it is possible to distinguish between events with different multiplicities and total sum energy.

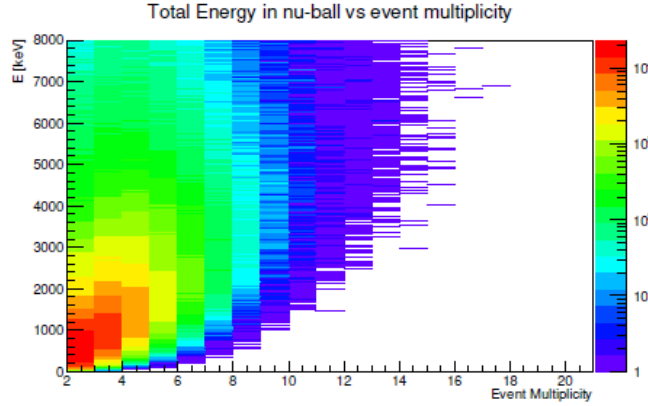


Fig. 3. Multiplicity *versus* total deposited energy in ν -ball spectrometer during activation of the ^{232}Th target.

4. Spectroscopy above the shape isomer in ^{238}U

Study of fission shape isomers can provide information about the fission barrier energy landscape as well as characteristic of super-deformed state of atomic nuclei. In this work, we decided to study the shape isomer in ^{238}U . The goal of the experiment was to obtain information about population of the fission shape isomer, its decay, branching ratio, half life and fission barrier penetrability. Study of shape isomer in ^{238}U has some advantages for experimental work. First of all, it is known that the ground state in the super deformed minimum has energy of 2.558 MeV. Also, two isomeric transitions (IT) to the normal deformed states with energy of 1878 keV and 2513 keV are identified in previous works [7, 8]. The measured half life of that IT decay is 195(30) ns [7, 8]. Decay of this state can occur through IT or isomeric fission (IF) with ratio of IT/IF = 95/5 [8]. With an incident neutron energy between 3 MeV and 5 MeV, the ratio of the prompt fission to delayed fission is $\approx 10^{-4}$ [9]. Taking into account the prompt fission cross section and the IT/IF ratio, the cross section for population of superdeformed isomeric state in ^{238}U can be expected to be ≈ 1.5 mb. Because of this high cross section, the $^{238}\text{U}(n, n')$ reaction is ideal to populate the shape isomer. The LICORNE incident neutron energy was, therefore, arranged to be 3.5 MeV which will give the possibility to populate energy levels up to 1 MeV above the shape isomer in the superdeformed well. Using

the ν -ball spectrometer with the LICORNE pulsed neutron beam gives the possibility first, to study IT decay of fission isomer and then, to study its population to obtain information about level scheme above the shape isomer. The experiment used the same cylindrical ^{238}U target of mass of 81 g used in the previous experiment. However, the lithium primary beam energy was higher, at 18.5 MeV. The measured LICORNE neutron energy spectrum (from TOF) is presented in Fig. 4. Data were collected over a period of approximately 6 days. Prompt and delayed gamma spectra (from 100 ns to 300 ns after beam pulse) for a part of collected data are presented in Fig. 5.

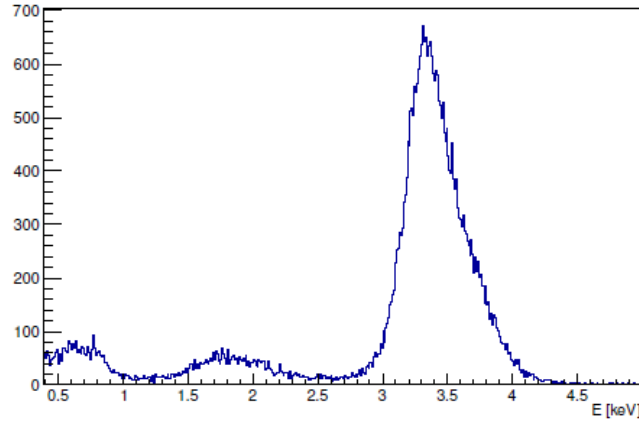


Fig. 4. Measured LICORNE neutron spectrum during the measurement of spectroscopy above the shape isomer in ^{238}U .

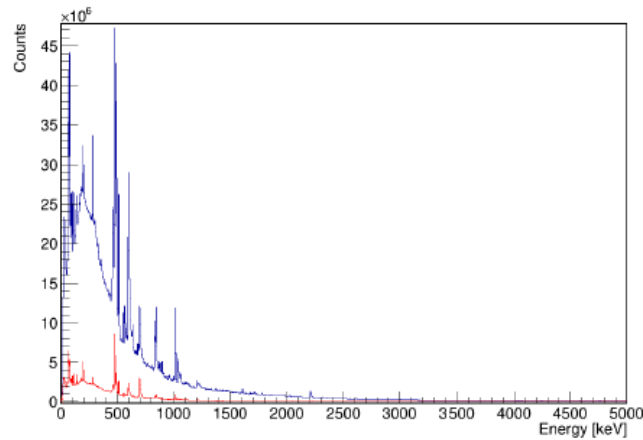


Fig. 5. (Color online) Prompt spectrum (top/blue line) and delay spectrum (bottom/red line) of Ge detectors during the measurement of spectroscopy above the shape isomer in ^{238}U .

The ability to make a selection of different events based on detected gamma multiplicity is presented in Fig. 6. No significant difference in the spectra (Fig. 6) is seen, which requires a further investigation.

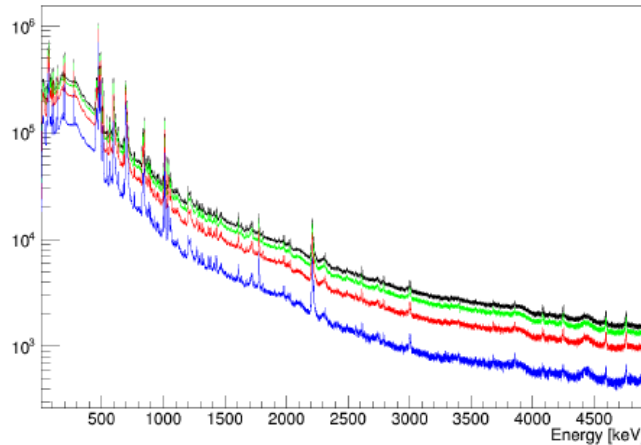


Fig. 6. (Color online) Delayed gamma spectra during the measurement of spectroscopy above the shape isomer in ^{238}U (from 100 ns to 300 ns after beam pulse) with prompt gamma multiplicity equal to or less than 1 and delay gamma multiplicity: equal or less than 1 (bottom/blue line), equal or less than 2 (second from the bottom/red line), equal or less than 3 (second from the top/green line) and equal or less than 4 (top/black line).

5. Conclusion

The coupling of the ν -ball hybrid spectrometer with the LICORNE neutron source was performed at the ALTO facility of the IPN Orsay. Two experiments concerning the gamma-ray spectroscopy of neutron-induced reactions were performed and the main ideas and experimental conditions have been described. The analysis of the collected data is in progress. New information about the structure of neutron-rich nuclei and the fission shape isomer in ^{238}U is expected.

REFERENCES

- [1] M. Lebois *et al.*, *Nucl. Instrum. Methods Phys. Res. A* **735**, 145 (2014).
- [2] J.N. Wilson *et al.*, *Acta Phys. Pol. B* **48**, 395 (2017).
- [3] D.N. Poenaru, M.S. Ivascu, D. Mazilu, *Chapter 2: Fission Isomer*, in: *Particle Emission from Nuclei, Volume II, Fission and Beta-delayed Decay Models*, D.N. Poenaru, M.S. Ivascu (Eds.), CRC PRESS, 1989, ISBN 0-8493-4646-3.

- [4] FASTER DAQ, <http://faster.in2p3.fr>
- [5] J.K. Hwang *et al.*, *Phys. Rev. C* **57**, 2250 (1998).
- [6] A.G. Smith *et al.*, *Phys. Rev. C* **60**, 064611 (1999).
- [7] P. Russo, J. Pedersen, R. Vandenboch, *Nucl. Phys. A* **240**, 13 (1975).
- [8] J. Kantele *et al.*, *Phys. Rev. C* **29**, 1693 (1984).
- [9] K.L. Wolf, J.W. Meadows, *Bull. Am. Phys. Soc.* **19**, KH1 595 (1974).



PRIRODNO-MATEMATIČKI FAKULTET
Univerzitet u Novom Sadu

FACULTY OF SCIENCES
University of Novi Sad

TRG DOSITEJA OBRADOVIĆA 3, 21000 NOVI SAD, SRBIJA (SERBIA)
tel +381.21.455.630 fax +381.21.455.662 e-mail dekanpmf@uns.ac.rs web www.pmf.uns.ac.rs
PIB 101635863 MB 08104620

Delovodni br.: 0603-803/20

Broj dosijea: 73d/12

Na osnovu člana 29. st. 1 Zakona o opštem upravnom postupku "Sl. glasnik RS" br. 18/2016, u skladu sa članom 112. Zakona o visokom obrazovanju "Sl. glasnik RS" br. 88/2017, uvida u matične knjige studenata doktorskih studija Prirodno-matematičkog fakulteta Univerziteta u Novom Sadu i zahteva Knežević Radenko Davida, iz Sonte izdaje se

UVERENJE

O STEČENOM VISOKOM OBRAZOVANJU TREĆEG STEPENA DOKTORSKIH STUDIJA

Knežević (Radenko) David

rođen 03.06.1988. godine u Kninu, opština Knin, država Republika Hrvatska, završio je visoko obrazovanje trećeg stepena-doktorskih studija, na studijskom programu Doktorske studije - Fizika, Departmana za fiziku Prirodno-matematičkog fakulteta Univerziteta u Novom Sadu, dana 28.09.2019. godine, sa prosečnom ocenom 10.00 (deset i 00/100), u toku studija i postignutim ukupnim brojem ESPB bodova 180.00 (slovima: sto osamdeset i 00/100) i stekao naučni naziv Doktor nauka-fizičke nauke. Naslov doktorske disertacije je: "Eksperimentalno određivanje parametara nuklearne strukture aktivacionim tehnikama"

Uverenje se izdaje radi lične upotrebe i zamenjuje diplomu do izdavanja iste.

Na osnovu člana 19. stav 1. tačka 7. Zakona o republičkim administrativnim taksama ("Sl. glasnik RS" broj 43/2003, 51/2003 - ispr., 61/2005, 101/2005 - dr. zakon, 5/2009 i 54/2009) ovo uverenje je oslobođeno takse.

Novi Sad, 28.10.2019.

